AD 681948

AD

USAAVLABS TECHNICAL REPORT 68-63

ADVANCED HIGH TEMPERATURE COMBUSTOR RESEARCH FOR SMALL GAS TURBINE ENGINES

By

Richard H. Andersen

October 1968

U. S. ARMY AVIATION MATERIEL LABORATORIES
FORT EUSTIS, VIRGINIA

CONTRACT DA 44-177-AMC-375(T)
CURTISS-WRIGHT CORPORATION
WOOD-RIDGE, NEW JERSEY

FEB 4 1969

A

This document has been approved for public release and sale; its distribution is unlimited.

Reproduced by the
CLEARINGHOUSE
for Federal Scientific & Technical
Information Springfield Va. 22151

199

Disclaimers

The findings in this report are not to be construed as an official Department of the Army position unless so designated by other authorized documents.

When Government drawings, specifications, or other data are used for any purpose other than in connection with a definitely related Government procurement operation, the United States Government thereby incurs no responsibility nor any obligation whatsoever; and the fact that the Government may have formulated, furnished, or in any way supplied the said drawings, specifications, or other data is not to be regarded by implication or otherwise as in any manner licensing the holder or any other person or corporation, or conveying any rights or permission, to manufacture, use, or sell any patented invention that may in any way be related thereto.

Trade names cited in this report do not constitute an official endorsement or approval of the use of such commercial hardware or software.

Disposition Instructions

Destroy this report when no longer needed. Do not return it to the originator.

DEPARTMENT OF THE ARMY
U. S. ARMY AVIATION MATERIEL LABORATORIES
FORT EUSTIS, VIRGINIA 23604

The object of this contractual effort was the investigation of several subelements of a small high-temperature combustor to generate technology precedent to a combustor component exploratory development program.

The conclusions and recommendations contained herein are concurred in. Results will be used in the planning of combustor programs for future gas turbine propulsion systems.

Task 1G 125901A 01409

Contract DA 44-177-AMC-375(T)

USAAVLABS Technical Report 68-63

October 1968

ADVANCED HIGH TEMPERATURE COMBUSTOR RESEARCH FOR SMALL GAS TURBINE ENGINES

Final Report

by

Richard H. Andersen

Prepared by

Curtiss-Wright Corporation
Wood-Ridge, New Jersey

for

U.S. ARMY AVIATION MATERIEL LABORATORIES
FORT EUSTIS, VIRGINIA

This document has been approved for public release and sale; its distribution is unlimited.

SUMMARY

The primary objective of the Advanced High Temperature Combustor Research Program was to generate the technology necessary to design a combustion chamber for a 2-5 lb/sec., 16:1 pressure ratio gas turbine engine with a 3000°F turbine inlet temperature.

Program effort was organized on the basis of three tasks:

TASK I - Parametric design studies were conducted to define fundamental combustor envelope restrictions and to select overall configurations and subsystems for experimental evaluation. This phase encompassed primary zone sizing and selection and the selection of optimum subsystem concepts for introducing fuel and diluent air into the system and for cooling the liners.

TASK II - Fundamental test evaluations of the subsystems selected in Task I were conducted to evaluate and optimize their performance. The extent of this evaluation is summarized below:

SUMMARY OF TESTS

SUBSYSTEM RIG TESTED	NO. OF CONFIG. TESTED	TEST HOURS		
		COLD	HOT	TOTAL
LINER COOLING TECHNIQUES	3	24	16	40
MIXING ZONE	4	33	-	33
FUEL PATTERNIZATION	3	39	-	39
PRIMARY ZONE				
CONFIGURATION SCREENING @ 5 ATM.	4	19:00	35:45	54:45
SELECTED CONFIGURATION EVALUATION	1	4:40	17:55	22:35
16 ATM. EVALUATION	1	4:20	3:00	7:20

TASK III - Preliminary combustor designs were conducted for a can and annular combustion chamber incorporating the results of the experimental evaluations performed in Task II.

The program has produced a demonstration of the technology necessary for the intended application, as confirmed by these results:

1. The experimental combustor was designed for use in a 2.0 lb/sec airflow engine and was operated successfully over a wide range of fuel-air ratios and at pressures up to 16 atmospheres. The designs meet the lower end of the specified 2-5 lb/sec engine airflow range, and are readily scaleable up to the 5 lb/sec level.

2. Good combustion efficiency was obtained over a wide range of fuel-air ratios and combustion chamber pressure levels, with both JP-4 and JP-5 fuel.

3. The unique liner configuration which utilized transpiration cooling proved to be durable in this first known application in a gas turbine combustion chamber. Further stringent testing is needed to fully qualify this component, which offers the prospect of a 50 - 65% saving in liner coolant requirements, thus allowing for a greater percentage of engine airflow for diluent purposes to trim the combustor exit temperature profile.

4. Data were obtained which indicate the mixing trends which prevail as the dilution zone geometry is varied. Data from another Curtiss-Wright design substantiate the trend.

5. Data presented herein from this program and from other sources pinpoint the two improvements required to attain the target outlet profile. These improvements are: (a) improved fuel feed systems to provide uniform distribution within the vaporizer tube; and (b) closer spacing of diluent air holes.

FOREWORD

United States Army Contract DA 44-177-AMC-375(T) was performed by the Curtiss-Wright Corporation to conduct design studies and experimental tests to provide basic technology and preliminary designs for a small combustor with a 3000°F exit temperature. The contract was administered under the direction of the Propulsion Division of the U.S. Army Aviation Materiel Laboratories (USAAVLABS).

The manager of the Small Gas Turbine Engine Program was Mr. T. Schober, and the managers of this Combustor Technology Contract were Messrs. A. Sneeden and D. Wagner. Principal contributing engineers were Messrs. N. Brookes, R. Andersen, J. Atkins, J. Durcan, J. Karph and B. Stahl. The overall guidance and technical direction provided by Mr. S. Lombardo are gratefully acknowledged.

The guidance of Mr. J. White and Mr. L. Bell of USAAVLABS is also gratefully acknowledged.

TABLE OF CONTENTS

TABLE OF CONTENTS (Continued)

LIST OF ILLUSTRATIONS

LIST OF ILLUSTRATIONS (Continued)

LIST OF ILLUSTRATIONS (Continued)

LIST OF ILLUSTRATIONS (Continued)

LIST OF ILLUSTRATIONS (Continued)

LIST OF ILLUSTRATIONS (Continued)

LIST OF ILLUSTRATIONS (Continued)

LIST OF ILLUSTRATIONS (Continued)

LIST OF TABLES

LIST OF SYMBOLS

1.0 Subsystems Concept Studies and Selection

A_p	=	Primary Zone Flow Area, $in.^2$
$\mathbb{C}$	=	Engine Center Line
D	=	Characteristic Dimension
f_{cc}	=	Combustor Overall Fuel-Air Ratio
f_p	=	Combustor Primary Zone Fuel-Air Ratio
K_1	=	Empirically Established Constant
L_p	=	Primary Combustion Zone Length, in.
N	=	Engine Speed, RPM
ΔP_T	=	Total Inlet Pressure to Combustor, in. Hg abs
P_T	=	Combustor Pressure Drop, in. Hg abs
q_j	=	Dynamic Head of the Primary Air Passing Through Headplate, in. HgA
q_p	=	Dynamic Head at the Primary Combustion Zone Exit, in. Hg abs
T_c	=	Liner Coolant Airflow Temperature, °F
T_{T_4}	=	Combustor Average Exit Temperature, °F
T_w	=	Liner Metal Wall Temperature, °F
W	=	Airflow, lb/sec
W_{cc}	=	Combustor Overall Airflow, lb/sec
W_p	=	Combustor Primary Zone Airflow, lb/sec

2.0 Liner Cooling Tests

A_e	=	Splash Plate Film Cooling Slot Exit Area, $in.^2$
A_o	=	Total Orifice Area, $in.^2$
A_s	=	Film Cooling Slot Total Exit Area, $in.^2$

LIST OF SYMBOLS (Continued)

C_F	=	Film Cooling Slot Flow Coefficient
C_p	=	Specific Heat at Constant Pressure, Btu/lb °R
D	=	Tangential Film Cooling Slot Channel Depth, in.; Splash Plate Film Cooling Slot Orifice Diameter, in.
g	=	Gravitational Constant, 32.2 ft/sec^2
H	=	Film Cooling Slot Height, in.
L	=	Film Cooling Slot Length, in.
$\dot{q}_r$	=	Incident Black Body Radiation, Btu/hr ft^2
$Q_{Radiation}$	=	Heat Flux into Specimen Due to Radiation, Btu/sec in.^{2}
$Q_{Heat\ Balance}$	=	Calculated Heat Flux Out of Specimen Due to Coolant Flow, Btu/sec in.^{2}
P_{s_e}	=	Film Cooling Slot Exit Static Pressure, in. Hg abs
P_{T_i}	=	Film Cooling Slot Inlet Total Pressure, in. Hg abs
R	=	Gas Constant, ft/°F
S	=	Distance Between Orifice Center Lines, in.
T_c	=	Coolant Air Inlet Temperature, °R
$\dot{W}_c$	=	Coolant Airflow Rate, lb/sec
θ	=	Relative Temperature (T/518.4), $^{\circ}R/^{\circ}R$
δ	=	Relative Pressure (P/29.92), in. HgA/in. Hg abs

3.0 Mixing Zone Rig Tests

H	=	Mixing Zone Duct Height, in.
L	=	Downstream Distance from Diluent Holes, in.
$(MV)_D$	=	Diluent Air Injection Momentum, lb ft/sec^2
$(MV)_p$	=	Primary Air Stream Momentum, lb ft/sec^2
n	=	Total Number of Local Temperatures Recorded

LIST OF SYMBOLS (Continued)

T_D	=	Diluent Air Inlet Temperature, °R
$\bar{T}_{exit}$	=	Overall Average Measured Exit Temperature, °R
T_L	=	Local Temperature, °R
T_{max}	=	Maximum Temperature, °R
T_p	=	Primary Air Inlet Temperature, °R
W	=	Distance Between Diluent Holes, in.
W_D	=	Total Diluent Airflow, lb/sec
W_p	=	Total Primary Airflow, lb/sec
σ	=	Standard Deviation

5.0 Primary Zone Combustion Rig Tests

f_p	=	Primary Combustion Zone Fuel-Air Ratio
H_d	=	Total Enthalpy of Diluent Air, Btu/sec
H_{exit}	=	Total Enthalpy of Combustor Exhaust Gas, Btu/sec
H_f	=	Ideal Effective Heat Value of Fuel, Btu/lb
H_p	=	Total Enthalpy of Preheated Primary Inlet Air, Btu/sec
P_s	=	Static Pressure, in. Hg abs
P_T	=	Total Pressure, in. Hg abs
T_{Local}	=	Local Combustor Exit Temperature, °R
T_m	=	Liner Metal Temperature, °F
T_{max}	=	Maximum Combustor Exit Temperature, °R
$\bar{T}_{overall}$	=	Average Measured Combustor Exit Temperature, °R
T_T	=	Total Temperature, °R
W_f	=	Fuel Flow, lb/hr
η_b	=	Combustion Efficiency, %

LIST OF SYMBOLS (Continued)

6.0 Preliminary Designs

f_{cc}	=	Combustion Chamber Fuel-Air Ratio
W_{bleed}	=	Combustor Bypass Flow Bleed Air, lb/sec
W_{cc}	=	Combustion Chamber Air Flow, lb/sec
W_e	=	Engine Air Flow, lb/sec

INTRODUCTION

The performance demands of advanced Army aircraft give rise to the requirement for small turbine engines having improvements in specific power, power to weight ratio, and specific fuel consumption. As part of a commitment to advance small gas turbine engine component technology, the U.S. Army awarded Curtiss-Wright a contract to extend the state of the art of small (2-5 lb/sec airflow) high temperature (3000°F) combustors. Technology gained from the combustor research activity, along with parallel turbine compressor and heat exchanger efforts, is directed toward future demonstration in an advanced, high performance engine.

The objective of this research program was to provide the basic technology and preliminary designs for a small high temperature rise combustor, as the first step toward demonstration in a research engine. Under this program, a combustor for a 2.0 lb/sec, 16:1 pressure ratio engine, rated at 3000°F turbine inlet temperature, was selected for study and test evaluation.

The research program involved parametric design studies to define fundamental combustor subsystems. The most promising concepts were then selected for test evaluation leading to optimization of system combustion efficiency, pressure loss, exit temperature distribution and other combustor characteristics, in terms of the overall objectives of the program.

As the result of these investigations the preliminary design of two combustors, one an end-mounted can configuration and the other an annular configuration, was completed. Each configuration incorporates transpiration cooled liner walls, and embodies the vaporizing concept of fuel introduction.

The design requirements were:

Total Engine Airflow, lb/sec	2.0
Combustor Inlet Pressure, atm	16
Combustor Inlet Temperature, °F	700
Combustor Efficiency, %	98.5
Combustor Pressure Loss, %	3
Turbine Inlet Temperature, °F	3000
Turbine Inlet Temperature Variation, °F	±200

1.0 SUBSYSTEMS CONCEPT STUDIES AND SELECTION

Analytical screening studies were conducted to identify the critical combustor design parameters needed to establish combustion chamber envelope restrictions and subsystem design requirements consistent with the particular requirements of a very small high temperature rise combustor. Specific designs were then selected for evaluation during the fundamental test phase of the program.

1.1 COMBUSTOR ENVELOPE RESTRICTIONS

Engine envelope restrictions on the combustor were established from preliminary engine designs derived on other programs at Curtiss-Wright. The conventional scaling methods outlined below were used to scale the reference engines to the power level required for the subject application.

$$\text{Power} \propto \text{Airflow} \qquad \text{Eq. (1)}$$

$$\frac{W_2}{W_1} = \left(\frac{D_2}{D_1}\right)^2 \qquad \text{Eq. (2)}$$

$$\frac{N_2}{N_1} = \frac{D_1}{D_2} \qquad \text{Eq. (3)}$$

where W = airflow

D = characteristic dimension

N = RPM

Subscript 2 = scaled (new) unit

1 = reference unit

Equation (1) expresses the concept that power output is directly proportional to airflow.

Equation (2) is based on maintaining the same geometric proportions of the designs.

Equation (3) is based on maintaining the same tip speed, which provides the same outlet conditions for the turbomachine element (either compressor or turbine), since the Mach number is identical.

This method assumes that other significant aerodynamic parameters, such as Reynolds number, are not seriously affected by the change in scale.

The combustor interfaces (compressor exit and turbine inlet dimensions) derived on this basis are presented in Figure 1. Both end- and mid-mounted combustion chamber designs were considered. Combustion chamber envelope restrictions were established for a 2.0 lb/sec total engine airflow and are applicable to the complete 2 to 5 lb/sec airflow range, since no problem is envisioned in scaling upward to new conditions. An allowance was made for the total downstream cooling air bleed amounting to 28.5% of the total engine airflow, or 0.57 lb/sec. This cooling requirement is based on estimates made for gas generator performance analyses performed by Curtiss-Wright under a separate USAAVLABS contract (Reference 1). The gas generator cycles investigated during this earlier program included the engine design point operating conditions (16:1 pressure ratio and a 3000°F turbine inlet temperature) and airflow range required for the combustion chamber under consideration herein. These results were therefore used directly to define the combustion chamber airflow (1.43 lb/sec) for which the combustor envelope restrictions were derived.

The combustor design criteria used to define the critical combustion chamber dimensions are presented in Figures 2, 3 and 4. An overall combustor fuel-air ratio of 0.040, which was established from Reference 1, is required to provide the design-point temperature rise of 2300°F. The primary zone combustion efficiency characteristic demonstrated on other Curtiss-Wright combustors was utilized to provide an estimate of the proportion of combustor air required by the primary combustion process. This characteristic is presented in the upper portion of Figure 2. The relationship between primary zone fuel-air ratio, f_p, and overall combustor fuel-air ratio, f_{cc}, for a range of primary zone to combustor airflow ratios, Wp/W_{cc}, is shown in the lower portion of Figure 2. A design-point primary zone fuel-air ratio of 0.075 was selected to ensure high design-point efficiency and a wide combustion stability characteristic. As shown in Figure 2, approximately 54% of the combustor flow must thus be allocated for primary combustion, leaving a balance of 46% of combustor flow to satisfy liner cooling and dilution zone requirements.

Design experience at Curtiss-Wright indicates that the overall combustor pressure loss and the primary zone cross-sectional area are dictated by primary zone mixing characteristics. An empirical equation utilized by this contractor to establish favorable primary zone mixing characteristics may be expressed in the following fundamental form:

$$q_j/q_p = K_1 \qquad \text{Eq. (4)}$$

where q_j = dynamic head of the primary air passing through the headplate

q_p = dynamic head at the primary zone exit

K_1 = a constant, established empirically

Current state of the art at Curtiss-Wright indicates a minimum requirement of K_1 equal to 21. This criterion (K_1 = 21) was utilized to establish the relationships between total pressure loss and primary zone flow area, as illustrated in Figure 3. In this figure, curves are drawn for design-point primary zone fuel-air ratios of 0.075 and 0.064. The value of 0.064 is considered to be the upper limit of primary zone fuel-air rat' which could be utilized in the design of a spray-atomizing type of combus. system.

The overal: length of the combustor is established by satisfying the requirements of the primary combustion zone and the diluent mixing zone. The length of the primary combustion zone, L_p, is dependent on two criteria: an aerodynamic mixing requirement and a primary zone residence time requirement. In the design of small-scale combustors such as the subject application, the residence time criterion is predominant in establishing primary zone length. The residence time is based on the mean through flow velocity within the primary combustion zone. The current state-of-the-art value of 3.5 milliseconds was utilized in the derivation of the curves of Figure 4 which relate primary zone length to total pressure loss for design-point primary zone fuel-air ratios of 0.075 and 0.064. For the target total pressure loss of 3% of inlet total pressure, it is seen that a primary zone length of approximately 3.9 inches is required. The length of the dilution zone was established by holding the ratio of diluent zone length to diluent zone passage height equal to the approximate current state-of-the-art value of 1.5.

1.2 COMBUSTION CHAMBER CONFIGURATIONS

Six candidate engine configurations were initially reviewed to establish engine design restrictions and a target combustor envelope. These configurations fall under three broad engine packaging categories:

1. Engines with in-line components (compressor, combustor, turbine)
   a. Mid-mounted can combustor with transition duct
   b. Mid-mounted in-line annular combustor
   c. Reverse flow annular combustor-over-turbine
2. Engines with end-mounted combustors
   a. End-mounted annular combustor
   b. End-mounted can combustor
3. Engines with offset combustors

   Mid-mounted tangential can combustor

Of these, the end-mounted combustion chamber configurations were considered to be the most desirable for extensive evaluation and application in a small high temperature gas turbine. Most of the test data accumulated

during this program has been directed toward the evaluation of such combustor designs.

As noted in the preceding section, it was estimated that 28.5 percent of the total engine flow will be required for air bleed and turbine cooling. Approximately 54 percent of the remaining air will be required for primary combustion. Thus, cooling air available to trim the combustor exit profile and for cooling the liners is minimal. Liner cooling air requirements are especially critical.

A chart covering the combustor designs considered is presented in Table III. The mid-mounted can with transition duct, and the mid-mounted tangential can shown in Figure 5, were both eliminated from further consideration due to the large liner surface areas and accompanying increase in cooling air requirements which are inherent to these designs with their complicated transition sections. The mid-mounted annular combustor and the reverse flow annular combustor-over-the-turbine design concepts, shown in Figures 6 and 7, were considered undesirable since a large number of fuel introduction points would be required. This would increase the fuel system complexity and thereby increase the possibility of contamination problems. It should be noted that these comments must be traded off against compensating advantages in a given engine packaging problem.

Basic envelopes for end-mounted annular and can configurations are presented in the full-scale sketches in Figure 8. As can be seen, these designs represent an optimum between large combustor volume, small liner surface area, and wide combustion zone annuli. Both configurations are free of complex transition sections. These designs also facilitate relatively simple fuel introduction systems, as will be discussed in a later section. From the combustor designer's viewpoint, then, the end-mounted combustor has definite advantages over other designs.

1.3 LINER COOLING TECHNIQUES

The design of combustors for high temperature, high performance and maximum durability involves consideration of four principal types of liner failures: buckling due to high temperature gradients, cracking due to thermal cycling, corrosion due to the action of impurities in high performance fuels, and oxidation due to high metal temperatures. These four types of failure are largely temperature dependent, and the most positive solution appears to be control of the gas film temperature adjacent to the chamber walls together with an effective application of methods for cooling the chamber walls. This solution serves a dual purpose; (1) it provides the boundary conditions necessary for low combustor liner temperatures; and (2) it provides reduced gas film temperatures at the turbine nozzle inner and outer shrouds. The quantity of cooling air required is a function of flame radiation heat flux, inlet air temperature, chamber pressure, chamber surface area to be cooled, film effectiveness, and convection cooling coefficients.

As shown in Section 1.1, an increase in the combustor exit temperature requires an increase in the percentage of total engine airflow for both

primary combustion and turbine cooling. Thus, a smaller percentage of air is available for liner cooling and dilution purposes.

These characteristics when combined with the geometric limitations of liner construction (wall thickness, cooling air metering hole size, sheet metal tolerances, etc.) produce a very difficult thermal design. In order to establish the design criteria for liner cooling in advanced small size combustors, an experimental and analytical study program was conducted. The initial step in this program was to select the cooling schemes to be evaluated experimentally and in parametric trade-off studies.

Various liner cooling schemes were qualitatively analyzed for application in an advanced high temperature combustor. These cooling techniques are shown schematically in Figure 9. A tabulation of the results of this analysis is presented in Table IV. As indicated in this table, the three liner cooling methods selected for experimental evaluation were:

1. Tangential Film Cooling Slots
2. Splash Plate Film Cooling Slots
3. Transpiration Cooling

The regenerative cooling technique, which takes advantage of the additional convective cooling capacity afforded by passing the primary combustion air over the liners, was rejected due to the high pressure drop inherent to the aerodynamics of this system. The impingement cooling technique, which allows selective convective cooling of the liners, also requires a higher pressure drop than was desired for the subject application. This system has the added disadvantage of requiring a second liner wall. Partial cooling of the liners using the engine fuel supply as a coolant, or as a heat sink, was not considered to be desirable or necessary for the subject application. The development of refractory coatings or new high temperature materials was outside the scope of this program. They could be used with any of the three selected techniques, however.

Of the three liner cooling methods selected for experimental evaluation, transpiration cooling is obviously the most desirable due to its lower coolant requirement. This is graphically demonstrated in Figure 10. The curves in this figure were produced using the preliminary liner cooling requirements established during the qualitative analysis of the various liner cooling techniques considered. As shown on this figure the cooling air required for film cooled liners (assuming .013 lb/sec in^2) is greater than that available for the engine size under study. The combustor airflow split with transpiration cooled liners, on the other hand, has approximately 20 percent of the combustor airflow available to trim the combustor exit temperature profile. Transpiration cooling has the added advantage of low stresses (less than 1000 psi) whereas typical film cooling systems result in higher stresses which limit liner life.

1.4 FUEL INTRODUCTION METHODS

The method of introducing fuel into a combustion chamber is an important parameter in the overall design of the system. Fuel-air mixing and preparation in the combustor directly affect the ignition delay time of the combustion process. Since the ignition delay time is several times as large as the reaction time, a minimization of this parameter has a significant effect on the envelope requirements of the primary zone and therefore the liner surface areas to be cooled. This aspect of fuel-air preparation also has side effects on ignition, stability range, flame luminosity and fuel supply system complexity, pressure requirements and weight. Engine reliability and overhaul life are subsequently affected. The selection of a fuel introduction method must be predicated upon the trade-offs which are advantageous from the overall engine viewpoint. In the final analysis, the fuel supply and combustor systems must be studied as an integral system, with efforts directed toward matching the performance of the two, as well as physically mating them.

In selection of fuel admission methods, consideration was given not only to applying classic fuel injection methods such as spray atomization and vaporization, but also to the adaptation of less commonly used methods such as fuel slingers and air-assist nozzles. However, further evaluation indicated that the complications incurred by the use of exotic fuel introduction systems were not warranted for this system application. A chart showing the fuel introduction systems considered during this phase of the program is given in Table V.

The three fuel introduction designs selected for test evaluation were the annular "vaporizer", "mushroom" vaporizer and an educer-simplex atomizer system. These systems are shown incorporated in their respective combustor applications in Figures 11, 12, and 13. As is evident, the end-mounted combustion chamber design lends itself to relatively simple fuel injection systems.

The operation of both vaporizer designs is identical in concept. Fuel is introduced to the system from a relatively low pressure fuel supply system and premixed with air in the "vaporizer". The quantity of primary air allocated to the "vaporizer" provides a fuel-air ratio of 0.25 within the vaporizer at the design fuel flow. It has been established that this ratio is sufficient to avoid fuel "cracking" and deposition while maintaining maximum carburetion and preheating of the fuel. Carbureting and preheating the fuel within the vaporizer prior to injection into the primary combustion zone reduces ignition delay time and minimizes the required primary zone residence time. Primary air for combustion passes through primary air cups on the headplate and enters the primary zone as fan-shaped jets. These axial jets divide the primary zone into sectors and create a degree of coarseness in the fuel-air mixture within the primary zone that provides combustion stability over a wide operating range. Strong recirculating patterns conducive to good mixing and flameholding are established.

A high level of combustion efficiency has been demonstrated by vaporizing type combustors over a wide range of fuel-air ratios. The combustors are characteristically smoke-free with relatively low flame radiation to

combustor liners. A relatively high design point primary zone fuel-air ratio may be utilized, which permits the use of a minimum proportion of primary air and a maximum proportion of air available for cooling and dilution. These systems are amenable to development of multifuel capability, since critical spray patterns and tight limits on spray droplet size (which are influenced by fuel viscosity) are not required. The fuel system is relatively insensitive to contamination.

The annular design, shown in Figure 11, has the added advantage that it provides a simple access path for routing air to both the inner liner and the turbine cooling system. The "mushroom" type vaporizer tube described in Figure 12 is a lighter design and has demonstrated excellent performance on larger combustion chambers, with multiple fuel injection points.

The educer-atomizer design, shown in Figure 13, applies an advanced afterburner flameholder device to primary combustion zone design in order to create advantageous fuel-air mixing and fuel preparation. An ejector action is set up in the primary zone by passing all the primary air over a conical shroud at high velocity. The pressure differential induced causes a strong reverse circulation of hot gases from the interior of the shroud. A rich mixture of fuel and air is formed within the shroud by the fuel spray from a simple atomizer nozzle onto the internal walls of the shroud. Since the shroud is wetted by fuel and is itself in a high temperature environment, it serves as a vaporizer as well as a mixer. The rich mixture is aspirated through the upstream end of the shroud, mixes with additional air as it passes over the exterior of the shroud, and burns in the downstream wake.

Other configurations considered for the primary zone were fuel spray atomizers and fuel slingers. Conventional atomizing injectors are considered less desirable because of the high associated radiant heat flux and increased smoke emission.

A single air assist atomizer was rejected because of the unavailability of high pressure air at engine starting conditions. One atomizing configuration indicating promise is shown in Figure 14. This configuration features two opposing duplex atomizers. The atomizers would be staged during engine operation in order to satisfy engine turndown requirements. This configuration was rejected for this program since introduction of fuel and air from the centerbody requires the combustor design to be highly integrated with the turbine design.

The use of a fuel slinger was also rejected for use in the subject combustor. For the end-mounted combustors under consideration an excessive shaft overhang was required to drive the slinger. A highly integrated design with respect to the turbine and associated critical speed problems were evident. The use of a separate drive was rejected since it would prejudice the engine reliability.

1.5 DILUENT AIR INTRODUCTION METHODS

The combustor exit temperature distribution is primarily a function of the primary combustion zone exit conditions coupled with the geometric relationships within the diluent mixing zone. The significant diluent geometric relationships are: the ratio of diluent mixing length to combustion zone passage height, the ratio of slot length to width, and the ratio of slot length to circumferential spacing. The most important of these is the diluent mixing length to combustion passage height ratio. Values from 1.0 to 1.8 for this ratio have been used at Curtiss-Wright with good mixing performance on large engine designs. Momentum requirements for diluent mixing are generally dictated by the pressure drop and airflow through the primary combustion zone.

The method of diluent air introduction is strongly dependent on the primary zone design and on the overall design restrictions on the combustor system. Logical candidates are single-sided entry (from the outer secondary passage) and double-sided entry (from both secondary passages).

The single-sided entry is more attractive because it substantially reduces the requirement to transfer airflow to the inner liner. This is especially relevant to the end-mounted can configuration where air to the inner liner must be supplied through the first-stage turbine stators. The validity of the approach is established by test results from another Curtiss-Wright combustor program where a pattern factor of 0.164 was achieved with single-sided entry and a (mixing length to annular height) ratio of one.

2.0 LINER COOLING TESTS

In small, advanced high temperature combustors, the designer generally faces the problem of increased liner cooling airflow requirements with a subsequent reduction in available air for gas temperature profile control. The designer must also efficiently utilize the available cooling air pressure drop and produce satisfactory film cooling airflow characteristics in small size configurations.

The increase in liner cooling airflow requirements in small size combustors is caused by:

1. Increased liner surface areas per unit combustor mass flow brought about by the use of higher combustor length to diameter ratios.

2. Increased combustor gas and coolant temperatures.

3. Increased radiation at the higher pressure levels.

Efficient use of the available cooling air pressure drop and the generation of a satisfactory film cooling airflow characteristic is made difficult in small size combustors by:

1. Sheet metal fabrication procedures which limit the practical slot height to 0.020 inch minimum.

2. Area tolerances which limit the coolant flow control accuracy in small size film cooling slots.

An experimental program was conducted to determine and evaluate flow characteristics in 0.020-inch film coolant slots and the heat transfer characteristics of transpiration material in a radiation environment. The 0.020-inch slot height represents the approximate height that would be used in film-cooled combustor liners for high temperature, high pressure, small size combustors.

Transpiration is recognized as the most efficient means of film cooling and therefore is ideal from a thermal standpoint for consideration in high temperature, high pressure, small size combustor applications having large liner surface areas per unit of combustion mass flow. Transpiration cooling characteristics in a radiation environment were unknown, however, and therefore required evaluation in a rig prior to the fabrication of a full-scale, transpiration cooled combustor liner.

2.1 TANGENTIAL SLOT COLD FLOW TESTS

Cold flow tests were conducted to evaluate the coolant flow characteristics of a tangential film cooling slot. Relationships between the flow and pressure drop across the slot and the slot length, channel depth, coolant bypass flow and approach velocity were investigated. A slot height of 0.020 inch was studied.

A series of seven cold flow tests was conducted with flat, tangential film cooling slots measuring 1.56 inches wide by 0.020 inch high. A schematic of the test rig and instrumentation is shown in Figure 15. Tables VI and VII list the configurations and reduced data for each of the tests.

The influence of the film cooling slot length on the coolant flow characteristic is shown in Figure 17. Three configurations of slot lengths L = 0.20, 0.35, and 0.50 inch corresponding to slot aspect ratios of 10, 17.5, and 25 respectively were cold flow tested over a 1.5% to 33% range of total to static pressure drop across the slot.

The flow characteristics obtained show that the coolant flow increases as the slot length is decreased. An approximate 20% increase in flow is achieved when the slot length is reduced from 0.50 inch to 0.20 inch, and an approximate 10% increase in flow is achieved when the slot length is reduced from 0.50 inch to 0.35 inch.

The influence of coolant bypass flow on the film cooling flow characteristics is shown in Figures 18, 19 and 20. Two configurations with slot lengths of 0.35 and 0.50 inch (which correspond to slot aspect ratios of 17.5 and 25 respectively) and two configurations of channel depth of 0.188 and 0.401 inch were tested over a 1.5% to 33% range of slot pressure drops.

The coolant approach velocity was varied by permitting a portion of the flow to bypass the tangential slot. Table VII lists the slot flow, the bypass flow, and the coolant velocity approaching the slot for each test.

The results of these tests indicate that the coolant flow characteristics of a tangential film cooling slot can be correlated by Equation 5 below for a slot aspect ratio, L/H, between 10 and 17.5 when the total to static pressure drop across the slot is between 3% and 5%. Equation 6 gives the correlation for a slot aspect ratio between 17.5 and 25 when the pressure drop is between 2% and 5%.

$$\frac{\dot{W}_c \sqrt{T_c}}{P_{T_i}} = 0.491\, A_s \left(\frac{2g}{1.4\,R}\right)^{\frac{1}{2}} \left(\frac{P_{T_i} - P_{S_e}}{P_{T_i}}\right)^{\frac{1}{2}} \qquad \text{Eq. 5}$$

$$\text{for } 10 < \frac{L}{H} < 17.5 \qquad .03 < \frac{\Delta P}{P} < .05$$

$$\frac{\dot{W}_c \sqrt{T_c}}{P_{T_i}} = 0.491\, A_s \left(\frac{2g}{1.75\,R}\right)^{\frac{1}{2}} \left(\frac{P_{T_i} - P_{S_e}}{P_{T_i}}\right)^{\frac{1}{2}} \qquad \text{Eq. 6}$$

$$\text{for } 17.5 < \frac{L}{H} < 25 \qquad .02 < \frac{\Delta P}{P} < .05$$

where $\dot{W}_c$ = coolant flow rate - lb/sec

T_c = coolant temperature - °R

P_{T_i} = slot inlet total pressure - in. Hg abs

A_s = slot area - $in.^2$

g = gravitational constant - ft/sec^2

R = gas constant - ft/°F

P_{S_e} = slot exit static pressure - in. Hg abs (discharge to the atmosphere)

Slot length does have a measurable influence on the coolant flow. A slot length of 0.20 inch will yield 20% more flow than a slot length of 0.50 inch over a 1% to 5% range in coolant slot pressure differential. The characteristic of flow versus slot length is approximately linear within the 1% to 5% range of coolant slot pressure differentials. The effect of bypass flow on the flow characteristics of a tangential film cooling slot can be neglected for this range of pressure drop.

2.2 SPLASH PLATE COLD FLOW TESTS

Cold flow tests were conducted on splash plate film cooling slots to evaluate their coolant flow characteristics as affected by slot geometry and pressure differentials across the slot. The influence of slot bypass flow was not investigated for this configuration since splash plate film cooling slots are generally used where the coolant air velocities are relatively low. As shown in the preceeding section, bypass flow had little effect on the flow characteristics of tangential film cooling slots.

A schematic of the test rig and instrumentation is shown in Figure 21. The range of splash plate test geometries investigated is listed below.

Slot Length/Slot Height	10 to 25	(L/H)
Orifice Diameter/Slot Height	1.3 to 3.4	(D/H)
Slot Length/Orifice Diameter	3.8 to 20	(L/D)
Orifice Diameter/Orifice Spacing	0.2 to 0.5	(D/S)
Slot Area/Orifice Area	1 to 5	(A_e/A_o)

A series of nine cold flow tests was conducted with flat, splash plate film cooling slots measuring 1.326, 1.368, and 1.53 inches wide by 0.020 inch high. Tables VIII and IX list the configurations and test data for each of the tests.

The influence of the splash plate film cooling slot length on the coolant flow characteristics is shown in Figures 23, 24 and 25. Three configurations of slot lengths of 0.20, 0.35 and 0.50 inch (corresponding to slot aspect ratio (L/H) of 10, 17.5, and 25 respectively) were cold flow tested over a 1.6% to 33% range of total to static pressure drop across the slot. The flow characteristics obtained show that the coolant flow increases as the aspect ratio (L/H) is decreased. An approximate 5% to 10% increase in flow is achieved when the aspect ratio is reduced from 25 to 10. The influence of aspect ratio on coolant flow appears to be independent of the splash plate area ratio.

The influence of the splash plate orifice solidity (D/S) on the coolant flow characteristics was found to be negligibly small. In Figures 23, 24 and 25 the aspect ratios and area ratios are identical and the flow characteristics ($W\sqrt{\theta}/\delta$ vs $\Delta P/\delta$) are practically identical for orifice solidities of 0.196 and 0.050.

The influence of splash plate area ratio on the coolant flow characteristics is shown in Figure 27 to be very strong. Within the range of area ratios tested ($1 < A_e/A_o < 5$), the splash plate flow coefficient quadruples from an original value of 0.16 to a value of 0.64.

The flow coefficients used in Figure 26 were obtained from the correlation curves shown in Figures 23, 24 and 25. The flow coefficient is defined as

$$C_F = \frac{\left(W_c \sqrt{\theta} / \delta A_{slot}\right)_{Actual}}{\left(W_c \sqrt{\theta} / \delta A_{slot}\right)_{Ideal}} \qquad \text{Eq. 7}$$

The relationship between $\left(W_c \sqrt{\theta}/\delta A_{slot}\right)_{Ideal}$ and $\Delta P/\delta$ is shown in Figure 28.

The results of these tests indicate that the most significant parameter influencing the coolant flow rate is the area ratio. Within the range of area ratios tested ($1 < A_e/A_o < 5$), the splash plate flow coefficient (C_F) quadrupled.

Test evaluation also indicates that orifice solidity has no significant influence on coolant flow within the range of test configurations and that the slot aspect ratio has only a slight influence on coolant flow within the range of $10 < L/H < 25$.

2.3 TRANSPIRATION COOLING TESTS

As mentioned previously, data were required for transpiration cooling characteristics in a radiation environment. The required data were obtained using a straight-through can-type combustor with a single atomizing fuel injector as a radiation source. The combustor was adapted to measure radiation in the downstream portion of the primary combustion zone where, it was felt, maximum radiation intensity occured. The radiation intensity at this point was determined for various operating conditions of the

combustor. The external test hardware was then switched to allow transpiration tests to be conducted at the same point on the combustor. The radiation measurement test model and instrumentation are shown in Figure 29. The incident flame radiation was measured directly with a modified Leeds and Northrup No. 8891-C-S double-mirror Rayotube together with a Leeds and Northrop potentiometer. The modification consisted in replacing the standard quartz window in the Rayotube with a sapphire window to allow transmission of significant flame radiation out to a wavelength of 5 microns. To prevent leakage from the combustor a second sapphire window was installed in the combustor housing as shown in Figure 30. The Rayotube with the sapphire windows in place was calibrated at Leeds and Northrup against a blackbody target. Table I presents the calibration data. The temperature, T (°R), and the incident blackbody radiation, $\dot{q}_r$ (Btu/hr ft^2), are related by Stefan-Boltzman Law

$$\dot{q}_r = 0.1713 \times 10^{-8} T^4 \qquad \text{Eq. 8}$$

Using the calibration data and the above equation, the potentiometer output in millivolts (mv) can be directly related to the incident radiation $\dot{q}_r$ as shown in Figure 31.

TABLE I. CALIBRATION DATA FOR 8891-C-S LEEDS AND NORTHROP RAYOTUBE USING TWO SAPHIRE WINDOWS

Temperature	(°R)	2260	2560	2960	3160
Millivolts	(mv)	0.395	0.680	1.250	1.863

A series of seven flame radiation measurement tests was conducted; three of these tests were reproducibility checks. The combustor exit pressures and temperatures were varied between 2 atm and 4.75 atm, and 575°F and 1070°F, respectively. The test data for each of seven tests are plotted in Figure 32. This figure indicates that at the lower heat inputs into the combustor (124 Btu/lb air and 180 Btu/lb air), the flame radiation increased with increasing combustor pressure. This trend was followed only partially at the higher heat inputs (220 Btu/lb air and 257 Btu/lb air). Radiation intensity increased up to about 3.5 - 4.0 atm and decreased above that pressure. This apparent decrease in radiation intensity with increasing pressure probably represents a shift in the radiant flame front away from the Rayotube viewing port as the combustor flow conditions changed. The maximum radiation intensity recorded was 0.9×10^5 Btu/hr ft^2.

A schematic of the flow system and instrumentation used for the cooling tests is shown in Figure 33. A Rigimesh N155 alloy porous metal specimen 0.034 inch-thick with a permeability of 1.8×10^{-11} was selected for this series of tests since its flow characteristics closely approximate that of the primary zone rig combustor liners. The round specimen, 1 inch in diameter, was TIG welded along its periphery to a

stainless steel holder, and two chromel-alumel thermocouples (0.003 inch diameter leads) were installed on the coolant side of the specimen. The specimen holder was then mounted in the test fixture and installed in the combustor housing as shown in Figure 34.

The test procedure consisted of injecting cold air through the test specimen and recording its metal temperature while the combustor operating conditions were maintained constant. The specimen temperature was recorded by a Brown potentiometer while the flows were measured with a Fisher and Porter flowrator.

A series of six cooling tests was conducted for combustor operating conditions similar to those of the radiation measurement tests. The metal temperature of the transpiration specimen, for the various combustor operating conditions tested, is presented as a function of coolant mass flow rate in Figure 35. The ratio of heat received by radiation, Q radiation, to heat rejected by transpiration cooling, Q heat balance, is shown in Figure 36 as a function of the ratios of coolant mass flux to hot gas stream mass flux tested. The radiation heat fluxes used for this graph were those measured during the radiation tests described earlier. The heat rejection flux was obtained from equation 9 below.

$$Q_{\text{heat balance}} = \dot{W}_c C_p (T_M - T_c) \qquad \text{Eq. 9}$$

where

$\dot{W}_c$ = coolant mass flow per unit porous specimen area, lb/sec in^2

C_p = specific heat at constant pressure, Btu/lb °F

T_M = measured porous specimen metal temperature, °F

T_c = coolant temperature (measured upstream of specimen), °F

As indicated in Figure 36, for the region where the coolant mass flux to hot gas stream mass flux ratio ($\rho V_c / \rho V_g$) is less than .095 the radiation heat flux is greater than that obtained by the transpiration material heat balance. This is believed to be caused by:

1. Inaccuracies in the coolant flow measurements at the low flow rates.

2. Supplementary cooling of the transpiration material at the low coolant flow rates.

The supplementary coolant flow is due to combustor cooling air leakage through the upstream portion of the oval cut-out in the combustion chamber wall. This oval cut-out was required to permit thermal expansion of the combustion chamber walls in the region of the fixed porous specimen holder. The convective heat transfer into or out of the porous specimen due to this supplementary film cooling is important only at the low transpiration coolant mass fluxes. Both the value and direction (into or out of the specimen) of this convective heat transfer is unknown. At higher mass flux ratios ($\rho V_c/\rho V_g > .095$) the strength of the transpiration coolant mass flux is sufficient to eliminate the effect of the supplementary cooling and the convective heat transfer can be neglected.

It is noted that for high mass flux ratios the radiation heat flux is from zero to 20 percent lower than that obtained from the transpiration material heat balance. It is believed that the heat exchanger effectiveness of the transpiration material, defined as the ratio $(T_{c_{out}} - T_{c_{in}})/(T_M - T_{c_{in}})$, is reduced as the coolant flux is increased. The heat exchanger effectiveness is shown as a dashed line on Figure 36. It is further believed that the transpiration material specimen tested represents an infinite heat exchanger in the region $\rho V_c/\rho V_g < .095$ and consequently has a heat exchanger effectiveness of 100% in this flow range, that is, the coolant temperature as it leaves the specimen, $T_{c_{out}}$, is equal to the specimen metal temperature, T_M. High heat exchanger effectiveness for transpiration materials means that smaller coolant flow rates are required to achieve acceptably low liner material temperatures. When 100% heat exchanger effectiveness is achieved the cooling system is used to its full potential and represents the best cooling that can be achieved for a given coolant flow. Transpiration cooling has demonstrated high (approximately 100%) heat exchanger effectiveness up to coolant to hot gas mass flux ratios of .095 and has shown that relatively high effectiveness (greater than 80%) can be retained for $\rho V_c/\rho V_g$ between .095 and .17. Thus, transpiration cooling appears to be ideally suited to combustor cooling systems, particularly in small scale combustors where high heat exchanger effectiveness is required to compensate for the large liner surface area to combustor airflow ratio which is inherent to the system.

3.0 MIXING ZONE RIG TESTS

A test program was conducted to provide fundamental data for a parametric study of the mixing process associated with multipoint injection of cold air into a hot air stream. In particular, the effects of mixing zone geometry and air stream momentum ratio on the mixing process were investigated.

Tests were conducted in a rectangular mixing zone duct. This section was installed in a cross-section duct as shown in Figure 37. Cut-outs were provided at the downstream end of the rectangular duct to allow for the installation of various diluent slot configuration plates. When installed these plates were flush with the inside wall of the mixing duct. Both single- and double-sided entry could be investigated. In addition, a 1/2-inch-thick plate could be inserted into the rectangular duct to change the effective duct height. This permitted the investigation of mixing zone scaling factors. Only single-sided entry diluent hole configurations could be tested with this plate in place.

The mixing zone inlet was bellmouthed and of sufficient length to insure straightening of the primary stream prior to diluent air injection. The downstream end of the mixing zone was fixed to a circular plate. This plate had an "O" ring seal to provide for differential thermal expansion between the rectangular mixing zone duct and the cross-section duct.

The mixing zone rig was mounted on the test stand as shown in Figure 38. Separate supply lines were used for the primary and diluent air, thus allowing independent variation of either flow. The primary air stream was heated to 700°F in a direct fired preheater and passed through a baffled duct prior to its entry into the rectangular mixing zone duct section. Cold (ambient temperature) diluent air was fed into the plenum formed by the cross-section duct, where it was slightly heated through convective heat transfer from the hot rectangular duct walls. This air then passed through the diluent holes and mixed with the preheated primary air stream. A back pressure value at the downstream end of the rig provided variation of pressure levels in the mixing zone.

Temperature profiles in the rectangular duct were measured at significant locations downstream of the plane of diluent air injection, to determine the mixing effectiveness of the mixing zone geometries tested. Temperatures were measured with a 3-element rake which could be moved across the width of the rectangular duct. The rake consisted of bare-wire iron-constantan thermocouples positioned at 23, 50 and 79 percent of the duct height. Temperatures were recorded for 17 probe locations across the duct, and at various axial planes downstream of the diluent holes. Sufficient instrumentation was included in the test rig to establish the inlet flow conditions of the diluent and primary air streams.

Four basic diluent hole and mixing zone geometries were evaluated. These are shown in Figure 39. Inlet primary air stream profiles were determined for each of the configurations by flowing only preheated primary air through the rectangular duct and obtaining a temperature profile across

the duct with the traversing probe. A maximum deviation of less than 2 percent of the total inlet temperature was established for all configurations. Test points were obtained by setting specific primary and diluent airflows and obtaining temperature profiles at various downstream locations in the mixing zone duct. The effects of varying combustion chamber fuel-air ratios on the mixing characteristics of each configuration were determined by varying the primary (preheated) airflow rate, thus changing the primary air to diluent air momentum ratio. The effect of varying diluent airflow rates while maintaining a constant primary airflow was also investigated. A tabulation of the test point conditions of primary and diluent airflows, temperatures and pressures, as well as the average exit temperature across the duct, T_{exit}, measured during the test, is presented in Table XI.

Test results are presented in Tables XII, XIII and XIV. Table XII lists the primary to diluent air momentum and velocity ratios, and the ratio of the average temperature at each duct height location to the overall average exit temperature. Diluent holes for the single-sided entry configurations were at the "tip" location of the rectangular duct. The ratio of the maximum temperature recorded in the duct to the overall average temperature is also presented in this table.

Tables XIII and XIV present overall stream mixing efficiencies for selected points. The mixing efficiency is expressed by two factors. The first is a measure of the average degree of mixing of the two streams and is defined by the Standard Deviation Factor (SDF). This factor is expressed as:

$$SDF = \frac{\sigma}{\Delta T} = \sqrt{\frac{\Sigma\left(T_L - \bar{T}_{Exit}\right)^2}{n-1}} \Big/ \left(T_p - \bar{T}_{Exit}\right) \qquad \text{Eq. 10}$$

where T_L = local measured temperature, °F

T_p = primary air inlet temperature, °F

$\bar{T}_{Exit}$ = overall average measured temperature, °F

n = number of local temperatures recorded

$\Delta T = T_p - \bar{T}_{Exit}$

σ = Standard deviation

The second factor is the Maximum Temperature Factor (MTF), as defined by the difference of the maximum temperature recorded during a point and the overall average exit temperature divided by the primary air stream average temperature drop.

$$MTF = \frac{T_{max} - \bar{T}_{Exit}}{T_p - \bar{T}_{Exit}} \qquad \text{Eq. 11}$$

where T_{max} = Maximum Exit Temperature

In the case where a portion of the primary air stream passes through the mixing zone without being cooled (no mixing), the value of the MTF will be unity. For the case of ideal mixing, the maximum temperature equals the average temperature and the MTF is zero. The standard deviation factor (SDF) is also zero for the case of perfect mixing.

Table XIII represents test points of similar diluent to primary air stream momentum ratios and mass flow rates for the configurations tested, for varying downstream distance from diluent injection to duct height ratio (L/H). Table XIV represents test points of varying momentum ratios for an L/H ratio of about 2.0. The data on these tables were used to establish the correlation parameters described below.

A qualitative view of the mixing process for the configurations and conditions tested can be obtained from the temperature contour profiles presented in Figures 40 and 41. These contour maps show isotherms which were extrapolated from the temperature readings taken with the traversing thermocouple rake during testing. Figure 40 presents typical contour maps obtained during testing of the Configuration 1 mixing zone geometry. The three maps represent the temperature contours for axial distance downstream of the diluent holes to duct height ratios, L/H, of 0, 1.0 and 2.5. The diluent to primary stream momentum ratio, $(MV)_D/(MV)_p$ is approximately equal to unity for all three. Diluent holes were located along the tip wall of the duct.

Immediately downstream of the diluent holes (L/H = 0), hot spots are located at the tip section of the duct between the diluent holes. The diluent jets have penetrated to the hub of the duct and are flattened along its length. Further downstream, the cold jets appear to be reinforcing each other midway between diluent holes and are ballooning upwards, dividing the original two hot spots into three parts. At an L/H ratio of 2.5, the mixing process has progressed to the point where the hot spots have been completely divided by the diluent air. It should be noted that the hot spots are now axially in line with the diluent holes. It appears that this last pattern represents a state where the diluent flow has been completely turned in the direction of the primary air stream flow. Once formed, this pattern continues to persist downstream, with mixing occurring through convection between the hot and cold areas. At the larger L/H ratios investigated during the testing of Configuration 4, similar contour patterns were seen to persist to an L/H ratio of 4.03, as shown in Figure 41.

The Configuration 4 isotherm contour map also serves to illustrate how sporadic occurrences affect the maximum temperature factor. It is noted in Figure 41 that the diluent jet on the left-hand side of the duct did not penetrate as far as the other four. The net result is that the highest temperature observed in the lower contour map (L/H = 4.03) occurs at the bottom left-hand corner of the duct. The other peak temperatures are located at the tip section of the duct. It is also noted that these peak contours are shifted slightly to the left.

The mixing efficiencies of the configurations tested are shown as functions of mixing zone geometry and stream momentum ratio in Figures 42, 43 and 44. Figure 42 presents the MTF and SDF as a function of the distance from diluent injection to the duct height ratio, L/H, for a nominal primary to diluent stream momentum ratio of 1.0. Since these curves represent two different diluent slot spacing to duct height ratios, W/H, they can be used to determine the relationship between mixing efficiency and W/H. This was done for the single-sided entry configurations by picking off mean values of mixing efficiency from the curves at various L/H values and plotting them as shown in Figure 43.

Figure 44 represents the mixing efficiencies of the mixing zone geometries tested in both the mixing zone rig and the primary zone rig, as a function of the diluent to primary stream momentum ratios. Also imposed on the MTF curve is a typical point obtained during testing of a large advanced gas turbine combustor after its mixing geometry had been fully developed.

Figures 45 and 46 present the radial temperature profiles of the mixing zone geometries tested for a nominal L/H = 2.5, and a diluent to primary stream momentum ratio of approximately 1.0.

As can be seen in Figure 42, the MTF decreases rapidly over a short distance downstream of the diluent holes, and then tends to level out. The initial drop appears to be associated with the turbulent mixing of the normal jet streams in the vicinity of the diluent holes. Once the diluent stream assumes the same direction of flow as the primary air stream, mixing is through convective, rather than mass, heat transfer and occurs at a lower rate. Since the SDF is a measurement of the average degree of mixing, it does not illustrate the persistence of hot streaks through the mixing zone as well as the MTF does. It appears that double-sided entry of the diluent air offers a greater potential for efficient mixing, and should be used where practical in combustor designs. The similarity of the curves for Configurations 1 and 4 indicates that the mixing efficiency is not significantly changed by scaling.

Mixing efficiency is also a strong function of the diluent to primary stream momentum ratios, as shown in Figure 44. All of the mixing geometries tested appear to fall on the same general curve. However, the mixing efficiency of the fully developed combustor (shown on the upper curve of Figure 44) was far superior to that of any of the geometries tested in the mixing zone rig. The diluent hole pattern for this combustor was for single-sided diluent injection with a slot spacing to annular height ratio, W/H, of less than 1.0.

The effect of W/H on mixing efficiency is shown in Figure 43. For the mixing geometries tested, it is evident that closer spacing between diluent holes yields better average mixing, especially at large distances downstream from the holes. The results of the large-scale combustor development program, which incorporated a W/H geometry less than 1.0, indicate that superior mixing can be achieved through close spacing of the diluent slots. It should also be noted that the mixing zone length to annular height ratio of this combustor was approximately 1.0.

It can be concluded that the best mixing efficiencies can be achieved with minimum spacing between diluent holes and double-sided injection where feasible. The mixing zone, when coupled to the primary combustion zone, should have the longest mixing length and highest diluent to primary air stream momentum ratio which are compatible with the basic combustor airflow distribution and envelope limitations.

4.0 FUEL PATTERNIZATION RIG TESTS

Cold flow rig tests were conducted to evaluate the fuel distribution of the fuel introduction systems selected for investigation in the primary zone rig tests. Fuel patternization at the exit plane of the fuel introduction systems was investigated as a function of the fuel feed system and the fuel and air velocity in the fuel introduction system. Tests covered a simulated range of the engine operating fuel introduction system fuel-air ratios.

Testing did not simulate the effect of vaporization of fuel at engine operating temperatures. The final analysis of the fuel feed and introduction systems developed during this series of tests was made under actual operating conditions in the primary zone rig evaluation phase of this program.

4.1 TEST PROCEDURE

Tests were conducted on the fuel patternization rig shown in Figures 47 and 48. The fuel introduction system to be tested was placed at the center of the rig and the air supply and fuel feed lines were attached. The rig was divided into eight pie-shaped compartments in which the fuel exiting from the fuel introduction system was collected. A port at the bottom of each compartment allowed the fuel to be drained into individual graduated flasks where it was measured.

Airflows within the fuel introduction systems were varied between 50 and 110 percent of rated airflow, with an inlet temperature of approximately 80°F and with atmospheric discharge. Emphasis was on the 100 percent airflow regime. Testing of the atomizer used for the primary zone configuration 3 rig test was conducted in still air.

Fuel flows were varied between 10 and 231 lb/hr, with emphasis on the lower (10-100 lb/hr) fuel flow range. The design fuel flows for the primary zone rig tests at 5 and 16 atmospheres pressure level are 65 and 208 lb/hr, respectively. Normal heptane was used as a liquid medium to correspond with an existing test stand set-up. The use of this fluid medium did not compromise the test results as density differences between heptane and the JP series of fuels were accounted for. Viscosity and vapor pressure differences have a negligible effect on patternization at the conditions tested.

Tests were conducted by setting a prescribed fuel and airflow to the fuel introduction system. After allowing the system to stabilize, the eight fuel ports were simultaneously switched to the graduated flasks where the individual port fuel flows were collected and measured. The total fuel flow and inlet pressure to the system were also recorded, as were the airflow and inlet air temperature and pressure.

4.2 TEST EVALUATION

Three fuel feed systems were evaluated for the annular vaporizer fuel introduction system of the Configuration 1 primary zone rig. The modifications of these fuel feed systems are shown in Figure 49. Build 1 consisted of a single point tangential fuel feed tube with an inside diameter of 0.125 inch. The fuel patternization of this system is shown in Figure 50. The ratio of the individual port flow to the ideal average port flow, expressed as the percentage of variance from the mean, is compared to the circumferential location of the port in this and subsequent graphs. It is evident that a severe maldistribution of fuel results with this system. Build 2 was an attempt to improve the fuel patternization of the system by increasing the fuel velocity at the point of injection into the annular vaporizer. The fuel feed tube was restricted at the exit plane to a 0.060 inch diameter. The fuel distribution improved slightly with this system, as is shown in Figure 51. In an attempt to further improve the fuel patternization, the airflow passage area of the annular vaporizer was increased in Build 3. This further increased the ratio between the fuel injection and local airflow velocities. The test results of this system are shown in Figure 52. As indicated the increased fuel injection velocity (momentum) carried the fuel completely around the vaporizer annulus and helped to improve the fuel distribution. However, further improvement in fuel patternization was required, and it was obvious that this could not be accomplished practically in this case with single point tangential feed. Substantial peak flows which are a function of the fuel-air velocity ratio are inherent to the system.

Single point axial fuel feed at the centerline of the annular vaporizer was investigated in Build 4. The fuel patternization of this system is presented for varying fuel and airflows in Figures 53 and 54 respectively. The maldistribution is primarily a function of the airflow distribution arising from the annular vaporizer inlet geometry. Proper centerbody inlet geometry coupled with either a single axial tube or duplex atomizer fuel feed system should have superior fuel distribution.

Build 5 of the fuel feed system to the annular vaporizer evaluated the patternization of a multipoint radial fuel injection system. An annular ring manifold with eight 0.020-inch-diameter, equally spaced, drilled holes was inserted in the annular vaporizer as shown in Figure 49. The construction of this ring is illustrated in Figure 55. The manifold was fed by a single tangential fuel feed tube. The fuel patternization of this system over a wide range of fuel and airflow rates was superior to any of the other systems tested, as shown in Figures 56 through 58. Subsequent testing of this fuel feed system on the primary zone rig indicates that the hole size tolerance is very critical in this design. A multipoint tangential fuel feed system, although not tested, has a good potential for further improving fuel patternization in an annular vaporizer fuel introduction system.

Two fuel feed systems were evaluated for the mushroom vaporizer fuel introduction system of the Configuration 2 primary zone rig. The first fuel feed system investigated used a single tangential fuel feed tube, as shown

in Figure 59. The results of the test on this system are presented in Figure 60. The maldistribution of fuel is similar to that obtained with the single point tangential fuel feed system tested with the annular vaporizer, and is a function of the fuel and air velocity ratio. Although this system has proved to be very effective in larger engine designs where many mushroom vaporizers were used, it is not acceptable for this (single vaporizer) application. In an attempt to improve the fuel patternization, a single point axial fuel feed was used in Build 2. The exit of the 0.125 inch inside diameter fuel tube was positioned at the inlet to the vaporizer tube as shown in Figure 59. Fuel patternization was improved at the high fuel flows but not at the lower flows. Test results are presented in Figure 61. The fuel feed tube was moved close to the vaporizer dome in the third build of this system, such that the fuel would impinge upon it. The fuel patternization obtained with this system is presented in Figure 62.

The fuel impingement velocity on the vaporizer dome was increased in Build 4 by locally reducing the exit diameter of the fuel feed tube from 0.125 inch to 0.040 inch, as shown in Figure 59. Improvement in the fuel patternization was obtained for all but the lowest fuel flow tested, as indicated in Figure 63.

Since the fuel patternization tests were conducted at ambient temperature, the effect of vaporization on the fuel distribution was not established. Mixing of the fuel and air in the primary zone due to the recirculation patterns set up by the introduction of primary air through the headplate is also unknown. Subsequent primary zone rig testing of the Build 4 fuel feed system in the mushroom vaporizer proved that significant fuel maldistributions in single vaporizer combustors persist through the primary zone as temperature gradients. Further development is required to establish better fuel feed systems for this application.

Testing of the simplex atomizer nozzle used for the primary zone Configuration 3 rig tests was conducted in still air to establish spray cone characteristics and fuel patternization. The fuel patternization test results are presented in Figure 64. Maximum deviations in port fuel flows occurred at the lower atomizer fuel flows. Cone spray patterns for increasing atomizer fuel flows are presented in Figures 65 through 67 for reference purposes. The spray cone collapsed in still air at a fuel flow rate of approximately 15 lb/hr, using normal heptane.

5.0 PRIMARY ZONE COMBUSTION RIG TESTS

Screening tests were conducted on three primary zone headplate configurations to evaluate their performance over a simulated engine operating range of fuel-air ratios. Initial screening tests were conducted at a nominal 5 atmospheres pressure level. The primary zone configuration which exhibited the most favorable characteristics for application in a small gas turbine engine was then tested at a 16 atmospheres pressure level, as a final evaluation of the system. Each of the primary zone configurations was evaluated on the basis of the following performance characteristics:

1. Combustion efficiency
2. Pressure drop
3. Circumferential exit temperature distribution
4. Liner cooling effectiveness
5. Coking characteristics
6. Flame stability
7. Ease of ignition
8. Multifuel capability
9. Component durability
10. Fuel system complexity

Approximately 85 hours of testing were completed, including 1.0 hour of rig burning time at a 16 atmospheres pressure level and 55.6 hours at 5 atmospheres.

5.1 TEST HARDWARE

The three primary zone configurations selected for initial test evaluation (See Section 1.0 - Subsystem Concept Studies and Selection) were:

1. Annular Combustor - Annular Vaporizer Configuration --- Figure 68
2. Can Combustor - - - Mushroom Vaporizer Configuration --- Figure 69
3. Can Combustor - - - Educer Atomizer Configuration --- Figure 70

A fourth primary zone configuration was also tested as an offspring of the initial test results:

4. Can Combustor - - - Annular Vaporizer Configuration --- Figure 71

All four are end-mounted combustor designs and incorporate transpirationally cooled liners.

The specific subsystems evaluated during the primary zone system tests were:

1. Annular Vaporizer Headplate Configuration
2. Mushroom Vaporizer Headplate Configuration
3. Educer - Atomizer Headplate Configuration
4. Transpirationally Cooled Outer Liner
5. Transpirationally Cooled Conical Inner Liner
6. Transpirationally Cooled Dome Inner Liner

The headplates and associated hardware were made from Hastelloy X material. Transpiration liners were fabricated from .030-inch-thick N155 alloy porous material. This woven sheet material was formed into the desired cone shape and then TIG welded along a helical seam. The final contour was achieved by conventional hydroforming.

Single piece construction of these liner sections would be desirable, thereby eliminating the weld along the length of the combustor which could be detrimental to the cooling effectiveness in that area. The development of single piece construction appears feasible by producing the basic material on a shaped mandril that duplicates the desired configuration. The development of this fabrication method was beyond the scope of this program but is recommended for future investigation. The method of welding might also be improved to minimize the weld bead and therefore the cooling problem. Techniques such as Electron Beam welding could be employed.

5.2 TEST INSTALLATION AND EQUIPMENT

During testing at 5 atmospheres pressure level, each of the primary zone configurations was mounted in a 10-inch-inside-diameter cross-section duct, as shown in Figure 72. This test setup allowed independent adjustment of the primary air stream inlet pressure, temperature and flow rate, from that of the diluent and cooling air. This provision effectively isolated the primary zone and permitted imposition of a wide range of inlet operating conditions without resorting to metering area modifications to both the primary and diluent air systems, as would be required if the two systems were fed from a common supply.

Another advantage of the split air streams was to permit the use of excess diluent air. This was required to reduce the temperature of the products of combustion to a level appropriate to modest cost temperature instrumentation and test equipment downstream of the primary zone.

Cooling air to the inner liner was fed through four tubes from the outer liner and diluent air plenum, as shown in Figure 72. Drilled holes along the axis of the tube provided film cooling of these tubes. Outer and inner liner cooling air temperatures were monitored separately.

The low pressure test stand installation of the cross-section duct is shown in Figure 73. A JP-4 fired preheater was used to raise the primary air to a desired inlet temperature. This preheated air was first passed through a baffled mixing duct to assure uniform primary inlet conditions. A back pressure valve was used downstream of the primary zone rig to vary the operating pressure level.

The air and fuel supply systems are shown schematically in Figure 74. ASME standard air metering orifices were used to determine the primary and diluent airflows. Calibrated fuel metering orifices and a flow-rotometer were used to measure fuel flows.

Testing of the selected primary zone configuration at the 16 atmospheres pressure level was conducted in a 15-inch-inside-diameter pressure vessel. The low pressure test equipment ducting, with the primary zone rig and associated instrumentation, was mounted in the pressure vessel as shown in Figure 75. A single air supply was used for this rig. The primary and diluent airflow split was maintained by the use of an orifice in series with the primary airflow. This orifice provided the higher back pressure in the diluent air stream required to overdilute the primary zone exhaust gases to a temperature level consistent with downstream test equipment duct limitations. A back pressure orifice and vernier valve were used to vary the operating pressure level within the vessel. A schematic of the air

and fuel supply systems for this test rig is presented in Figure 76. Air was supplied from a 1700-psi bottled air supply. The bottles were supplemented by compressors during blowdown. Total blowdown time was approximately one hour. An automatic pressure reducer maintained the required rig inlet pressure as the bottled air supply pressure dropped. Fuel flows were measured before the high pressure pumps, allowing for the use of the same low pressure flow-rotometers used during the 5 atmospheres tests.

5.3 TEST INSTRUMENTATION

A schematic of the instrumentation used to evaluate the performance of the primary zone configurations is shown in Figure 77.

Primary zone inlet air and exhaust gas temperatures were recorded using bare-wire chromel-alumel thermocouples and a Brown recorder. The exhaust temperature instrumentation section used to evaluate the combustion efficiencies of the primary zone rigs is shown in Figure 78. Combustion chamber exhaust gases, after passing through a mixing plenum, were accelerated through the 2-inch-diameter passage to minimize temperature errors due to thermocouple radiation losses to adjacent walls. The wall temperature of this duct was monitored to facilitate radiation error calculations. Iron-constantan bare-wire thermocouples were used to measure the effluent and liner cooling air temperatures.

During the extended evaluation phase of the program, 32 platinum - platinum 10% rhodium bare-wire thermocouples were installed in the inner liner support housing, as shown in Figure 79, to facilitate evaluation of the primary zone circumferential exit temperature distributions.

Temperature instrumentation to evaluate metal operating temperatures included shielded and unshielded thermocouples on the headplates, vaporizer components, and transpirationally cooled liners. A typical liner metal temperature thermocouple installation is shown in Figure 80. These thermocouples were attached to the "cold" side of the liners. Temperature sensitive paints proved to be relatively unsuccessful in evaluating liner temperature distributions.

Rig pressures were obtained through the use of mercury manometer banks and Wallace and Tiernan gauges. Where manometer banks were used, photographs were taken to establish instantaneous rig pressure relationships.

5.4 TEST PROCEDURE

Sufficient cold flow checks were initially conducted to establish airflow distributions within each of the rigs tested. Ignition of primary zone combustion was accomplished with the use of a standard, gas turbine, high energy (2 joules) igniter. No primer was used. Ignition was initiated at approximately 75% of the design-point primary air velocity at a 4 - 5 atmospheres pressure level (about 0.18 lb/sec primary airflow) at 700°F preheat. After ignition, the primary airflow was increased to achieve rated primary inlet Mach number at 5 atmospheres. For testing at 16 atmospheres pressure level, a stepwise increment of the fuel flow, airflow and back

pressure was required. A primary zone fuel-air ratio between 0.035 and 0.050, with 700°F preheat, was found to be sufficient during this process.

Primary zone performance was evaluated at a steady state condition of primary air, diluent air and fuel flows. A sufficient number of primary zone fuel-air ratios was run to establish the combustor performance characteristics from above the design point, down to lean blowout. Off-design performance was evaluated by running fuel-air curves for various primary air inlet temperatures while maintaining the rated inlet Mach number. Both JP-4 and JP-5 fuels were used.

Initial testing of all three primary zone configurations was conducted at a 5 atmospheres pressure level. The fuel introduction systems developed during testing of fuel patternization rigs were used. Simulated design primary inlet conditions of temperature, velocity and Mach number were maintained throughout this series of tests. Evaluation of the primary zone exit temperature distribution was not conducted at this point.

Further evaluation of the three primary zones at off-design conditions was performed before the final selection of the configuration to be tested at 16 atmospheres was made. In preparation for this series of tests, modifications were made to the fuel introduction systems where deemed necessary. Platinum - platinum 10% rhodium thermocouples were attached at the exit plane of the primary zone to evaluate circumferential exit temperature distributions. The diluent hole pattern in the outer liner was also modified to improve diluent mixing. Additional headplate instrumentation was installed to establish operating metal temperatures.

5.5 TEST EVALUATION

A detailed description of each of the primary zone configurations and modifications tested will enhance the evaluation of the resulting data. This description is also presented in tabular form in Table XV.

Primary zone Configuration 1 is an end-mounted annular combustor design as shown in Figure 68. The specific components of this configuration are an annular vaporizer headplate, a conically shaped, transpirationally cooled inner liner and a transpirationally cooled outer liner. A photograph showing these components in an exploded view is given in Figure 81. The outer liner is common to all of the primary zone configurations tested. The first build of this configuration incorporated the eight-point radial fuel feed system developed during fuel patternization rig tests. This system incorporated a machined ring manifold with eight .020-inch radially drilled holes. This ring was brazed to the inside of the headplate annulus as shown on the bottom part of Figure 68. Fuel feed to the internal manifold was from a single inlet tube. Post-test inspection of this system indicated that leaks had developed between the internal manifold and the side wall of the vaporizer. In preparation for the extended evaluation testing of this configuration, the fuel feed system was changed to an external fuel manifold, as shown on the upper part of Figure 68. As an experimental expedient, the cover plate for this manifold was brazed in place. This second build also included a four-point axial fuel feed system which consisted

of four equal lengths of stainless steel tubing brazed to the upstream face of the vaporizer (also shown in Figure 68). These tubes were fed from a common supply. During the initiation of testing for Build 2, a malfunction in the preheater system resulted in a primary inlet temperature in excess of the liquidus of the braze holding the external fuel manifold cover. As a result, most of the testing of this build was conducted with the use of the four-point axial fuel feed system. Post-test inspection showed that the braze from the cover plate had been deposited, in part, on the inner liner. Damage to the liner was local and consisted of residues from the braze clogging the porous material. This is shown in Figure 82. This damage was minimal and did not hinder testing.

The third build of this configuration incorporated a welded cover plate on the external fuel manifold. All parts had been ultransonically cleaned and reinstrumented prior to Build 3 testing. Additional headplate temperature instrumentation and a thermocouple in the area of braze deposit on the inner liner were also included. In preparation for evaluation of the circumferential exit temperature distribution, a new diluent hole pattern was incorporated into the outer liner. This change was a result of test evaluation of prior primary zone and mixing zone test data. The revised diluent slot geometry is shown in the photograph of Figure 83. The eight existing slots were halved in length by butt-welding inserts of transpiration material. An additional eight slots were then eloxed into the liner to produce 16 uniform, equally spaced slots. As mentioned previously, the outer liner was common to all primary zone configurations, and was used for all of the tests.

The Configuration 2 primary zone was an end-mounted can combustor design. The main components, shown in Figure 69, are the mushroom vaporizer headplate with axial fuel feed system and a transpirationally cooled, dome shaped, inner liner. The hardware associated with Builds 1 and 2 of this configuration were the same except for additional headplate instrumentation and the revised diluent hole pattern which were included in Build 2.

Primary zone Configuration 3 was an end-mounted can design, as shown in Figure 70. This design used an educer-atomizer fuel feed system and the dome shaped, transpirationally cooled liner. Build 2 differed from the original in that the headplate was rotated 180° with respect to the atomizer nozzle. This was an attempt to trace a high metal temperature gradient on the educer recorded during Build 1 testing. Additional headplate instrumentation and the revised diluent hole pattern in the outer liner were included.

Primary zone Configuration 4 was a hybrid of the Configuration 1, Build 3, headplate and the dome shaped inner liner of the second and third configurations. This combination was selected for evaluation on the basis of the superior performance characteristics demonstrated by these components. This configuration facilitated the evaluation of the annular vaporizer headplate incorporated in an end-mounted can combustion chamber design, as well as a comparison between annular and can combustion chamber performance characteristics. This configuration was also selected for testing at the 16 atmospheres pressure level. Prior to the testing in the high pressure facility, all parts were ultrasonically cleaned and reinstrumented.

Combustion efficiency was calculated by means of a total enthalpy balance of the form:

$$\text{Combustion efficiency, } \eta_b = \frac{H_{exit} - Hp - Hd}{W_f H_f} \times 100\% \qquad \text{Eq. 12}$$

where

H_{exit} is the total enthalpy of the exhaust gases based on the total rig airflow, the fuel-air ratio of the overall system, and the mean exhaust gas temperature; Btu/sec.

Hp is the total enthalpy of the preheated primary zone inlet air, based on primary airflow, preheater fuel-air ratio, and mean primary air rig inlet temperature, assuming 100% preheater combustion efficiency; Btu/sec.

Hd is the total enthalpy of the cold diluent inlet air, based on the diluent airflow (including liner cooling air) and the mean inlet temperature; Btu/sec.

W_f is the primary zone fuel flow rate; lb/sec.

H_f is the ideal effective heating value of the fuel, based on the mean exit gas temperature, and the lower heating value of a sample of the fuel used; Btu/lb.

The test data presented are not corrected for radiation losses from the exhaust gas thermocouples to their cooler surrounding walls. Analysis based on wall temperatures recorded during the extended evaluation phase of primary zone rig testing indicated a maximum error in calculated combustion efficiencies to be in the order of 1 percent. This error is less than the anticipated scatter in test data and its inclusion was not considered to be warranted. This facilitated comparison between the preliminary and extended evaluation test results without prejudicing the data. However, the results presented are slightly conservative.

The combustion efficiency characteristics for all of the configurations tested are presented in Figures 84 through 88. The combustion efficiency is related to the primary zone fuel-air ratio in these figures. The design goal characteristic curve is included for reference purposes.

The total pressure loss for each of the three headplate configurations is presented in Figures 89, 90 and 91. The data have been corrected to the design-point primary zone inlet air conditions, and the design goal is included for reference purposes.

Typical circumferential exit temperature distributions for the various configurations of the primary zones tested are presented in Figures 92 through 95. The ratio of the local temperature and the overall average exit temperature is related to the local circumferential location in these figures.

Temperatures were obtained from 32 platinum-platinum 10% rhodium thermocouples equally spaced around the exit plane of the primary zones. All of the data was obtained with the revised diluent hole pattern in the outer liner. The locations of the 16 diluent holes are indicated at the top of each figure for reference purposes. Blank areas indicate that a thermocouple has been lost at that location. In all cases, peak temperatures were measured behind the diluent air holes, with the passage between holes being cooler. This same phenomenon was noted during testing of the mixing zone rig. The severe point-to-point saw-tooth pattern is due, in part, to the overdilution of the exhaust gases with cold (less than 200°F) diluent air. This excess diluent air was required to prevent overtemperaturing downstream test equipment hardware and ducting. Another contributing factor to the saw-tooth pattern is the diluent hole pitch to annulus height ratio. Analysis of the mixing zone test data has shown that a smaller ratio would have resulted in better mixing characteristics. This is substantiated by post-test photographs of carbon deposit patterns on the inner liners. These patterns were also present in the mixing zone rigs and can be traced to soot produced by the preheater. The photograph shown in Figure 96 represents the diluent pattern of the original eight diluent holes. The photograph presented in Figure 97 represents the diluent pattern for the revised diluent hole configuration, which had twice as many holes, with one-half the pitch. For this case, the patterns appear to be slightly overlapped. A further reduction in the diluent hole pitch would produce a greater overlapping of these patterns.

Post-test photographs of the Configuration 2 and 3 headplate assemblies are shown in Figures 98 and 99 respectively. Post-test photographs of the primary zone Configuration 4, Build 1, hardware are presented in Figures 100 through 104.

5.6 DISCUSSION OF RESULTS

Table XVI is a comparative review of the major aspects of the four primary zone configurations. Valid comparisons can be made for the information obtained for primary zone Configurations 1, 2 and 3 and for Build 1 of primary zone Configuration 4. The information presented for these configurations represents the results of extensive testing under similar conditions on the same test facility. The information available for the primary zone Configuration 4, Build 2, represents limited test data obtained on a new facility, and is presented for reference purposes.

As shown in Figures 84 through 88, a high level of combustion efficiency at the design primary zone fuel-air ratio was demonstrated by all configurations during testing in the low pressure facility. Combustor performance with JP-5 fuel was indistinguishable from that with JP-4.

A comparison of the efficiency afforded by the four- and eight-point fuel feed systems tested on the annular vaporizer fuel introduction system is presented in Figure 85. As shown, the combustion efficiency was consistently 2 to 3 percent higher when the eight-point fuel feed system was used. This may be explained by the poor circumferential exit temperature distribution exhibited by the four-point fuel feed system at high fuel flow. The

maldistribution of fuel in the primary zone may have lead to incomplete combustion. Although the Configuration 2 primary zone also exhibited a poor circumferential exit temperature distribution (corresponding to a fuel introduction maldistribution), the volume of the primary zone of this configuration was approximately 19 percent greater. The correspondingly greater residence time associated with this can combustor configuration, as compared to that of the annular configuration, explains why the combustion efficiency was greater even though the fuel distribution was worse.

The combustion efficiency of the simplex atomizer-educer primary zone configuration at lean primary zone fuel-air ratios was the poorest of any of the configurations tested. A staged fuel feed system (duplex nozzle) is obviously required.

The combustion efficiency characteristic of the annular vaporizer-can combustor configuration was consistent with the design goal when tested on the low pressure test facility. The test data from both the low and high pressure test facilities are included in Figure 88 for comparative purposes. Testing on the high pressure facility was conducted at both the 5 and 16 atmospheres pressure level, to obtain direct comparison of both facility and pressure changes on the combustor performance. The open circles on Figure 88 represent the combustion efficiencies calculated from the data recorded on the low pressure test facility. The open squares are for comparable inlet pressures and airflows as recorded on the high pressure test facility. The closed squares are combustion efficiencies obtained at the 16 atmospheres pressure level.

The exceedingly high values for combustion efficiency obtained during the initial primary zone combustion tests on the high pressure facility were discounted for the following reasons:

1. Higher exhaust gas and liner temperatures were recorded during this series of tests than during subsequent testing at similar inlet conditions, indicating that the internal rig flow conditions did not correspond with those of the later tests.

2. Post-test inspection of the pressure vessel indicated that the bolts sealing the downstream flange had become loose during this initial series of tests.

Each of the above indicates that the high calculated efficiencies were a result of a leak of unknown magnitude in the diluent airflow passage.

The limited number of points which remain indicate that the combustion efficiency is not seriously affected by high pressures. The variations between the four points are in the same order of magnitude as those at constant pressure. The difference in the level of the two series of data points is believed to be primarily due to the change in test facilities.

The lean blowout characteristics of primary zone Configurations 1, 3 and 4 were consistent with the design goal of a primary zone fuel-air ratio of 0.013. The leanest operating condition obtained with the Configuration 2 design was a 0.022. Data are shown in Table XVI and Figures 84 through 88.

The combustor headplate pressure loss of all three headplate designs was equal to or less than the 3-percent design goal.

A comparison of the circumferential exit temperature distributions of the first three primary zone configurations is presented in Figure 92. As mentioned previously, the severe point-to-point saw-tooth pattern is due to the overdilution of the primary exhaust gases with cold diluent air, and the relatively wide pitch between diluent holes. However, the profiles presented in this figure are representative of the fuel patternization and mixing in the primary zone. Severe fuel and temperature maldistributions such as occurred in the Configuration 2 primary zone are evident. The profiles presented in this figure are, in general, representative of those obtained at other operating conditions of fuel flow and inlet temperatures. Changes in fuel flow rates did have a significant effect on the circumferential exit temperature distribution of primary zone Configuration 1 when the four-point axial fuel feed system was used. As shown in Figure 93, as the fuel flow increases, distinct temperature peaks become evident. Since low fuel flow points were run both before and after the high fuel flow points, and since the peaks occur only at the higher fuel flows, it is evident that the temperature peaks are a function of the fuel feed system. The peaks also line up with the fuel introduction points of the four-point system, except at the 225° location. Post-test flow checking of the four-point fuel feed system showed that the fuel feed tube at this location was clogged. It can be expected that with this passage open, the same trend would be noted, with four peaks developing. The circumferential exit temperature distribution of the eight-point fuel feed system in this configuration was uniform throughout the fuel flow range tested. Similar indications were seen for the eight-point system with the higher fuel flow rates associated with 16 atmospheres tests, as will be discussed later.

Further comparison of the exit temperature distribution of the first three primary zones is presented in Figure 94. The ratio of the maximum recorded temperature and the overall average temperature is given as a function of the primary zone fuel-air ratio in this figure. The maldistributions in temperatures noted in the four-point axial fuel feed system of primary zone Configuration 1 are clearly shown. It is evident that only the eight-point fuel feed system incorporated in primary zone Configuration 1 and the atomizer-educer fuel introduction system of Configuration 3 had generally flat maximum temperature profiles over the range of fuel flows tested.

The severe exit temperature maldistribution exhibited by the mushroom vaporizer fuel introduction system indicates that the axial fuel feed tube and exit orifice must be very precisely aligned with the axis of the mushroom vaporizer if an even fuel distribution is to be achieved. Alternately, other fuel feed systems could be incorporated in this design. Although this system has proved very effective in larger engine applications where many mushroom vaporizers (multipoint fuel introduction) were used, it is not acceptable for this (single vaporizer) application unless further modification to the fuel feed system is made.

The circumferential exit temperature distribution of primary zone Configuration 4 obtained on the high pressure facility is shown in Figure 95. A

post-test fuel feed orifice flow calibration on the eight-point fuel feed system is also presented on this curve as the ratio of the actual measured fuel flow and the ideal average fuel flow per hole. It is evident that the maldistribution of fuel at the lower fuel flows associated with the low pressure test was wiped out due to mixing with the primary air in the vaporizer and primary zone. At the higher fuel flows associated with the high pressure test, the fuel flow maldistribution was significant enough to override the mixing characteristics of the vaporizer and primary zone. A severe local peak in the exit temperature resulted. A similar occurrence was noted in the four-point fuel feed system at lower fuel flows. The solution of this problem consists of a more uniform circumferential fuel distribution in the annular vaporizer. Two straightforward methods for accomplishing this objective are delineated in the preliminary design section, and should be utilized in any development program derived from this technology.

No coking or durability problems were encountered during the testing of the primary zone rigs. Operating temperatures of the vaporizing components at high fuel flows were low.

Improvements in fuel distribution to the vaporizing components at lower fuel flows would substantially reduce their operating temperatures at lean operation. A severe temperature gradient was noted in the educer cone of primary zone Configuration 3. This gradient has been traced to eccentricities in the headplate components. No durability problems were encountered during primary zone testing of the vaporizer components.

Primary zone Configuration 3 required a higher energy igniter than the others. However, the position of the igniter for this design was not optimized. Also, improving the fuel spray quality through the use of a duplex nozzle would aid ignition.

Smoke emission tests conducted on the annular vaporizer-can combustion chamber of primary zone Configuration 4 indicated that the exhaust gases were smoke-free at both the 5 and 16 atmospheres pressure operating levels. A comparison of the smoke emission of this configuration and the others was not obtained.

The overall results of testing the various primary zone configurations indicate that the design parameters developed at Curtiss-Wright for large gas turbine engines can be applied to the design of primary zones for application in a high temperature rise, small gas turbine combustor. The annular vaporizer fuel introduction system has demonstrated the greatest potential for achieving a uniform fuel patternization in the primary zone, which is coincident with a uniform circumferential exit temperature. Further development of the fuel feed supply is required, however, to fully realize this potential. This headplate design has also demonstrated good combustor performance over a range of primary zone fuel-air ratios which are consistent with those of a 2300°F temperature rise combustor. A high degree of performance was demonstrated for both the end-mounted annular and can combustion chamber configurations. Further engine trade-off studies would be required to determine the desirability of the lower liner

cooling air requirements of a can configuration as opposed to the added complexity of routing the cooling air through the turbine section. The annular vaporizer headplate design is also applicable to a mid-mounted annular combustor. This may be accomplished by passing the main shaft through the center of an expanded annular vaporizer, and redesigned conical inner liner.

Due to overdilution of the combustion exhaust products at the exit plane of the primary zone, a true evaluation of the mixing zone was not obtained. Tests on a separate mixing zone rig and information obtained during testing of the primary zone rig indicate that superior mixing and a corresponding superior exit temperature distribution would be obtained by a further reduction in the distance between diluent holes.

A full evaluation of the transpirational liners used during this series of tests was not within the scope of this program. All of the liners were in very good condition after testing. The only damage noted was due to the local braze deposit on the conical inner liner sustained during testing Build 2 of primary zone Configuration 1. Even with this damage, the liner successfully completed 17-1/2 additional hours of hot testing. The data accumulated indicate that transpiration cooling of the liners offers excellent potential, particularly for application in small, high temperature rise combustors.

6.0 PRELIMINARY DESIGNS

Preliminary flight-weight engine designs have been conducted for both an annular and a can combustion chamber configuration based on the technology developed in this program. These combustion chamber designs, which are presented in Figures 105 and 106, are sized for a small gas turbine with an overall engine airflow of 2.0 lb/sec and a compressor pressure rise of 16 to 1. It has been assumed that engine turbine cooling airflow requirements amount to 28.5 percent of the total engine airflow. The design point airflow distribution for both preliminary combustor designs is presented in Table II. The target combustion chamber performance goals for these preliminary designs are given in Table XVII.

TABLE II. USAAVLABS HIGH TEMPERATURE COMBUSTOR AIRFLOW DISTRIBUTION

	(lb/sec)	(% W_{cc})	(% W_e)
Compressor Discharge	2.0		100
Air Bleed	.57		28.5
Combustor Flow	1.43	100	71.5
Headplate	.7698	53.83	38.49
- Vaporizer	.231	16.16	11.57
- Primary Air Cups	.5388	37.67	26.92
- Slots	.4988	34.87	24.92
- Cooling	.04	2.80	2.00
Balance Available for Liner Cooling and Dilution	.6602	46.17	33.01

Both designs are for end-mounted combustion chamber configurations and incorporate annular vaporizer fuel introduction system headplate designs and transpirationally cooled liners.

The two configurations (Figures 105 and 106) which are proposed as alternates provide for end-mounted installations of either a full annular or can type. The end-mounted annular combustor offers relatively simple routing of coolant air to the inner liner. The end-mounted can combustor has a smaller liner surface area than does the annular design, but requires routing of the inner liner cooling air through the turbine stators. The annular vaporizer fuel introduction system headplate design exhibited excellent performance characteristics during test evaluation in the primary zone rig. A high level of combustion efficiency over a wide range of fuel-air ratios, with both JP-4 and JP-5 fuels was demonstrated. Tests at 5 and

16 atmospheres pressure level indicate that the products of combustion are smoke free. This performance is due to the premixing of the fuel with primary air prior to its introduction to the primary combustion zone. The major portion of the primary air for combustion passes through eight primary air cups on the headplate and enters the primary zone as fan-shaped jets. These axial jets divide the primary zone into sectors and create a degree of coarseness in the fuel-air mixture within the primary zone that provides combustion stability over a wide operating range.

The annular vaporizer headplate design is easily adapted to either annular or can combustion chamber configurations, as shown in Figures 105 and 106. An annular vaporizer headplate could also be incorporated in a mid-mounted annular combustor if the engine design is such that the shaft can be passed through the center of a scaled up annular vaporizer.

A uniform fuel feed distribution in the annular vaporizer is essential for optimum combustor performance, since it relates directly to the circumferential exit distribution of the primary zone. A uniform fuel distribution in the vaporizer will also lower the vaporizer metal surface temperatures sufficiently to assure long operating life. Although the system exhibits excellent premixing characteristics, significant maldistribution in the fuel feed will result in high peak exit temperatures. The fuel feed system presented in the preliminary designs should yield a better fuel distribution in the annular vaporizer than was obtained during testing of the primary zone rig. Fuel is metered through a set of eight precalibrated orifice inserts, and fed into the annular vaporizer tangent to the outside wall. A varying area external manifold is used to maintain a relatively constant pressure gradient across all the orifices. The swirl imparted to the fuel by this system should distribute it evenly around the vaporizer annulus.

This program did not involve an extensive evaluation of transpiration cooling as applied to combustion chamber liners. However, the test data accumulated on the transpirationally cooled liners used during test evaluation of the primary zone rig were very favorable. Although further stringent testing is required to fully qualify this component with respect to liner operating temperatures and endurance characteristics, it has been included in the preliminary designs as being the best choice for the subject application. The prospect of a 50 to 65 percent saving in liner coolant requirements offered by this cooling technique is particularly significant in high temperature rise combustors, since it allows for a greater percentage of the engine airflow for diluent purposes to trim the combustor exit temperature profile.

Recent investigations of transpiration materials indicate that nichrome wire has superior oxidation resistance and higher temperature properties than does the N-155 wire used to form the liners tested in this program.

Manufacturing development is needed to optimize fabrication of the liners. Based on coordination with suppliers, and utilization of technology developed in filament winding of plastic structures, it appears that optimum properties would be obtained by winding the nichrome wire on a mandril, thus eliminating any welds. Two inner liners would probably be wound

simultaneously (back-to-back) and cut apart after the sintering process which bonds the wire mesh together.

The combustor envelopes formed by the liners in the preliminary designs are identical to those tested, and have proved to be sufficient to attain high combustor efficiency.

The inner liners are supported in both configurations through pins in the downstream fish-mouths, which allows for easy maintenance of the liners. The outer liner is welded to the headplate.

Single-sided diluent injection geometry was maintained in the preliminary design of the end-mounted can combustor to minimize the airflow to the inner liner, since it must be passed through the turbine stators. A large number of small diluent holes is provided in the outer liner to insure a uniform turbine inlet profile. Since a more direct routing of air to the inner liner is provided in the end-mounted annular combustor design, double-sided diluent injection can be used in this configuration.

Both of these designs will require testing at simulated engine operating conditions to evaluate their mixing efficiencies, as well as their resultant combustor exit radial temperature profile. As noted in Section 5.5, a complete evaluation of the mixing zone was not obtained during testing of the primary zone rig and the design combustor exit circumferential temperature distribution was not demonstrated. It is obvious that for the very high temperatures being considered this is an especially critical area and will require particular attention in any future development program.

The igniter used for the preliminary designs is a high energy (2 joules/second) surface gap spark plug. Its location is the same as that on the primary zone rig. This position provided good ignition characteristics during testing with preheated inlet air. Testing at simulated engine starting conditions will be required to qualify this ignition system.

CONCLUSIONS

Testing of the primary zone rigs, under Task II of this program, has demonstrated primary zone performance characteristics which are consistent with the objectives of this program. The annular vaporizer fuel introduction system has shown the greatest potential for achieving uniform fuel patternization to the primary zone and is compatible with both annular and can combustion chamber designs.

Test data accumulated on the transpirationally cooled liners indicate that this unique liner cooling technique offers excellent potential, particularly for application in small, high temperature combustors.

Further development testing will be required to qualify the preliminary designs which were derived from the technology developed in this program. In particular, qualifications of the transpiration liners and further development of the fuel feed and diluent introduction systems, to obtain uniform exit temperatures, are required.

RECOMMENDATIONS

Further development testing will be required in three specific areas to fully qualify the preliminary designs and technology derived during this program. These areas are the fuel feed system, the diluent air introduction method and the transpiration cooled combustor liners.

Testing of the multipoint tangential fuel feed system proposed in the preliminary designs will be required to evaluate and optimize this system. This testing should be directed toward obtaining a uniform fuel patternization with the minimum number of fuel introduction points and a maximum orifice size. Initial testing could be conducted on a cold flow rig, but final qualification should be conducted in a primary zone rig to evaluate fuel patternization as measured by the combustor circumferential exit temperature distribution.

At the same time the annular vaporizer operating tempertures could be evaluated, as well as fuel system contamination resistance.

Testing of the diluent air introduction designs proposed in the preliminary engine designs should be conducted to evaluate their mixing efficiencies. This testing should be conducted at design diluent air temperature and pressure drop to establish combustor circumferential and radial exit temperature distributions.

Further evaluation of transpiration cooled combustion chamber liners will be required to fully qualify this component. Testing should be conducted at simulated engine operating conditions of coolant temperature, coolant flow and pressure drop to obtain realistic transpiration metal operating temperature. Contamination, oxidation resistance and cyclic endurance testing of the transpiration liners at simulated operating conditions would also be desirable. Optimization of fabrication techniques for manufacturing transpiration liners without axial welds should also be undertaken. Investigations in this area would include winding and sintering techniques as well as alternate wire material compositions. Alternate perforating techniques such as photoetching or electric discharge machining should also be investigated.

End-Mounted Combustors

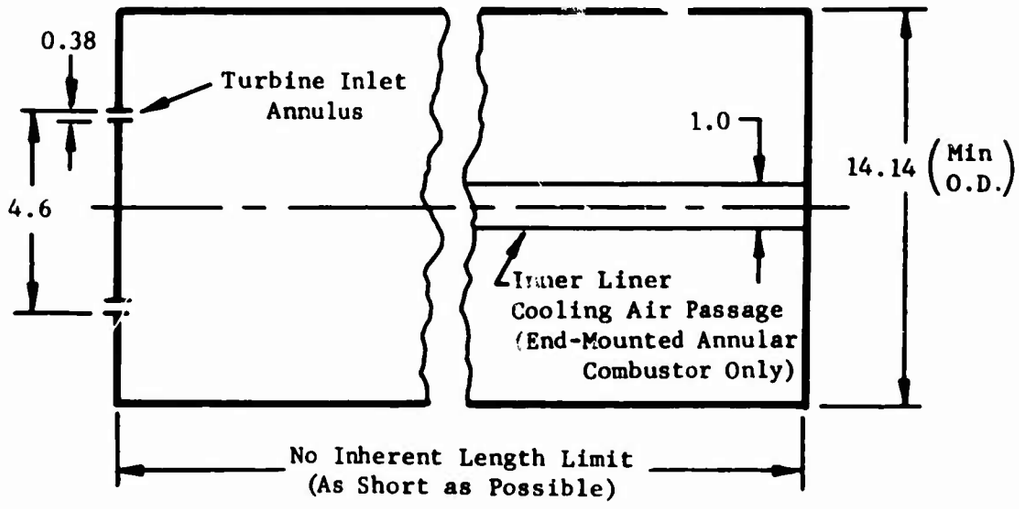

Combustor Between Compressor and Turbine

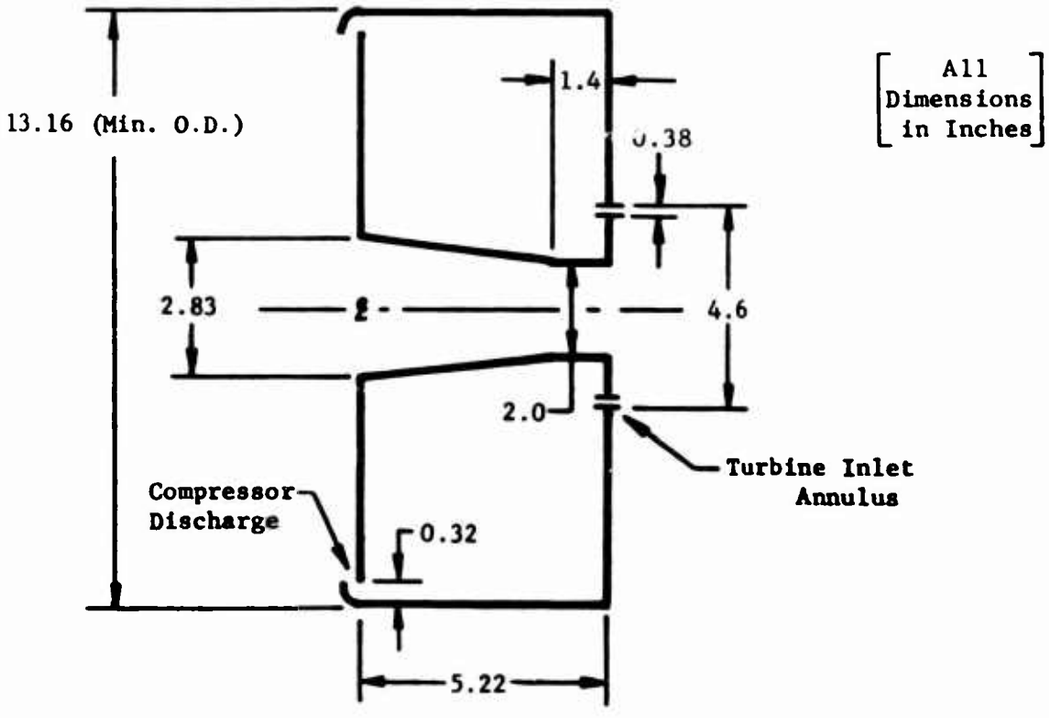

Figure 1. Engine Combustor Cross Section Envelope Restrictions.

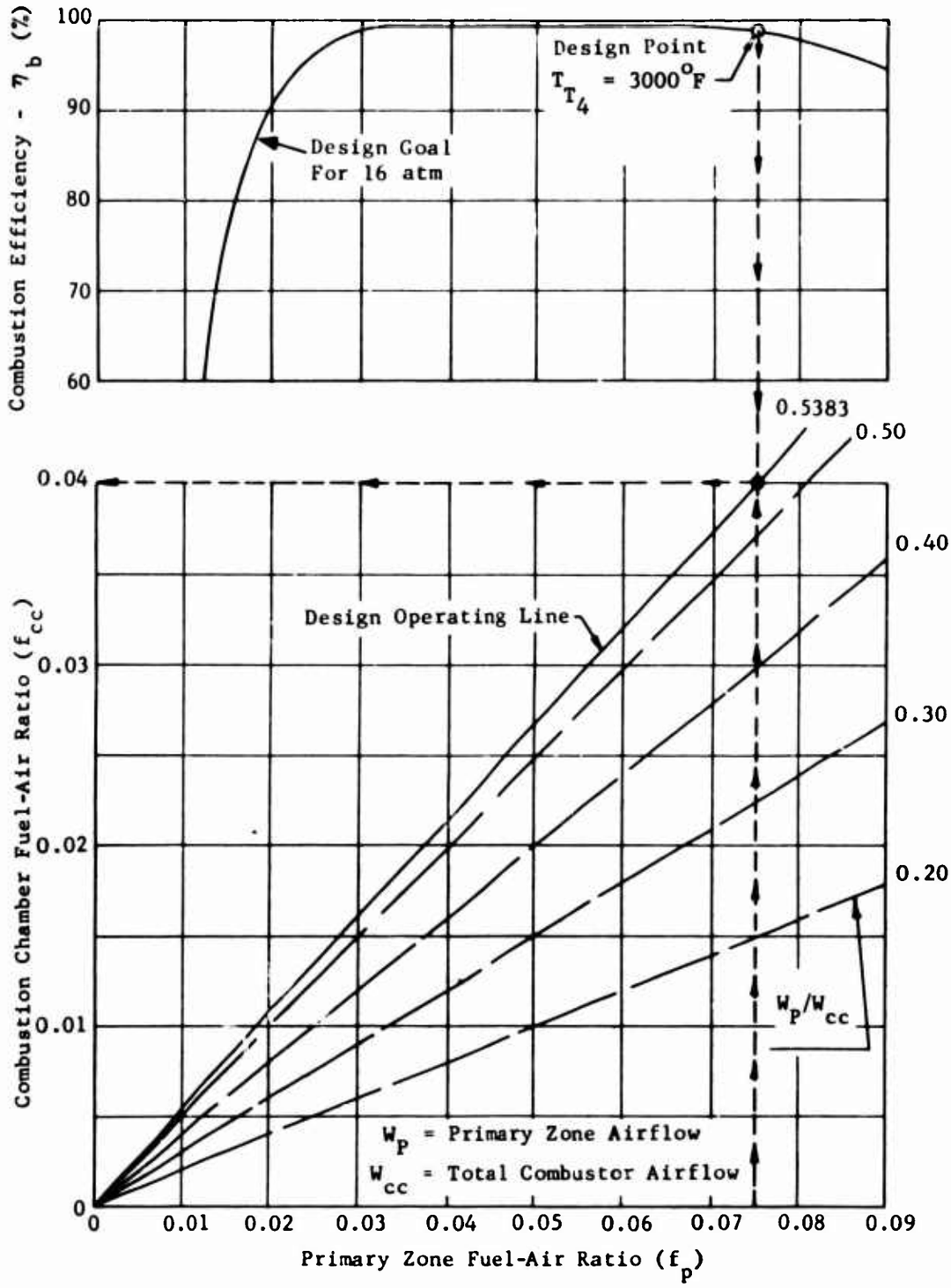

Figure 2. Design Goal Combustion Efficiency Characteristics and Fuel-Air Ratios.

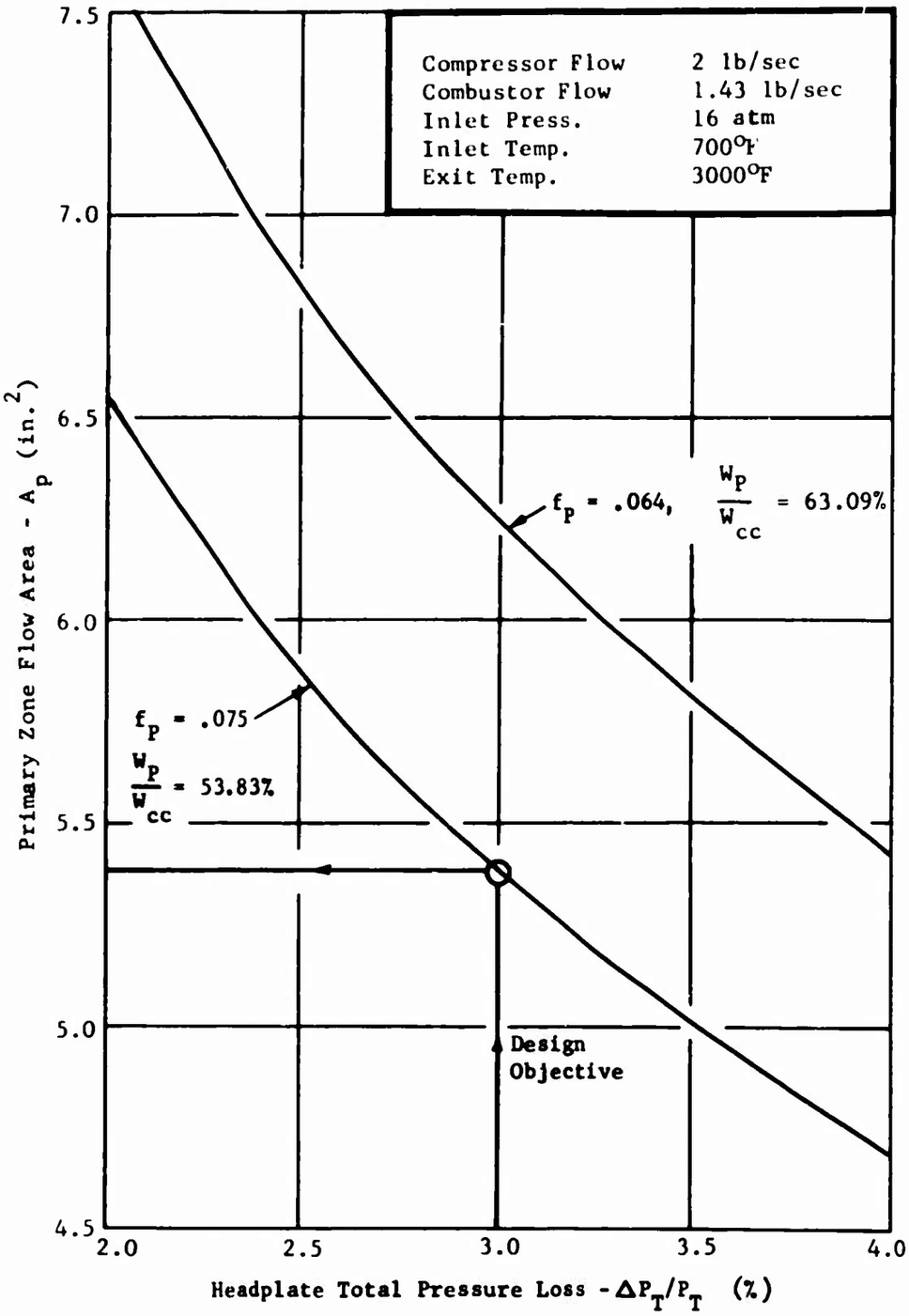

Figure 3. Primary Zone Flow Area as a Function of Headplate Total Pressure Loss.

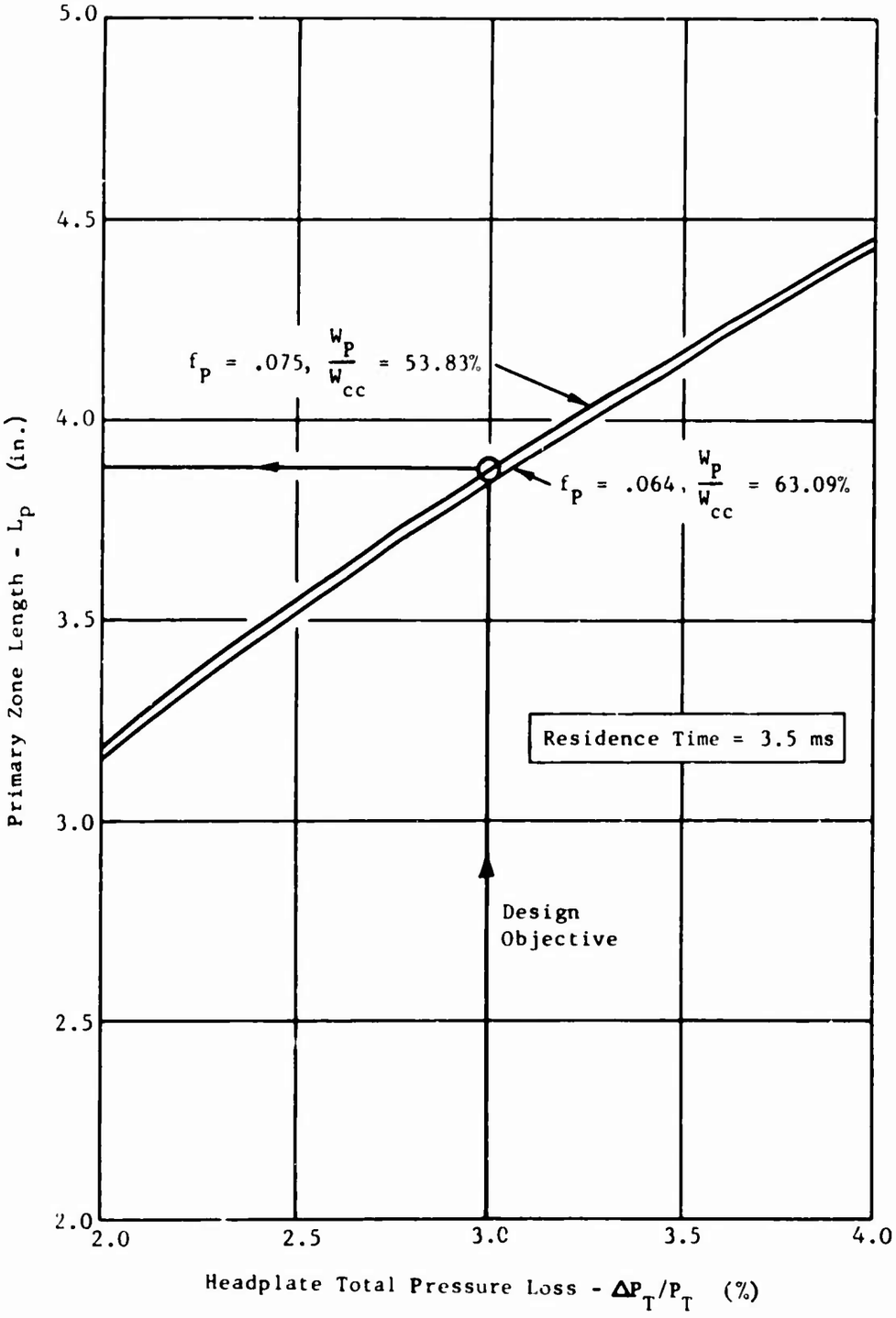

Figure 4. Primary Zone Length as a Function of Headplate Total Pressure Loss.

TABLE III. SUMMARY OF COMBUSTION CHAMBER CONFIGURATIONS CONSIDERED FOR SUBJECT APPLICATION

Combustor Design	Advantages	Disadvantages
Mid-Mounted Can with Transition Duct	1. Small number of fuel introduction points	1. Excessive liner surface area with prohibitive liner cooling air requirements 2. Complex transition duct
Mid-Mounted In-Line Annular Combustor	1. Simple engine air routing 2. Relatively short engine configuration	1. Large number of fuel introduction points required 2. Narrow combustion zone annuli
Reverse Flow Annular Combustor-Over-Turbine	1. Short engine configuration 2. Simple engine air routing	1. Large number of fuel introduction points required
End-Mounted Annular Combustor	1. Small liner surface area 2. Simple inner liner cooling air routing 3. Small number of fuel introduction points 4. Large combustion zone annuli	1. Complicated engine air ducting
End-Mounted Can-Annular Combustor	1. Minimum liner surface area 2. Single fuel introduction point 3. Large combustion zone annuli	1. Complicated inner liner cooling air routing 2. Complex engine air routing
Mid-Mounted Tangential Can	1. Short engine configuration	1. Excessive liner surface area with prohibitive liner cooling air requirements 2. Complex transition duct and scroll

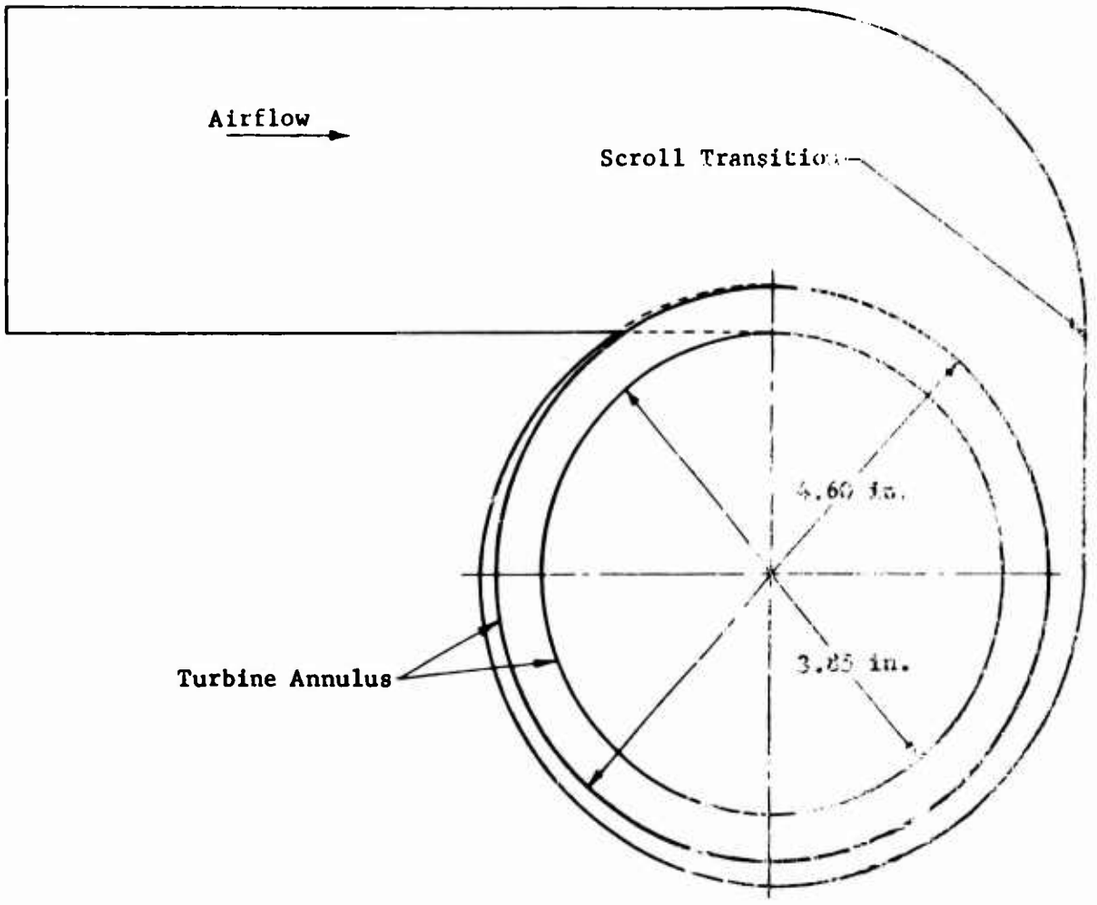

Figure 5. Mid-Mounted Tangential Can Combustor Envelope Schematic

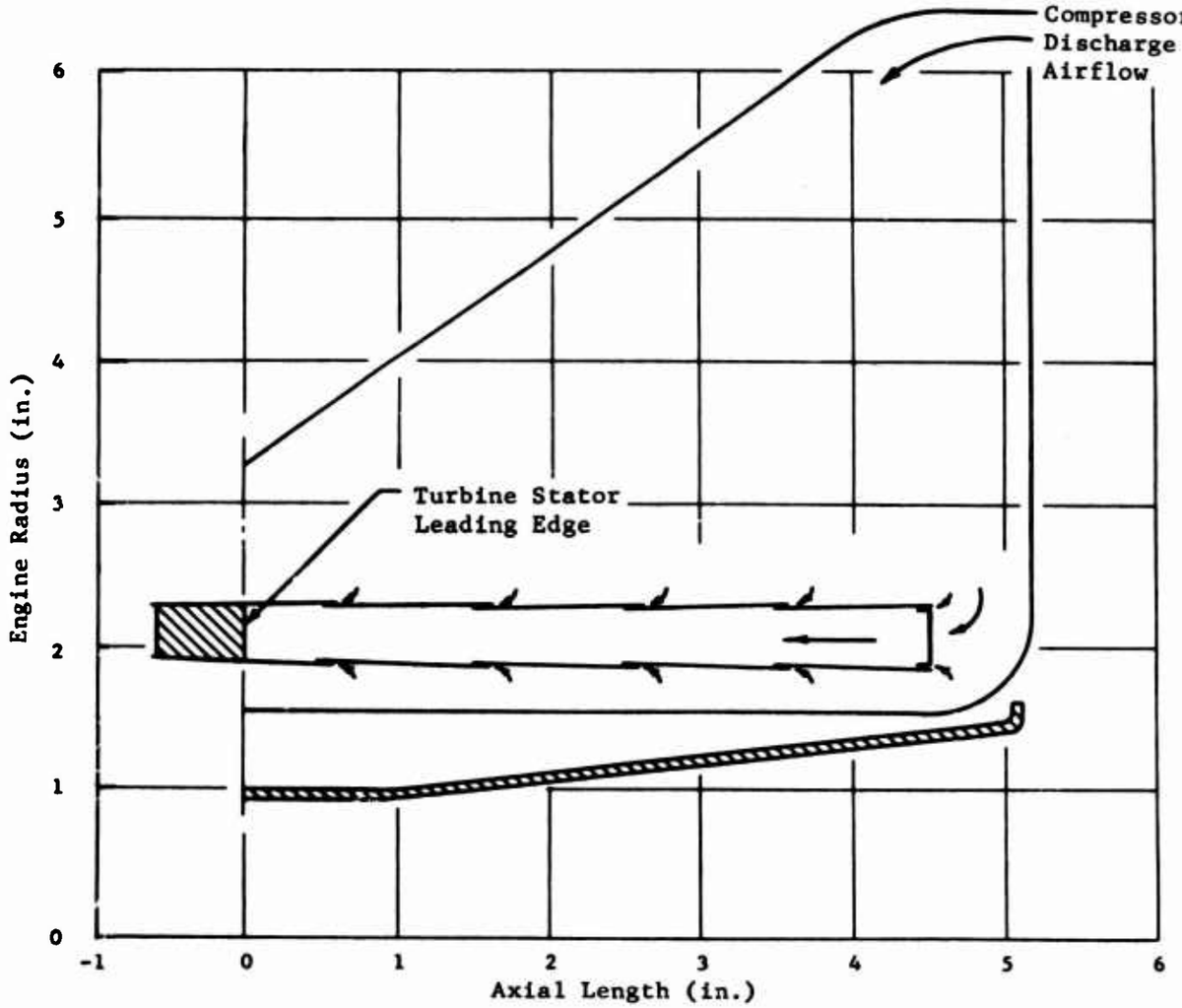

Figure 6. Mid-Mounted In-Line Annular Combustor Envelope Schematic.

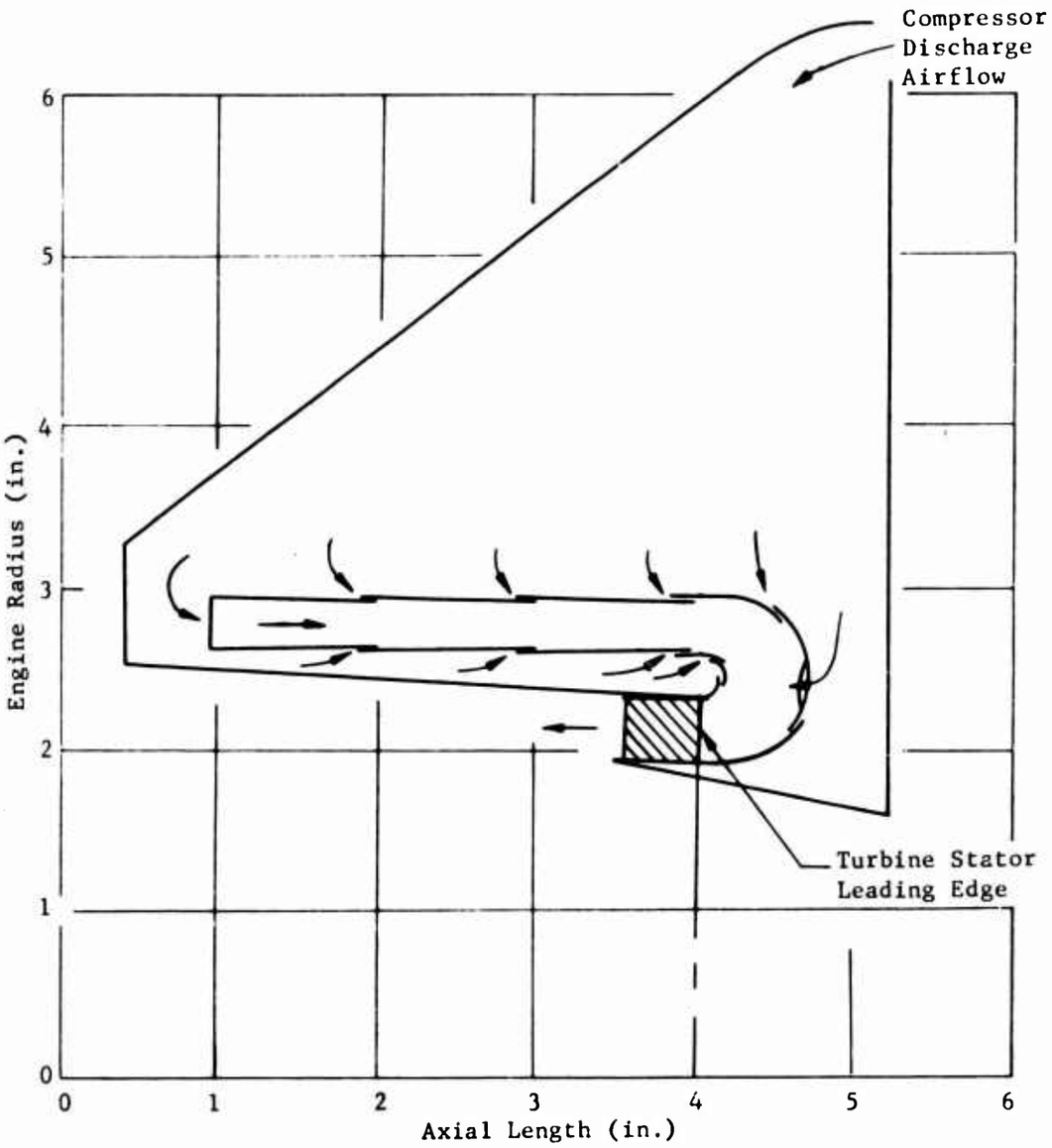

Figure 7. Mid-Mounted Reverse Flow Annular Combustor-Over-The-Turbine Envelope Schematic.

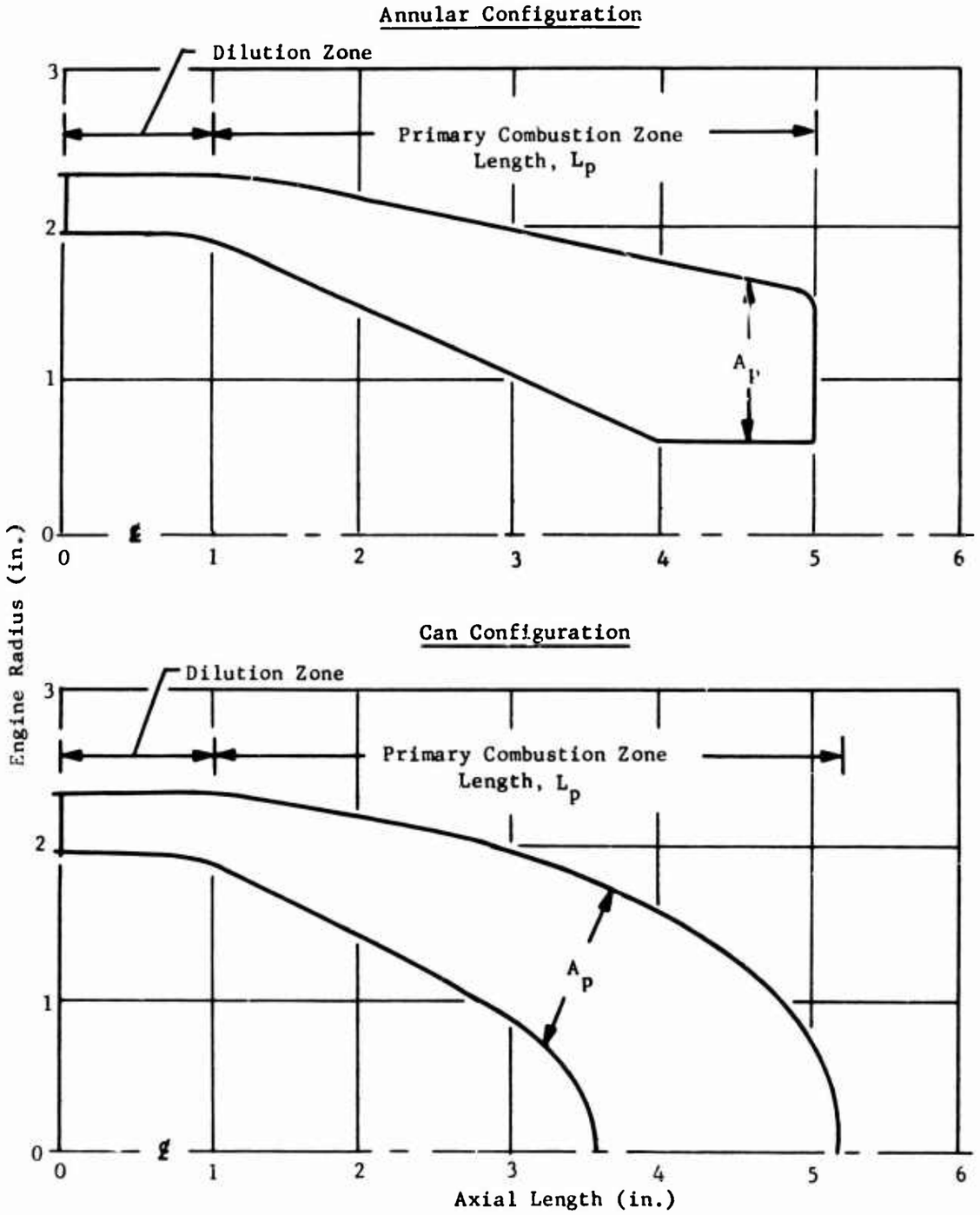

Figure 8. Schematic of Basic End-Mounted Combustor Envelopes.

Tangential Film Cooling

Splash Plate Film Cooling

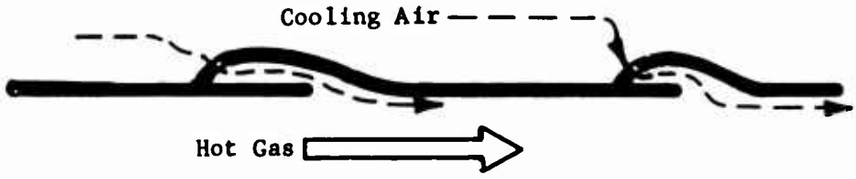

Transpiration Cooling

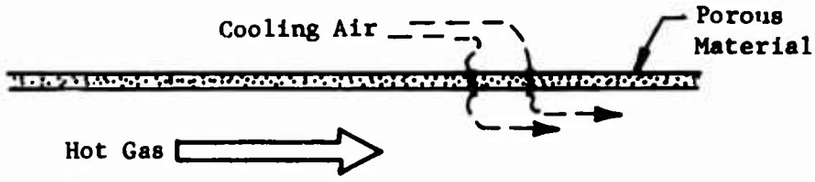

Regenerative Cooling

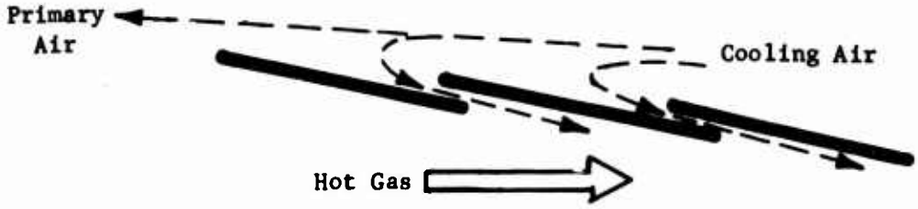

Impingement Cooling

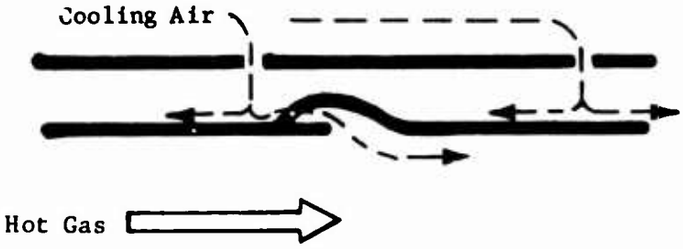

Figure 9. Liner Cooling Techniques Investigated During Subsystems Concept Studies.

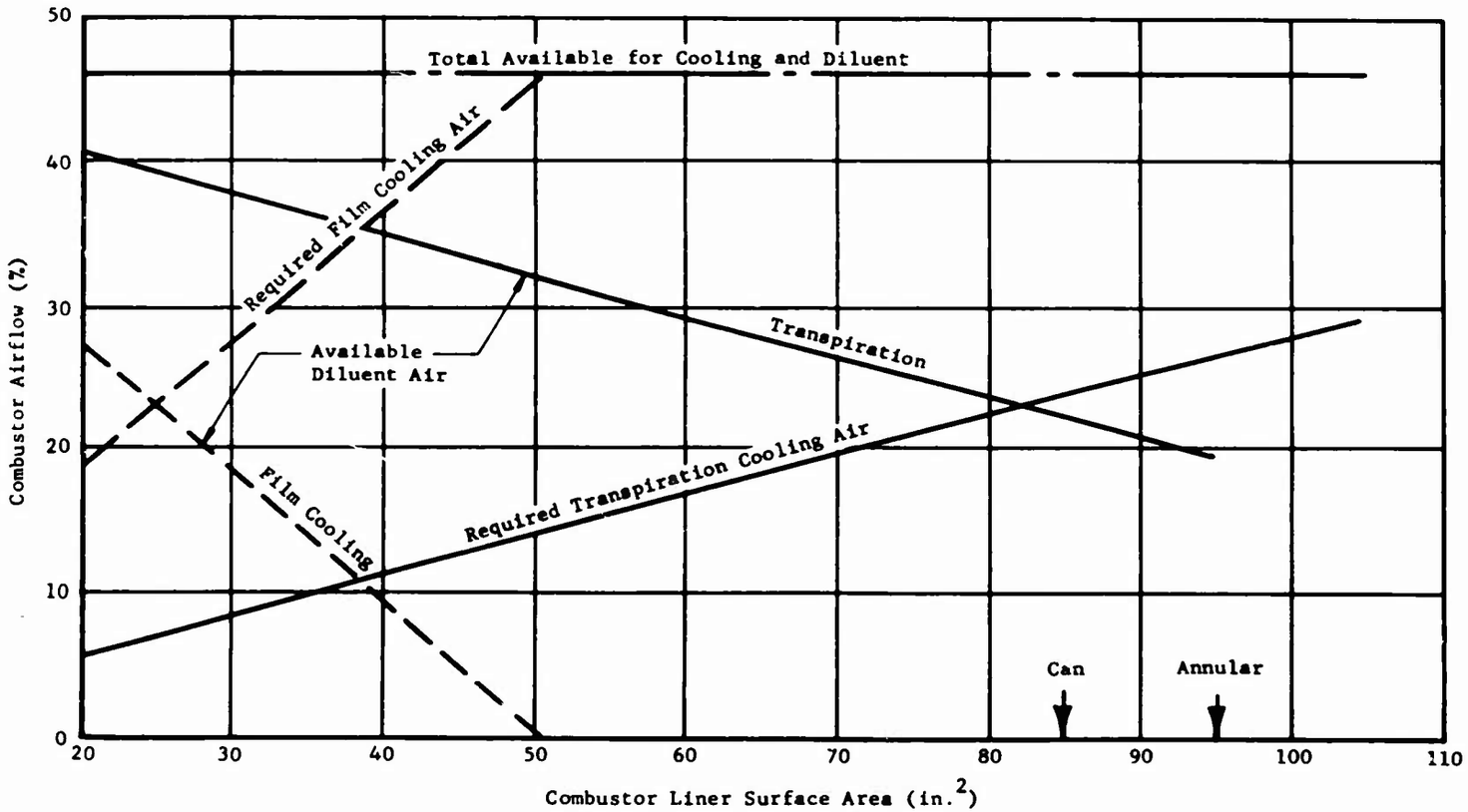

Figure 10. Preliminary Combustor Airflow Split for Transpiration and Film Cooled Liners.

TABLE IV. SUMMARY OF COMBUSTION CHAMBER LINER COOLING METHODS CONSIDERED FOR SUBJECT APPLICATION

Cooling Method	Applicable To This Program	Preliminary Liner Cooling Requirement	Considered In Exper. Program	Included in Later Parametric Study	Comments
a) Film Slots	X	.013 $\left(\frac{lb}{sec\ in^2}\right)$	X	X	2300°F Combustor Temp. at T_c = 700°F, T_w = 1600°F, 16 atm
b) Splash System	X		X	X	
c) Transpiration	X	.004	X	X	
d) Regenerative	X	<.007		X	Pressure drop higher than (a)
e) Impingement	X	<.007		X	Pressure drop higher than (a)
f) Coatings & Materials	X	<.007		X	Can be used with a, b, d, or e
g) Modified Transpiration					Proprietary - Not available to Curtiss-Wright
h) Partial Fuel Cooled					

TABLE V. SUMMARY OF FUEL INTRODUCTION SYSTEMS CONSIDERED FOR SUBJECT APPLICATION

Fuel Introduction Method	Advantages	Disadvantages
Mushroom Vaporizer	1. Low pressure fuel supply. 2. Carburates, pre-mixes and preheats fuel and air. 3. Low flame luminosity. 4. Smoke-free combustion. 5. Stable combustion over wide operating range. 6. Insensitive to fuel viscosity variation due to temperature changes.	1. Potential for excessive metal temperatures on vaporizer element. 2. Possible need for added fuel system component to assure ignition.
Annular Vaporizer	Same as for mushroom vaporizer plus: 1. Central annulus can be used for inner liner and turbine section cooling air route. 2. Engine shaft can be passed through center annulus.	Same as for mushroom vaporizer plus: 1. Heavier design than mushroom vaporizer.
Atomizer-Educer	1. Good atomization of fuel. 2. Educer action helps pre-mix and preheat fuel and air.	1. Potential for excessive metal temperatures on educer element. 2. Possible need for added fuel system component to assure ignition.
Simplex Atomizer	1. Good atomization of fuel. 2. Fuel introduction system not in high temperature environment.	1. Requires high pressure fuel system. 2. Poor low end performance. 3. Luminous flame. 4. Relatively smoky.

TABLE V - Continued

Fuel Introduction Method	Advantages	Disadvantages
Air Assist Atomizer	1. Good fuel atomization over wide operating range.	1. Requires high pressure air supply (extra components). 2. Air pumping components reduce engine output.
Opposing Duplex Atomizers	1. Good fuel atomization over wide operating range.	1. Complex design. 2. Luminous flame. 3. Relatively high smoke output.
Fuel Slinger	1. Good fuel atomization over wide operating range. 2. Good circumferential fuel distribution. 3. Low pressure fuel supply.	1. Highly integrated engine design. 2. For end-mounted combustors, shaft overhang creates critical speed problem.

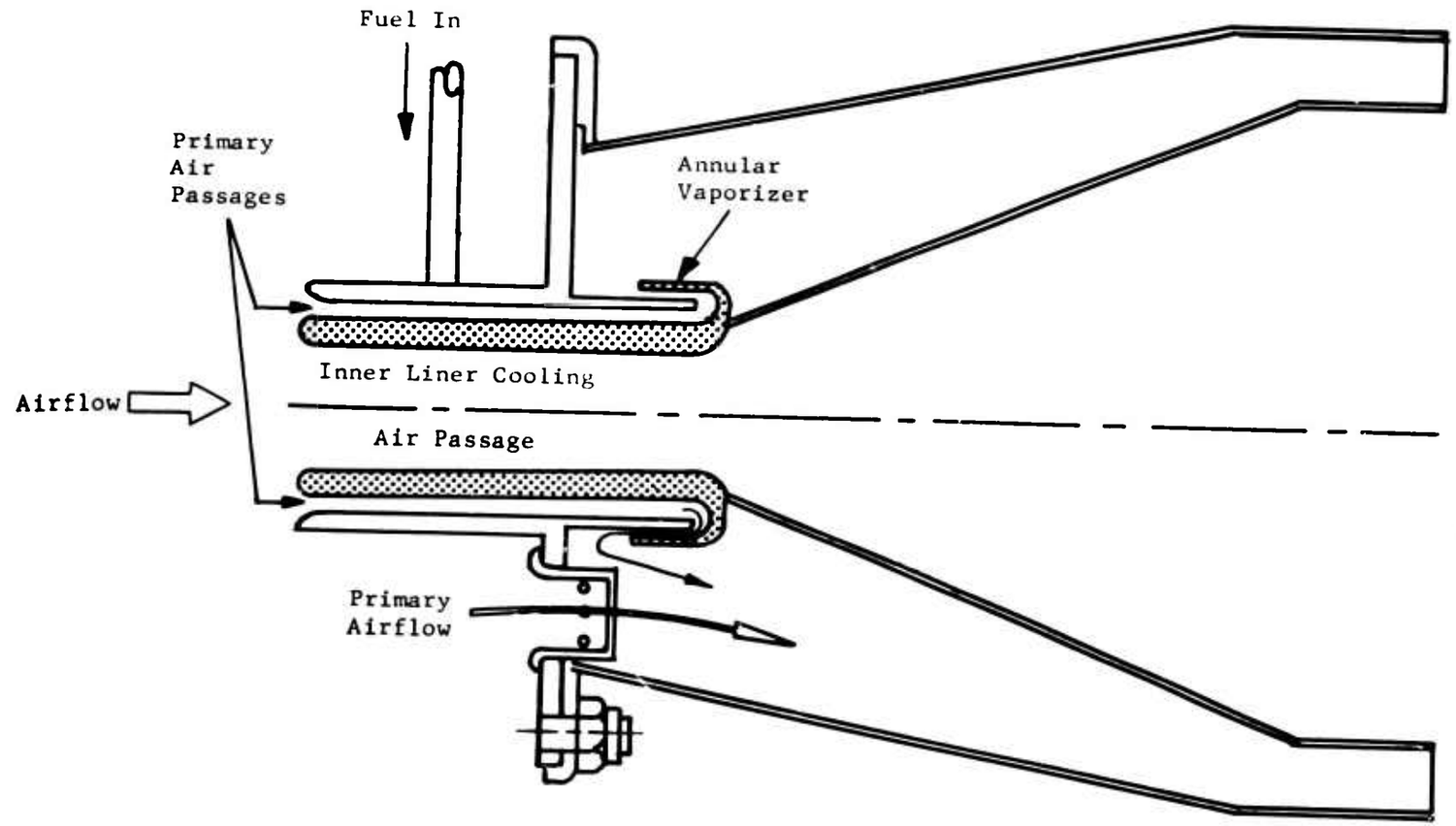

Figure 11. Annular Vaporizer Fuel Introduction System Concept Integrated with an Ent-Mounted Annular Combustor.

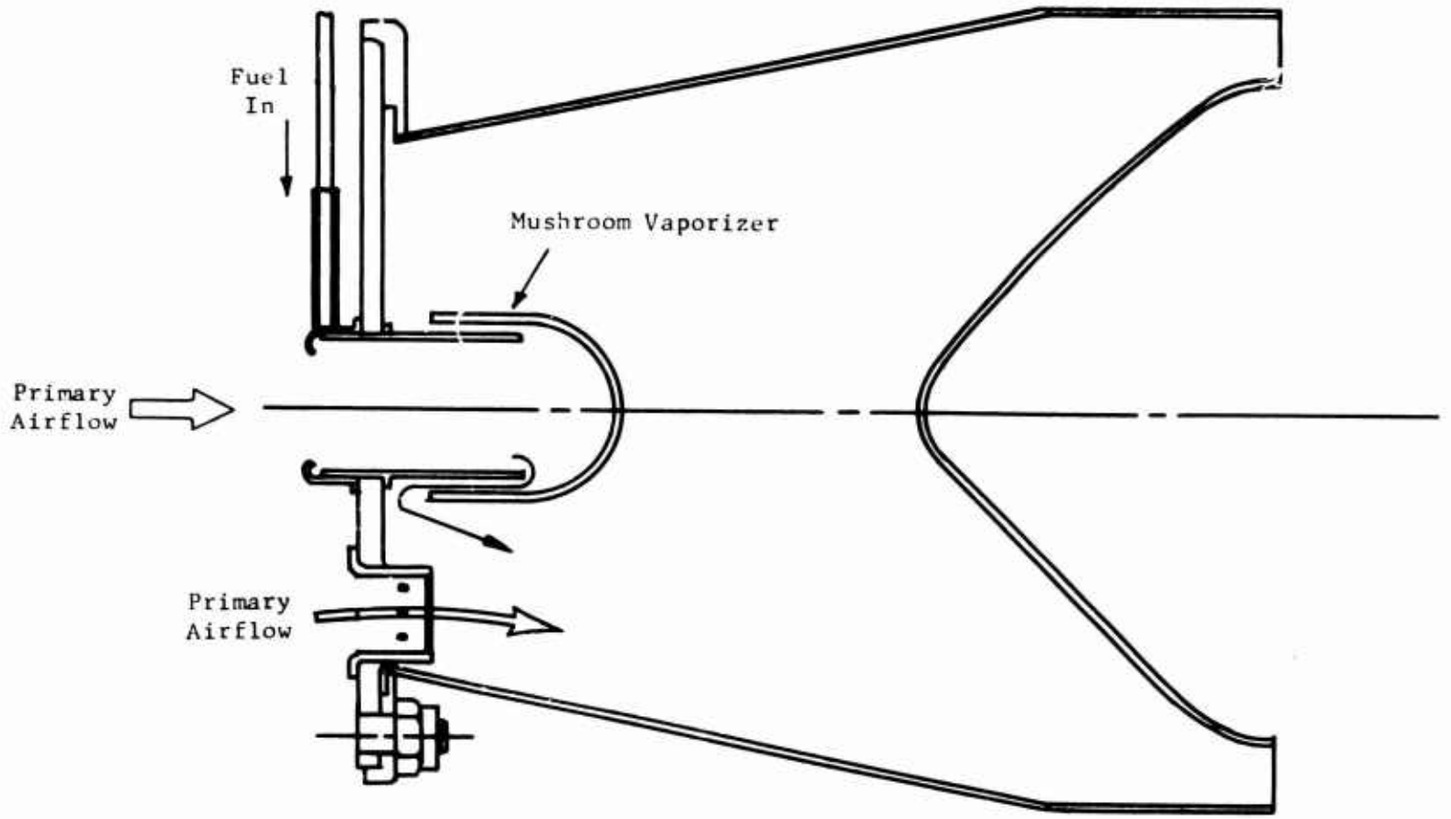

Figure 12. Mushroom Vaporizer Fuel Introduction System Concept Integrated with an End-Mounted Can Combustor.

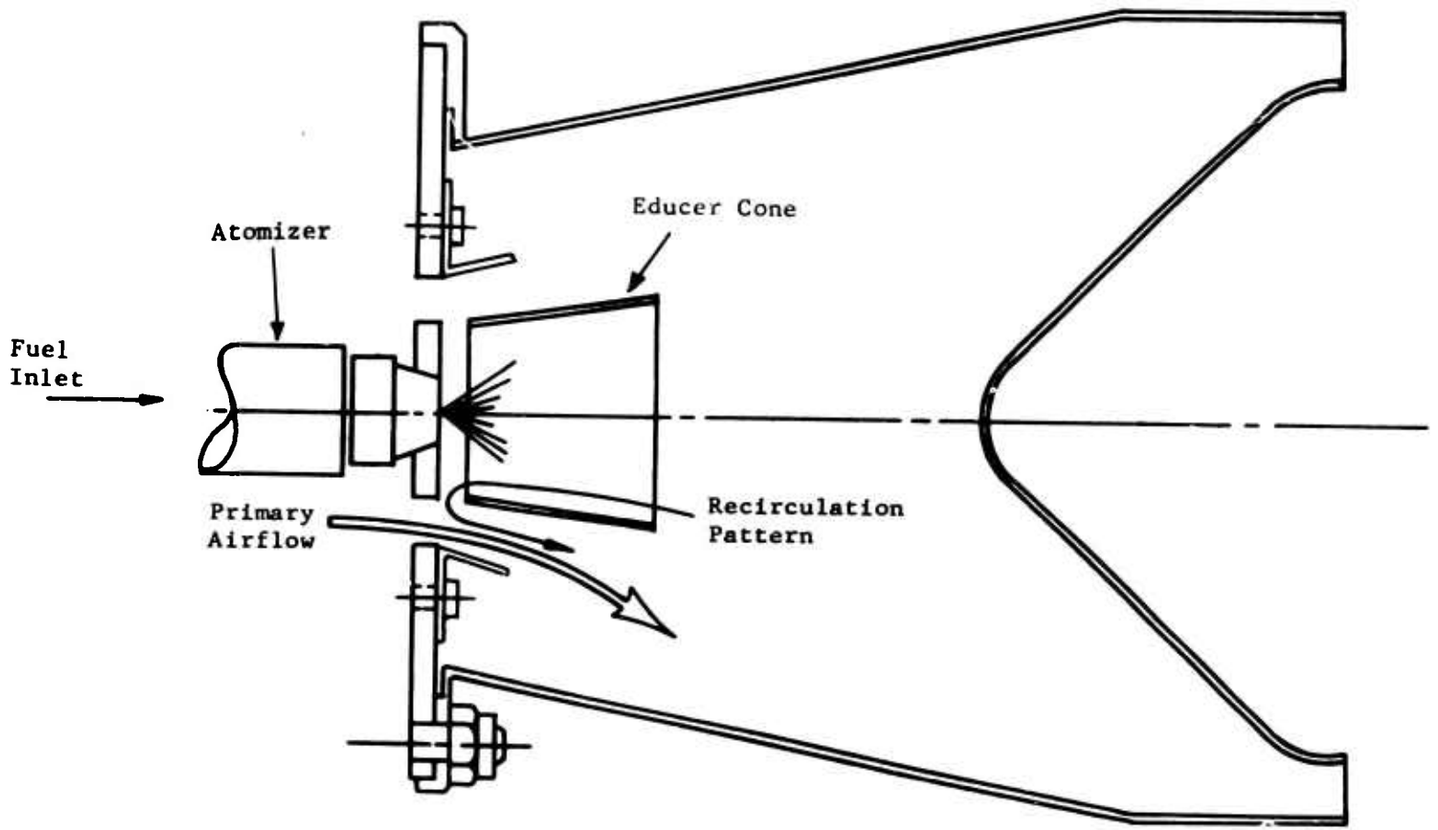

Figure 13. Atomizer-Educer Fuel Introduction System Concept Integrated with an End-Mounted Can Combustor.

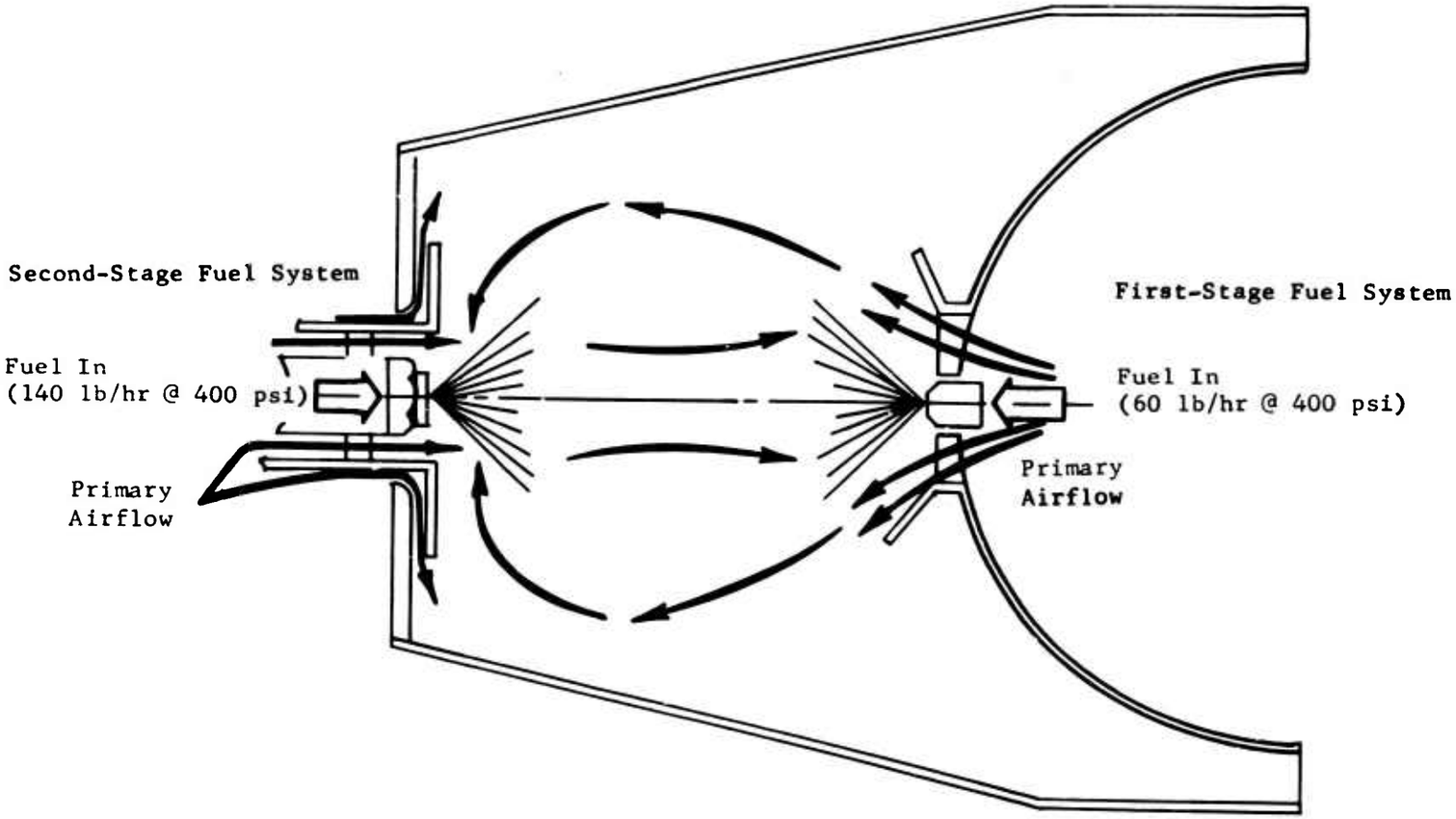

Figure 14. Atomizer Fuel Introduction System Concept Integrated with an End-Mounted Can Combustor.

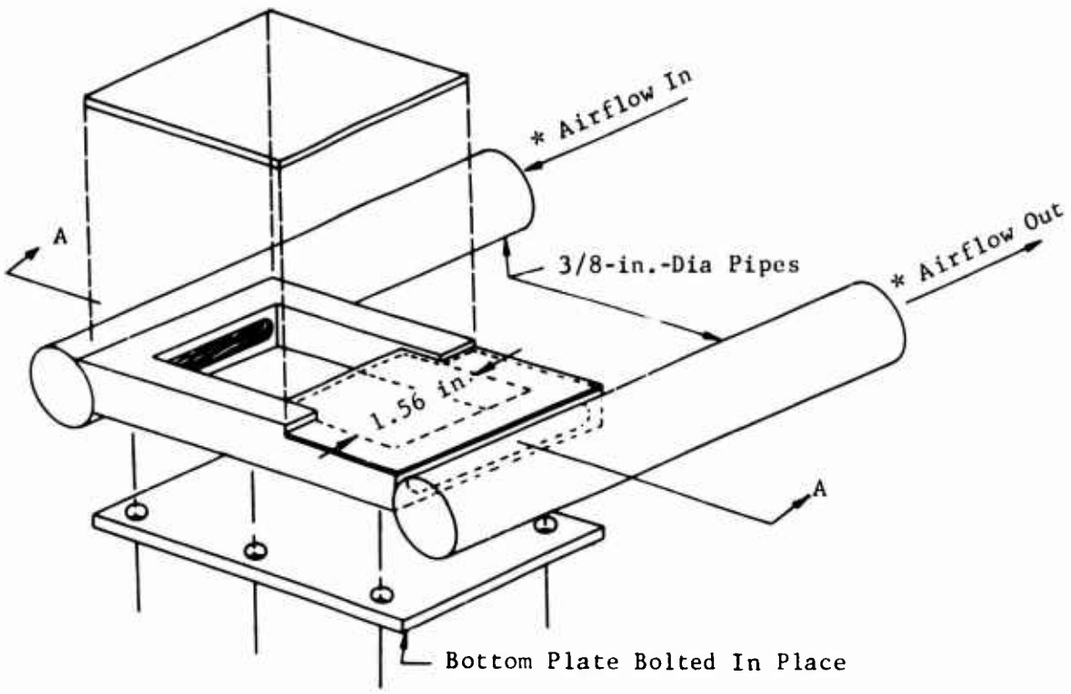

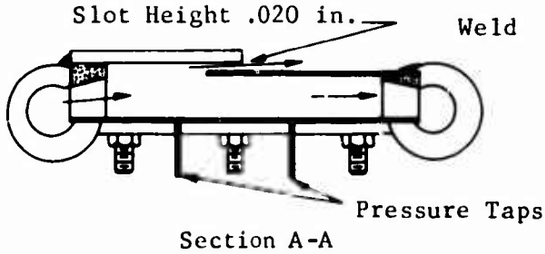

* Airflow In And Out Measured On Fisher Porter Flowmeters

Figure 15. Tangential Film Cooling Slot Flow Test Rig Schematic.

TABLE VI. TANGENTIAL FILM COOLING SLOT CONFIGURATIONS TESTED

Test No.	L (in.)	D (in.)	Bypass Flow (%)
1	0.50	0.188	0
2	0.50	0.401	0
3	0.50	0.401	~ 100
4	0.50	0.188	~ 100
6	0.35	0.401	0
7	0.35	0.401	~ 300
14	0.20	0.401	9

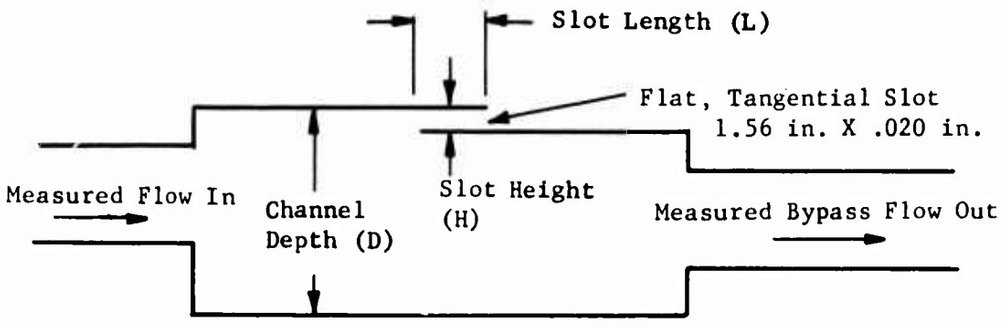

Figure 16. Definition of Tangential Film Cooling Slot Geometry.

TABLE VII. REDUCED TANGENTIAL FILM COOLING SLOT TEST DATA

Slot W_c (lb/sec)	P_{S_i} (in. Hg A)	P_{S_e} (in. Hg A)	Bypass W_c (lb/sec)	P_{T_i} (in. Hg A)	$V_{Approach}$ (ft/sec)
TEST 1					
.0018	30.26	29.76	0	30.262	12.37
.00221	30.46	29.76	0	30.463	15.2
.00298	30.76	29.76	0	30.766	20.2
.00432	31.76	29.76	0	31.773	28.4
.00528	32.76	29.76	0	32.78	33.6
.00627	33.76	29.76	0	33.78	38.8
.00983	39.76	29.76	0	39.817	51.6
.01196	44.76	29.76	0	44.835	56.0
TEST 2					
.00195	30.26	29.76	0	30.260	6.35
.00305	30.76	29.76	0	30.761	9.63
.00442	31.76	29.76	0	31.763	13.7
.00548	32.76	29.76	0	32.764	16.5
.00642	33.76	29.76	0	33.766	18.7
.0100	39.76	29.76	0	39.773	24.8
.01215	44.76	29.76	0	44.777	26.8
TEST 3					
.00209	30.41	29.76	.00181	30.412	12.6
.00696	34.06	29.76	.00637	34.087	38.6
.00582	33.16	29.76	.00564	33.180	34.1
.0104	39.46	29.66	.0108	39.518	53
.00448	31.81	29.66	.00437	31.822	27.4
.01305	44.66	29.66	.0127	44.737	56.8
TEST 4					
.00614	33.16	29.66	.00549	33.256	73.5
.00442	31.66	29.66	.00391	31.711	54.9
.00305	30.66	29.66	.0026	30.684	38.5
.00213	30.26	29.66	.00174	30.271	26.8
.01075	39.66	29.66	.01025	39.922	111.0
.01365	44.66	29.66	.01285	45.029	124.0

TABLE VII. - Continued

Slot W_c (lb/sec)	P_{S_i} (in. Hg A)	P_{S_e} (in. Hg A)	Bypass W_c (lb/sec)	P_{T_i} (in. Hg A)	$V_{Approach}$ (ft/sec)
TEST 6					
.00207	30.37	29.87	0	30.370	6.82
.00331	30.87	29.87	0	30.871	10.55
.005115	31.87	29.87	0	31.874	15.8
.005985	32.87	29.87	0	32.875	17.9
.00709	33.87	29.87	0	33.877	20.6
.01112	39.87	29.87	0	39.886	27.5
.0134	44.87	29.87	0	44.890	29.4
TEST 7					
.0060	33.97	29.87	.0154	34.04	62.0
.0081	35.05	29.87	.0233	35.216	88.3
.00995	37.87	29.87	.0267	38.054	95.4
.0124	40.02	29.82	.0343	40.304	115.0
.0102	37.82	29.82	.0295	38.086	103.5
.00545	32.82	29.82	.01695	32.899	67.3
.00375	31.82	29.82	.00995	31.857	42.4
.00198	30.82	29.82	.00586	30.830	25.1
TEST 14					
.00226	30.24	29.74	0	30.240	7.36
.00350	30.74	29.74	0	30.742	10.2
.004975	31.74	29.74	0	31.744	15.4
.006375	32.74	29.74	0	32.746	19.2
.007385	33.74	29.74	0	33.748	21.5
.01055	39.74	29.74	0	39.754	26.1
.0130	44.74	29.74	0	44.759	28.6
.00885	35.74	29.74	0	35.751	24.4
.01012	37.74	29.74	0	37.754	26.4
.01094	39.74	29.74	0	39.755	27.1
.01194	41.74	29.74	0	41.757	28.2
.01278	43.74	29.74	0	43.759	28.8

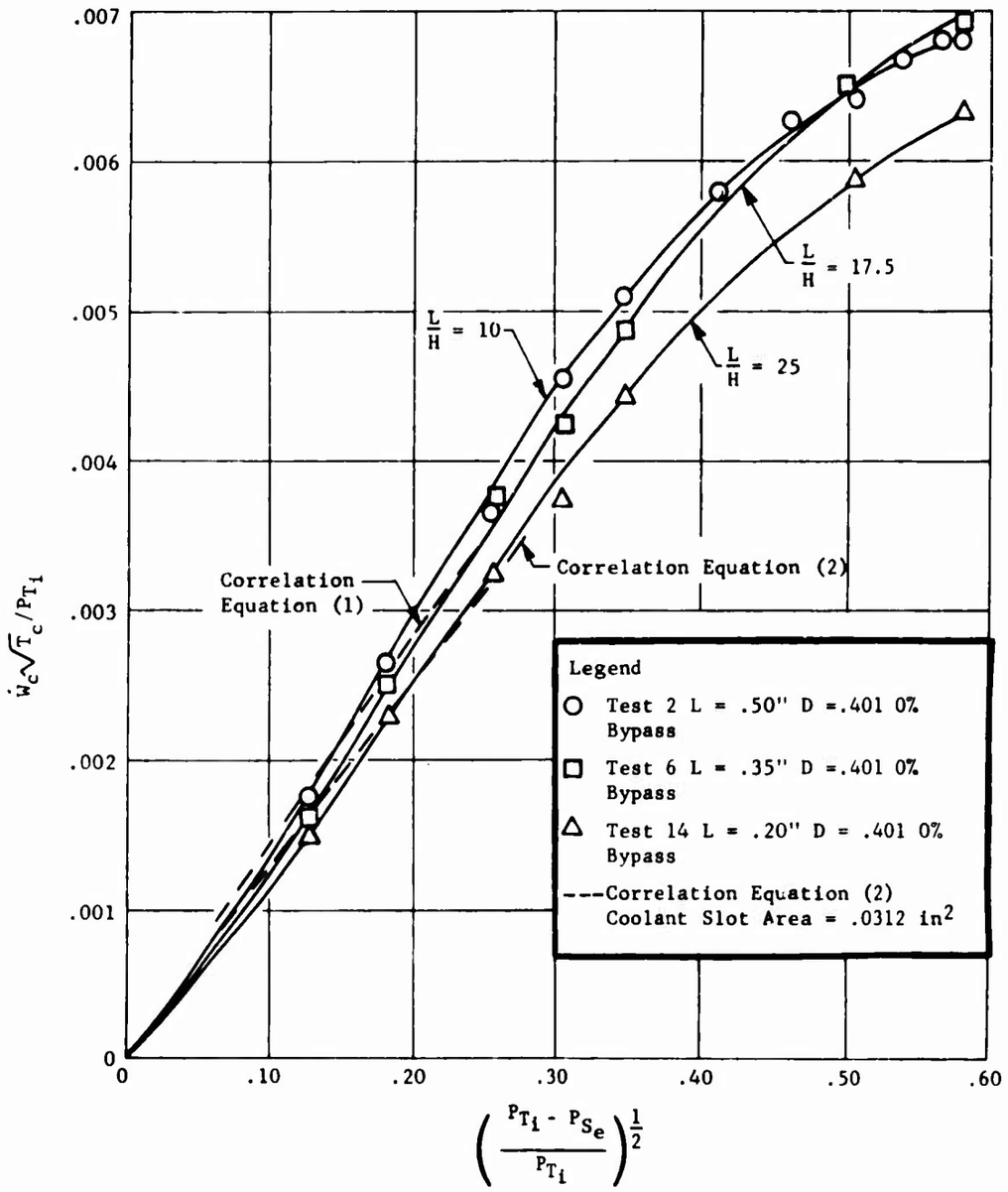

Figure 17. Influence of Tangential Film Cooling Slot Length for Zero Bypass Flow.

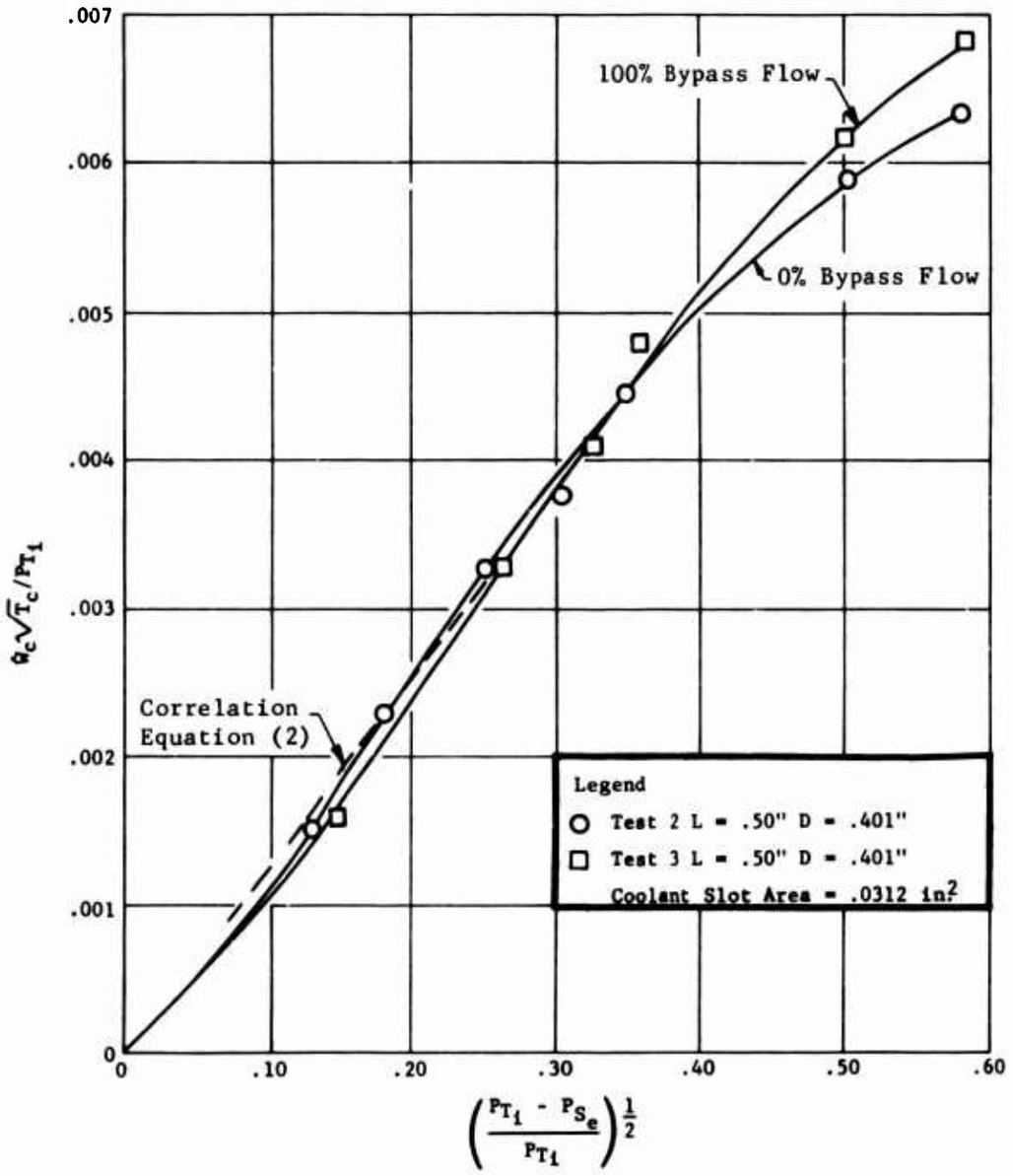

Figure 18. Influence of Coolant Bypass Flow on Tangential Film Cooling Slot Flow Characteristics.

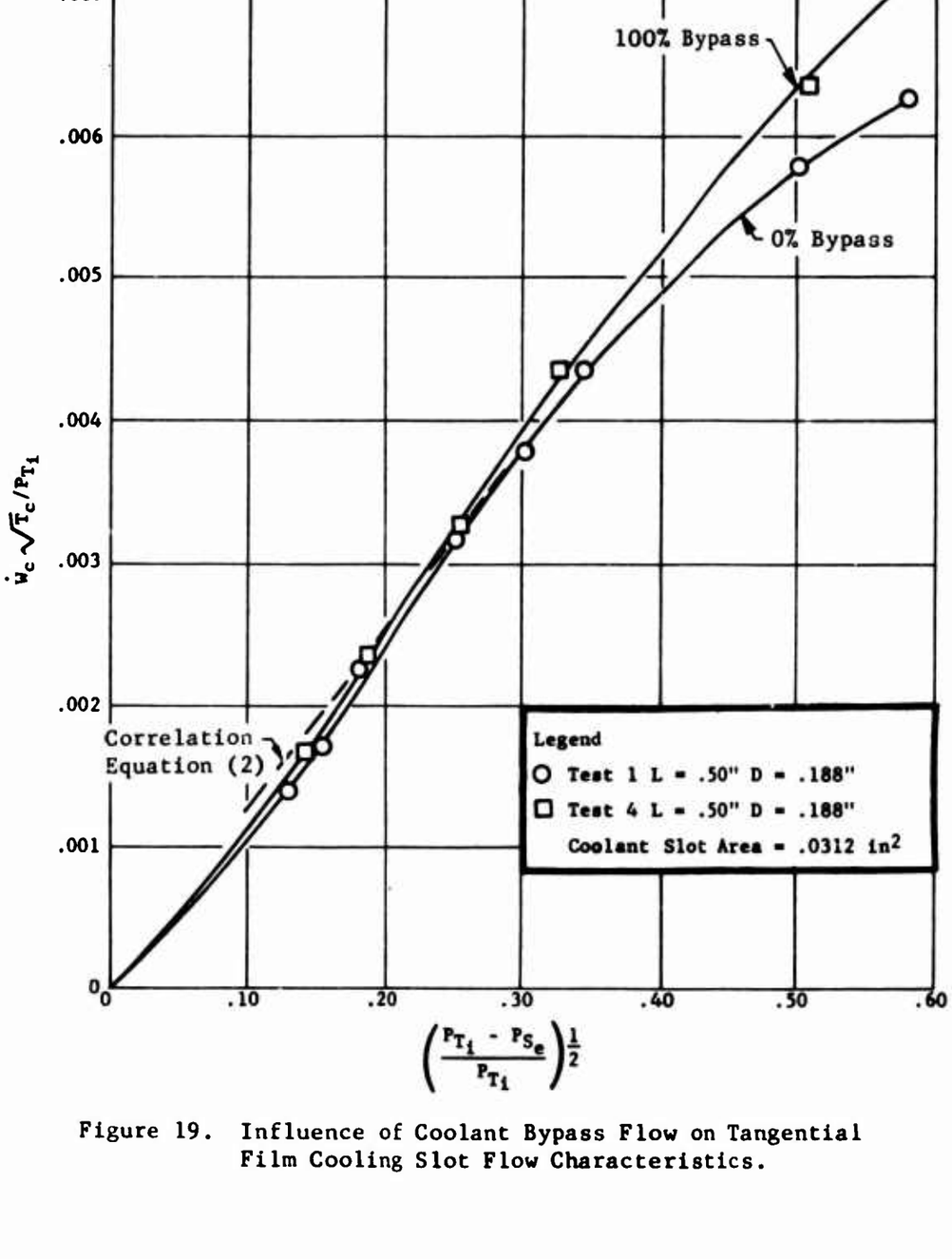

Figure 19. Influence of Coolant Bypass Flow on Tangential Film Cooling Slot Flow Characteristics.

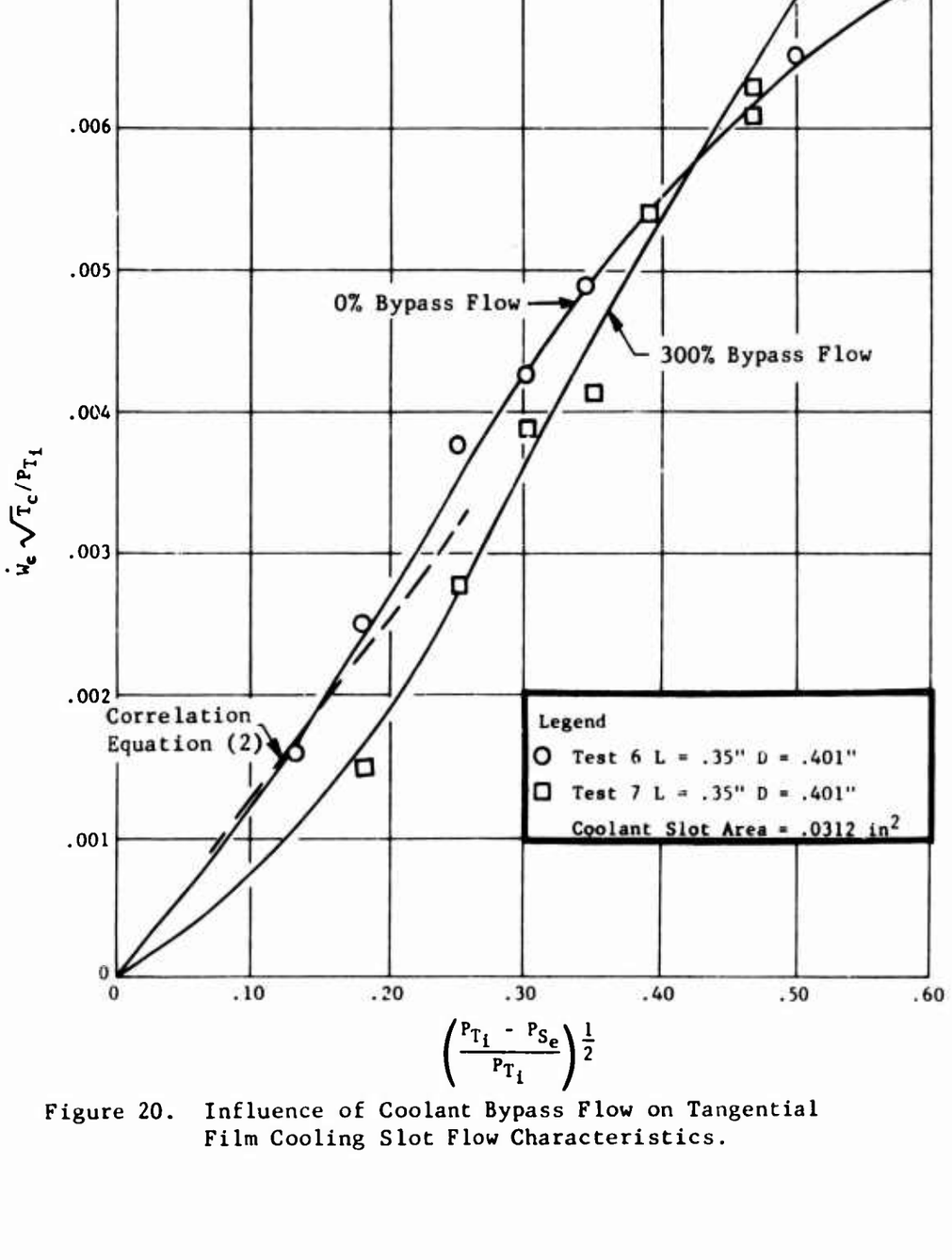

Figure 20. Influence of Coolant Bypass Flow on Tangential Film Cooling Slot Flow Characteristics.

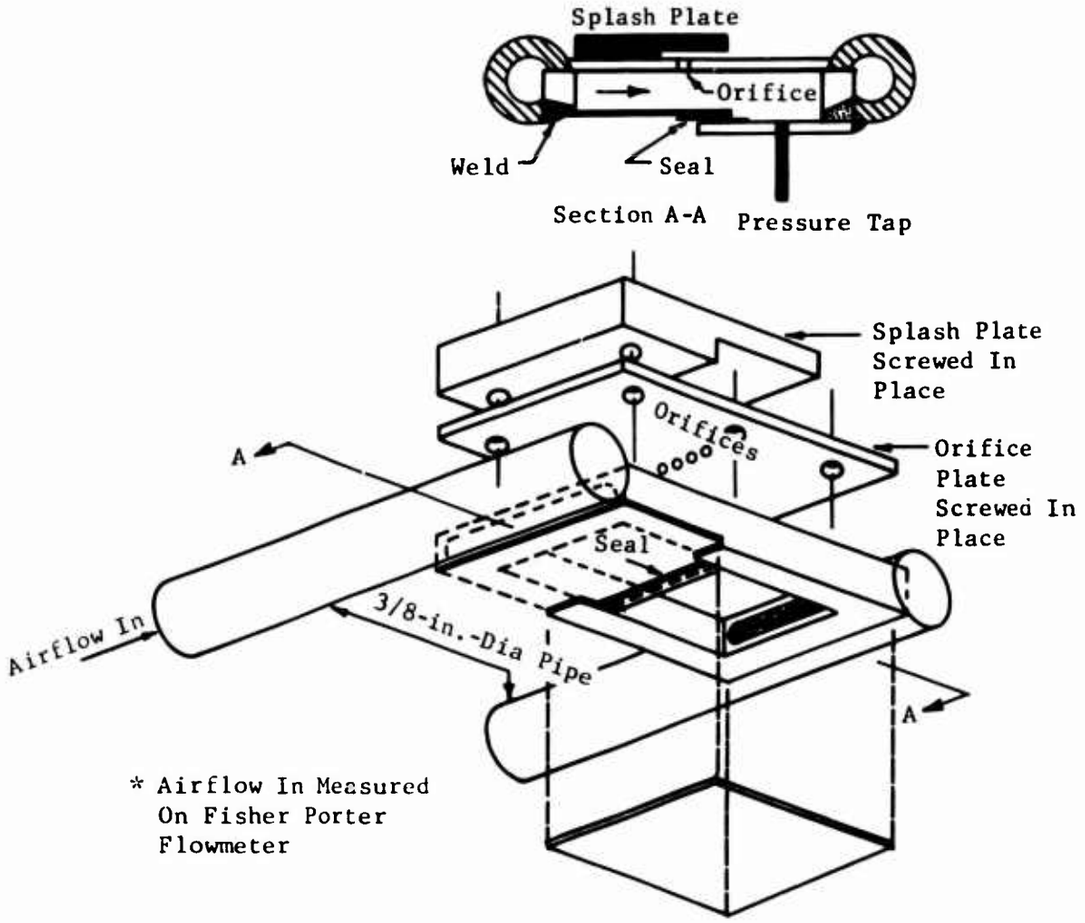

Figure 21. Splash Plate Film Cooling Slot Flow Test Rig Schematic.

TABLE VIII. SPLASH PLATE FILM COOLING SLOT CONFIGURATIONS TESTED

Test No.	L (in.)	L/H	D (in.)	Number of Holes	S (in.)	D/S	W (in.)	A_e/A_o ($in^2./in^2.$)
5	0.20	10	0.052	15	0.102	0.51	1.53	0.963
9	0.35	17.5	0.026	30	0.051	0.51	1.53	1.92
10	0.20	10	0.026	30	0.051	0.51	1.53	1.92
11	0.50	25	0.026	30	0.051	0.51	1.53	1.92
12	0.35	17.5	0.026	10	0.1326	0.196	1.326	5.0
13	0.50	25	0.026	10	0.1326	0.196	1.326	5.0
18	0.35	17.5	0.067	4	0.342	0.196	1.368	1.945
19	0.50	10	0.067	4	0.342	0.196	1.368	1.945
20	0.20	10	0.067	4	0.342	0.196	1.368	1.945

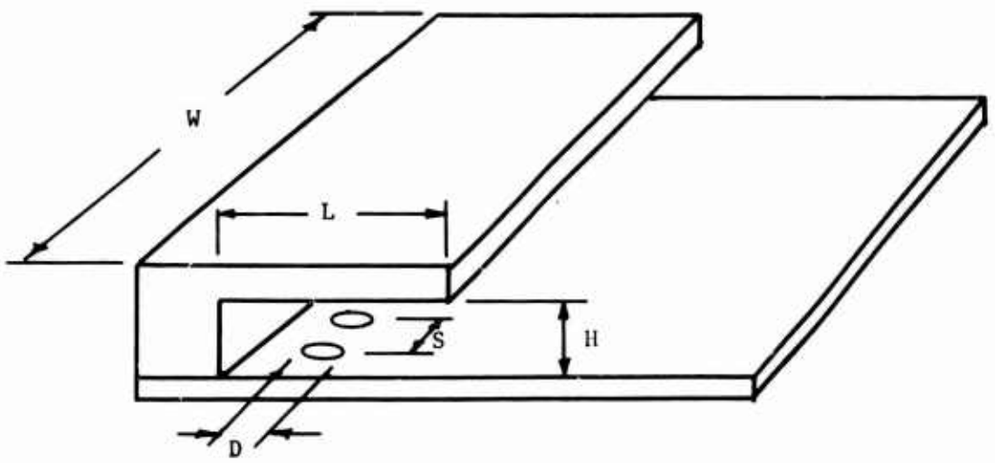

Figure 22. Definition of Splash Plate Film Cooling Slot Geometry.

TABLE IX. SPLASH PLATE FILM COOLING SLOT TEST DATA

Slot W_c (lb/sec)	P_{s_i} (in. Hg A)	P_{s_e} (in. Hg A)	T_c (°F)
Test 5			
.0103	45.36	29.76	85
.0079	39.76		
.00518	33.76		
.00417	32.76		
.00353	31.76		
.00247	30.76		
.00180	30.26		
Test 9			
.00382	36.72	29.82	84
.00290	33.82		
.00245	32.82		
.00192	31.82		
.00135	30.82		
.00088	30.32		
.00495	39.82		
.0065	44.82		
Test 10			
.00597	44.82	29.82	88
.0049	39.82		
.00289	33.82		
.00252	32.82		
.00198	31.82		
.00133	30.82		
.00096	30.32		
Test 11			
.00091	30.32	29.82	89
.00130	30.82		
.00186	31.82		
.00224	32.82		
.00275	33.82		
.0047	39.82		
.0058	44.82		
Test 12			
.00219	44.82	29.82	94
.00172	39.82		
.00104	33.82		
.000923	32.82		
.00075	31.82		
.00051	30.82		
.000333	30.32		

Slot W_c (lb/sec)	P_{s_i} (in. Hg A)	P_{s_e} (in. Hg A)	T_c (°F)
Test 13			
.00036	30.32	29.82	95
.00050	30.82		
.00073	31.82		
.00088	32.82		
.00103	33.82		
.00162	39.82		
.00200	44.82		
Test 18			
.00138	30.84	29.74	78
.00196	31.94		
.00229	32.74		
.00262	33.74		
.00442	39.74		
.0055	44.64		
.0039	37.74		
.00336	36.74		
Test 19			
.00552	44.74	29.74	79
.00438	39.74		
.00388	37.74		
.00332	35.69		
.00270	33.74		
.00233	32.74		
.00192	31.79		
.00124	30.74		
.00083	30.24		
Test 20			
.00091	30.24	29.74	71
.00131	30.74		
.00194	31.74		
.00246	32.74		
.00288	33.74		
.00352	35.74		
.00410	37.74		
.00466	39.74		
.00585	44.74		

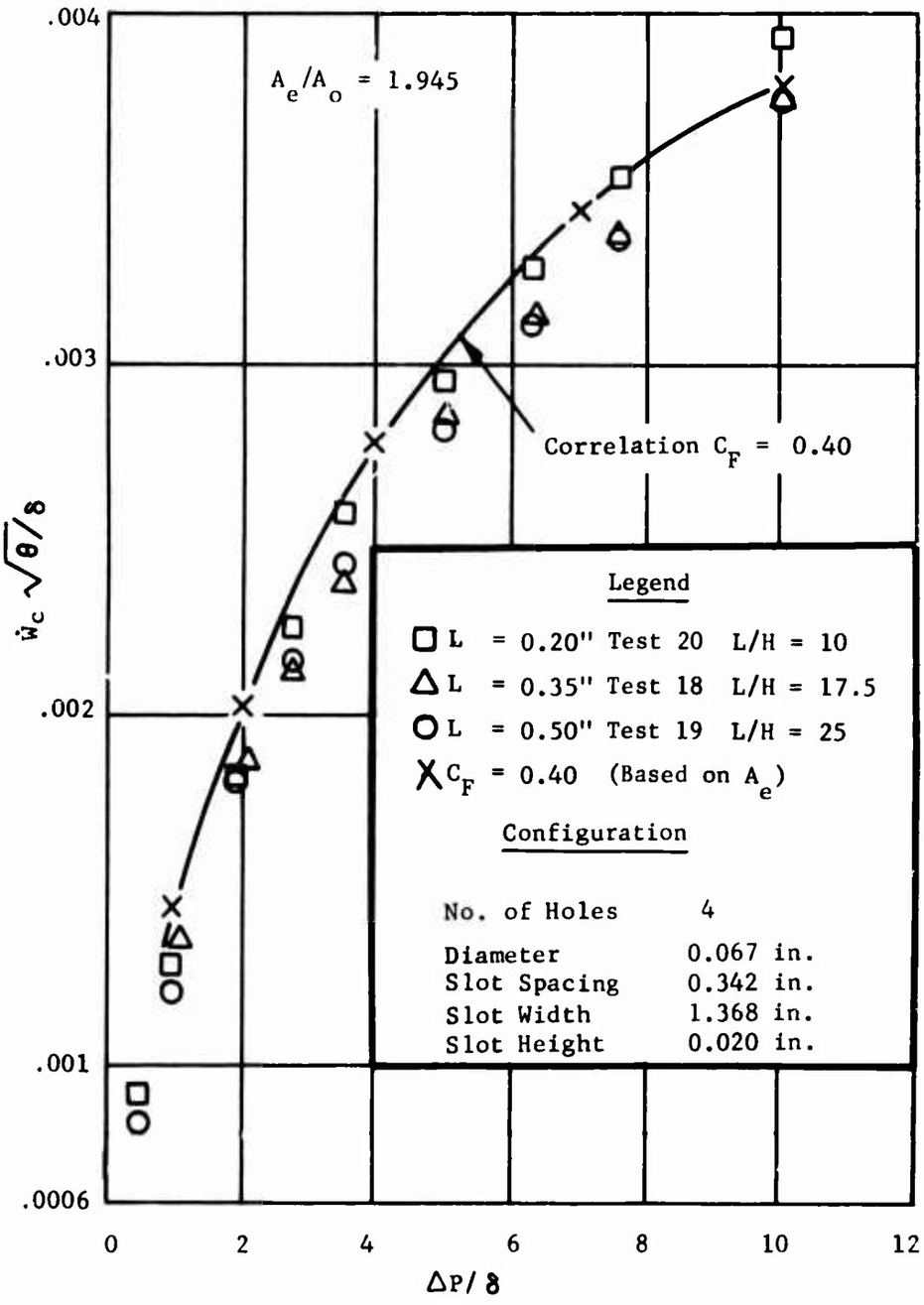

Figure 23. Influence of Splash Plate Film Cooling Slot Length on The Coolant Flow Characteristics.

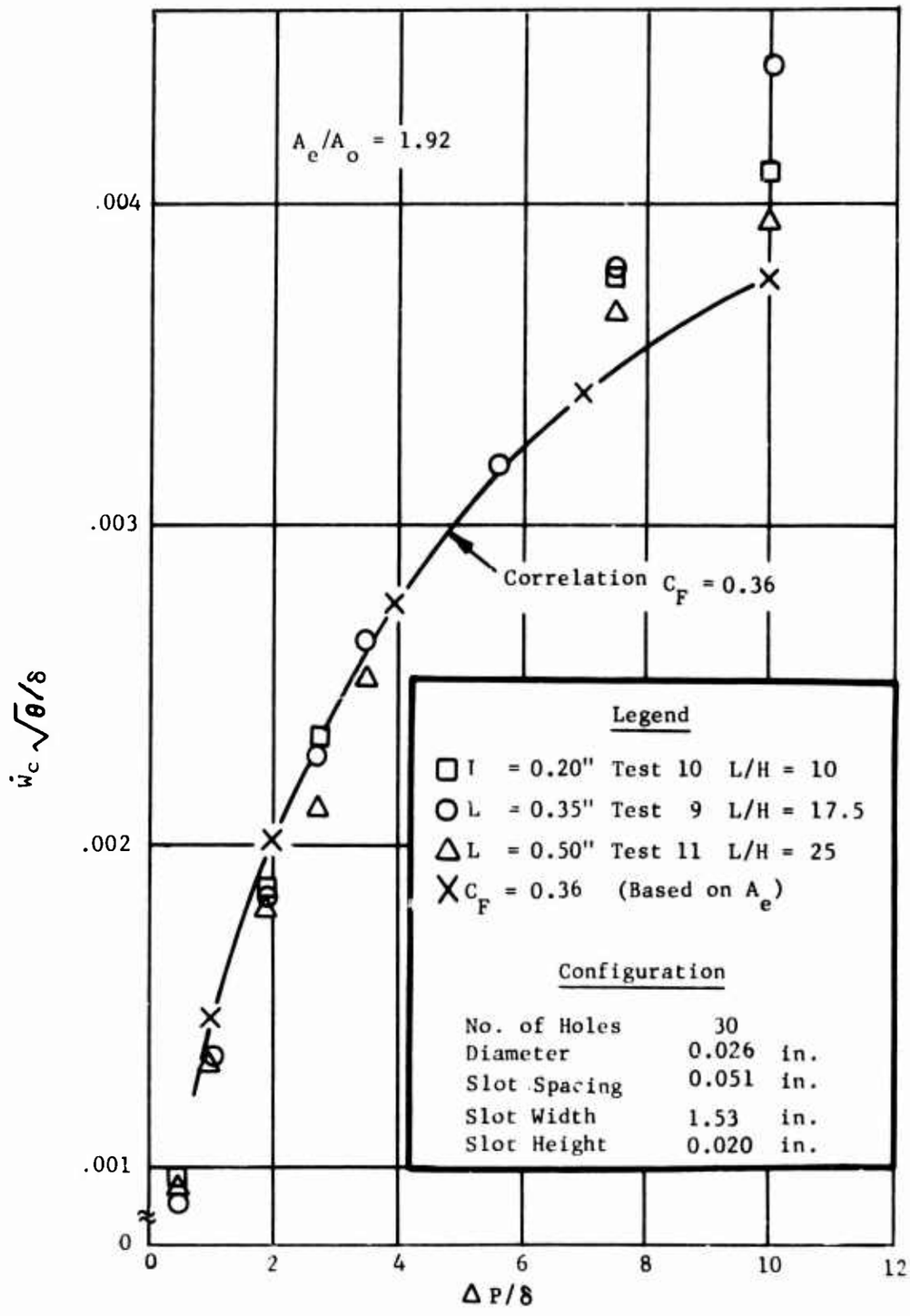

Figure 24. Influence of Splash Plate Film Cooling Slot Length on The Coolant Flow Characteristics.

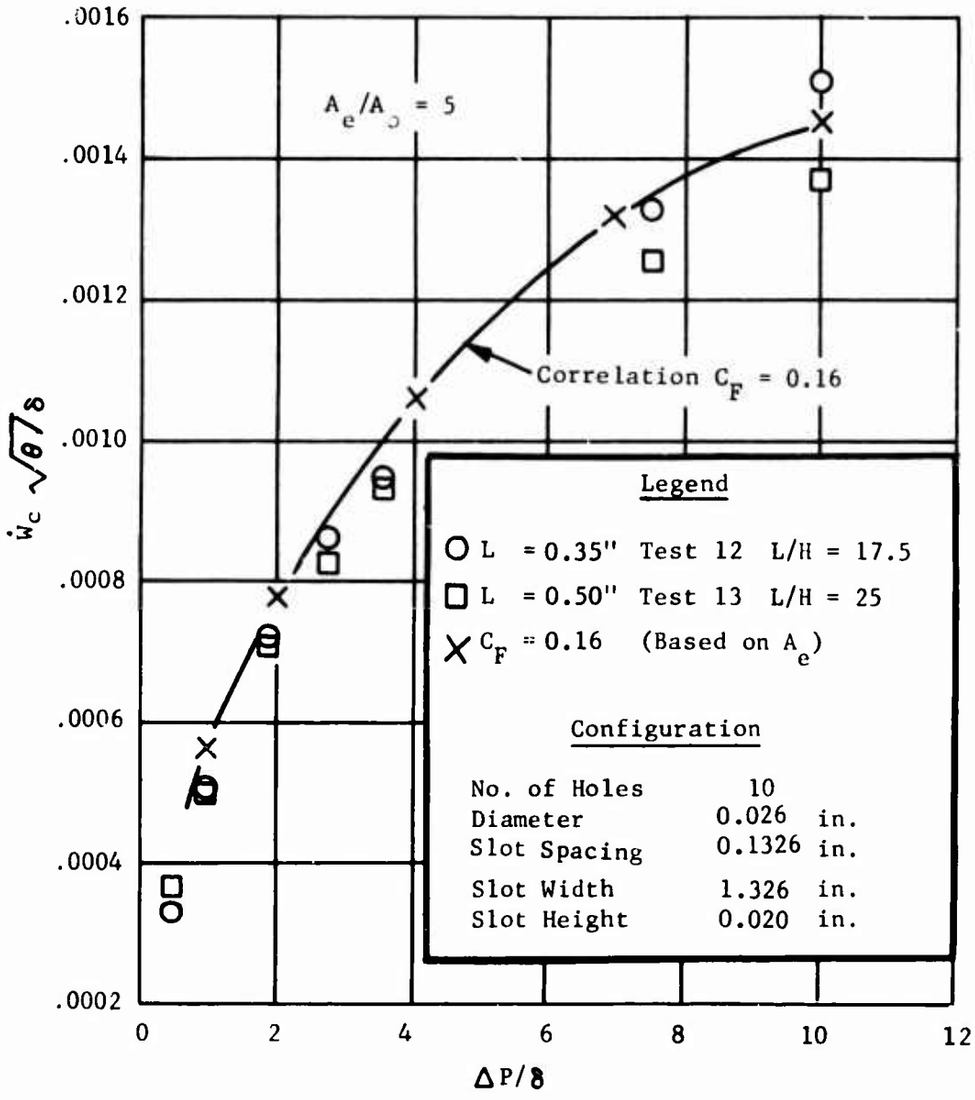

Figure 25. Influence of Splash Plate Film Cooling Slot Length on The Coolant Flow Characteristics.

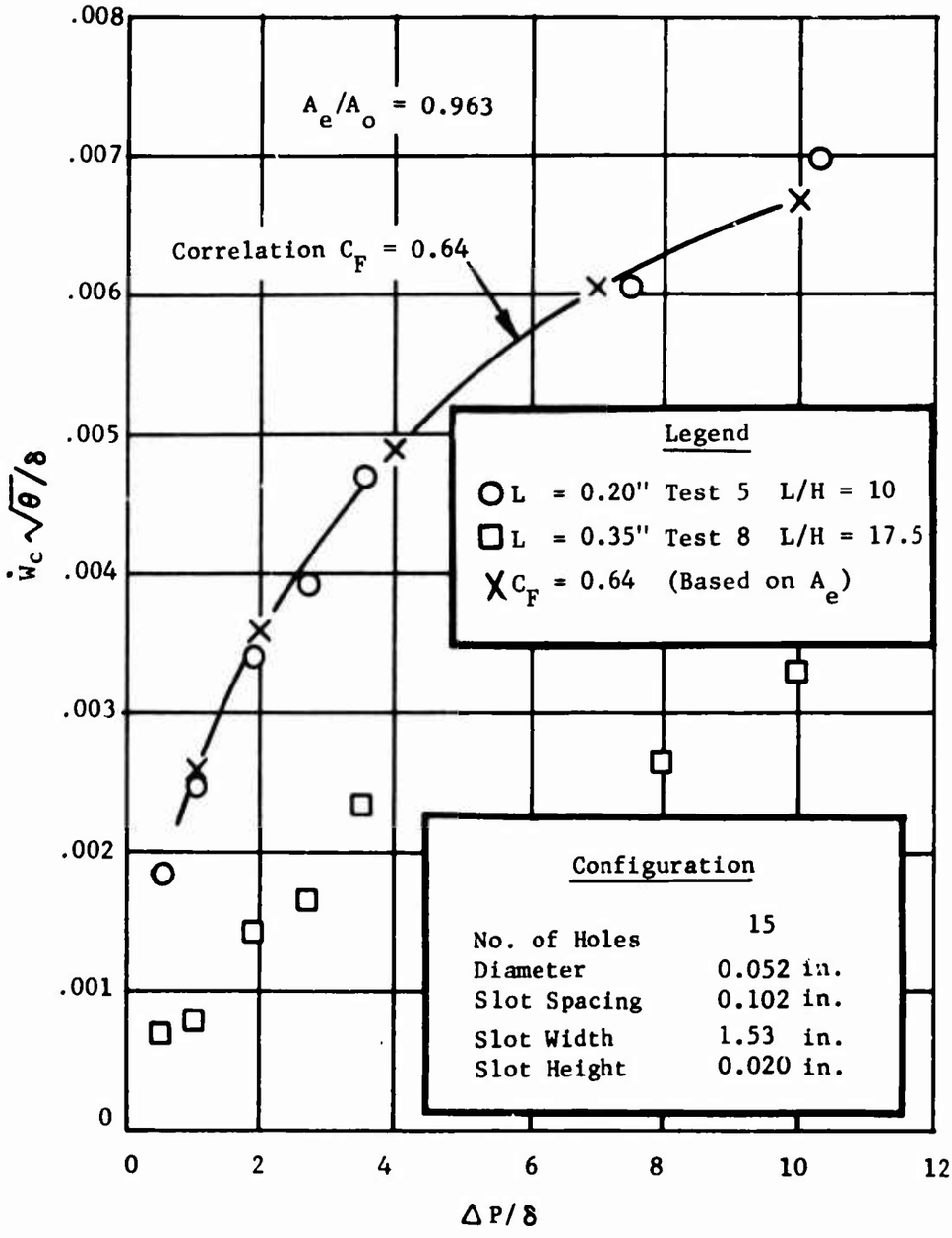

Figure 26. Influence of Splash Plate Film Cooling Slot Length on The Coolant Flow Characteristics.

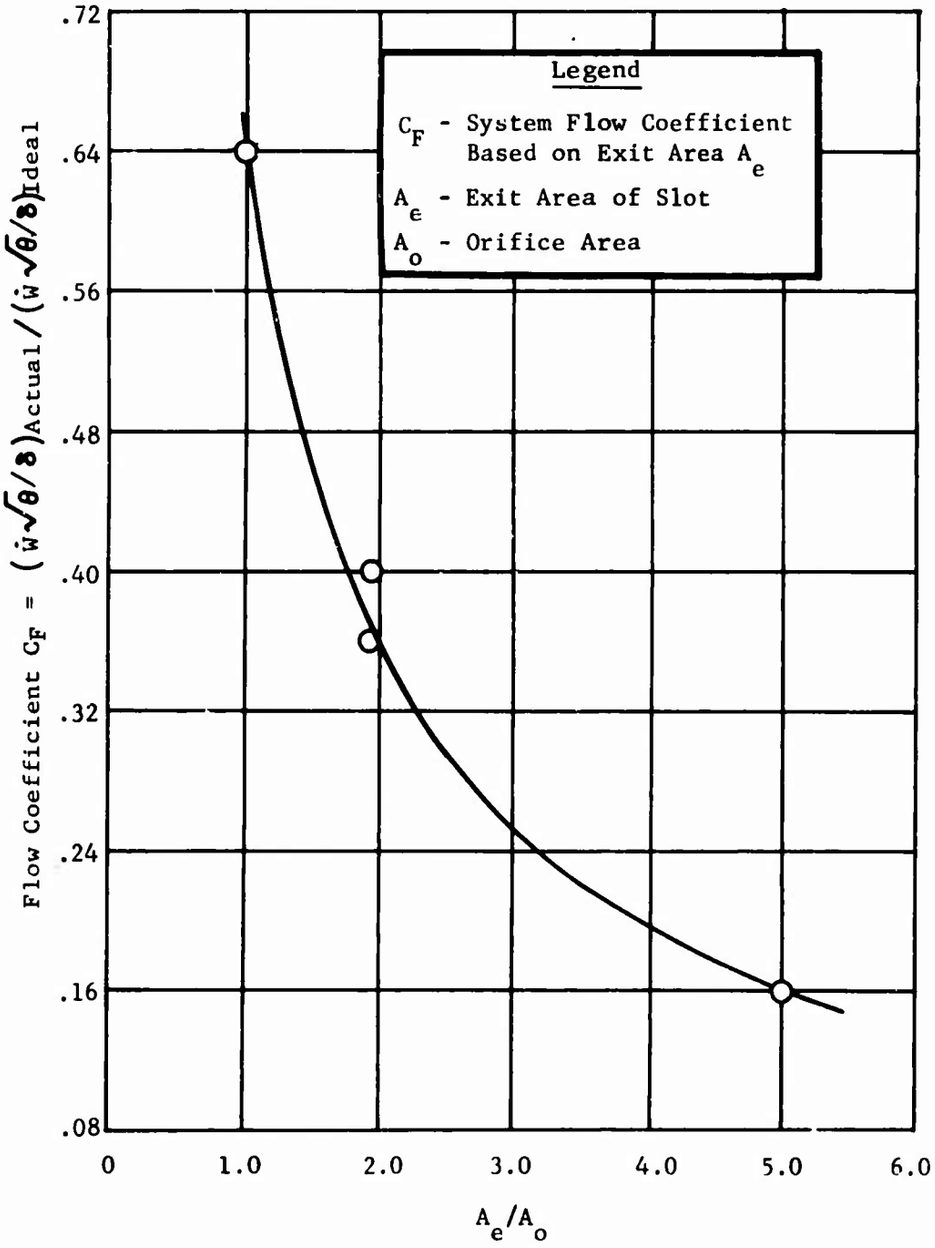

Figure 27. Influence of Splash Plate Area Ratio on Coolant Flow Characteristics.

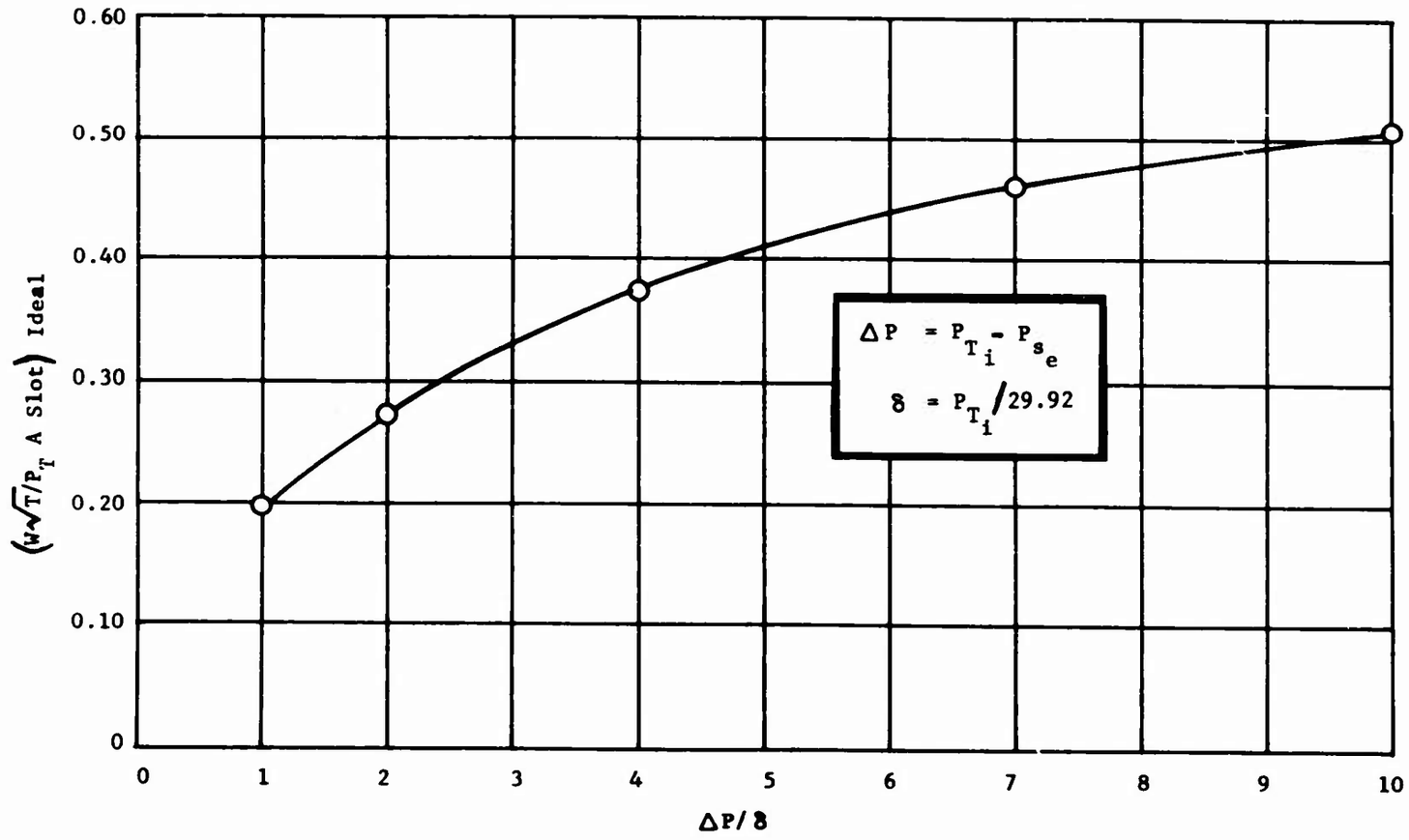

Figure 28. Ideal Splash Plate Flow Characteristic.

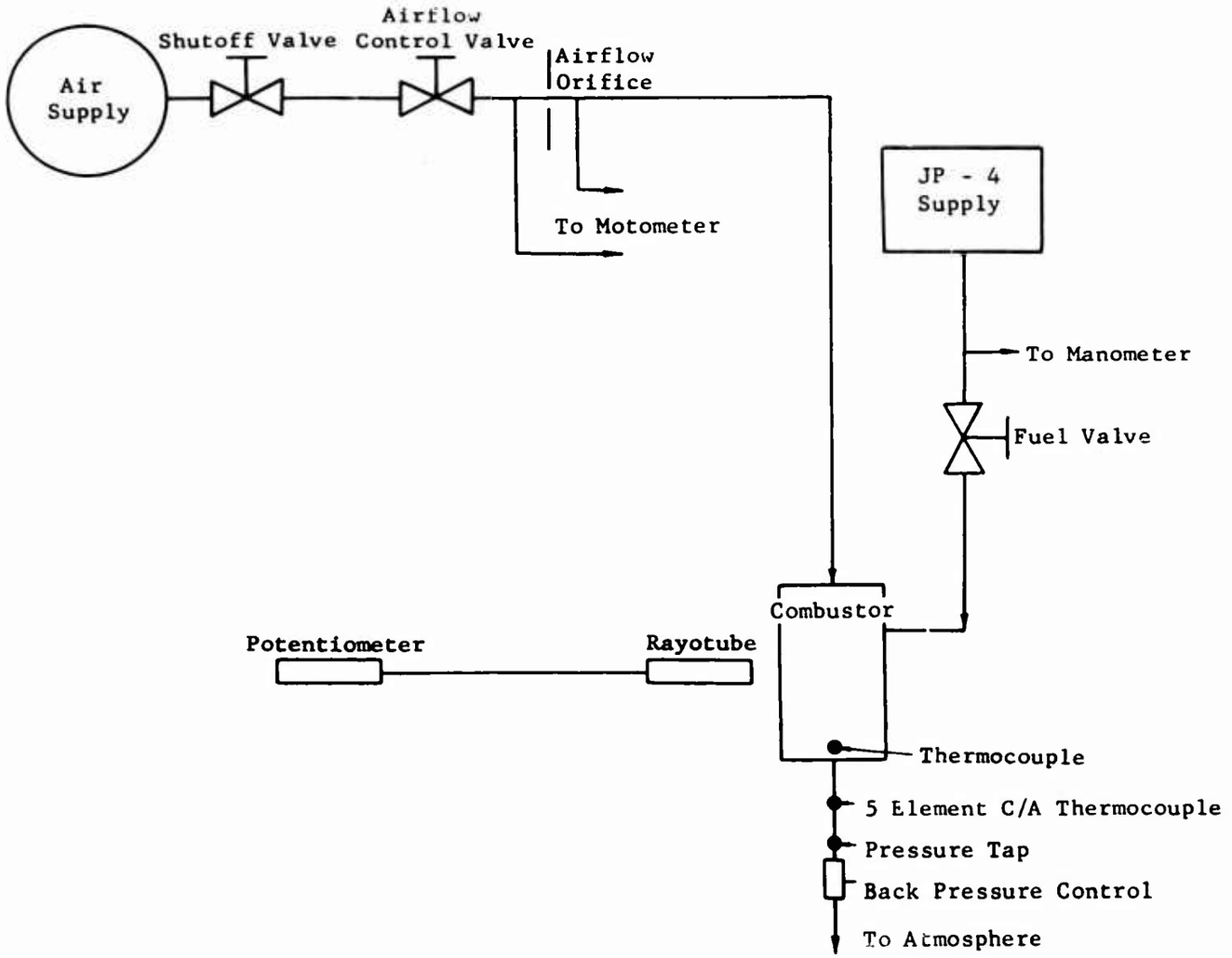

Figure 29. Radiation Measurement Airflow and Instrumentation Schematic.

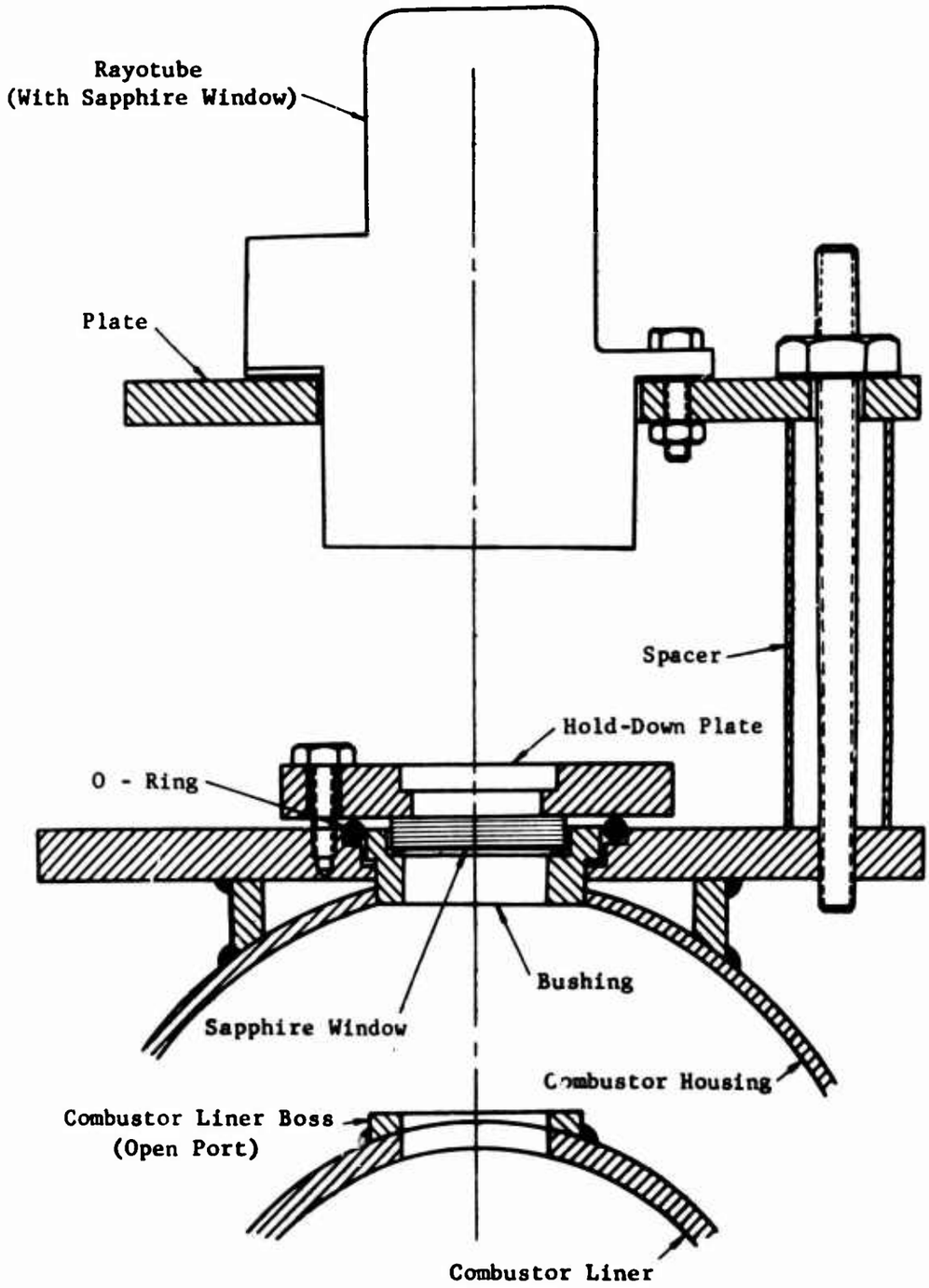

Figure 30. Radiation Measurement Assembly.

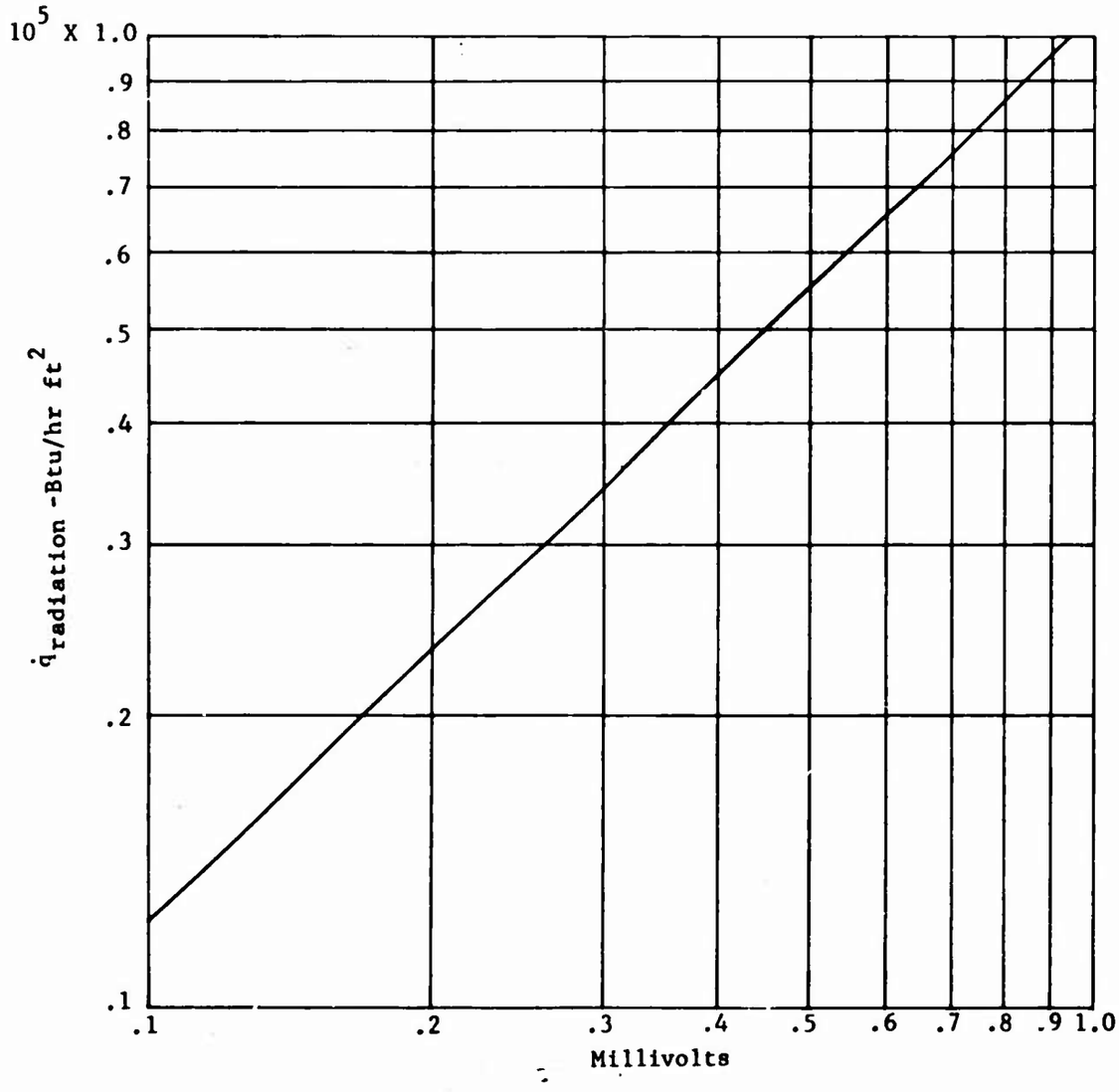

Figure 31. Calibration Curve for 8891-C-S Leeds and Northrup Rayotube Using Two Sapphire Windows.

TABLE X. COMBUSTOR OPERATING CONDITIONS FOR RADIATION MEASUREMENT TESTS

Test No.	Combustor Exit Gas Temperature (°F)	Combustor Inlet Air Temperature (°F)	Overall Fuel-Air Ratio	Heat Input Rate (Btu/lb air)	Combustor Exit Pressure Range (atm abs)	Symbol
1	1070	77	.01375	257	2-4	◇
2,3	937	75	.0118	220.6	2-4.3	○
4,5,6	780	75	.00952	178	2-4.75	△
7	577	77	.00665	124	2-4.6	□

(JP-4 Used for All Tests)

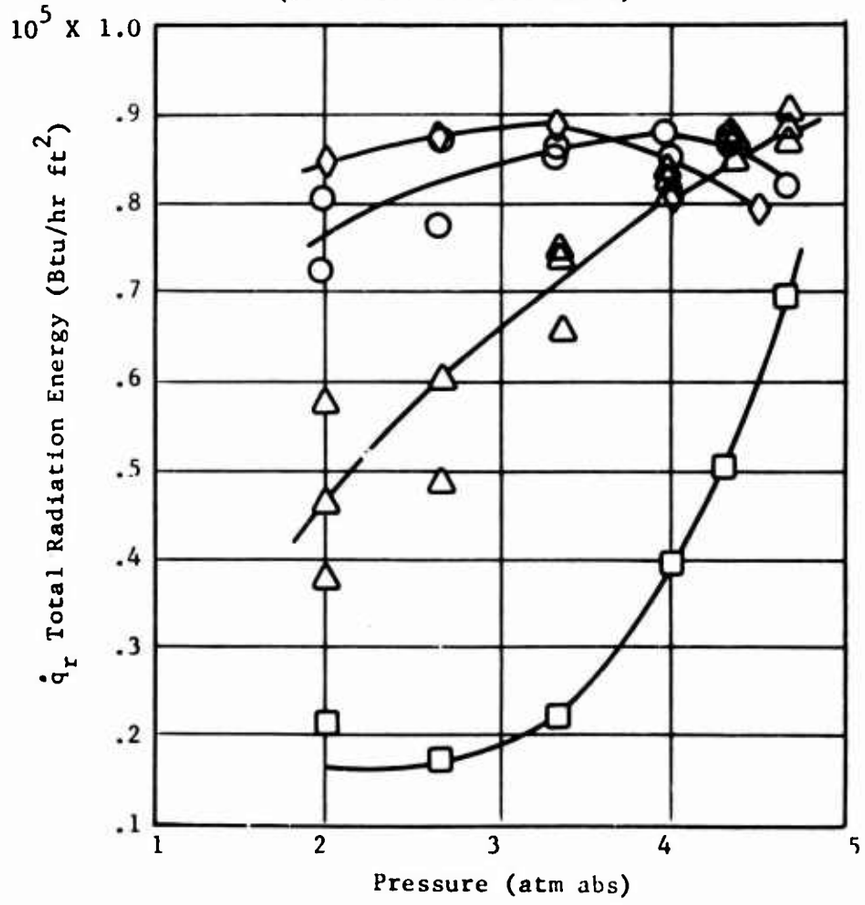

Figure 32. Flame Radiation as a Function of Exit Pressure for Heat Transfer Test Combustor.

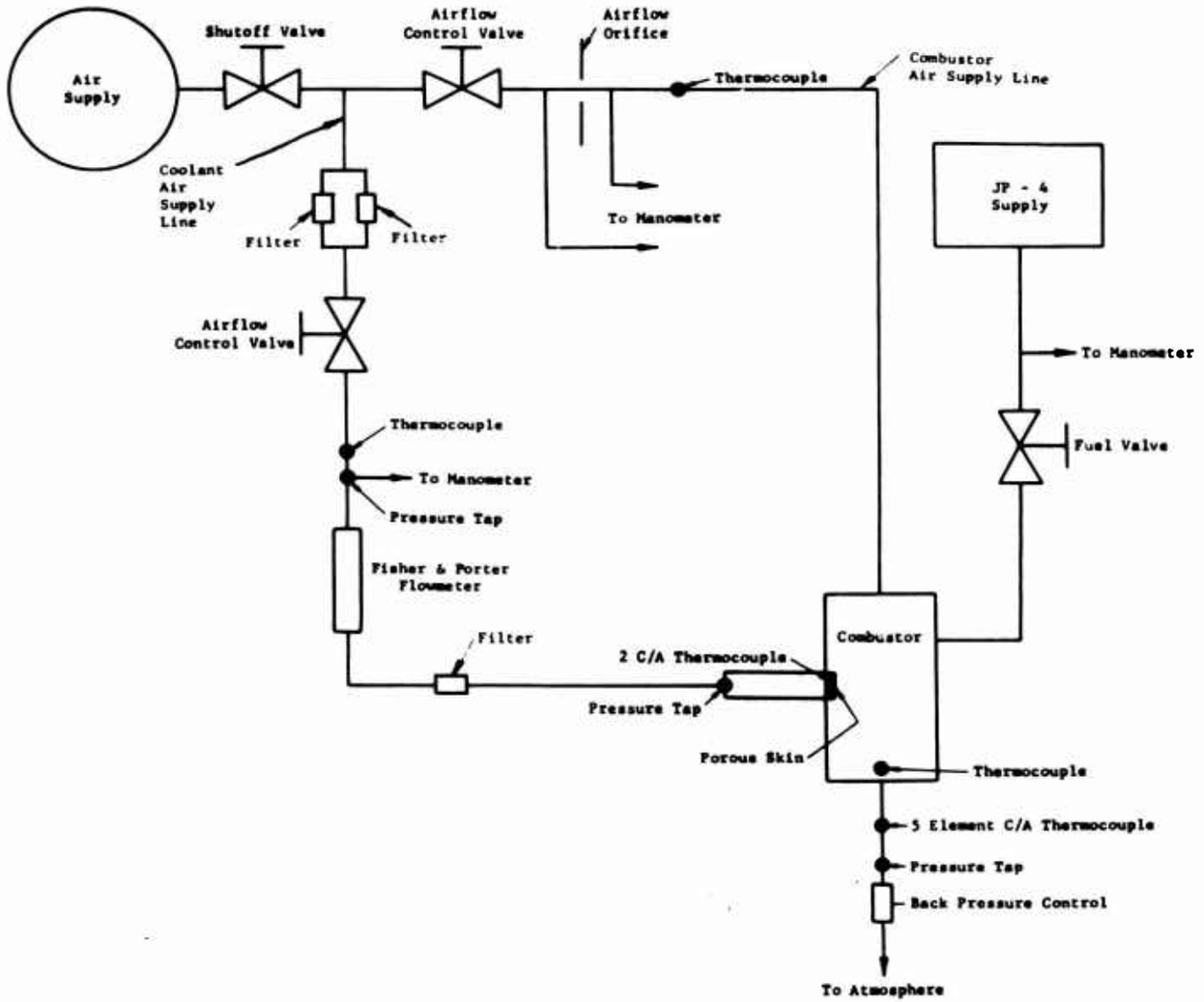

Figure 33. Transpiration Cooling Test Rig Airflow and Instrumentation Schematic.

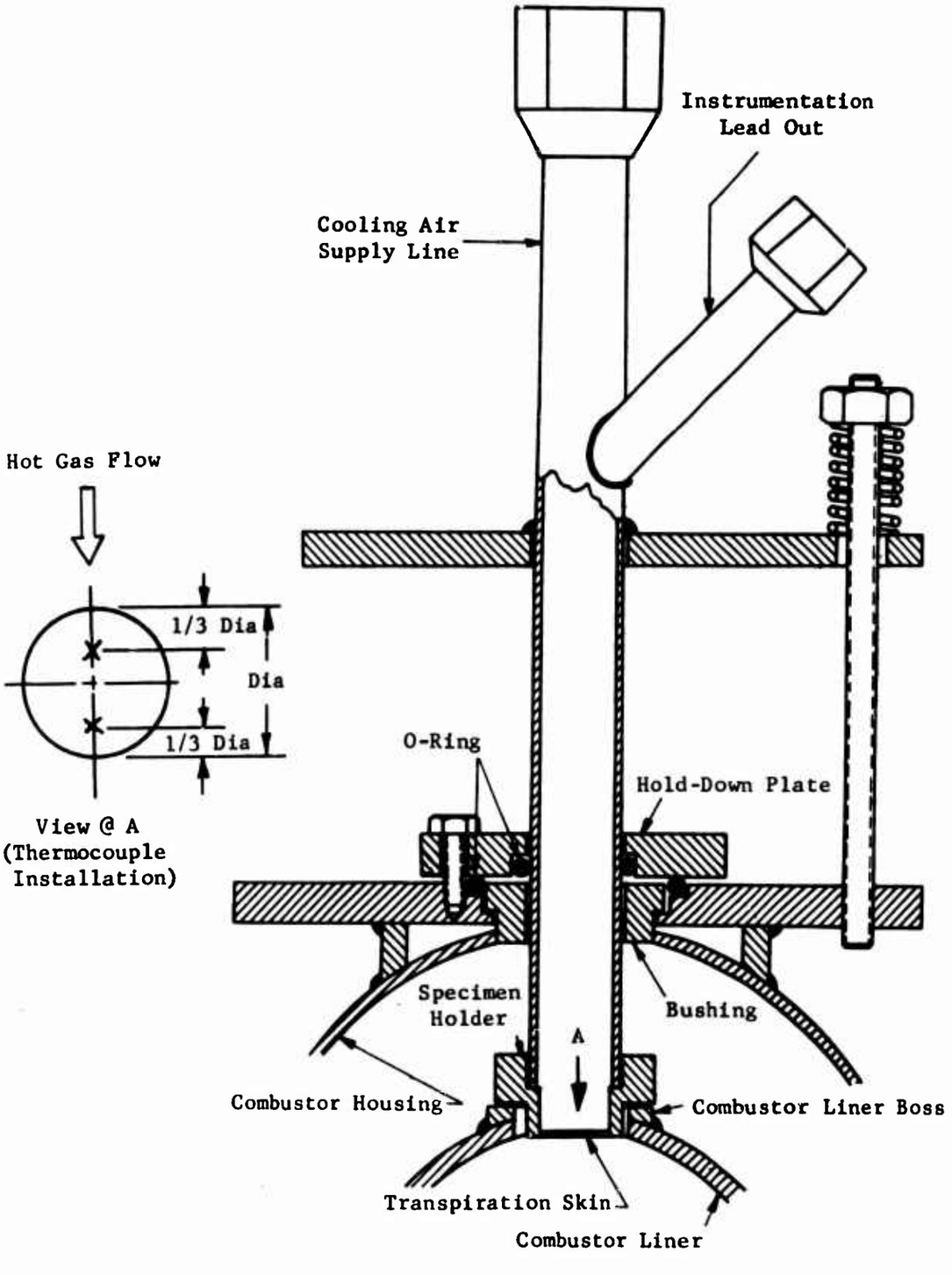

Figure 34. Transpiration Cooling Test Assembly.

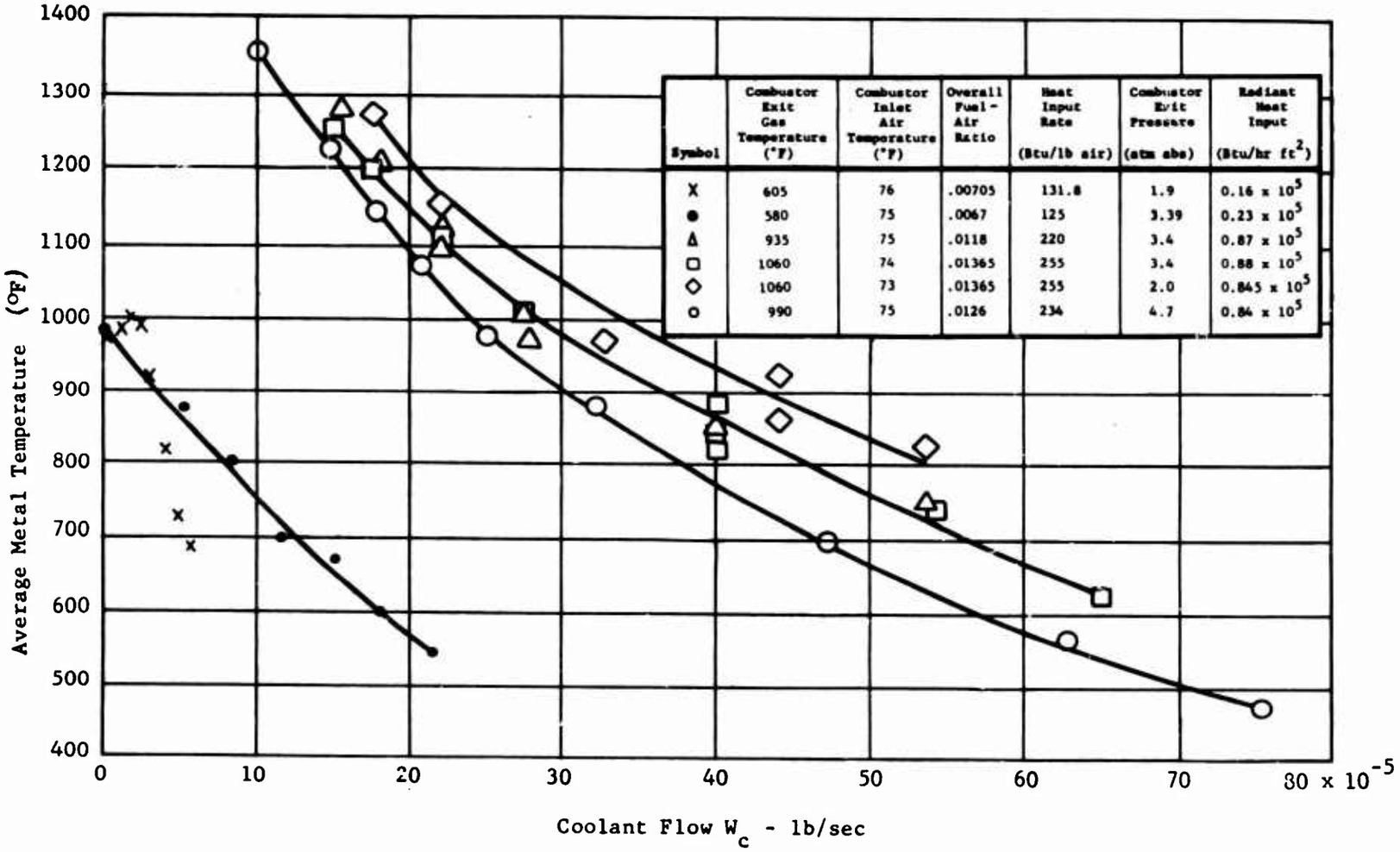

Figure 35. Transpiration Metal Temperature as a Function of Coolant Flow and Pressure.

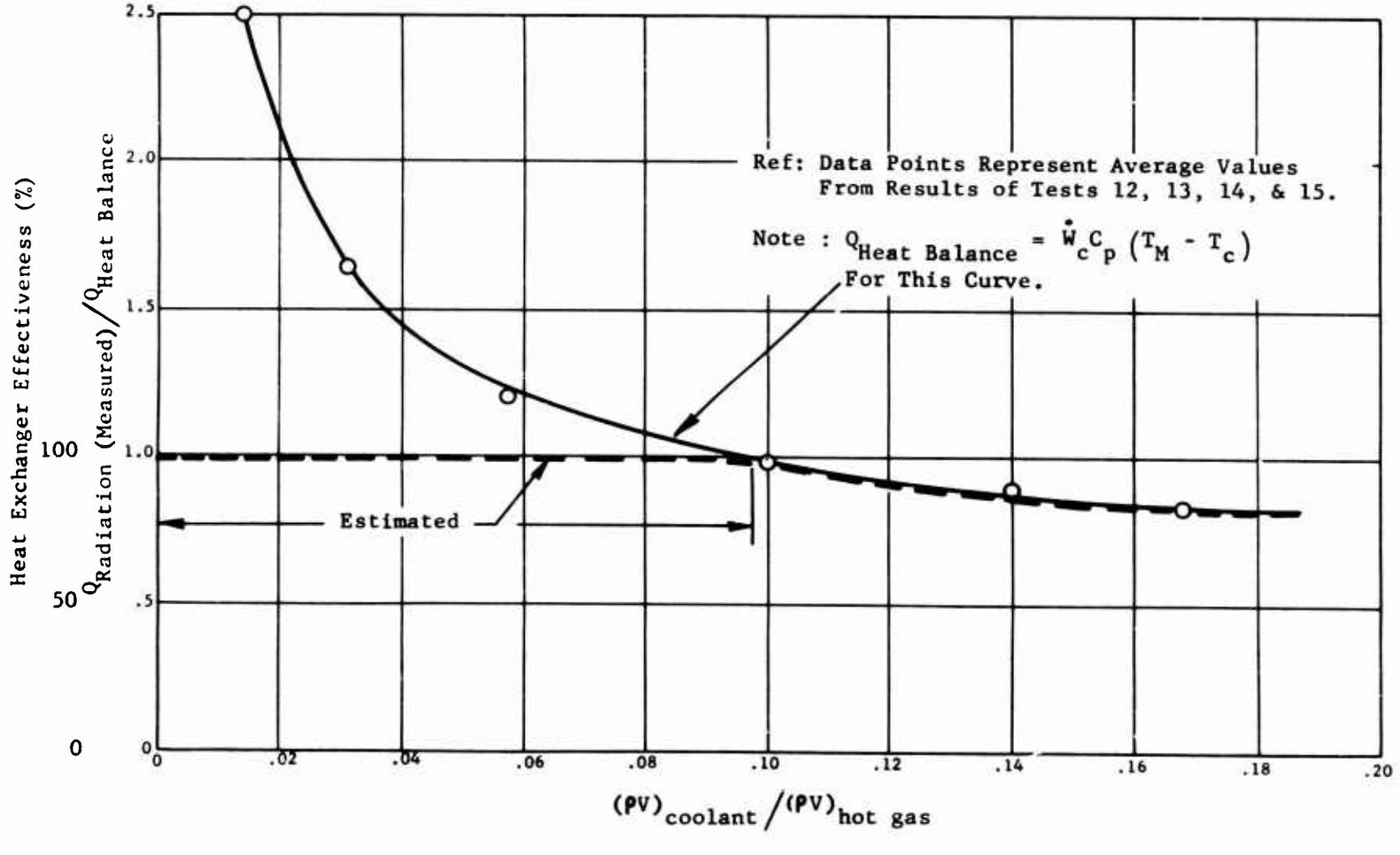

Figure 36. Transpiration Material Cooling Characteristics in a Radiation Environment.

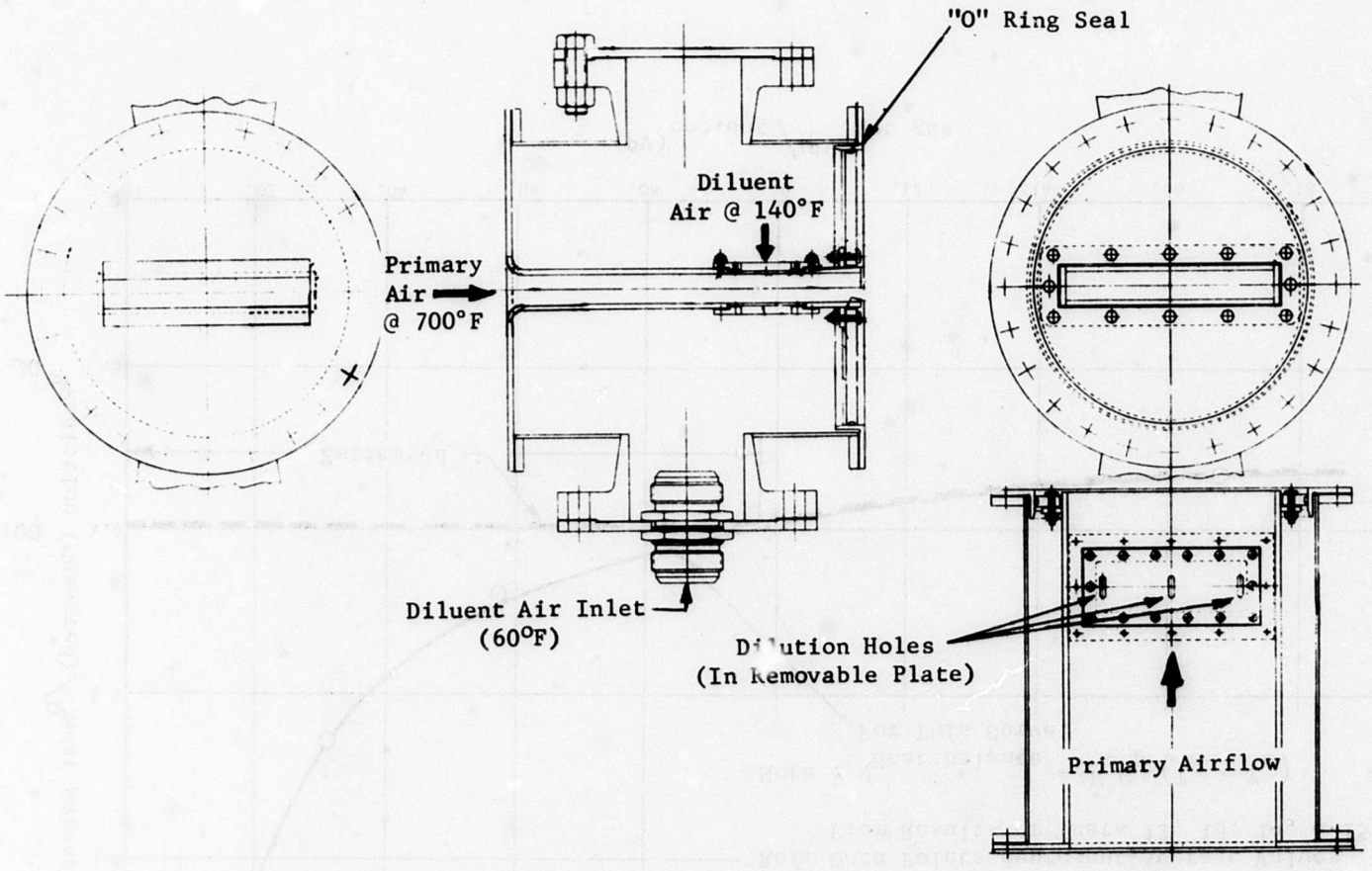

Figure 37. Rectangular Mixing Zone Duct Installed in Cross-Section Duct.

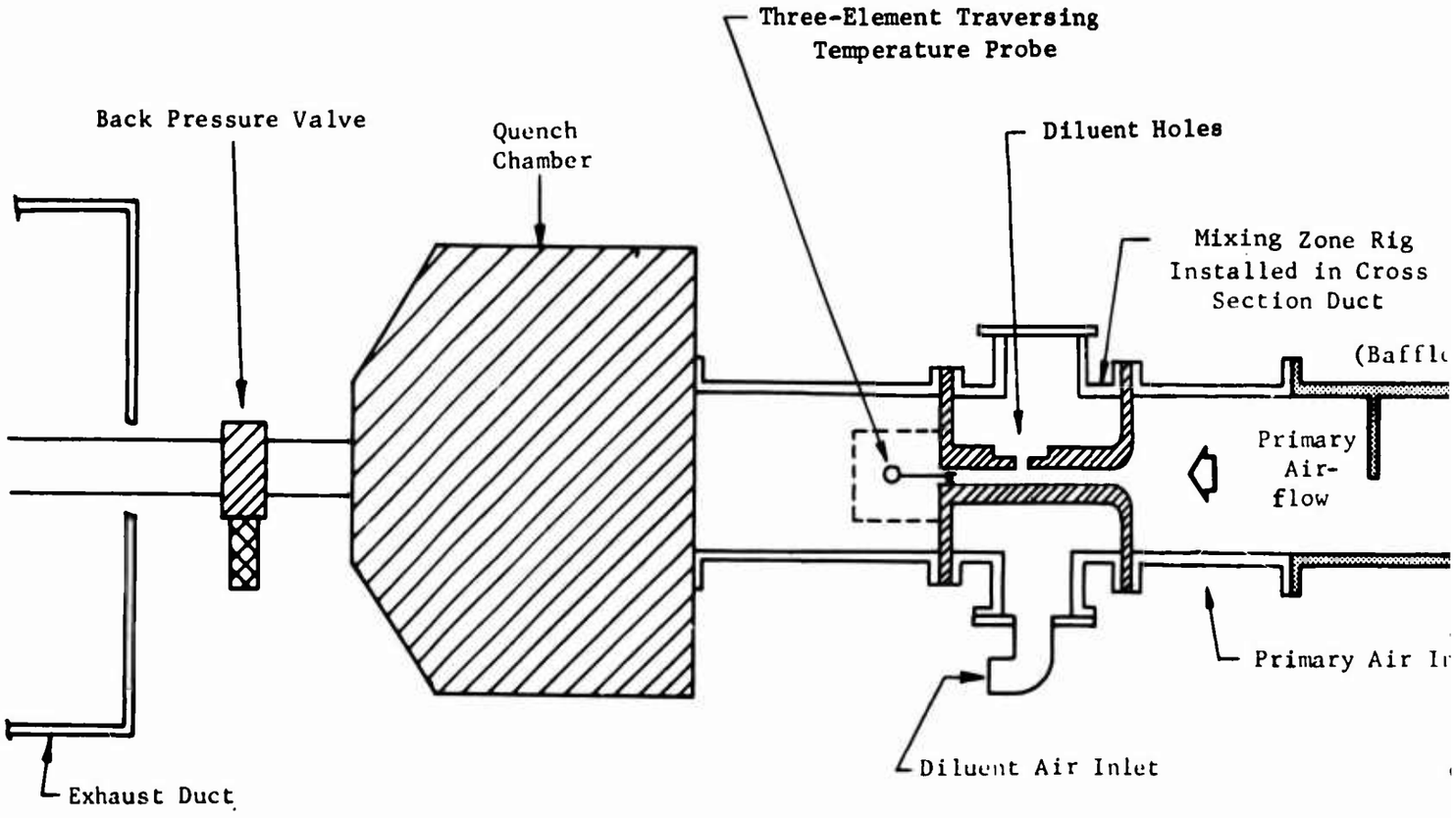

Figure 38. Mixing Zone Rig Test Stand Installation.

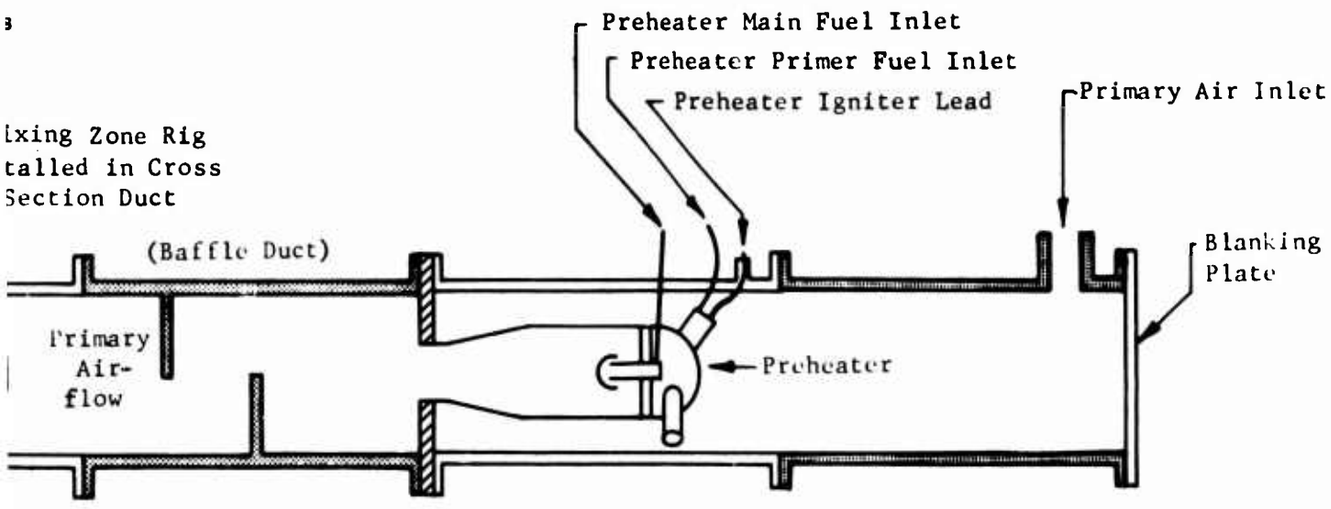

ɜ

ɪxing Zone Rig
talled in Cross
Section Duct

└ Primary Air Inlet Instrumentation Duct

B

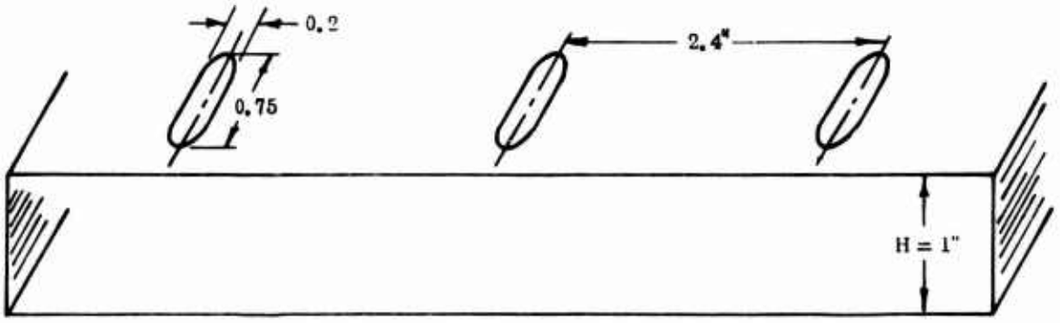

Configuration No. 1 - Simulation of 16 Slot, Single-Side Entry

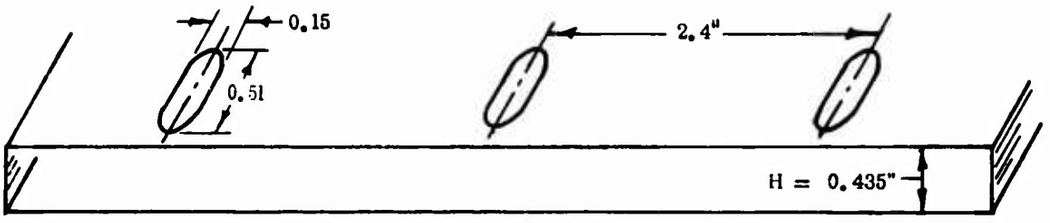

Configuration No. 2 - Simulation of 8 Slot, Single-Sided Entry

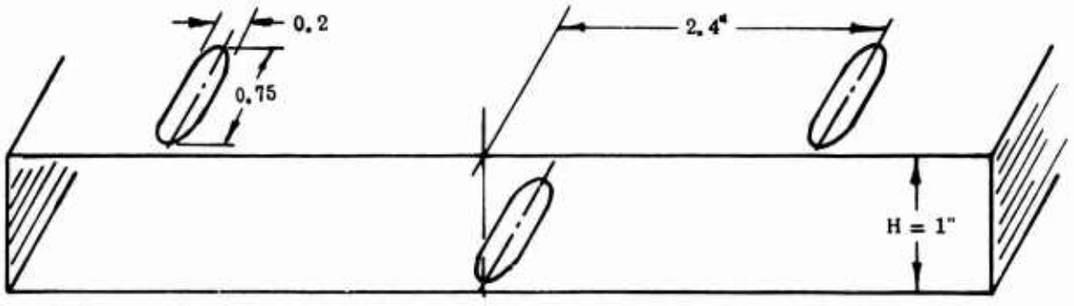

Configureation No. 3 - Simulation of 8 Slots on Each Liner.

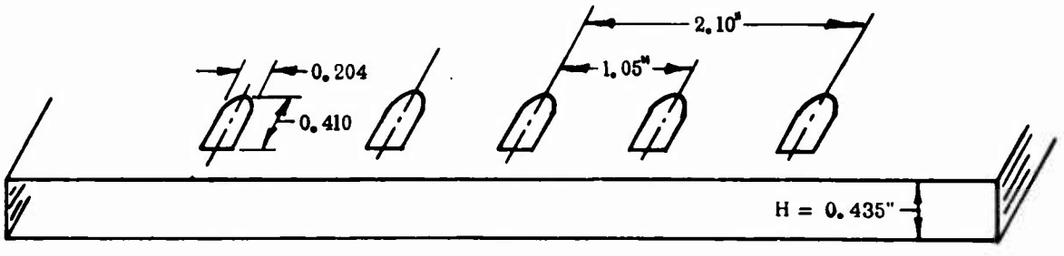

Figure 39. Basic Diluent Hole and Mixing Zone Geometries Tested.

TABLE XI. SUMMARY OF TEST POINTS RUN ON MIXING ZONE RIG

Config. Number	Point Number	Axial Plane (L/H)	W_p (lb/sec)	P_p Nominal ("HgA)	T_p (°F)	W_D (lb/sec)	ΔP_D Corrected ("Hg)	T_D (°F)	$\bar{T}_{Exit}$ (°F)
1	1	0	0.403	63	703	0.104	2.95	161	622
	2	1	0.403	63	705	0.105	3.02	160	631
	3	2.5	0.401	63	700	0.105	2.98	160	614
	4	2.5	0.359	63	700	0.105	3.00	160	595
	5	1	0.360	63	700	0.100	2.70	163	617
	6	0	0.359	63	700	0.100	2.70	163	612
	7	0	0.316	63	700	0.103	2.90	162	612
	8	1	0.314	63	700	0.102	2.90	162	601
	9	2.5	0.313	63	700	0.102	2.90	160	594
	10	2.5	0.283	63	700	0.106	3.05	160	564
	11	1	0.287	63	708	0.106	3.10	160	588
	12	0	0.287	63	708	0.106	3.10	160	597
	13	0	0.412	63	700	0.102	2.85	162	620
	14	1	0.399	63	700	0.094	2.40	155	625
	15	2.5	0.392	63	700	0.093	2.35	165	618
	16	2.5	0.390	63	700	0.113	3.50	157	603
	17	1	0.384	63	700	0.111	3.48	157	615
	18	0	0.388	63	700	0.113	3.58	157	610
	19	0	0.384	63	700	0.123	4.30	150	608
	20	1	0.400	63	700	0.122	4.10	148	602
	21	2.5	0.396	63	700	0.126	4.55	150	550
	22	2.5	0.401	63	700	0.085	1.90	170	625
	23	1	0.405	63	700	0.085	1.90	173	626
	24	0	0.384	63	700	0.081	1.74	175	618
2	1	2	0.410	163.7	691	0.112	4.6	160	613
	2	0	0.406	161.4	695	0.113	4.9	160	617
	3	1.15	0.403	160.8	700	0.105	4.6	160	616
	4	3.45	0.402	162.3	700	0.106	4.55	160	613
	5	5.75	0.404	165.3	700	0.110	3.8	160	609
	6	5.75	0.404	165.5	698	0.098	3.3	160	621
	7	3.45	0.401	166.3	700	0.098	2.1	160	621
	8	1.725	0.403	167	702	0.096	2.5	160	617
	9	-	Abort	-	-	Abort	-	-	-
	10	1.725	0.368	162.9	695	0.108	3.9	160	605
	11	3.45	0.363	163.8	705	0.107	3.5	160	604
	12	5.75	0.369	166.3	702	0.109	4.1	160	605
	13	-	Abort	-	-	Abort	-	-	-
	14	5.75	0.303	162.75	705	0.106	3.25	160	587
	15	3.45	0.302	165.5	702	0.112	1.25	160	595
	16	1.575	0.298	164	705	0.106	4.3	160	612
	17	0	0.302	166.6	702	0.109	4.15	160	617
	18	1.725	0.443	164.3	700	0.108	3.0	160	626
	19	3.45	0.453	166.75	700	0.110	2.5	160	628
	20	5.75	0.457	161.4	700	0.106	2.75	160	632

TABLE XI - Continued

Config. Number	Point Number	Axial Plane (L/H)	W_P (lb/sec)	P_P Nominal ("HgA)	T_P (°F)	W_D (lb/sec)	ΔP_D Corrected ("Hg)	T_D (°F)	$\bar{T}_{Exit}$ (°F)
3	1	1	0.405	63.5	700	0.106	3.06	194	616
	2	2.5	0.399	63.5	700	0.105	2.98	194	608
	3	0	0.400	63.5	700	0.104	2.89	194	617
	4	0	0.361	63.5	700	0.104	2.89	194	615
	5	1	0.365	63.5	700	0.105	2.98	194	621
	6	2.5	0.365	63.5	700	0.105	3.03	194	608
	7	2.5	0.313	63.5	700	0.104	2.89	194	596
	8	1	0.321	63.5	700	0.104	2.93	194	620
	9	0	0.324	63.5	700	0.105	2.98	194	618
	10	0	0.401	63.5	700	0.100	2.70	194	617
	11	1	0.404	63.5	700	0.100	2.70	194	622
	12	2.5	0.405	63.5	700	0.100	2.72	194	621
	13	0	0.383	63.5	700	0.113	3.5	165	609
	14	1	0.383	63.5	700	0.112	3.47	207	617
	15	2.5	0.380	63.5	700	0.112	3.43	205	601
	16	2.5	0.388	63.5	700	0.124	4.30	200	584
	17	1	0.391	63.5	700	0.125	4.37	195	612
	18	0	0.392	63.5	700	0.126	4.50	198	619
	19	1	0.392	63.5	700	0.125	4.50	210	624
	20	2.5	0.387	63.5	700	0.123	4.23	195	596
	21	2.5	0.389	63.5	700	0.083	1.80	215	595
	22	1	0.390	63.5	700	0.083	1.80	222	628
	23	0	0.389	63.5	700	0.083	1.795	220	619
	24	0	0.277	63.5	700	0.104	2.89	202	618
	25	1	0.282	63.5	700	0.105	2.98	198	609
	26	2.5	0.280	63.5	700	0.104	2.89	198	581
4	1	0.58	0.234	160.70	705	0.134	4.8	149	524
	2	-	Abort	-	-	Abort	-	-	-
	3	2.30	0.240	160.70	713	0.139	5.2	134	494
	4	4.03	0.240	160.75	703	0.139	5.2	139	479
	5	5.75	0.240	159.20	720	0.138	5.2	137	477
	6	5.75	0.240	159.80	705	0.147	5.9	140	459
	7	4.03	0.233	161.90	703	0.145	5.7	132	448
	8	2.30	0.236	160.30	715	0.147	5.9	144	479
	9	0.58	0.235	160.50	715	0.146	5.8	146	498
	10	0.58	0.242	162.45	700	0.146	6.3	144	488
	11	2.30	0.240	162.40	705	0.155	6.3	146	472
	12	4.03	0.245	163.95	695	0.154	6.4	145	471
	13	4.03	0.245	159.85	710	0.166	6.6	146	448
	14	2.30	0.245	159.98	700	0.166	6.6	146	476
	15	0.58	0.239	159.40	715	0.164	6.3	132	462
	16	2.30	0.238	146.00	700	0.075	1.57	165	548
	17	4.03	0.238	145.95	700	0.075	1.57	170	548
	18	-	Abort	-	-	Abort	-	-	-

TABLE XII. MIXING ZONE RIG - SUMMARY OF TEST DATA

Config. No.	Point Number	Axial Plane (L/H)	Diluent-To-Primary Momentum Ratio $(MV)_D/(MV)_P$	Diluent-To-Primary Velocity Ratio (V_D/V_P)	Mean Local to Overall Average Temp. Ratio $\bar{T}_L/\bar{T}_{Exit}$ - (°R/°R)			Max. Local to Overall Average Temp. Ratio $T_{Max.}/\bar{T}_{Exit}$ (°R/°R)
					Tip	Mean	Hub	
1	1	0	0.7142	2.763	1.061	1.000	0.938	1.095
	2	1	0.7286	2.797	1.061	1.004	0.934	1.078
	3	2.5	0.7268	2.789	1.019	0.995	0.985	1.055
	4	2.5	0.9119	3.130	1.014	0.996	0.988	1.085
	5	1	0.822	2.963	1.052	1.002	0.945	1.083
	6	0	0.8286	2.972	1.064	1.007	0.927	1.083
	7	0	1.1429	3.520	1.067	1.008	0.924	1.091
	8	1	1.1499	3.536	1.040	1.003	0.956	1.080
	9	2.5	1.1633	3.557	1.0040	1.0015	0.9943	1.082
	10	2.5	1.4905	3.999	0.9908	1.0008	1.0083	1.095
	11	1	1.4710	3.972	1.0245	1.0099	0.9654	1.098
	12	0	1.4775	3.982	1.0718	1.0036	0.9244	1.098
	13	0	0.6565	2.662	1.0553	0.9995	0.9450	1.078
	14	1	0.5938	2.520	1.0615	1.0057	0.9327	1.074
	15	2.5	0.6028	2.542	1.0196	0.9960	0.9842	1.075
	16	2.5	0.8995	3.110	1.0103	0.9966	0.9929	1.083
	17	1	0.9143	3.152	1.0518	1.0014	0.9466	1.078
	18	0	0.9171	3.144	1.0688	1.0072	0.9239	1.083
	19	0	1.1232	3.504	1.0728	1.0065	0.9205	1.095
	20	1	1.0146	3,326	1.0458	1.0024	0.9516	1.098
	21	2.5	1.1094	3.489	1.0055	0.9993	0.9950	1.080
	22	2.5	0.4711	2.230	1.0461	0.9913	0.9625	1.068
	23	1	0.4642	2.211	1.0568	1.0054	0.9376	1.075
	24	0	0.4710	2.234	1.0467	0.9861	0.9671	1.075
2	1	2.3	0.649	2.38	1.0392	1.002	0.9588	1.073
	2	0	0.692	2.48	1.0682	1.0071	0.9248	1.091
	3	1.15	0.634	2.423	1.0637	1.0048	0.9314	1.088
	4	3.45	0.638	2.42	1.033	1.0001	0.9670	1.064
	5	5.75	0.603	2.197	1.0139	0.9991	0.9870	1.053
	6	5.75	0.498	2.047	1.0212	0.9989	0.9799	1.046

TABLE XII - Continued

Config. No.	Point Number	Axial Plane (L/H)	Diluent-To-Primary Momentum Ratio $(MV)_D/(MV)_P$	Diluent-To-Primary Velocity Ratio (V_D/V_P)	Mean Local to Overall Average Temp. Ratio $\bar{T}_L/\bar{T}_{Exit}$ - (°R/°R)			Max. Local to Overall Average Temp. Ratio $T_{Max.}/\bar{T}_{Exit}$ (°R/°R)
					Tip	Mean	Hub	
	7	3.45	0.3975	1.638	1.0406	0.9965	0.9629	1.072
	8	1.725	0.427	1.783	1.0526	1.0051	0.9423	1.086
	10	1.825	0.717	2.44	1.0522	1.0018	0.9460	1.080
	11	3.45	0.691	2.34	1.0293	1.0009	0.9697	1.069
	12	5.75	0.738	2.49	1.0082	1.0024	0.9894	1.060
	14	5.75	0.950	2.704	0.9963	0.9994	1.0043	1.080
	15	3.45	0.625	1.686	1.0078	1.0033	0.9888	1.070
	16	1.725	1.130	3.170	1.0360	1.0050	0.9590	1.073
	17	0	1.113	3.070	1.0745	1.0049	0.9206	1.105
	18	1.725	0.435	1.776	1.0616	1.0038	0.9346	1.095
	19	3.45	0.384	1.588	1.0368	0.9985	0.9647	1.060
	20	5.75	0.384	1.757	1.0239	0.9970	0.9791	1.054
3	1	1	0.676	2.59	0.9825	1.011	1.0064	1.082
	2	2.5	0.679	2.59	0.9951	1.0099	0.9951	1.076
	3	0	0.660	2.55	0.9811	1.0018	1.0170	1.086
	4	0	0.809	2.82	0.9801	1.0100	1.0097	1.088
	5	1	0.815	2.83	0.9823	1.0242	0.9933	1.073
	6	2.5	0.822	2.85	0.9963	1.0069	0.9967	1.077
	7	2.5	1.076	3.25	0.9972	1.0027	1.0000	1.079
	8	1	1.035	3.19	0.9894	1.0223	0.9882	1.078
	9	0	1.029	3.19	0.9758	1.0185	1.0056	1.081
	10	0	0.608	2.45	0.9842	0.9971	1.0186	1.086
	11	1	0.602	2.43	0.9723	1.0139	1.0137	1.072
	12	2.5	0.607	2.45	0.9922	1.0095	0.9981	1.068
	13	0	0.86	2.92	0.9813	1.0089	1.0096	1.089
	14	1	0.853	2.91	0.9793	1.0236	0.9969	1.072
	15	2.5	0.858	2.92	1.000	1.0044	0.9955	1.083
	16	2.5	1.021	3.20	0.9977	1.0045	0.9977	1.072
	17	1	1.023	3.21	0.9876	1.0234	0.9888	1.073

TABLE XII. - Continued

Config. No.	Point Number	Axial Plane (L/H)	Diluent-To-Primary Momentum Ratio $(MV)_D/(MV)_P$	Diluent-To-Primary Velocity Ratio (V_D/V_P)	Mean Local to Overall Average Temp. Ratio $\bar{T}_L/\bar{T}_{Exit}$ - (°R/°R) Tip	Mean	Hub	Max. Local to Overall Average Temp. Ratio $T_{Max.}/\bar{T}_{Exit}$ (°R/°R)
	18	0	1.038	3.24	0.9826	1.0146	1.0026	1.080
	19	1	1.033	3.24	0.9916	1.0227	0.9855	1.075
	20	2.5	0.440	2.07	0.9831	1.0110	1.0057	1.055
	22	1	0.438	2.06	0.9803	1.0074	1.0122	1.075
	23	0	0.443	2.07	0.9896	0.9879	1.0223	1.080
	24	0	1.376	3.67	0.9782	1.0185	1.0031	1.085
	25	1	1.358	3.66	0.9894	1.0237	0.9867	1.076
	26	2.5	1.351	3.64	0.9868	1.0035	1.0096	1.059
4	1	0.575	3.35	4.24	0.9890	1.0205	0.9903	1.1532
	3	2.30	3.41	4.21	0.9860	1.0025	1.0114	1.1528
	4	4.00	3.45	4.27	0.9896	1.0005	1.0098	1.0863
	5	5.70	3.37	4.18	0.9969	1.0008	1.0022	1.0887
	6	5.70	3.89	4.53	0.9971	1.0008	1.0020	1.0664
	7	4.00	3.93	4.55	0.9974	1.0009	1.0015	1.0241
	8	2.30	3.91	4.54	0.9856	1.0052	1.0091	1.1717
	9	0.50	3.90	4.53	0.9724	1.0092	1.0183	1.1900
	10	0.50	4.12	4.66	0.9683	1.0113	1.0202	1.1812
	11	2.30	4.14	4.66	0.9882	1.0068	1.0048	1.1534
	12	4.00	4.11	4.68	0.9980	1.0002	1.0016	1.0743
	13	4.00	4.34	4.62	0.9992	1.0009	0.9998	1.1122
	14	2.30	4.37	4.66	0.9888	1.0065	1.0045	1.1542
	15	0.50	4.33	4.56	0.9707	1.0049	1.0243	1.1926
	16	2.30	1.01	2.31	1.0320	1.0080	0.9599	1.1306
	17	4.00	1.01	2.32	0.9851	1.0024	1.0123	1.1116

TABLE XIII. MIXING EFFICIENCIES FOR VARYING DOWNSTREAM DISTANCE TO DUCT HEIGHT RATIOS

Configuration	Test Point	L/H	σ	T_{Max} (°F)	$\left(\frac{\sigma}{T_P - \overline{T}_{Exit}}\right)^*$	$\left(\frac{T_{Max} - \overline{T}_{Exit}}{T_P - \overline{T}_{Exit}}\right)^{**}$
1	17	1.0	41.9	690	0.492	0.88
	18	0	65.4	700	0.735	1.0
	19	0	55.6	710	0.605	1.0
	20	1.0	50.5	705	0.515	1.0
	21	2.5	46.9	675	0.426	0.78
2	14	5.75	46	670	0.394	0.80
	16	1.73	48	680	0.515	0.73
	17	0	44	700	0.515	1.00
3	16	2.5	28.8	670	0.25	0.74
	17	1.0	47.4	690	0.537	0.72
	18	0	82.1	700	0.97	1.0
4	16	2.30	68.4	680	0.44	0.84
	17	4.03	51.1	660	0.33	0.71

* Standard Deviation Factor (SDF)

** Maximum Temperature Factor (MTF)

TABLE XIV. MIXING EFFICIENCIES FOR VARYING PRIMARY TO DILUENT AIR MOMENTUM RATIOS

Configuration	Test Point	$(MV)_D/(MV)_P$	σ	$T_{Max.}$ (°F)	$\frac{\sigma}{T_P - \bar{T}_{Exit}}$	$\frac{T_{Max} - \bar{T}_{Exit}}{T_P - \bar{T}_{Exit}}$
Mixing Zone	3	0.727	44.9	690	0.522	0.89
1	10	1.491	41.9	690	0.329	0.75
	21	1.109	46.9	675	0.426	0.78
2	1	0.649	31.0	680	0.392	0.86
	16	1.13	48.0	670	0.515	0.73
	18	1.12	48.9	680	0.515	1.00
	19	0.38	28.4	695	0.390	0.93
3	16	1.021	28.8	670	0.25	0.74
4	3	3.41	40	640	0.18	0.67
	14	4.37	41	620	0.18	0.64
	16	1.01	68.4	680	0.44	0.71
Primary Zone	184	2.26	296	1475	0.28	0.71
	185	2.25	434	2080	0.21	0.49
4.1 @ 5 Atm.	187	3.24	612	2300	0.26	0.46
	190	2.36	485	2190	0.23	0.50
	191	6.46	209	1205	0.14	0.40
	193	9.5	163	1000	0.08	0.30
4.2 @ 16 Atm.	215	1.35	535	2820	0.49	1.03
	216	2.09	446	2800	0.64	1.27
4.2 @ 5 Atm.	221	1.24	223	1930	0.35	0.69
	222	1.13	507	2730	0.33	0.97

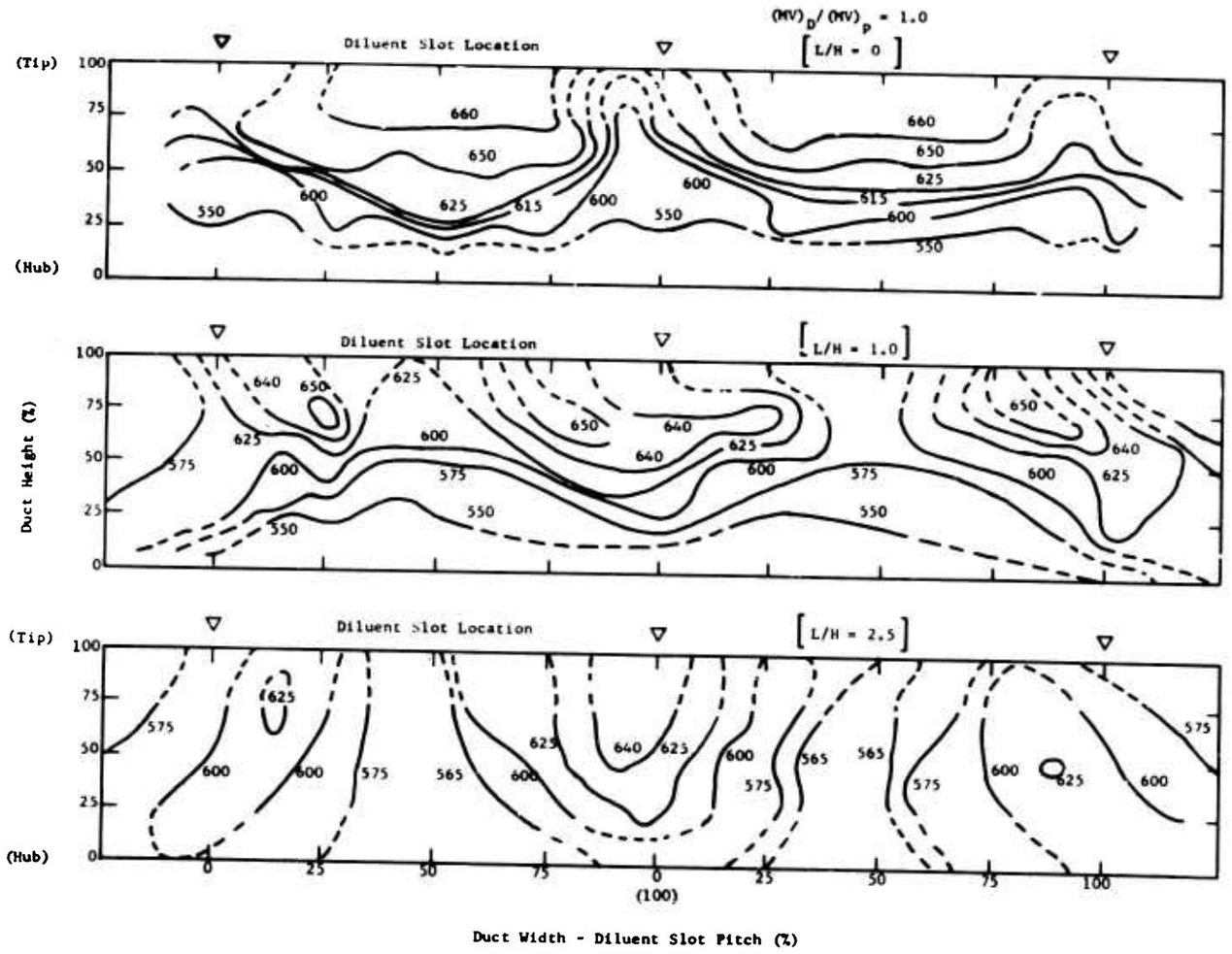

Figure 40. Typical Isotherm Contour Maps for Mixing Zone Configuration 1.

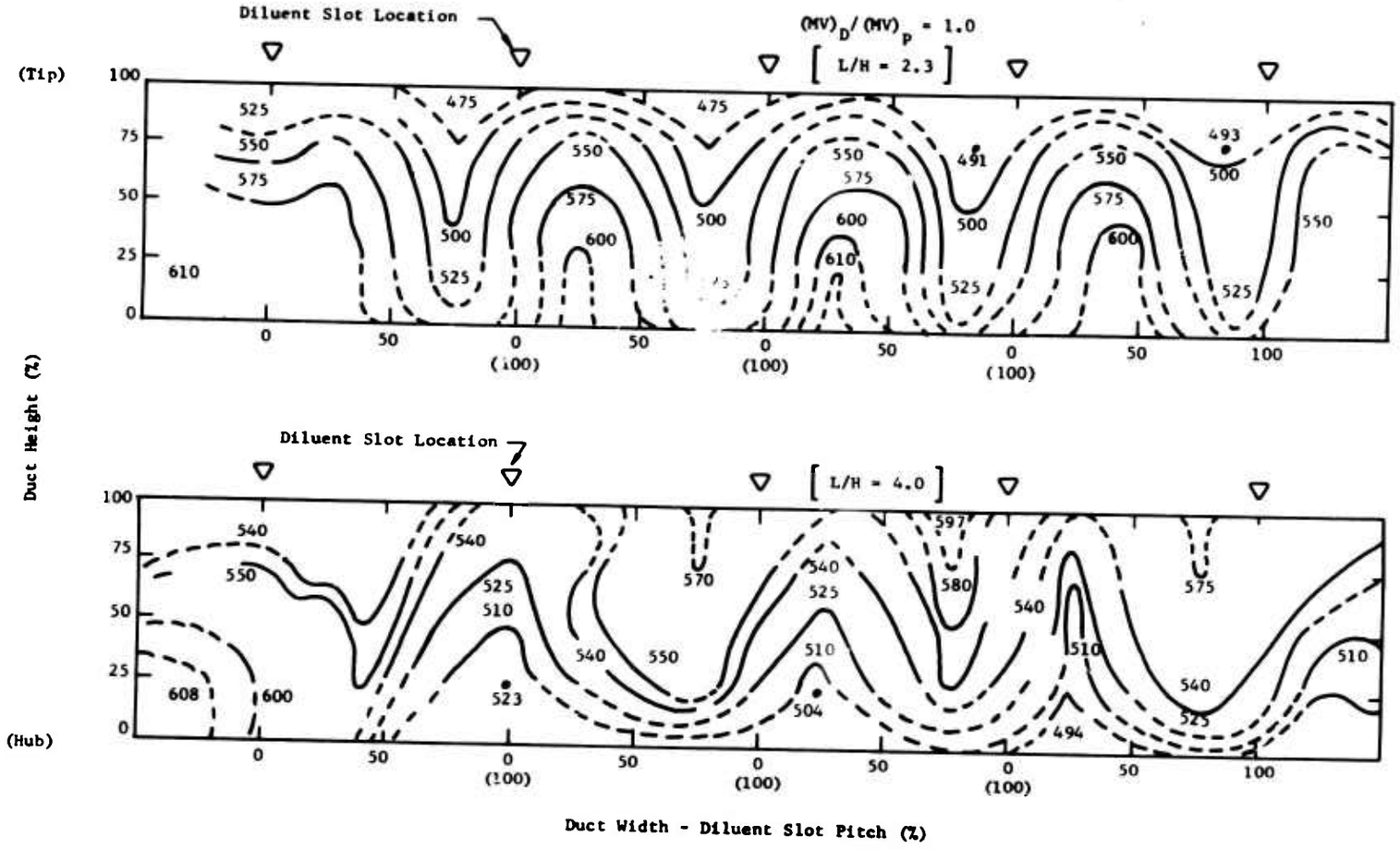

Figure 41. Typical Isotherm Contour Maps for Mixing Zone Configuration 4.

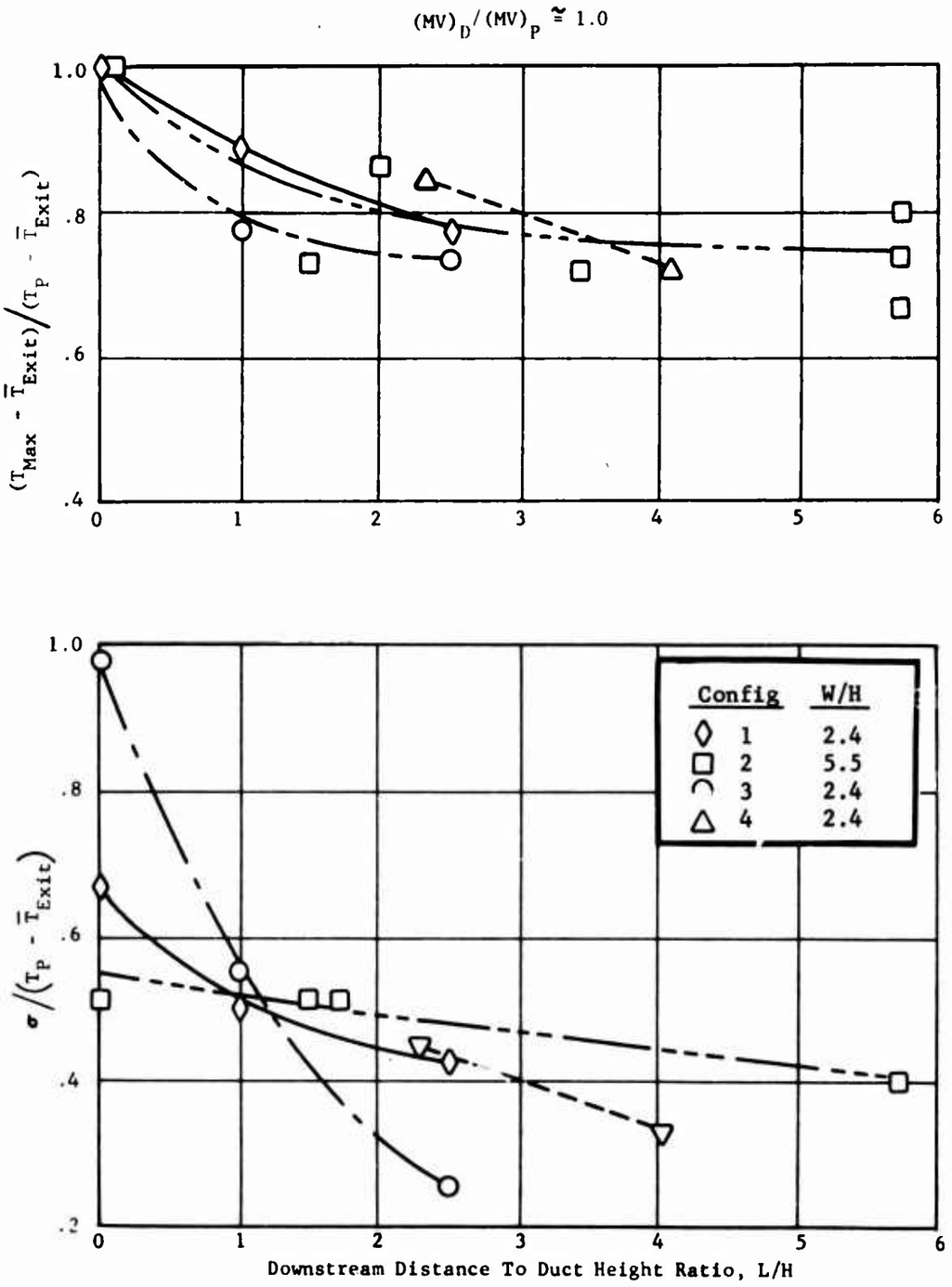

Figure 42. Mixing Efficiency as a Function of Downstream Distance to Duct Height Ratio.

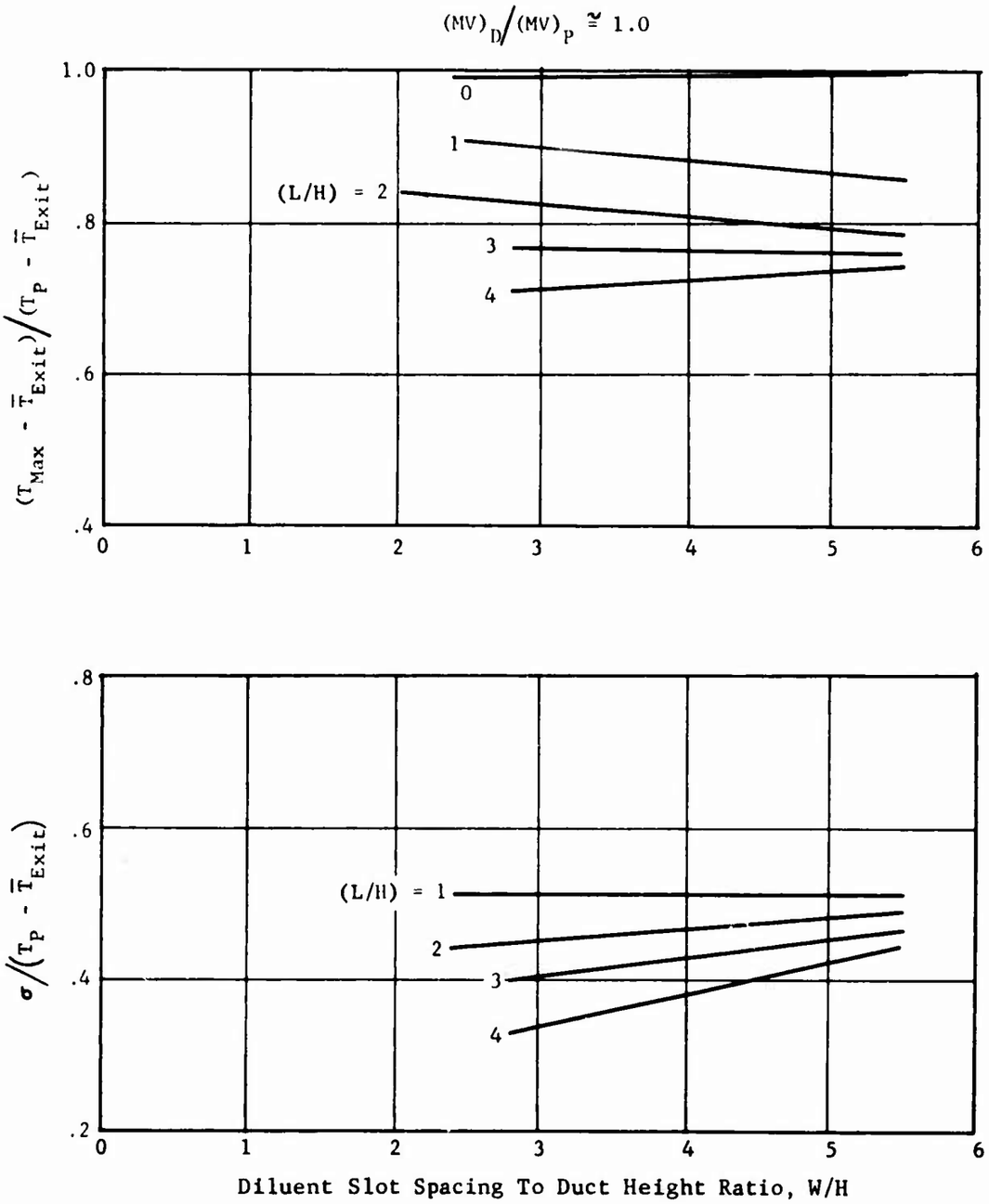

Figure 43. Mixing Efficiency as a Function of Diluent Hole Spacing to Duct Height Ratio.

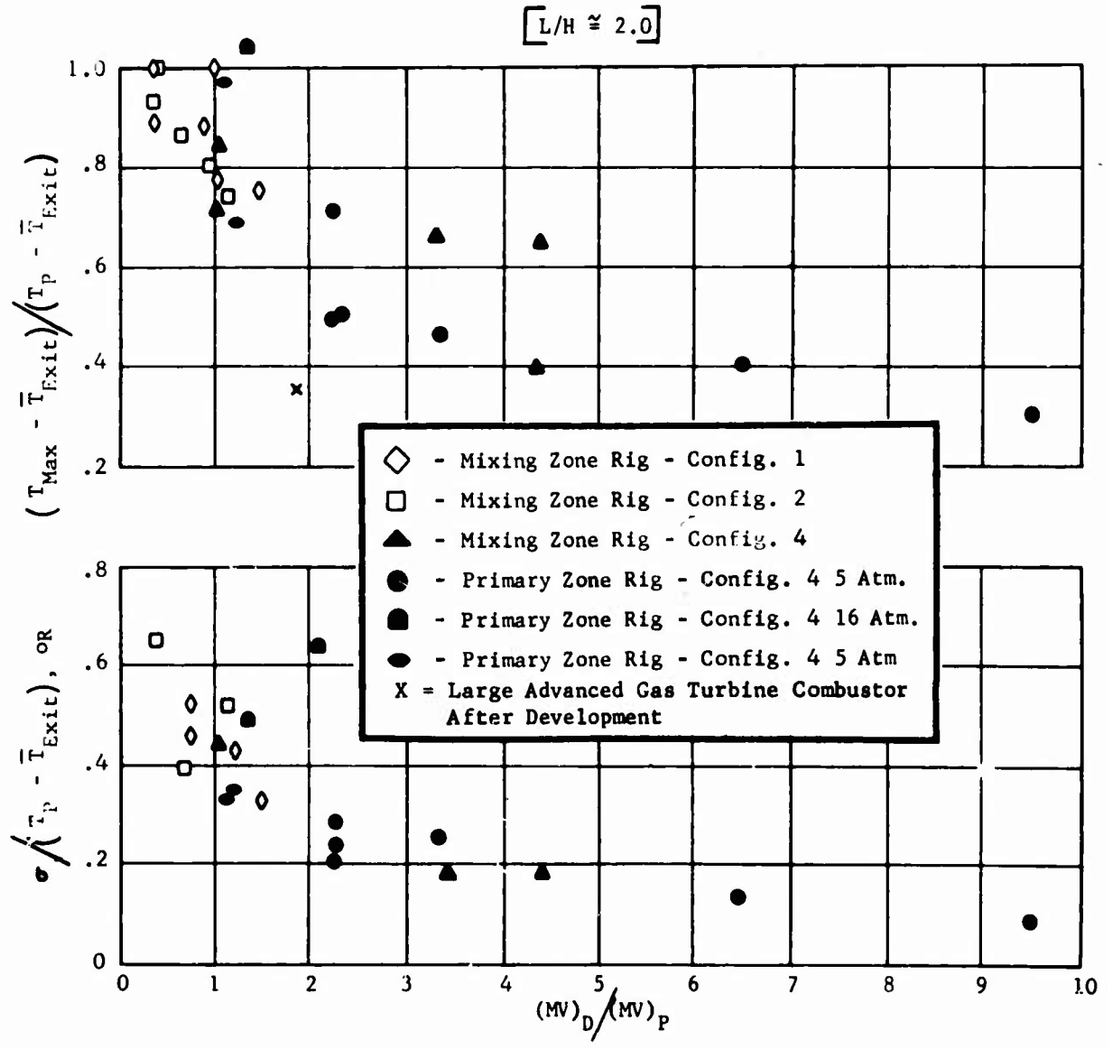

Figure 44. Mixing Efficiency as a Function of Diluent to Primary Air Stream Momentum Ratio.

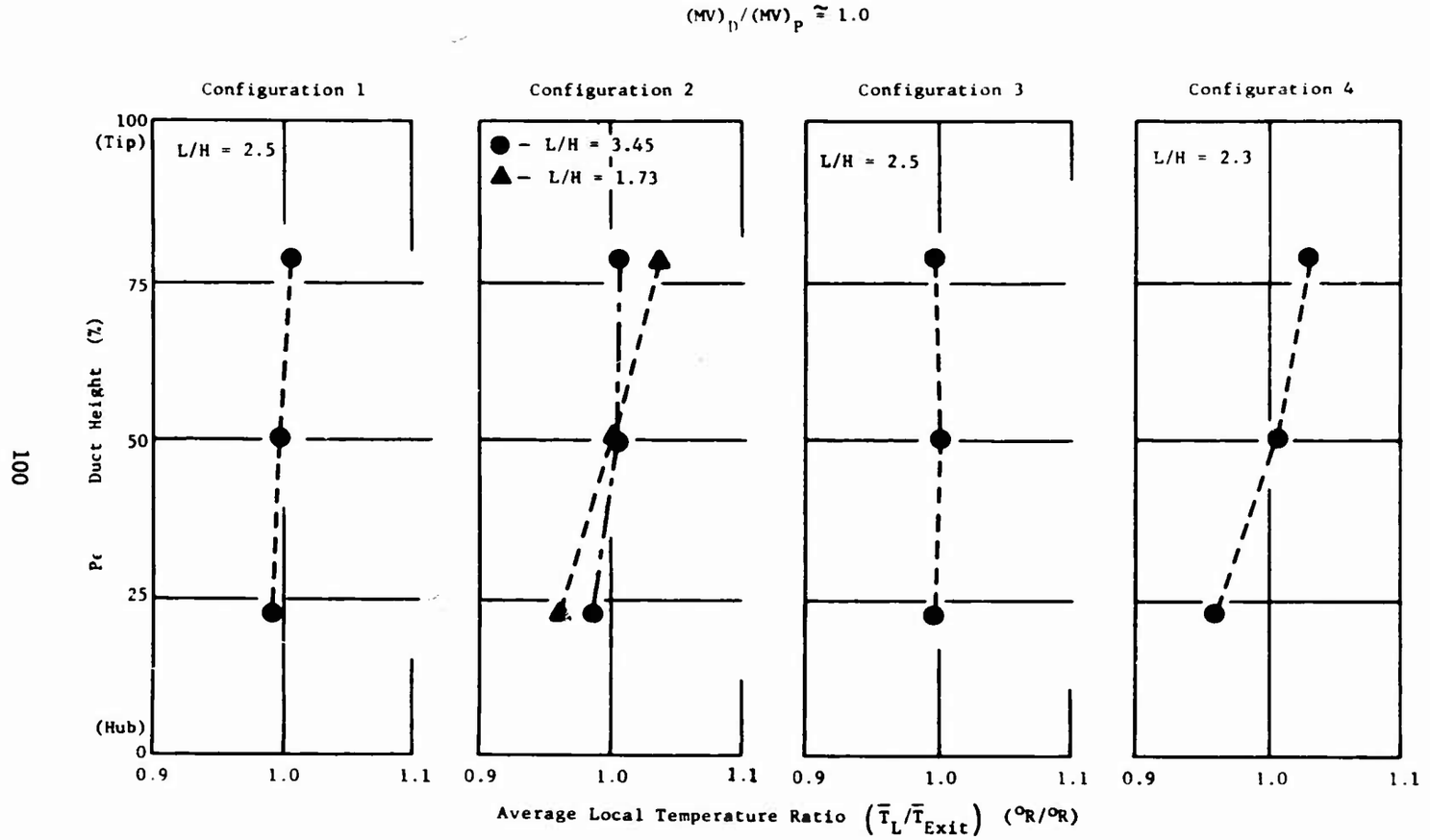

Figure 45. Typical Mean Temperature Profiles For Mixing Zone Configurations Tested.

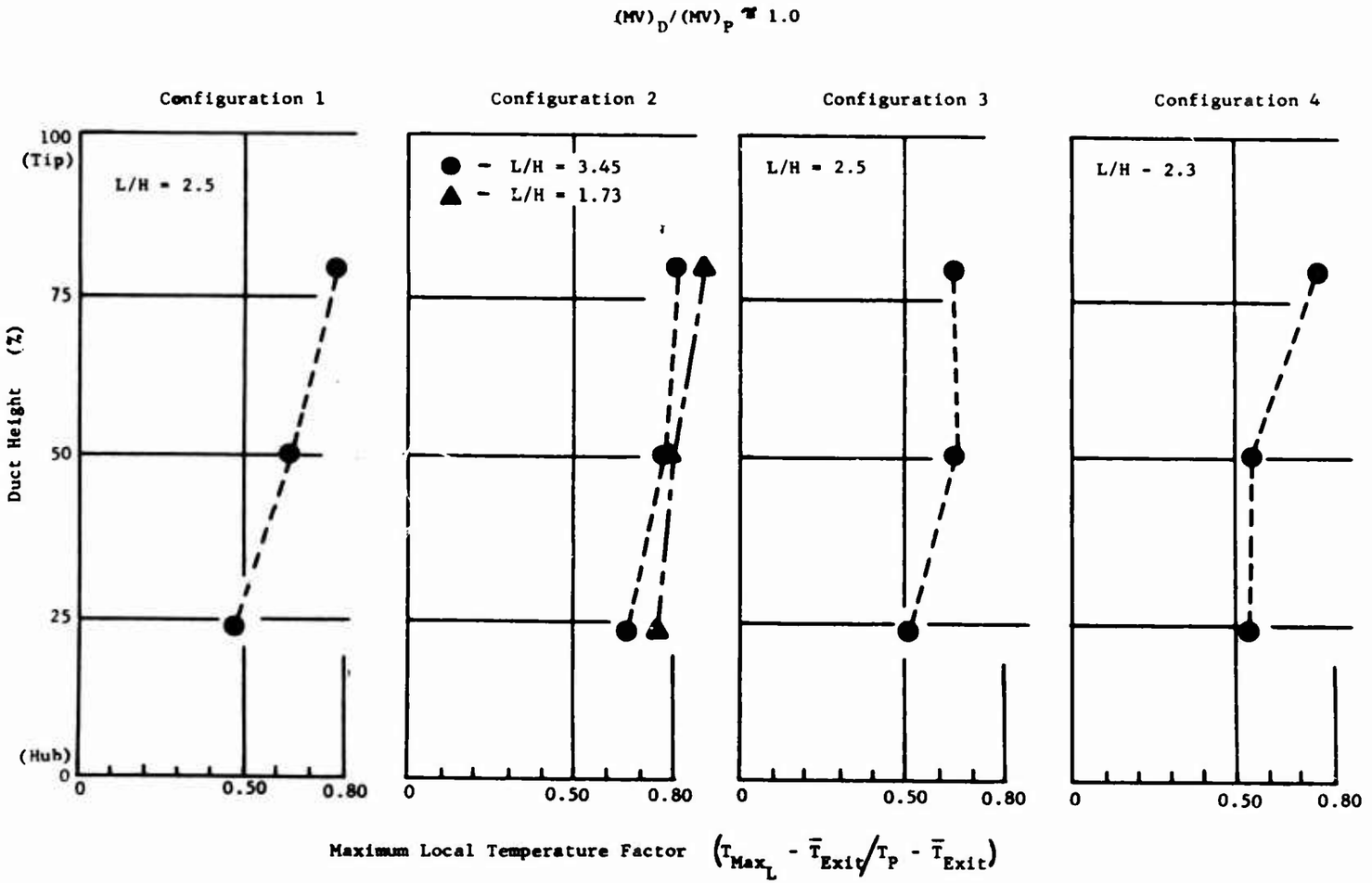

Figure 46. Typical Maximum Temperature Profiles for Mixing Zone Configurations Tested.

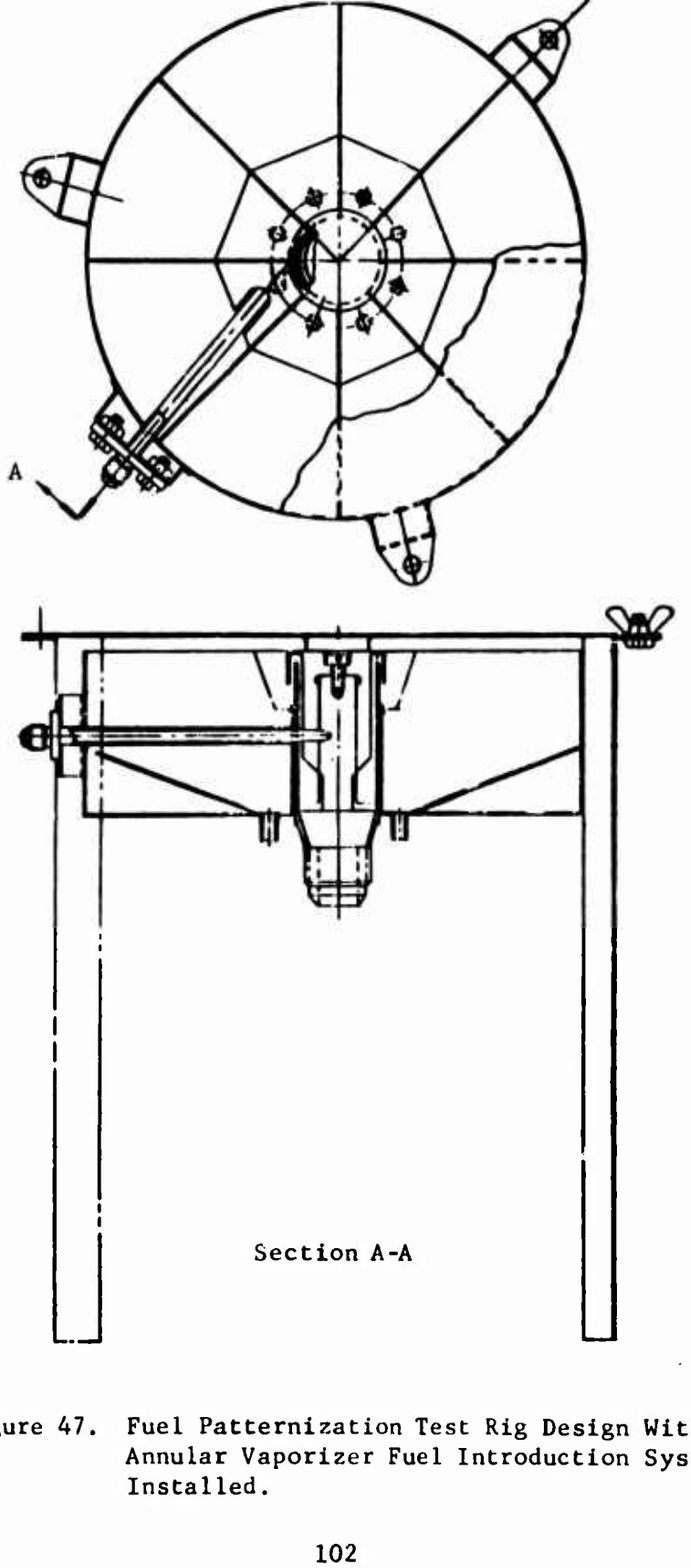

Figure 47. Fuel Patternization Test Rig Design With Annular Vaporizer Fuel Introduction System Installed.

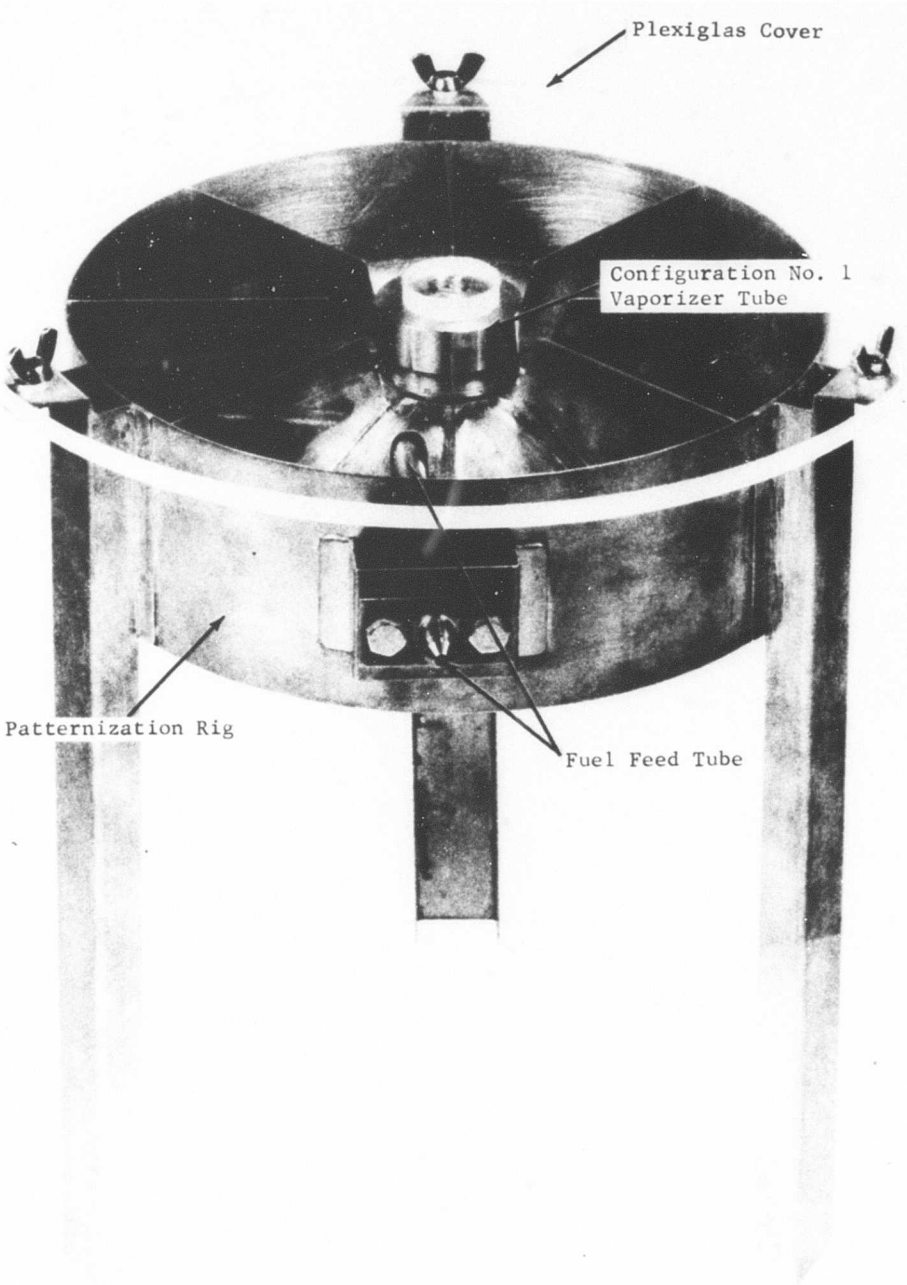

Figure 48. Photograph of Fuel Patternization Rig.

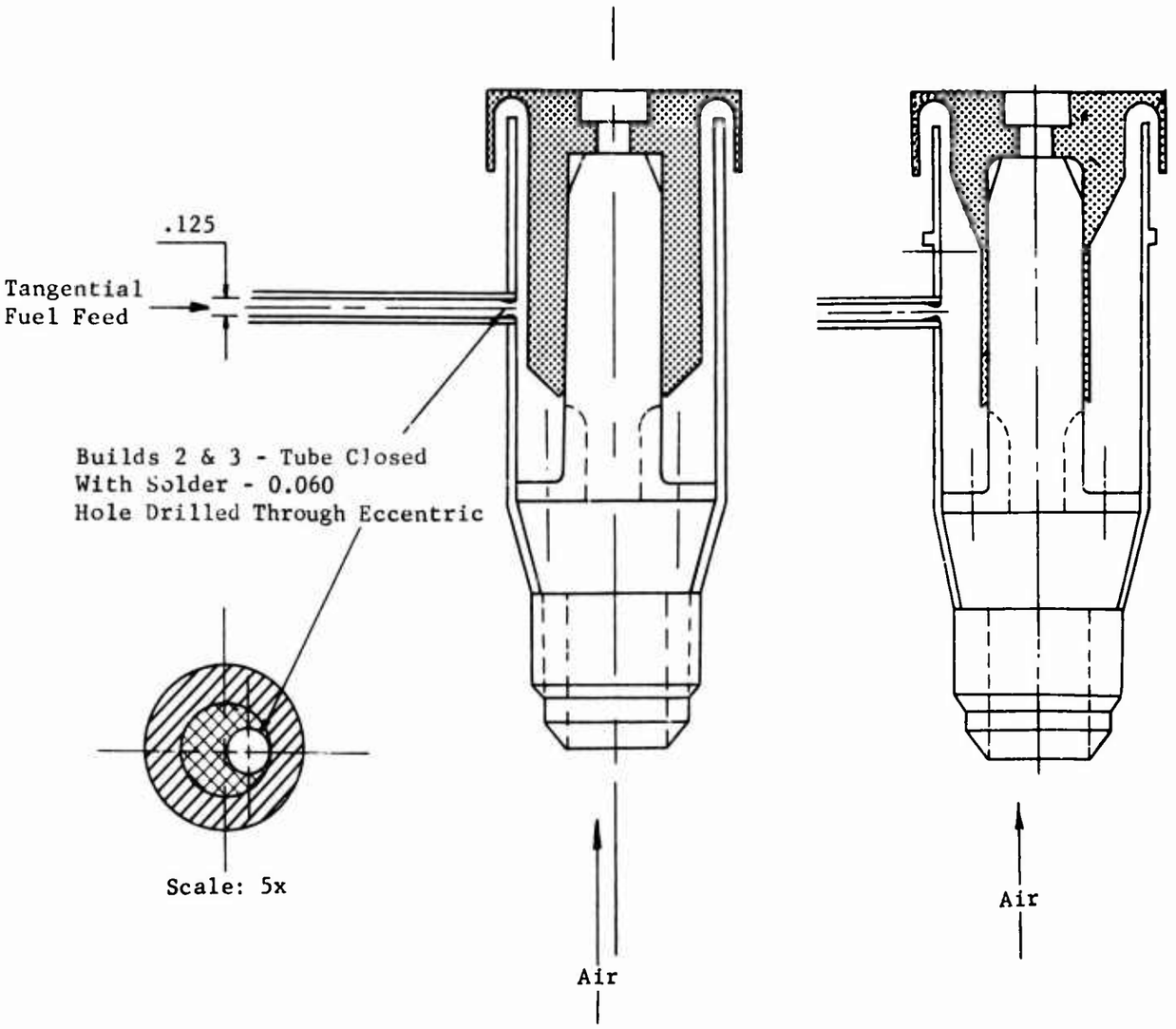

Figure 49. Fuel Feed Systems and Modifications Tested for Annular Vaporizer Fuel Introduction System.

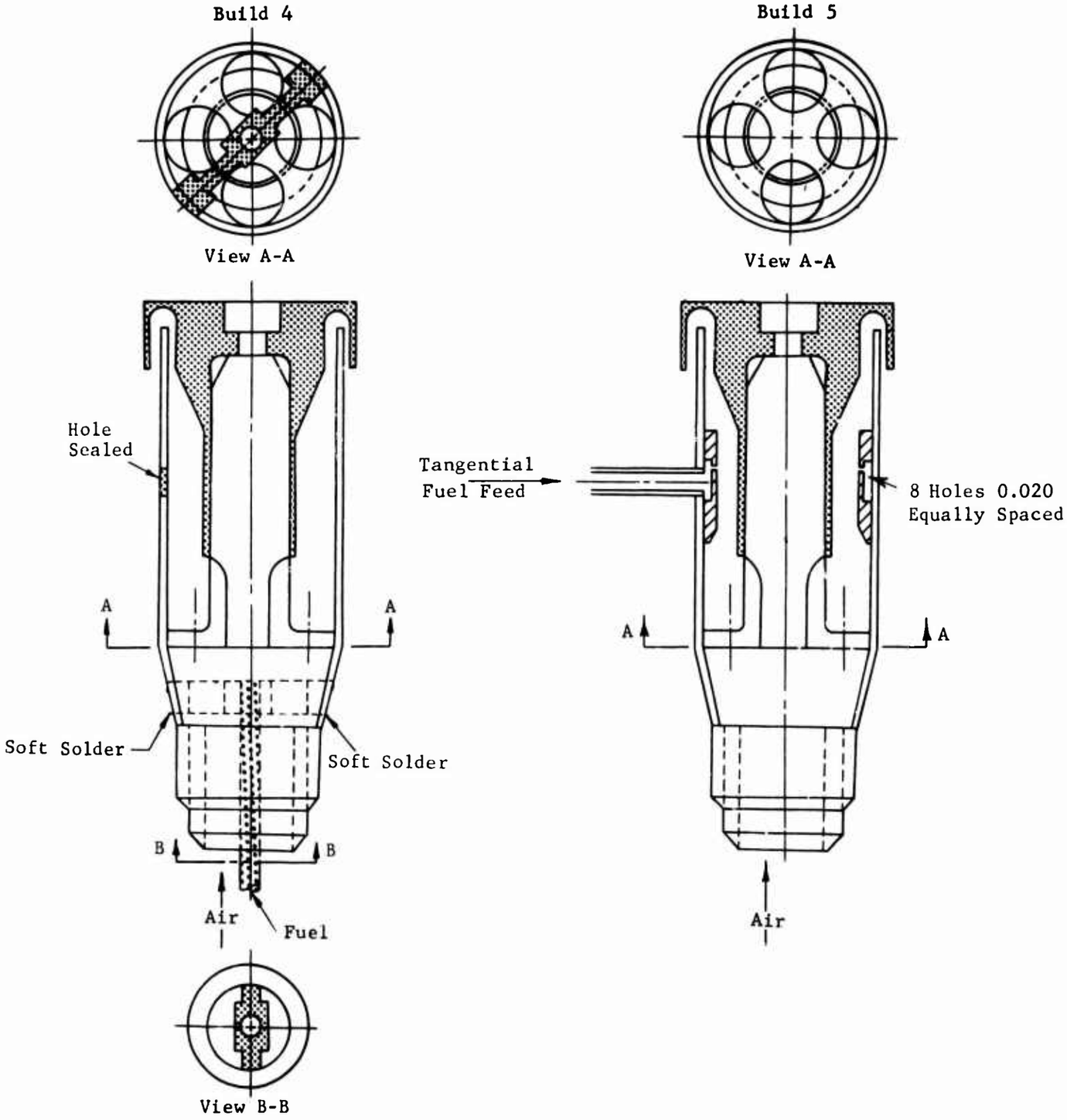
Build 4
View A-A
Hole
Sealed
A
A
Soft Solder
Soft Solder
B
B
Air
Fuel
View B-B
Build 5
View A-A
Tangential
Fuel Feed
8 Holes 0.020
Equally Spaced
A
A
Air

B

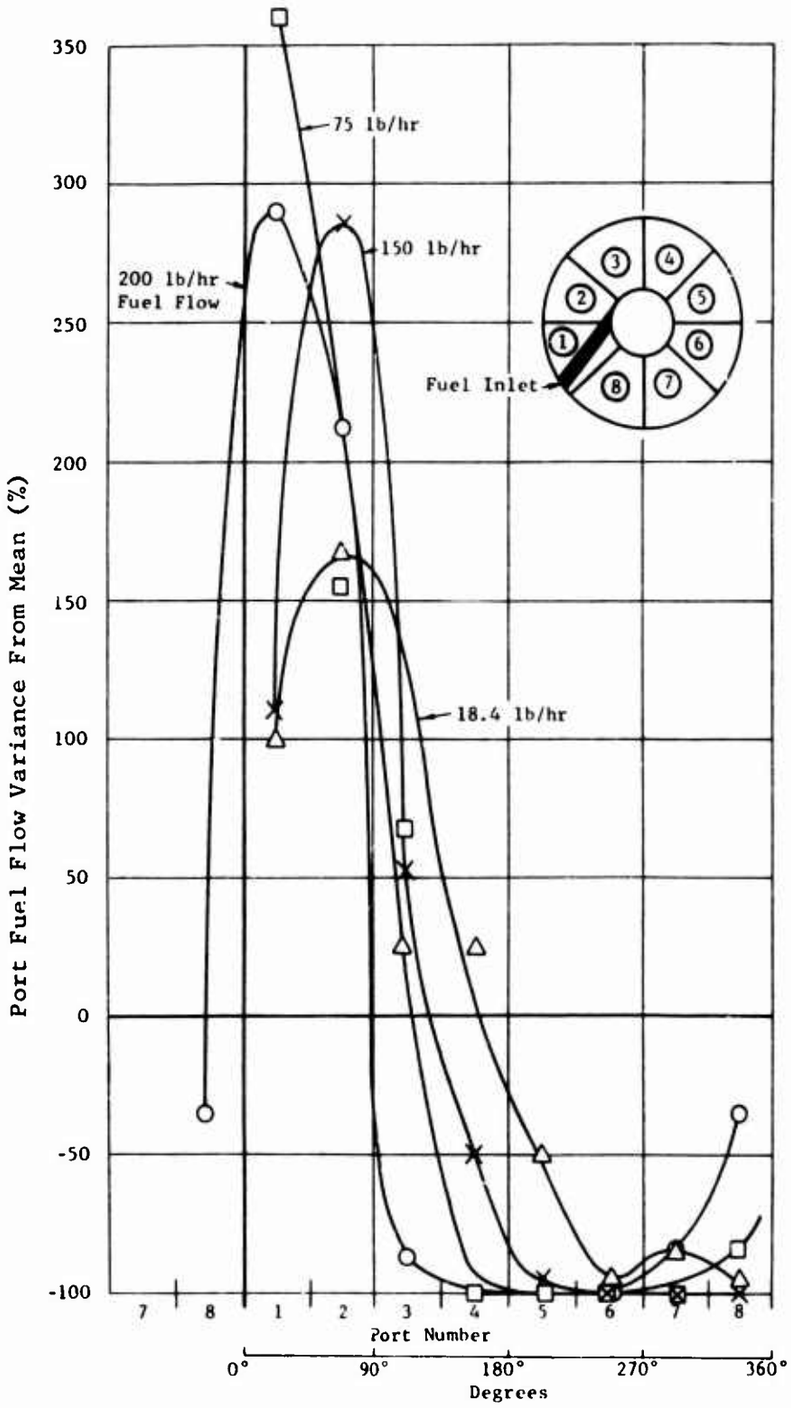

Figure 50. Fuel Patternization of Build 1 Single Point Tangential Fuel Feed for Varying Fuel Flows at 75 Percent Rated Airflow in Annular Vaporizer Fuel Introduction System.

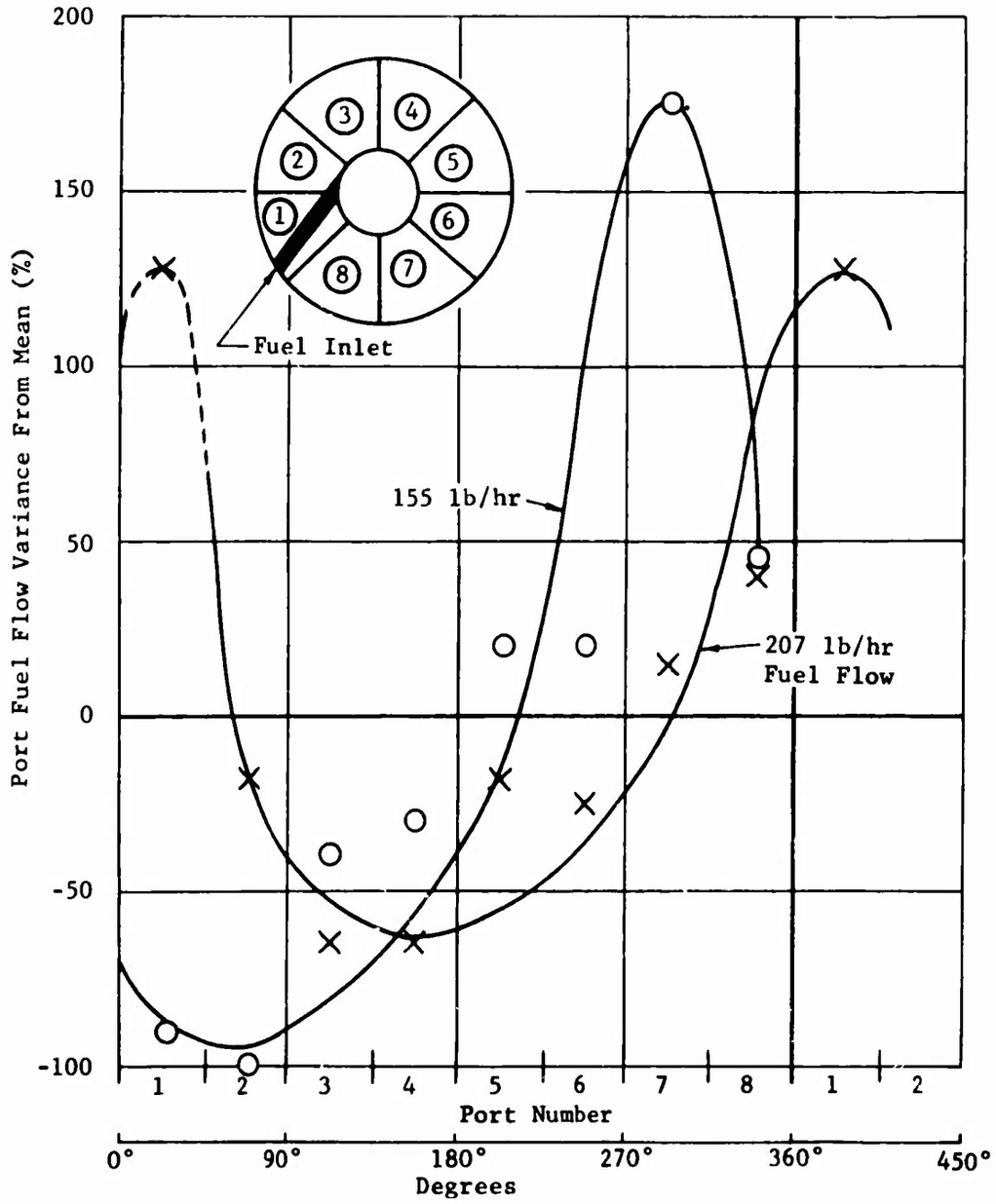

Figure 51. Fuel Patternization of Build 2 Single Point Tangential Fuel Feed for Varying Fuel Flows at 70 Percent Rated Airflow in Annular Vaporizer Fuel Introduction System.

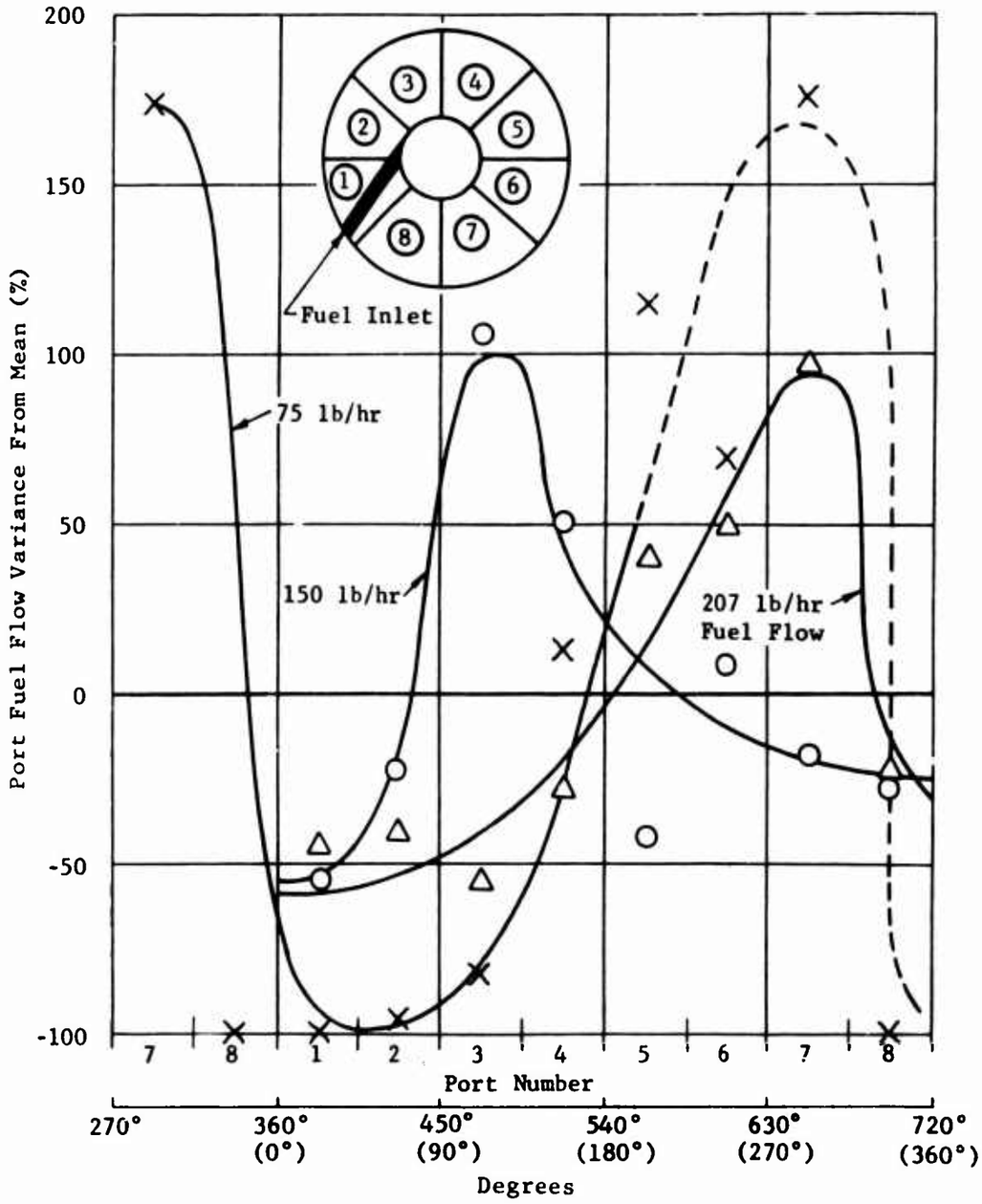

Figure 52. Fuel Patternization of Build 3 Single Point Tangential Fuel Feed for Varying Fuel Flow at Rated Airflow in Annular Vaporizer Fuel Introduction System.

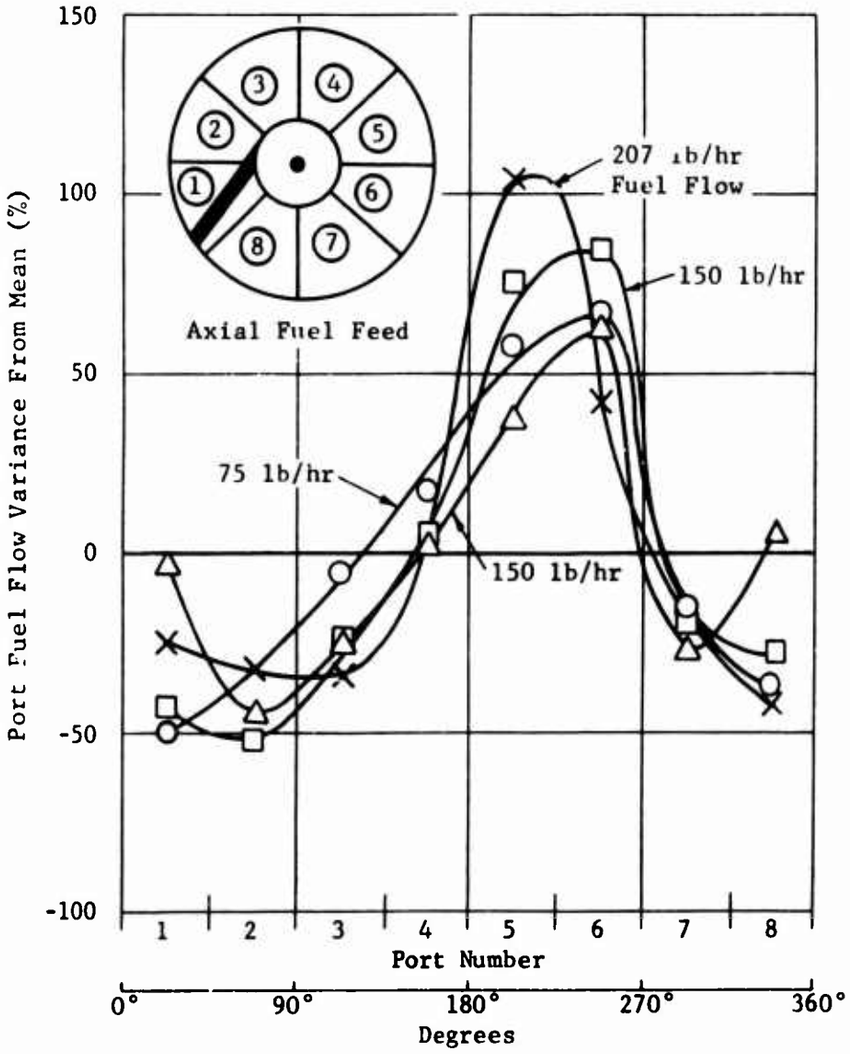

Figure 53. Fuel Patternization of Axial Fuel Feed System for Varying Fuel Flows at Rated Airflow in Annular Vaporizer Fuel Introduction System.

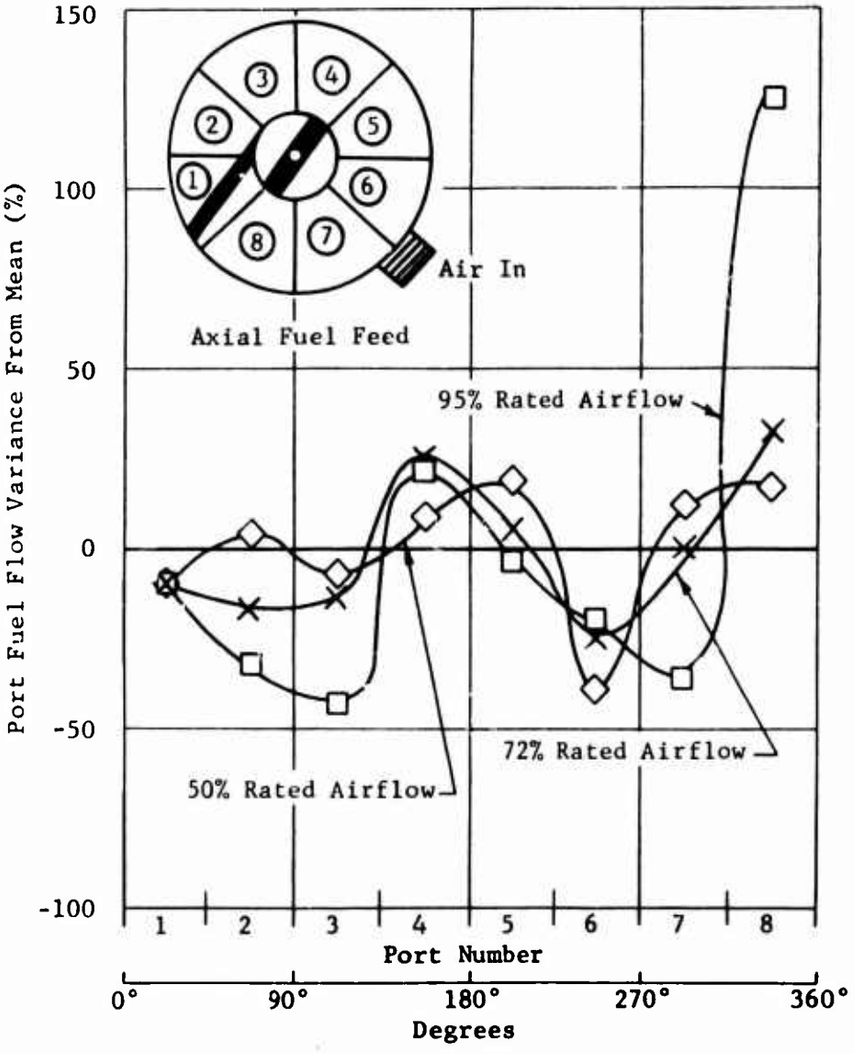

Figure 54. Fuel Patternization of Axial Fuel Feed System for Varying Airflows at Rated Fuel Flow in Annular Vaporizer Fuel Feed System.

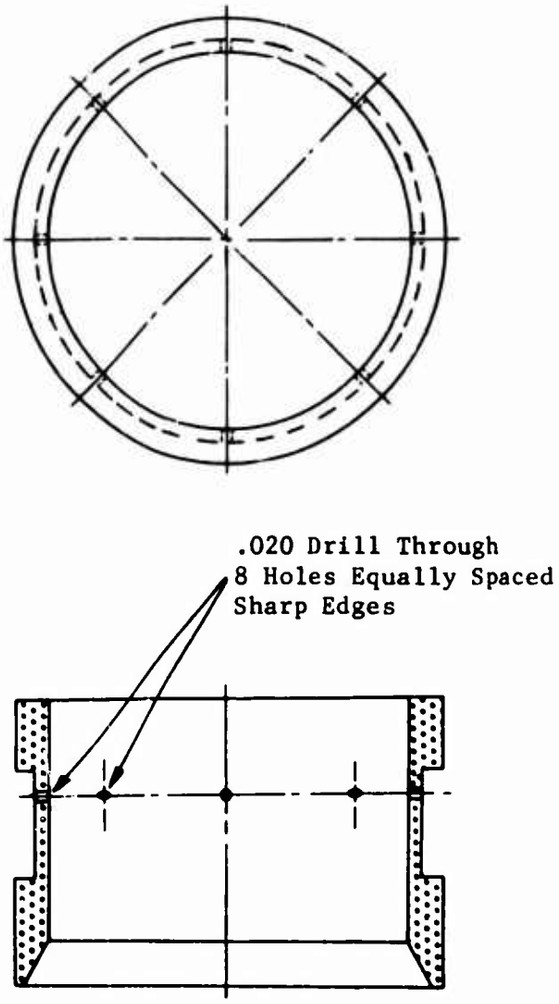

Figure 55. Internal Manifold Ring Insert For Eight-Point Radial Fuel Feed in Annular Vaporizer Fuel Introduction System.

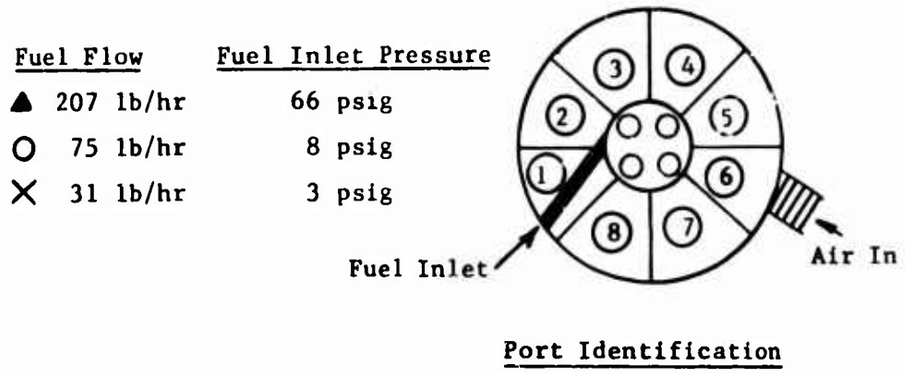

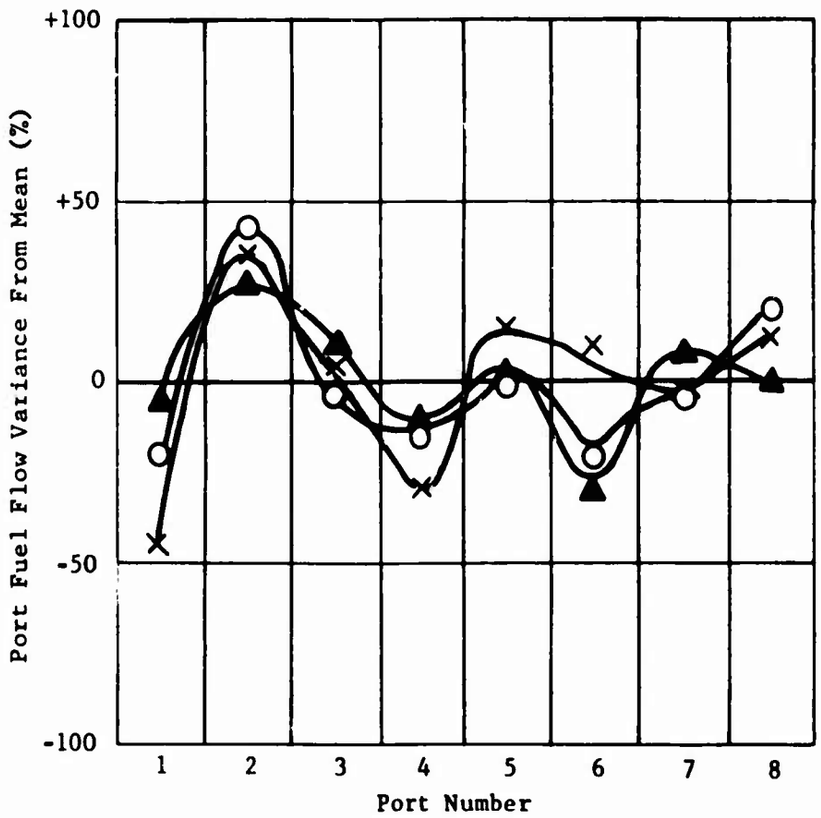

Figure 56. Fuel Patternization of Eight-Point Radial Fuel Feed System for Varying Fuel Flows at 50 Percent Rated Airflow in Annular Vaporizer Fuel Introduction System.

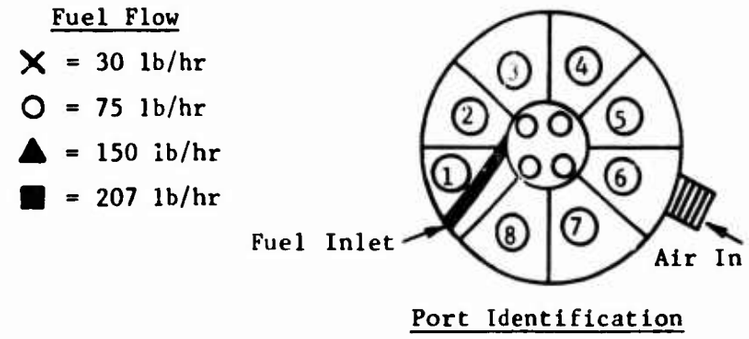

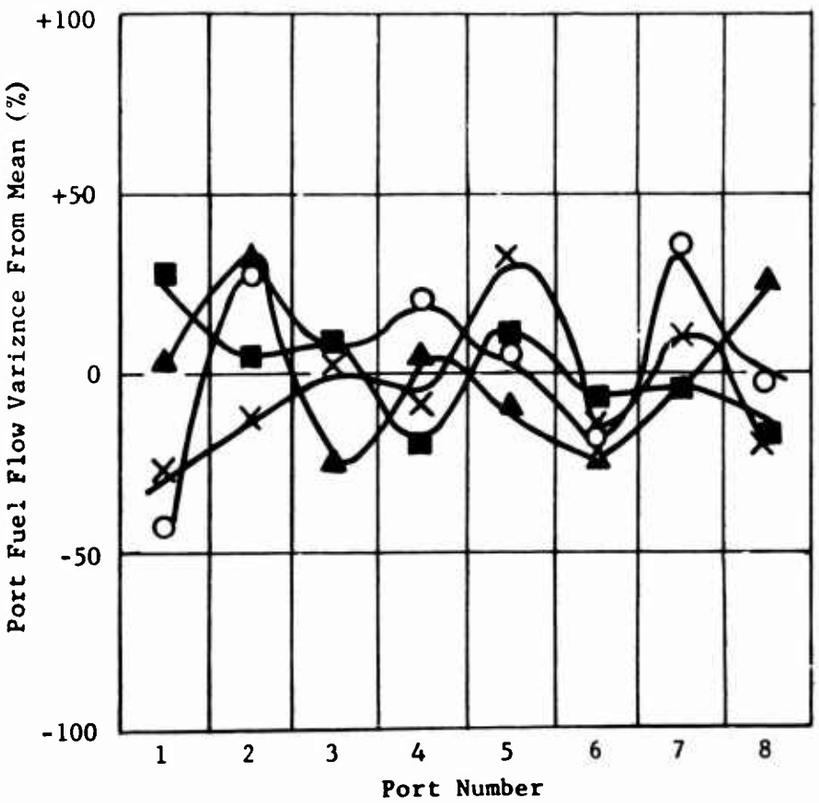

Figure 57. Fuel Patternization of Eight-Point Radial Fuel Feed System for Varying Fuel Flows at Rated Airflow in Annular Vaporizer Fuel Introduction System.

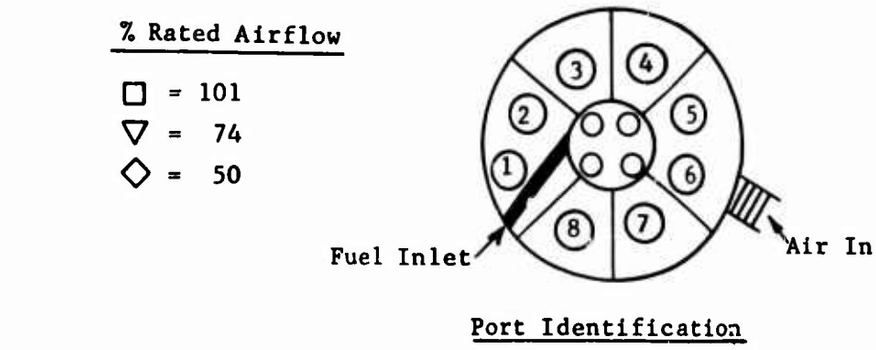

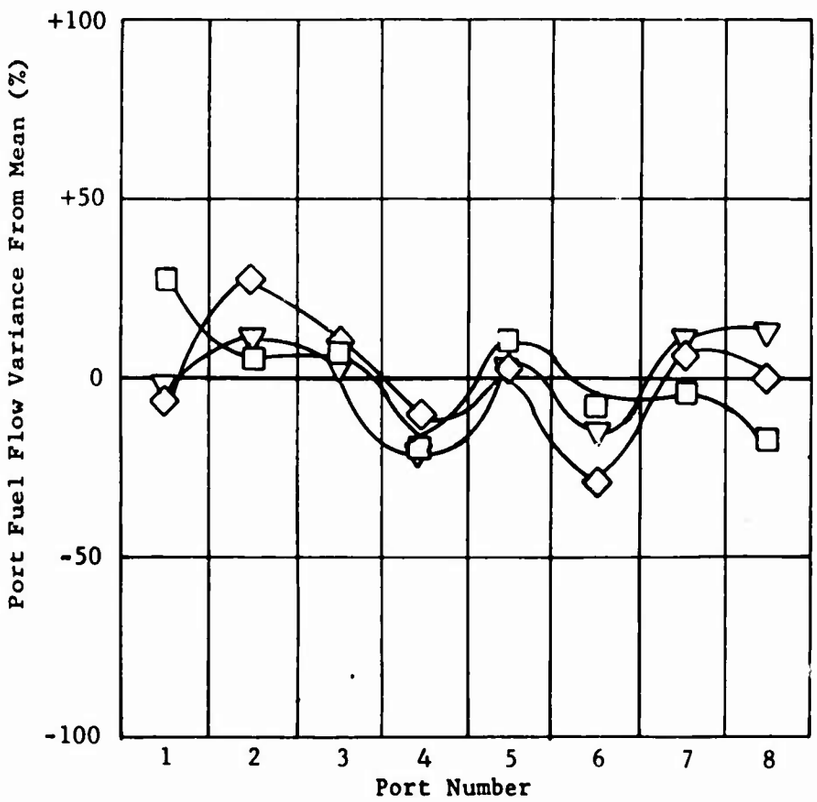

Figure 58. Fuel Patternization of Eight-Point Radial Fuel Feed System for Varying Airflows at Rated Fuel Flow in Annular Vaporizer Fuel Introduction System.

Tangential Fuel Feed - Build 1
0.125" Inner Dia.

Short Axial Fuel Feed - Build 2
0.125" Inner Dia.

Long Axial
3 --
4 --

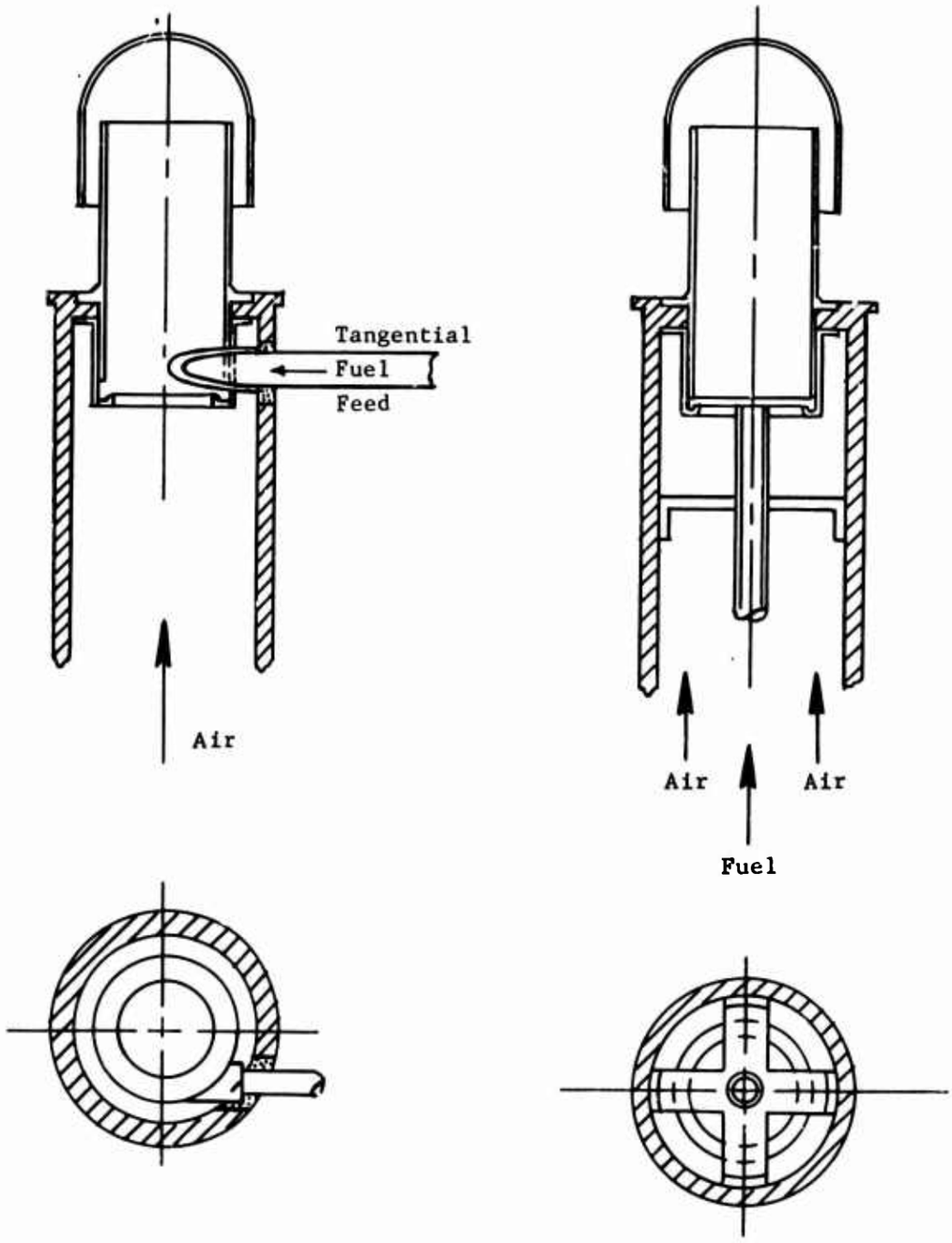

Figure 59. Fuel Feed Systems And Modifications Tested For Mushroom Vaporizer Fuel Introduction System.

Build 2

Long Axial Fuel Feed - Builds 3 & 4
3 -- 0.125" Inner Dia.
4 -- 0.040" Inner Dia.

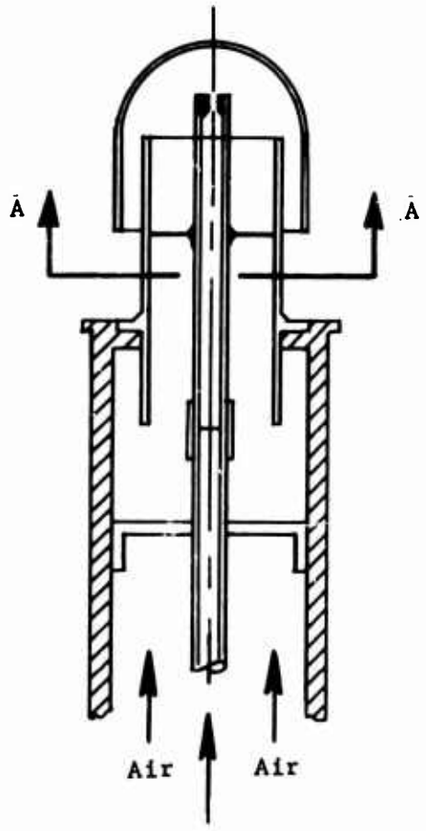

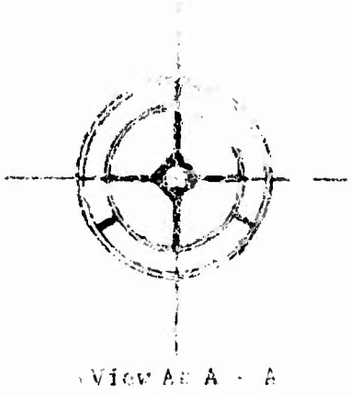

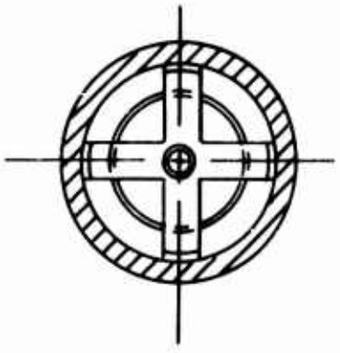

m Vaporizer

B

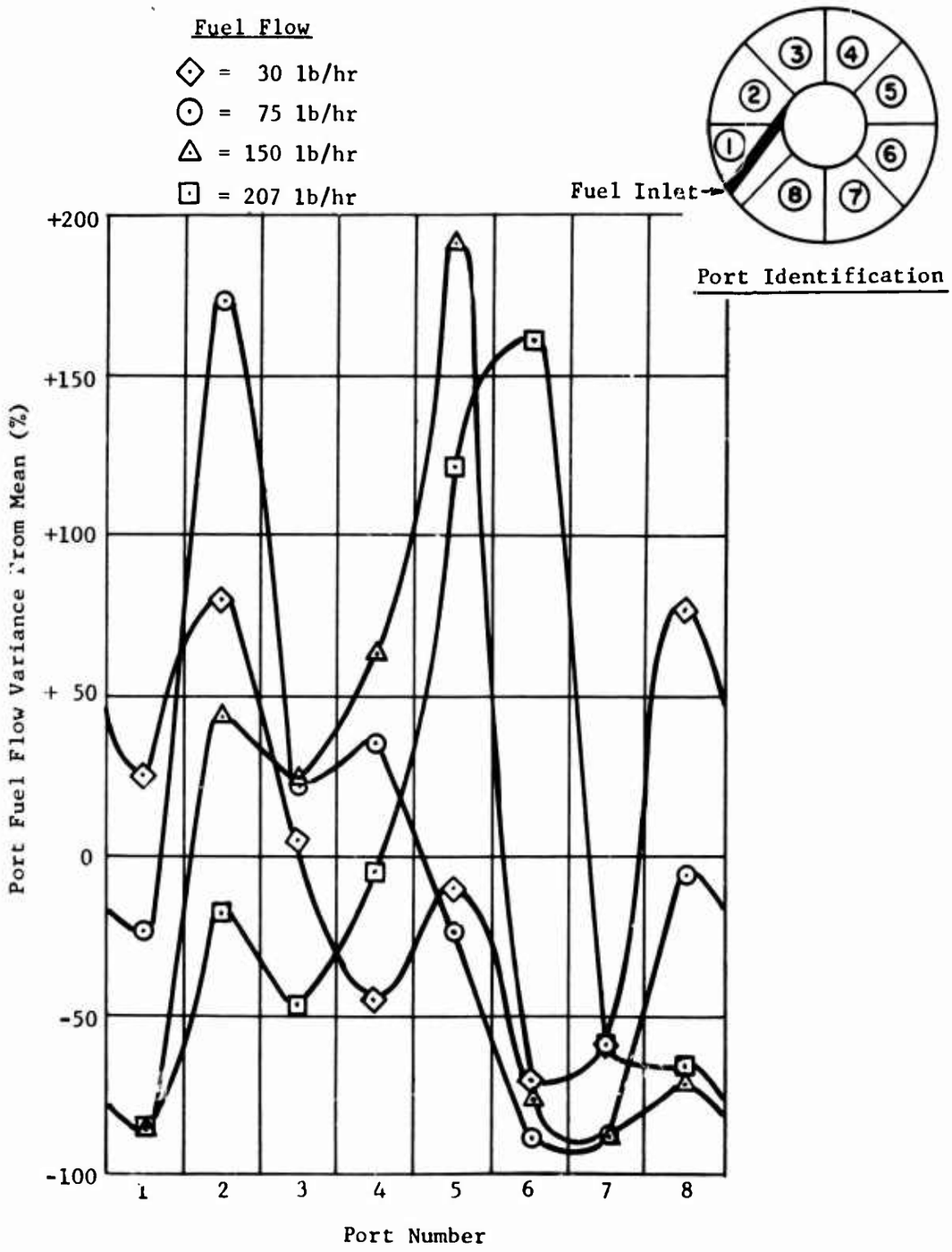

Figure 60. Fuel Patternization of Build 1 (Single Point Tangential Fuel Feed) for Varying Fuel Flows at Rated Airflow in Mushroom Vaporizer Fuel Introduction System.

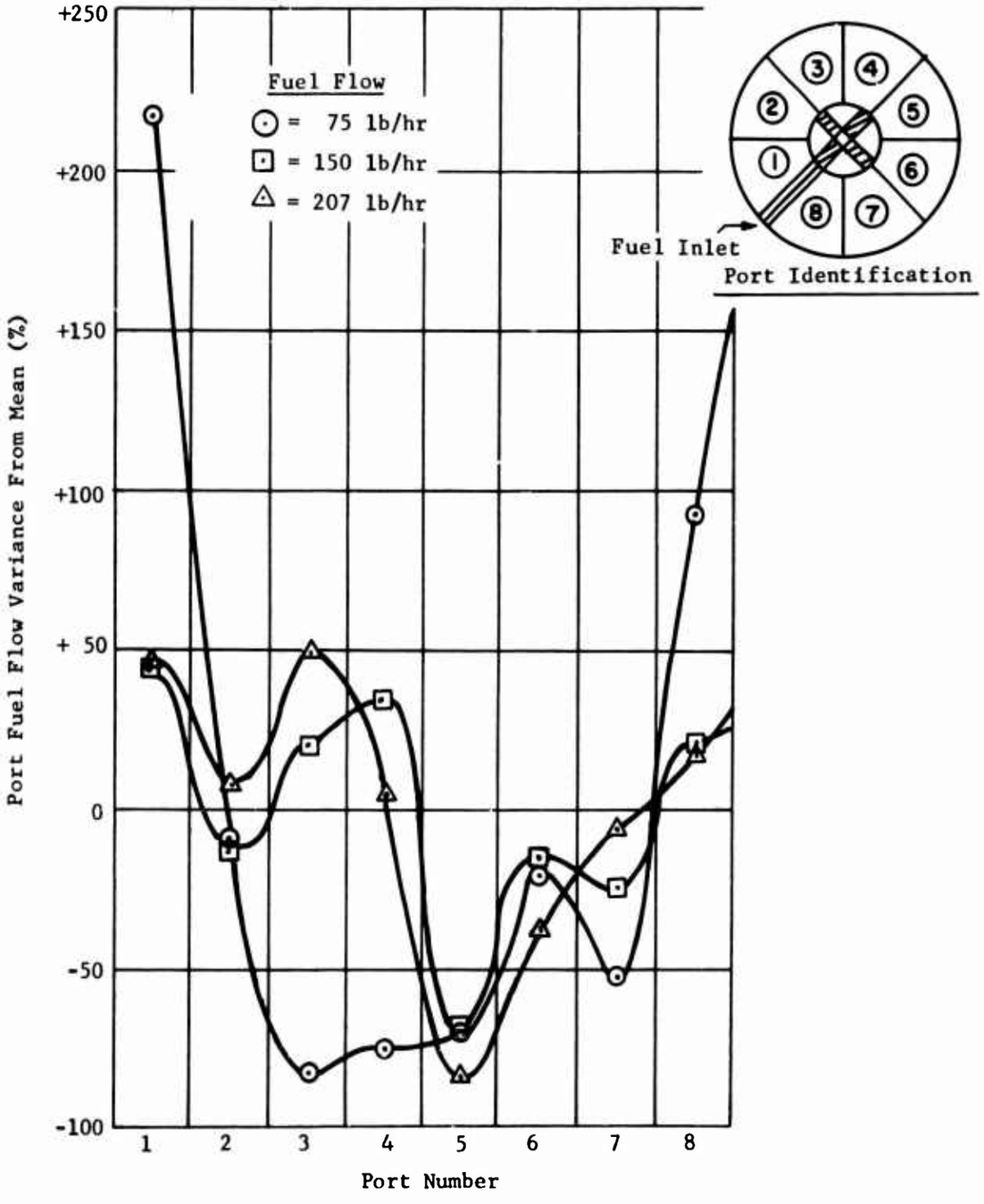

Figure 61. Fuel Patternization of Build 2 (Single Point Axial Fuel Feed) for Varying Fuel Flows at Rated Airflow in Mushroom Vaporizer Fuel Introduction System.

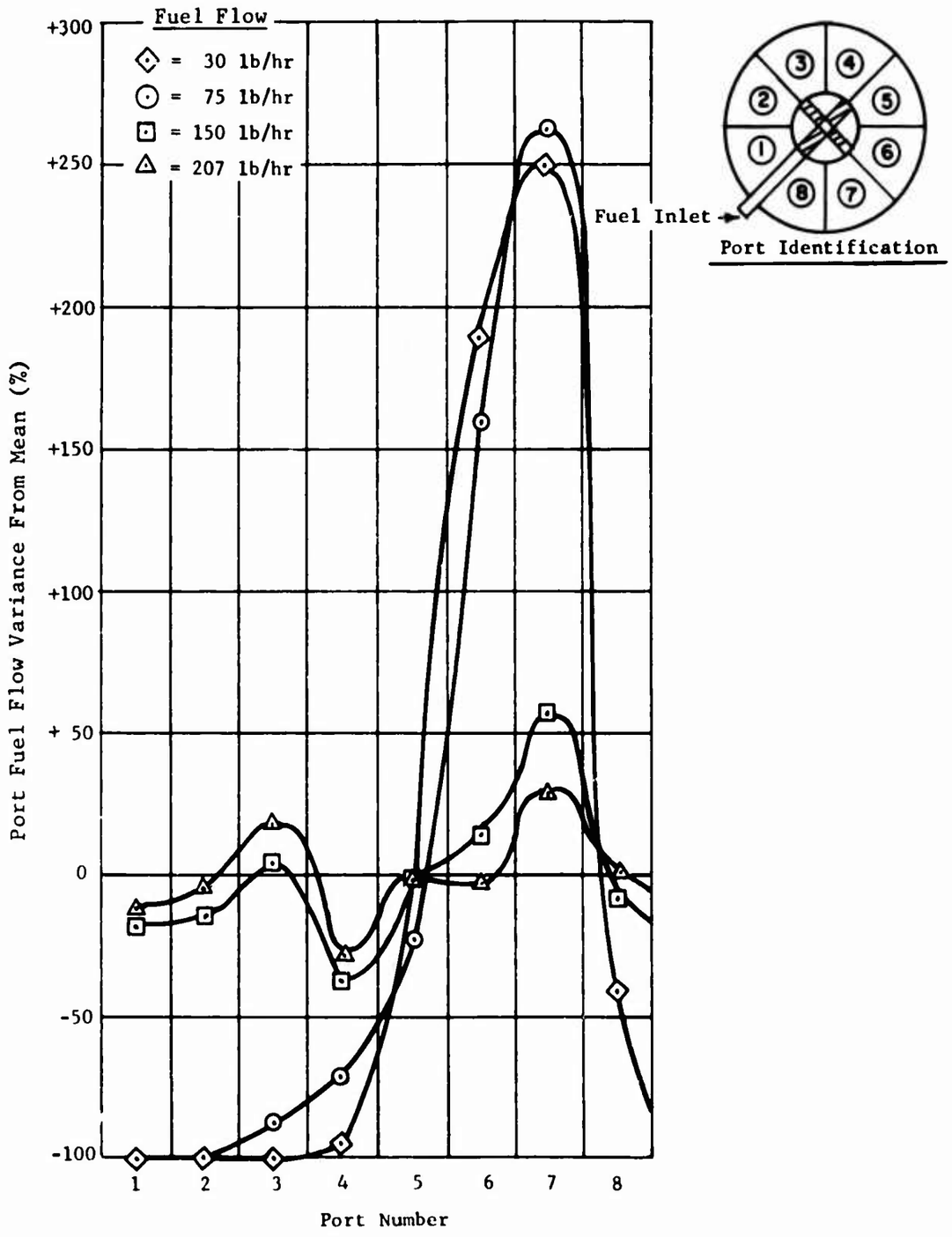

Figure 62. Fuel Patternization of Build 3 (Single Point Axial Fuel Feed) for Varying Fuel Flows at Rated Airflow in Mushroom Vaporizer Fuel Introduction System.

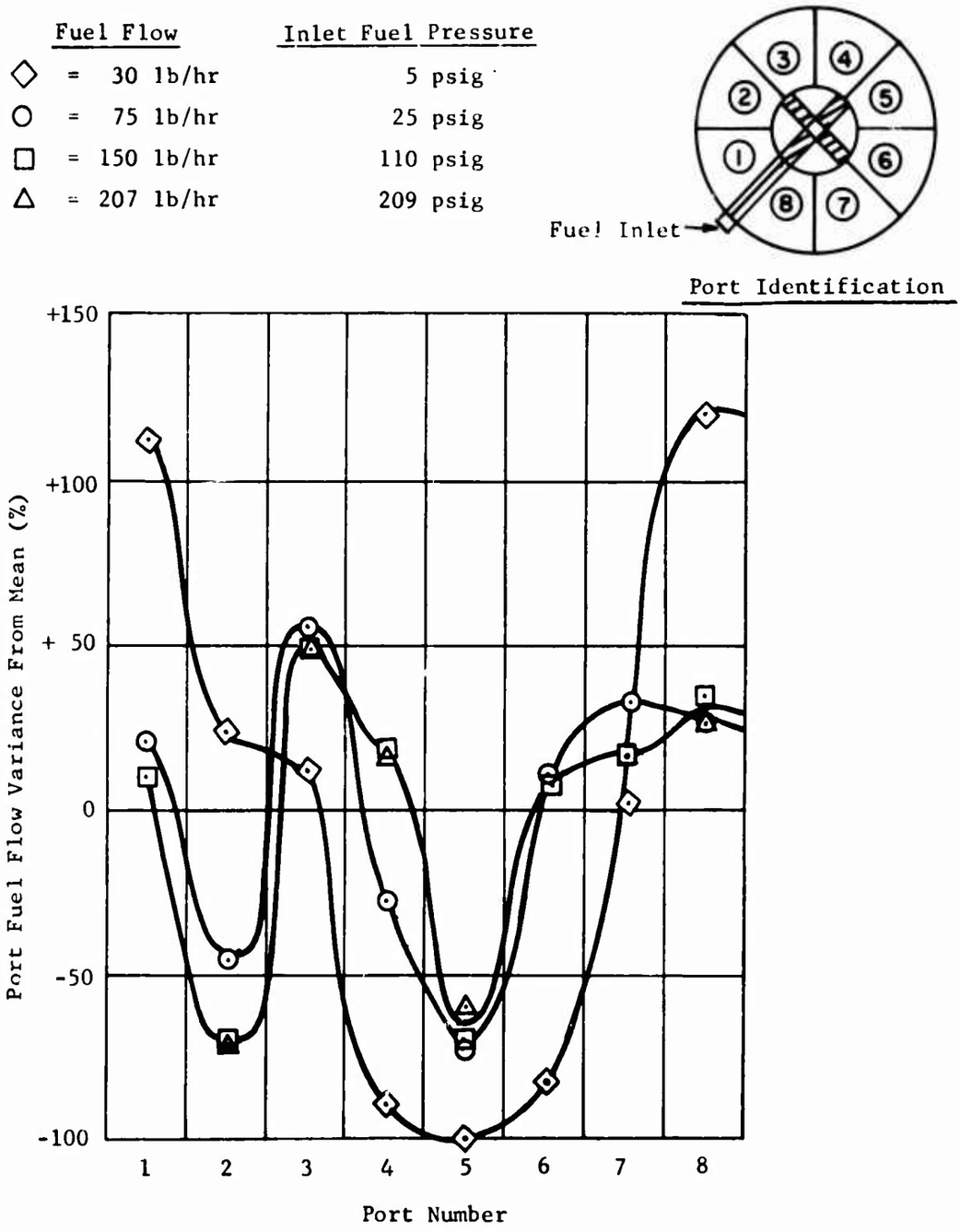

Figure 63. Fuel Patternization of Build 4 (Single Point Axial Fuel Feed) for Varying Fuel Flows at Rated Airflow in Mushroom Vaporizer Fuel Introduction System.

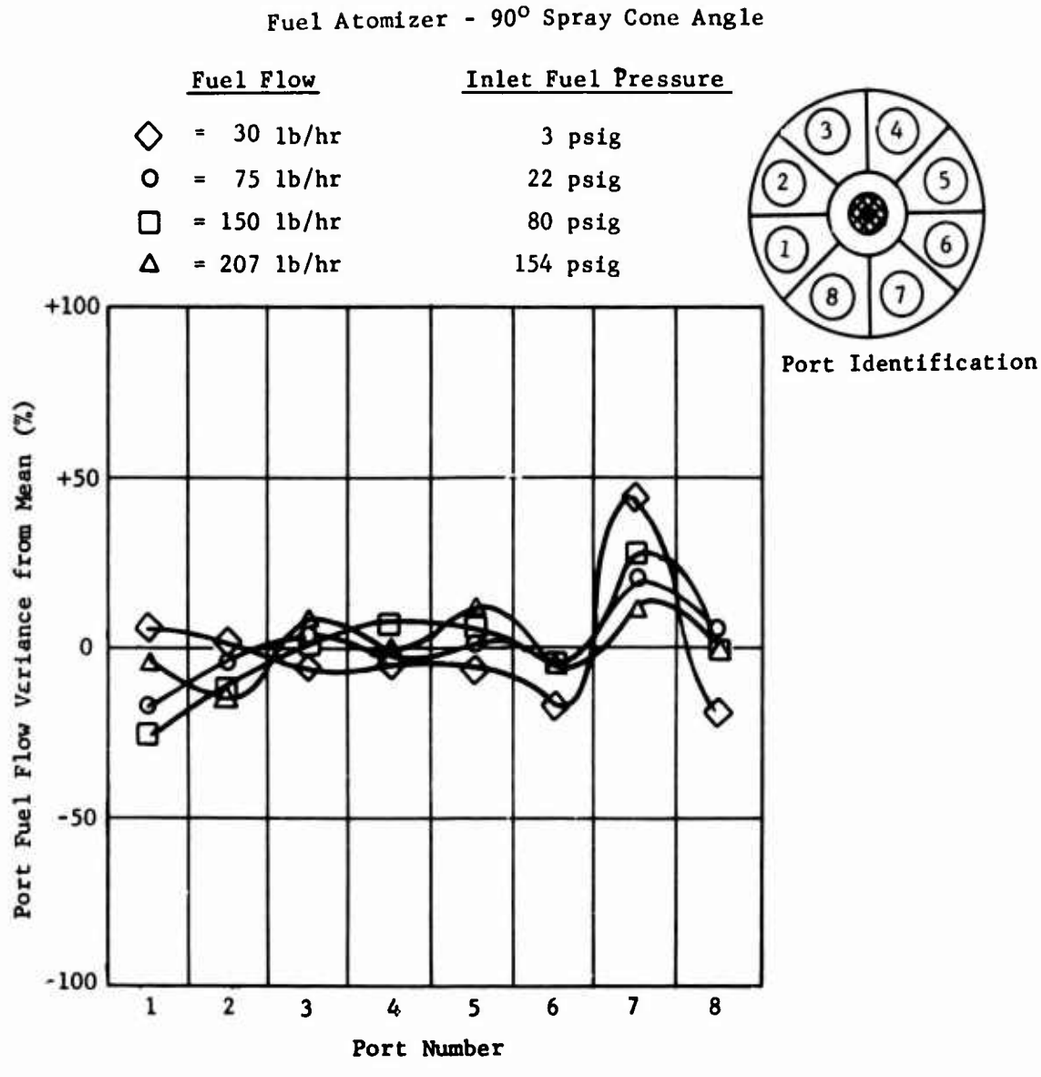

Figure 64. Fuel Patternization of Atomizer Nozzle Fuel Feed System for Varying Fuel Flows in Still Air.

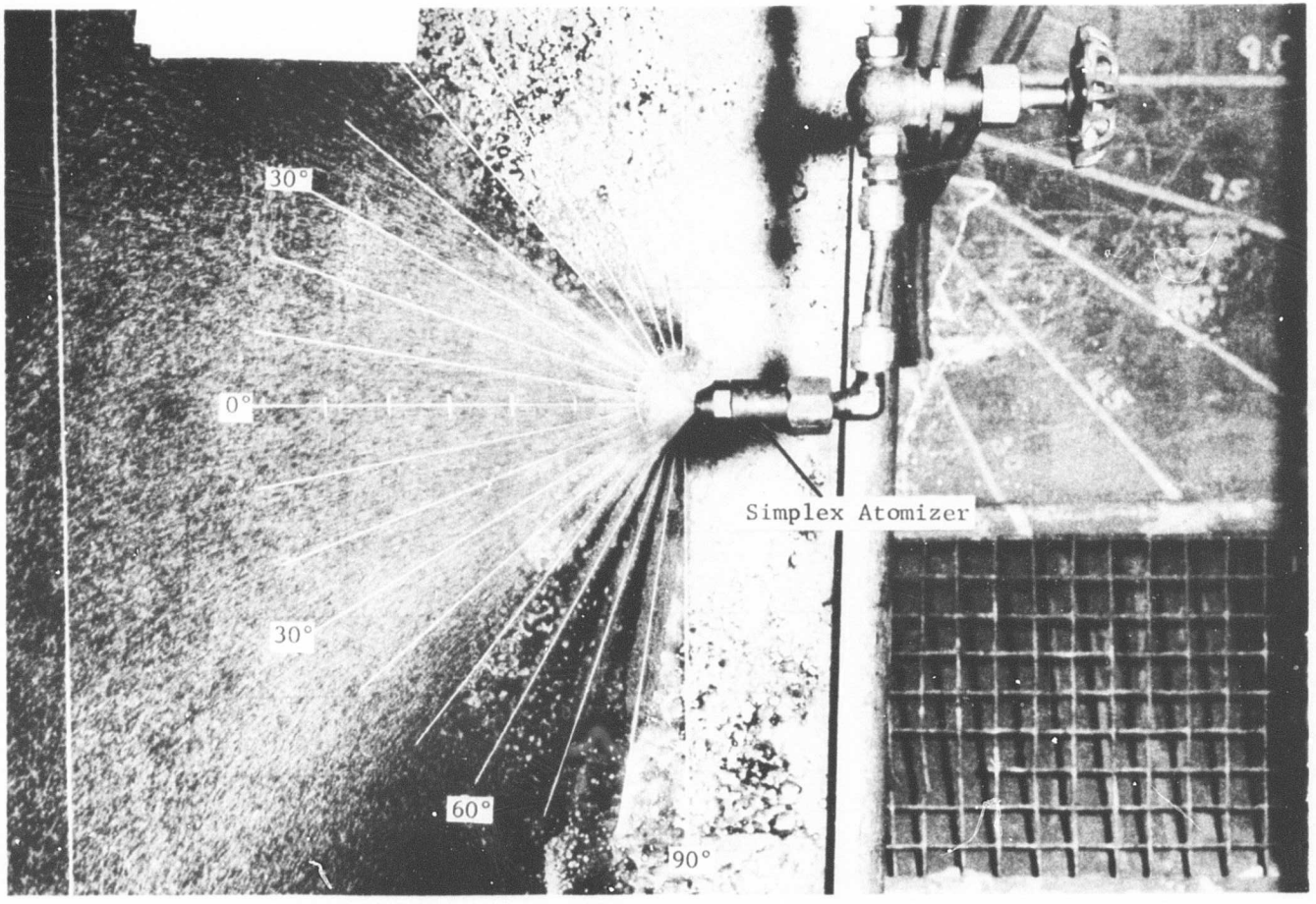

Figure 65. Spray Cone Pattern for Simplex Atomizer with 30 lb/hr Fuel Flow in Still Air.

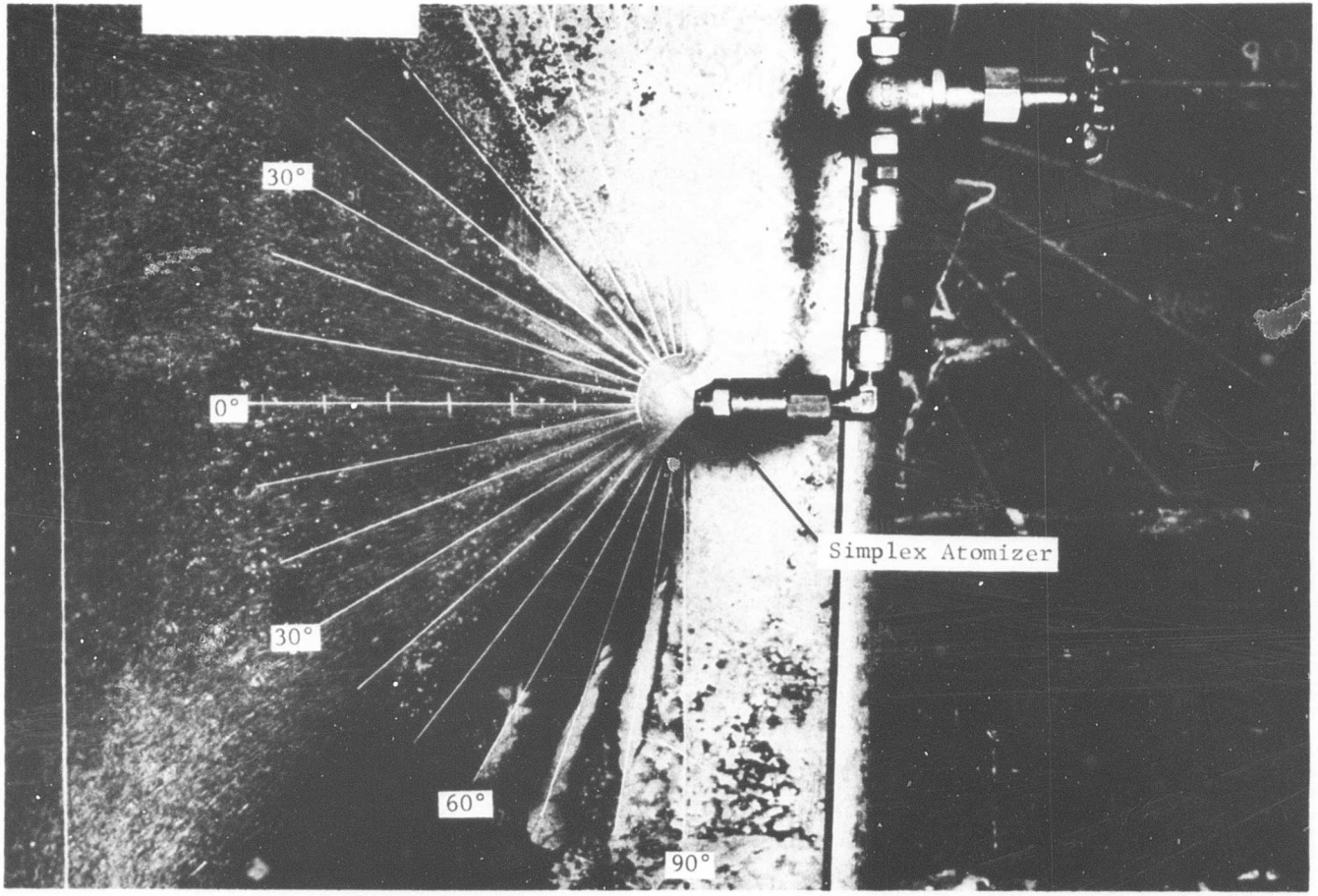

Figure 66. Spray Cone Pattern for Simplex Atomizer with 65 lb/hr Fuel Flow (5 Atmospheres Pressure Design Flow) in Still Air.

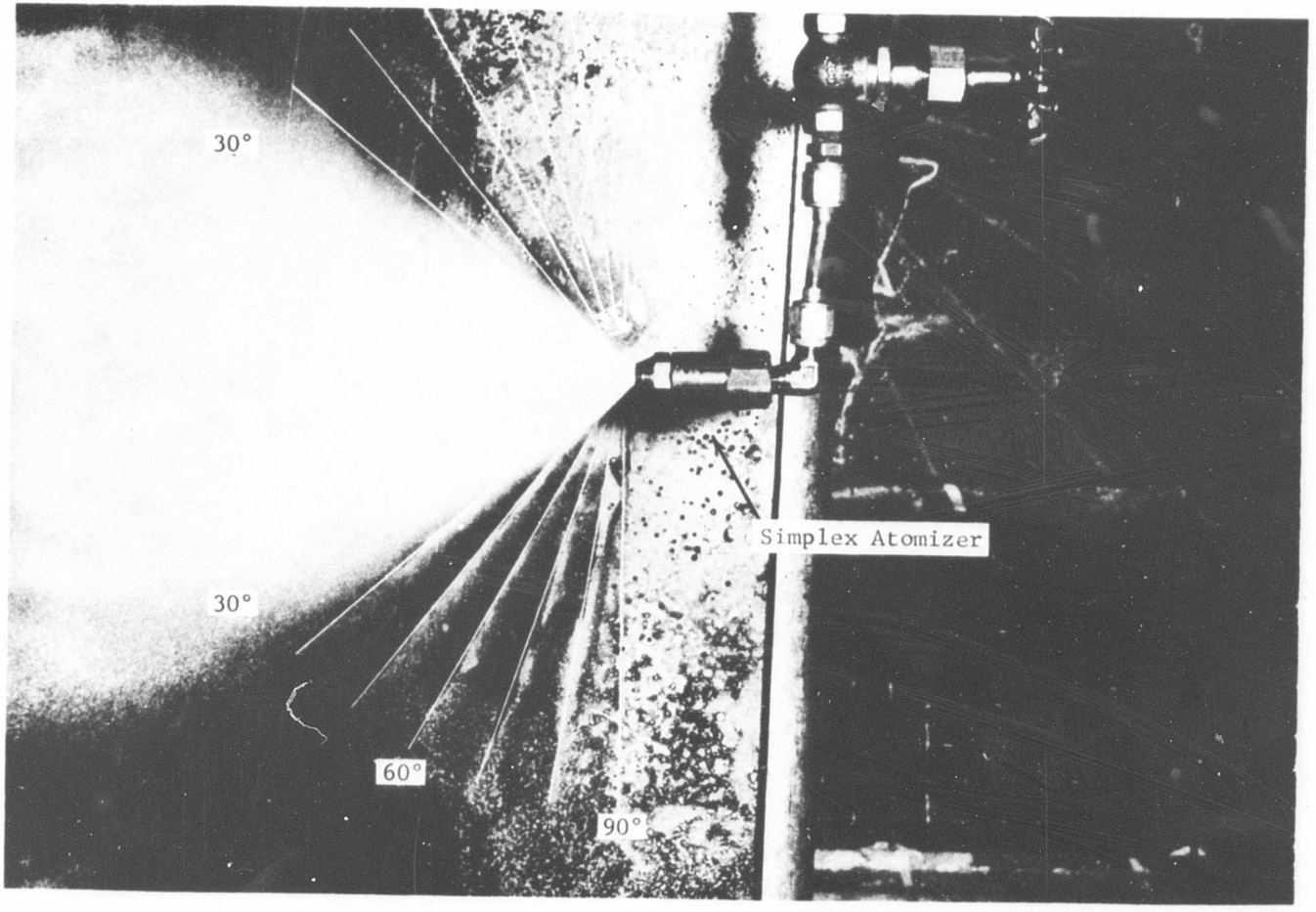

Figure 67. Spray Cone Pattern for Simplex Atomizer with 207 lb/hr Fuel Flow (16 Atmospheres Pressure Design Flow) in Still Air.

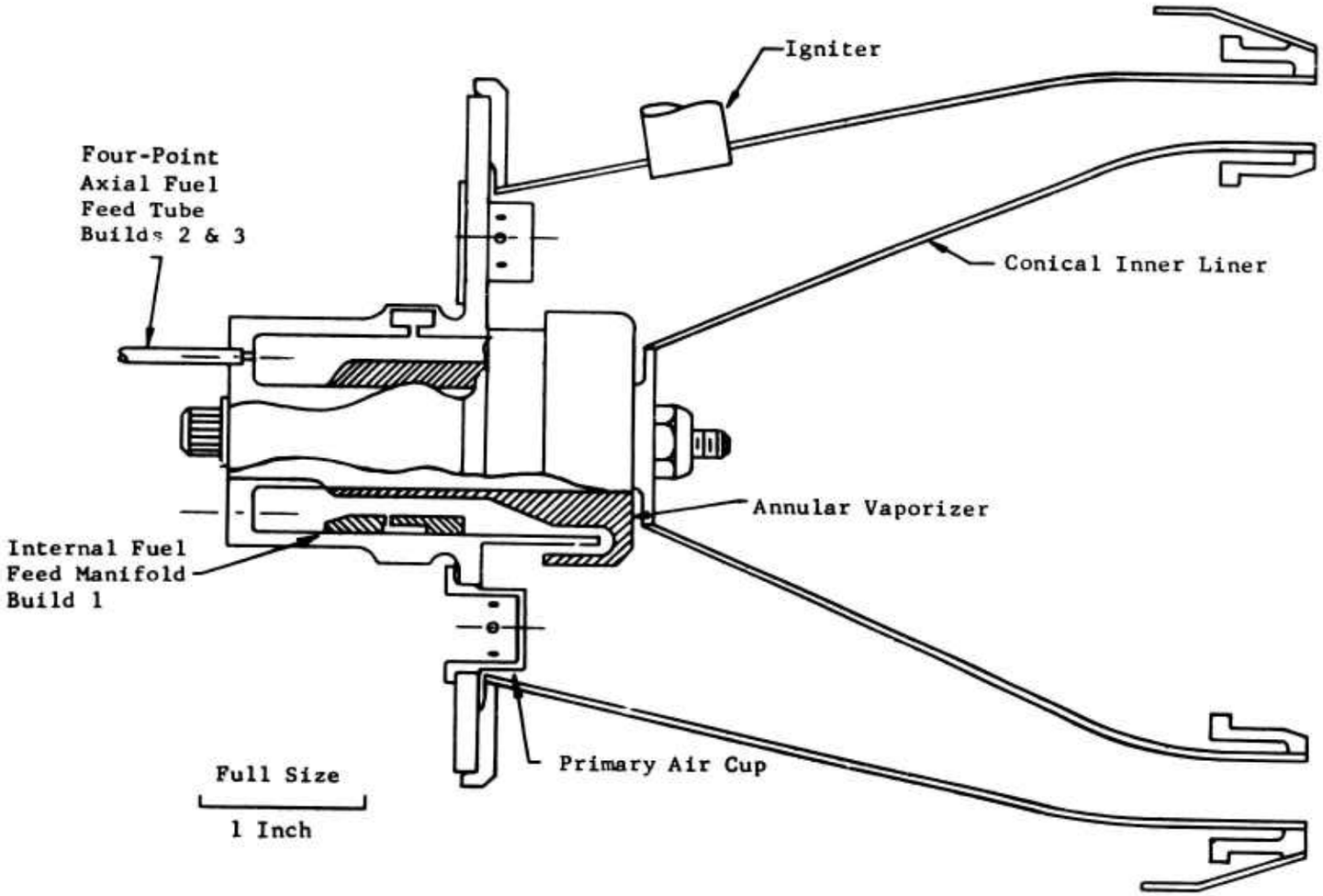

Figure 68. Primary Zone Configuration 1.

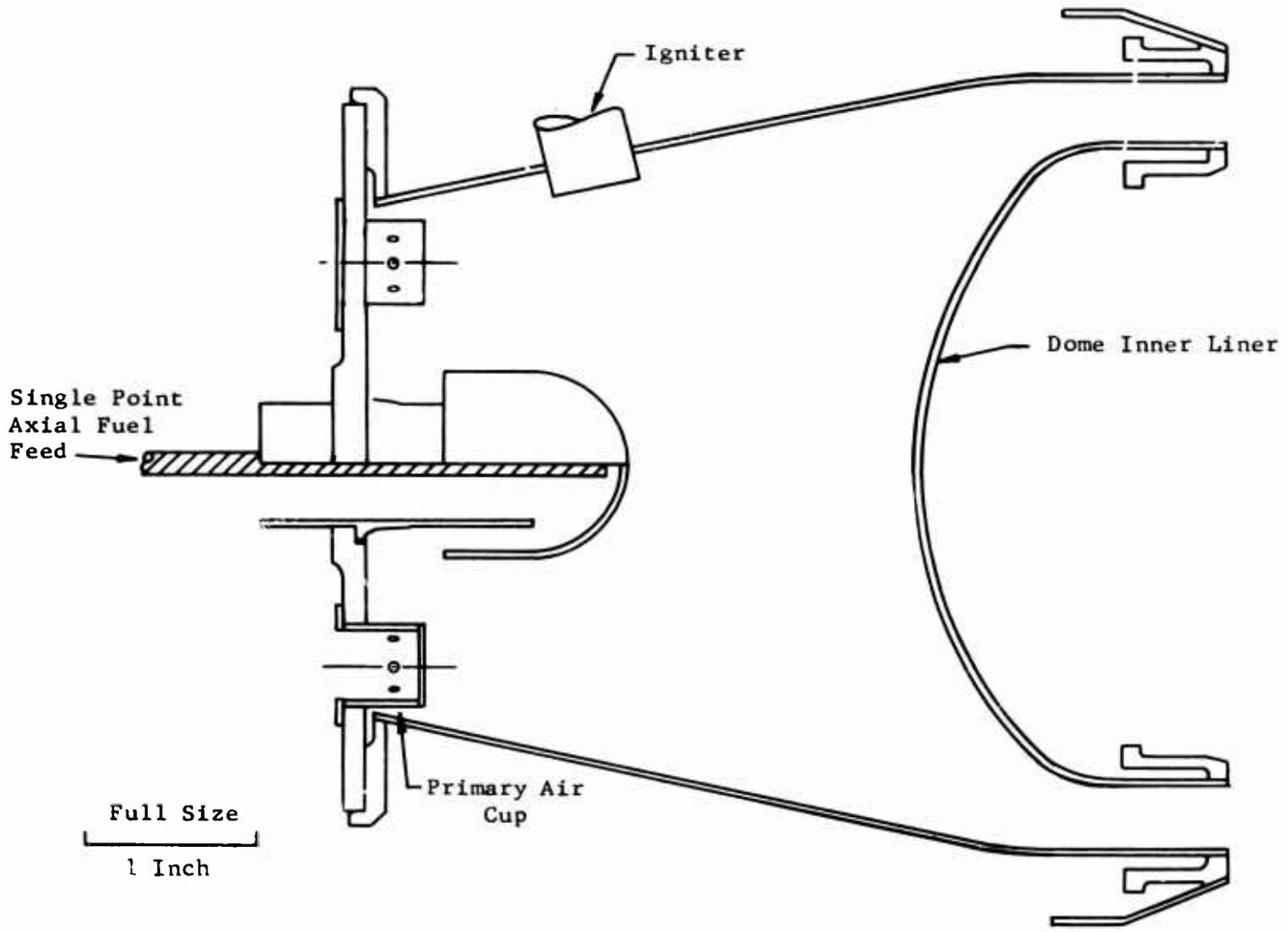

Figure 69. Primary Zone Configuration 2.

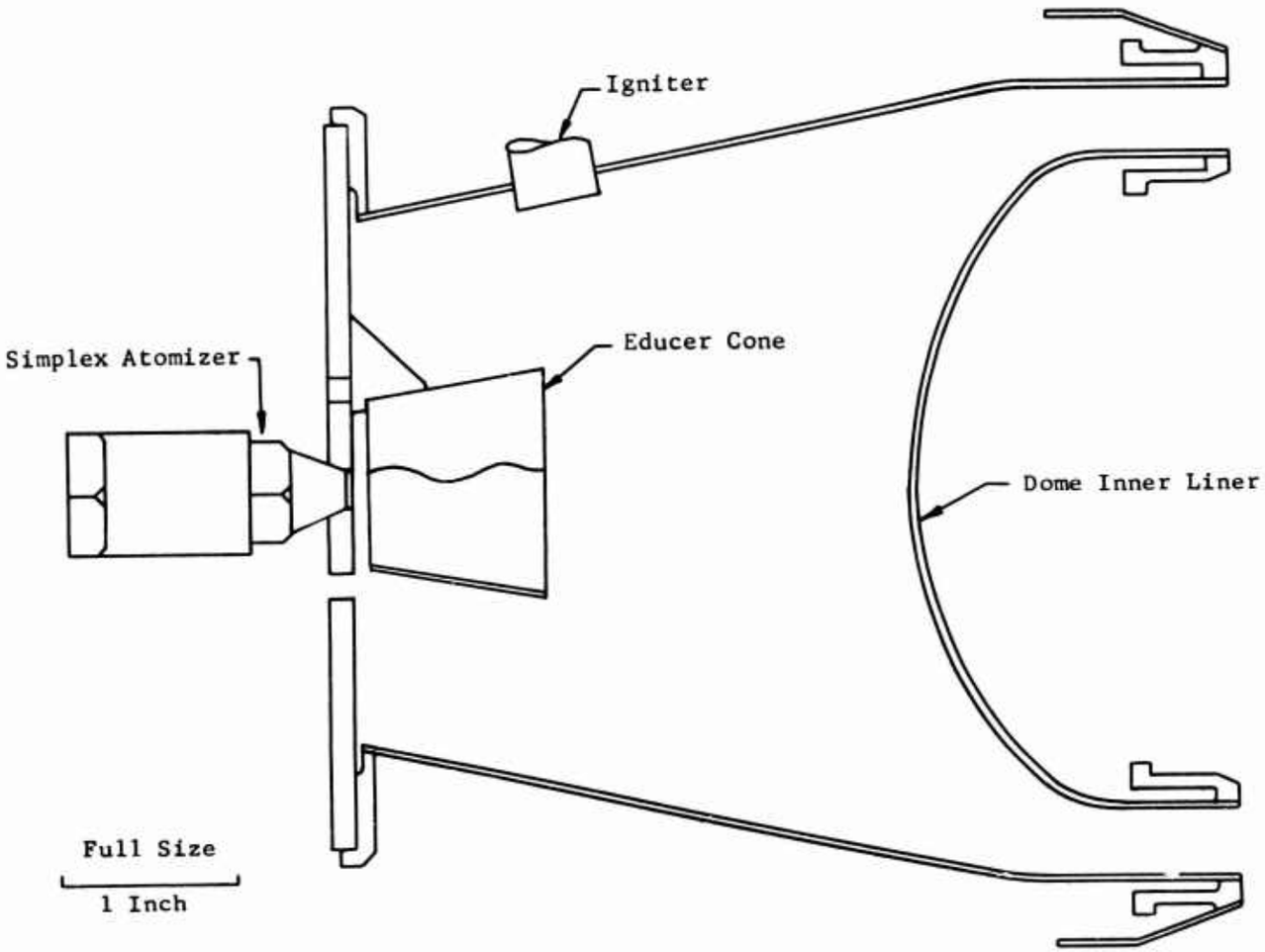

Figure 70. Primary Zone Configuration 3.

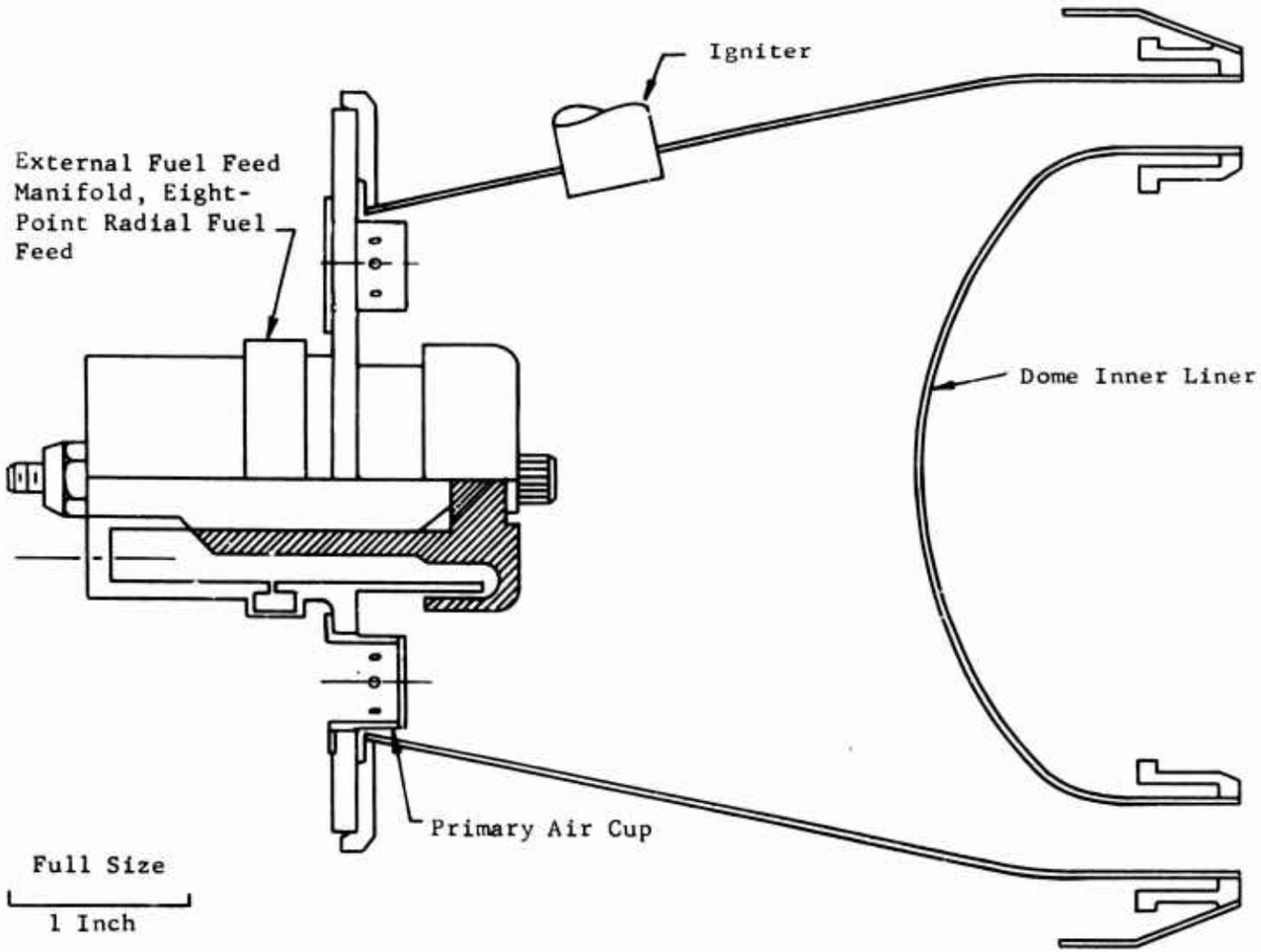

Figure 71. Primary Zone Configuration 4.

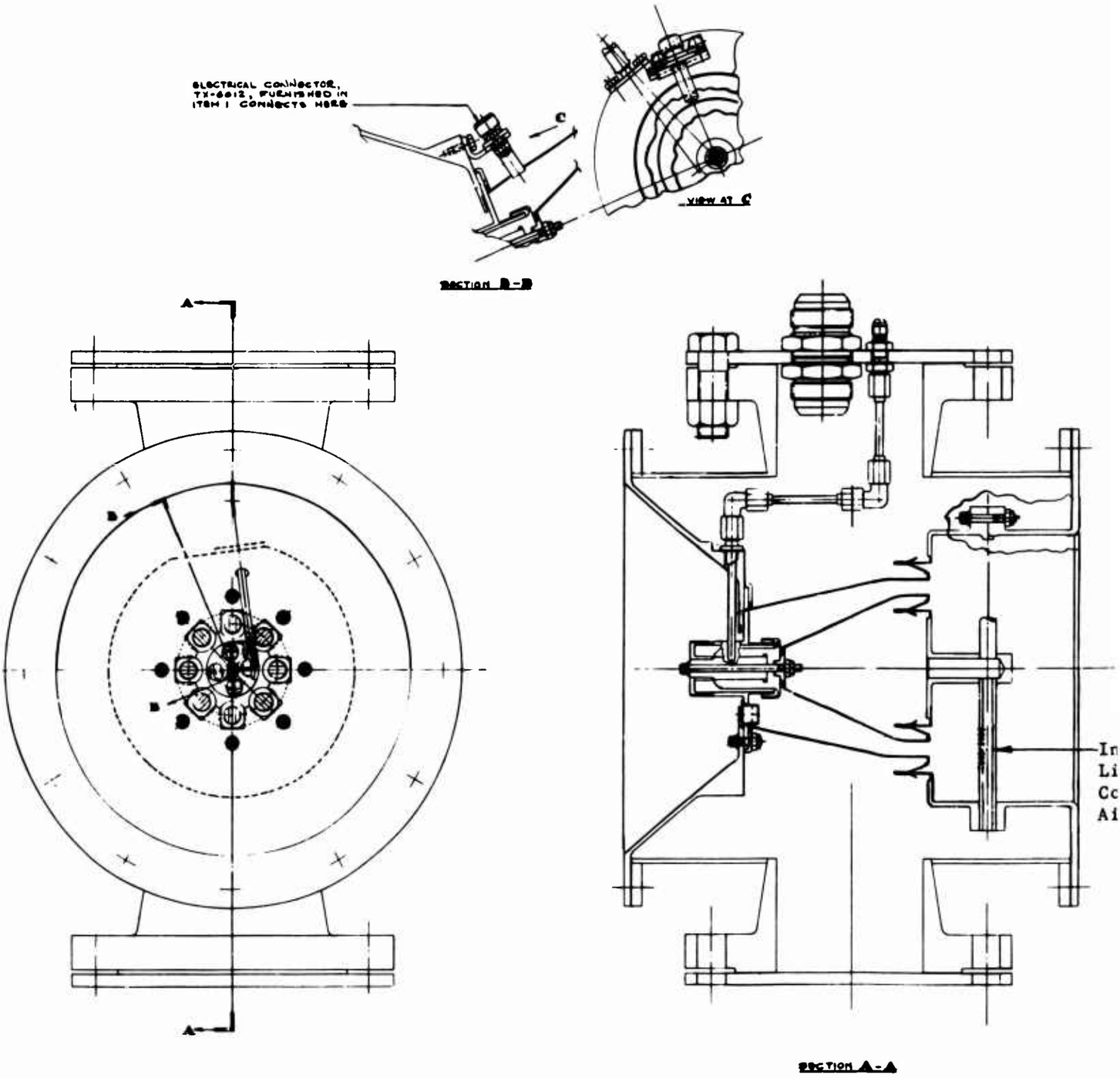

Figure 72. Primary Zone Rig Installation in Cross-Section Duct.

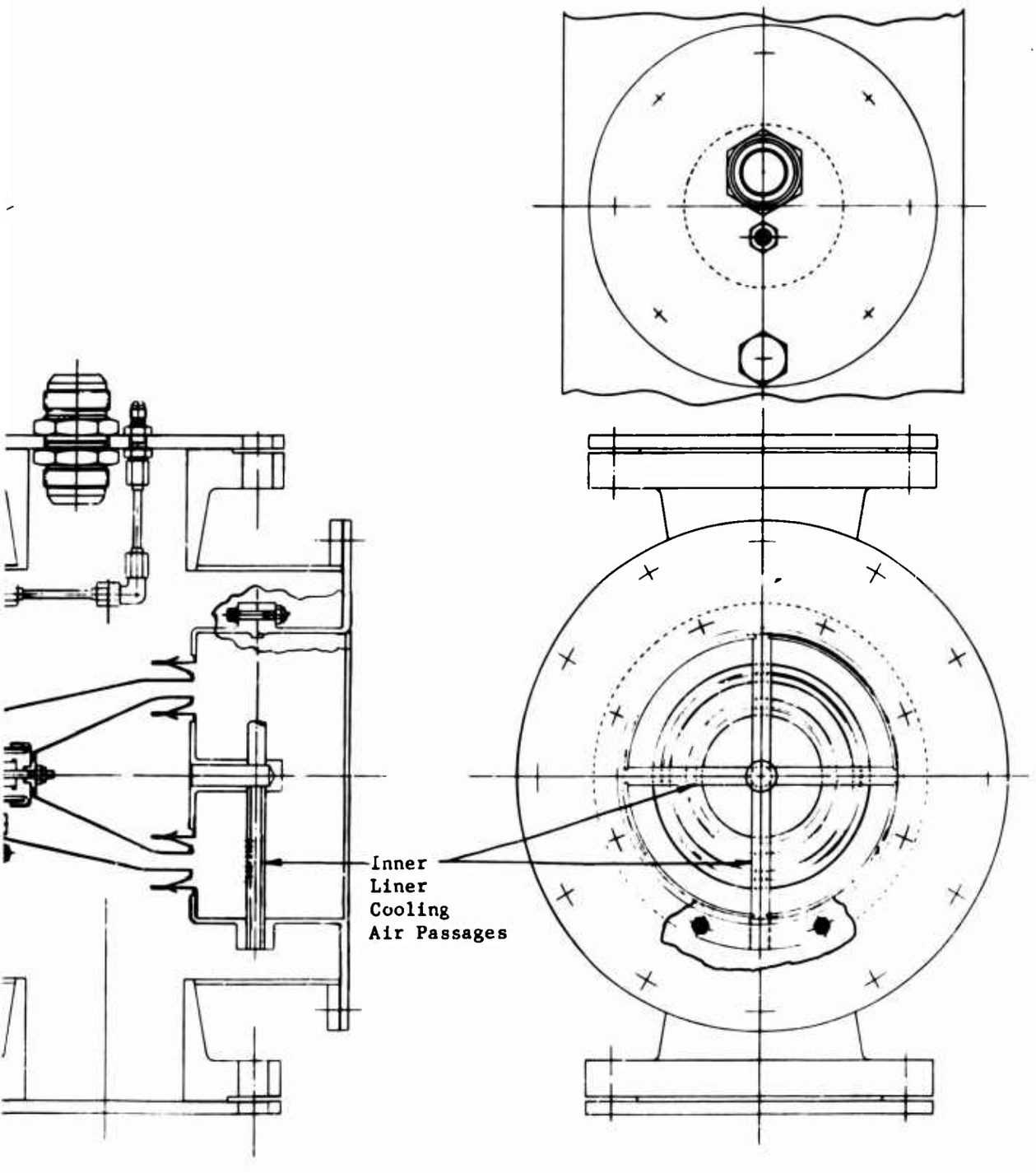

SECTION A-A

B

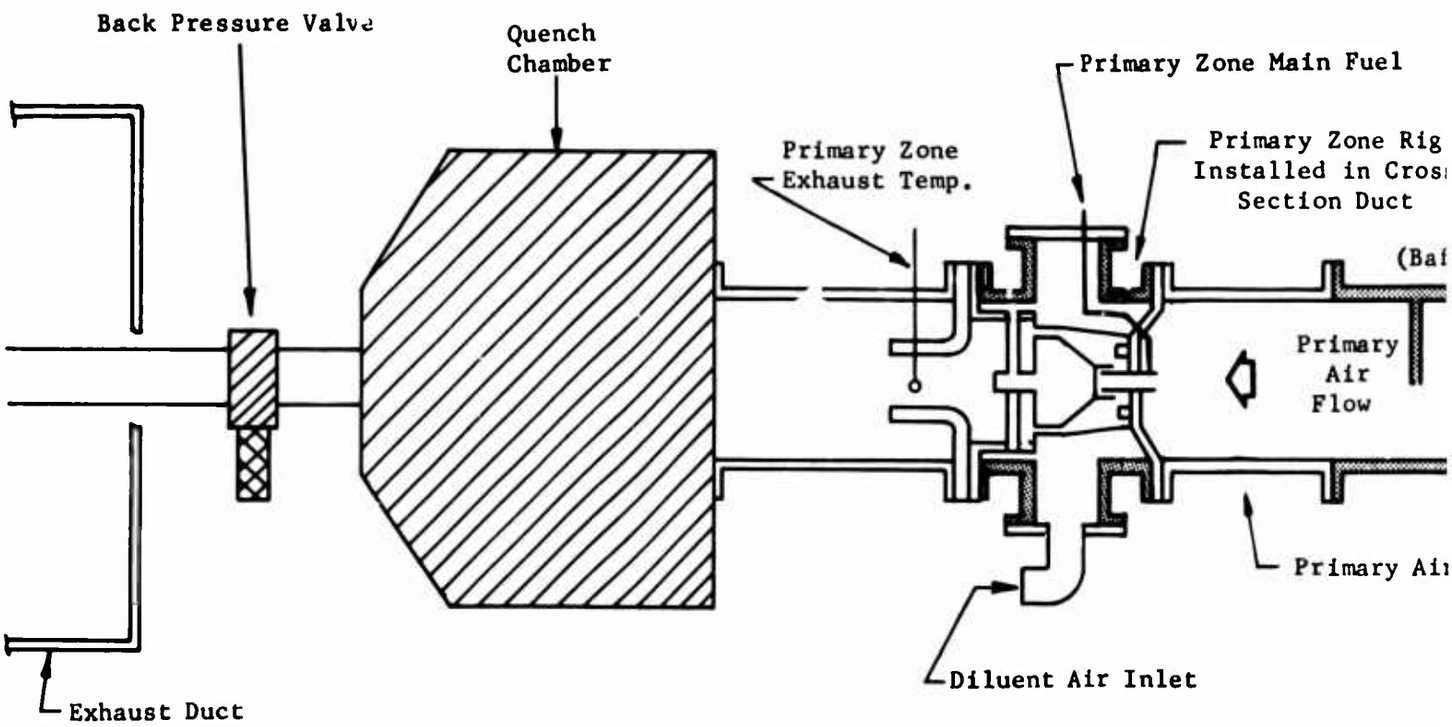

Figure 73. Primary Zone Rig Low Pressure Test Stand Installation.

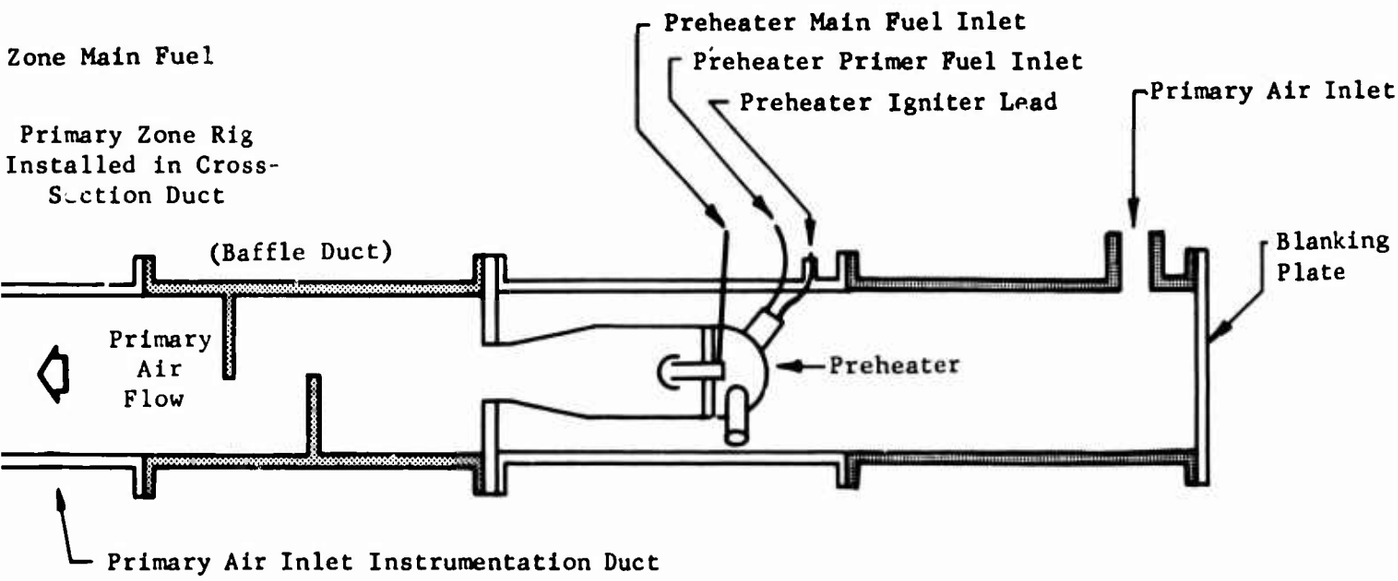
Preheater Main Fuel Inlet
Preheater Primer Fuel Inlet
Preheater Igniter Lead
Primary Air Inlet
Zone Main Fuel
Primary Zone Rig Installed in Cross-Section Duct
(Baffle Duct)
Blanking Plate
Primary Air Flow
Preheater
Primary Air Inlet Instrumentation Duct

B

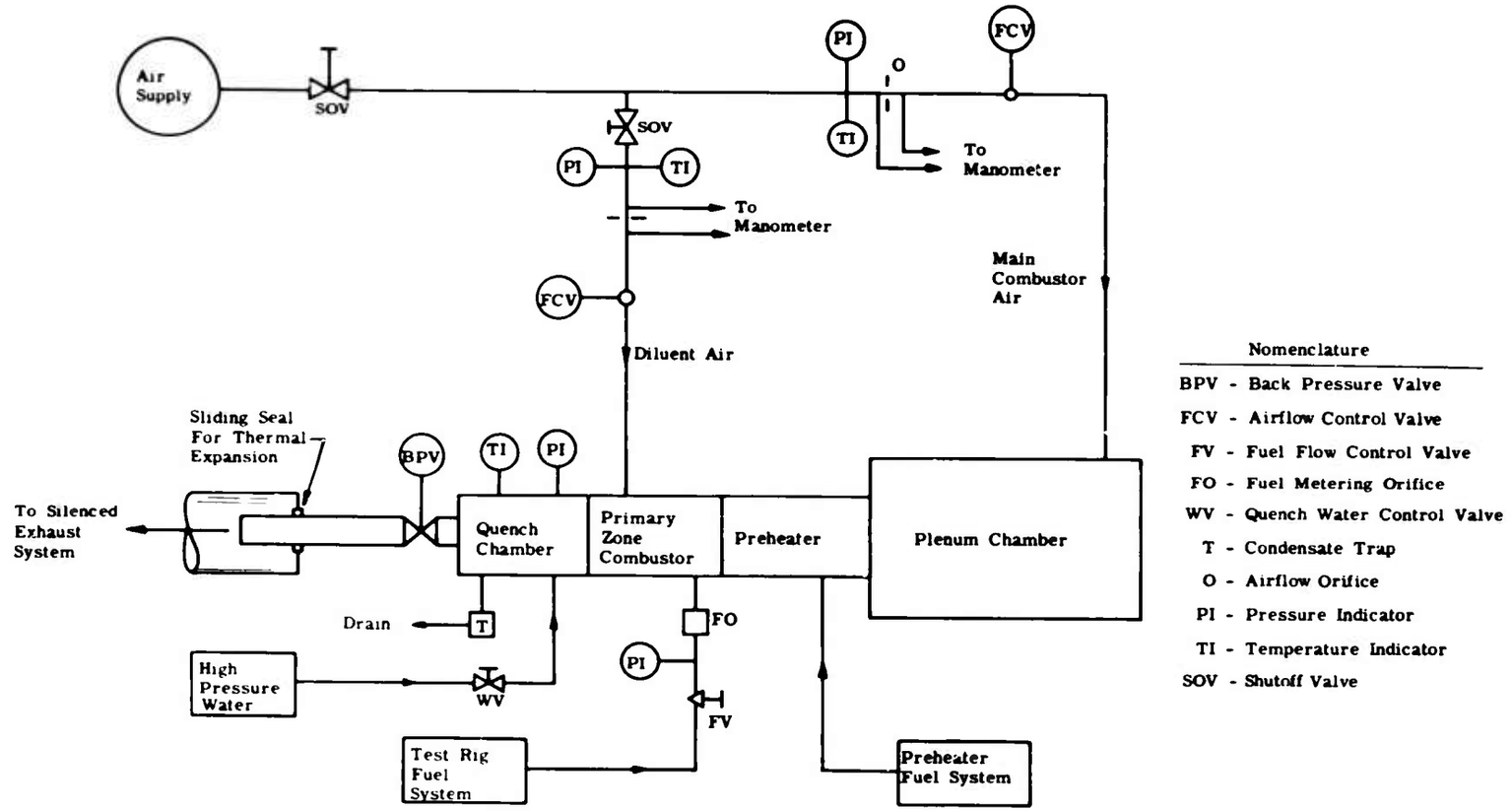

Figure 74. Primary Zone Rig Low Pressure Test Facility Fuel and Air Supply Schematic.

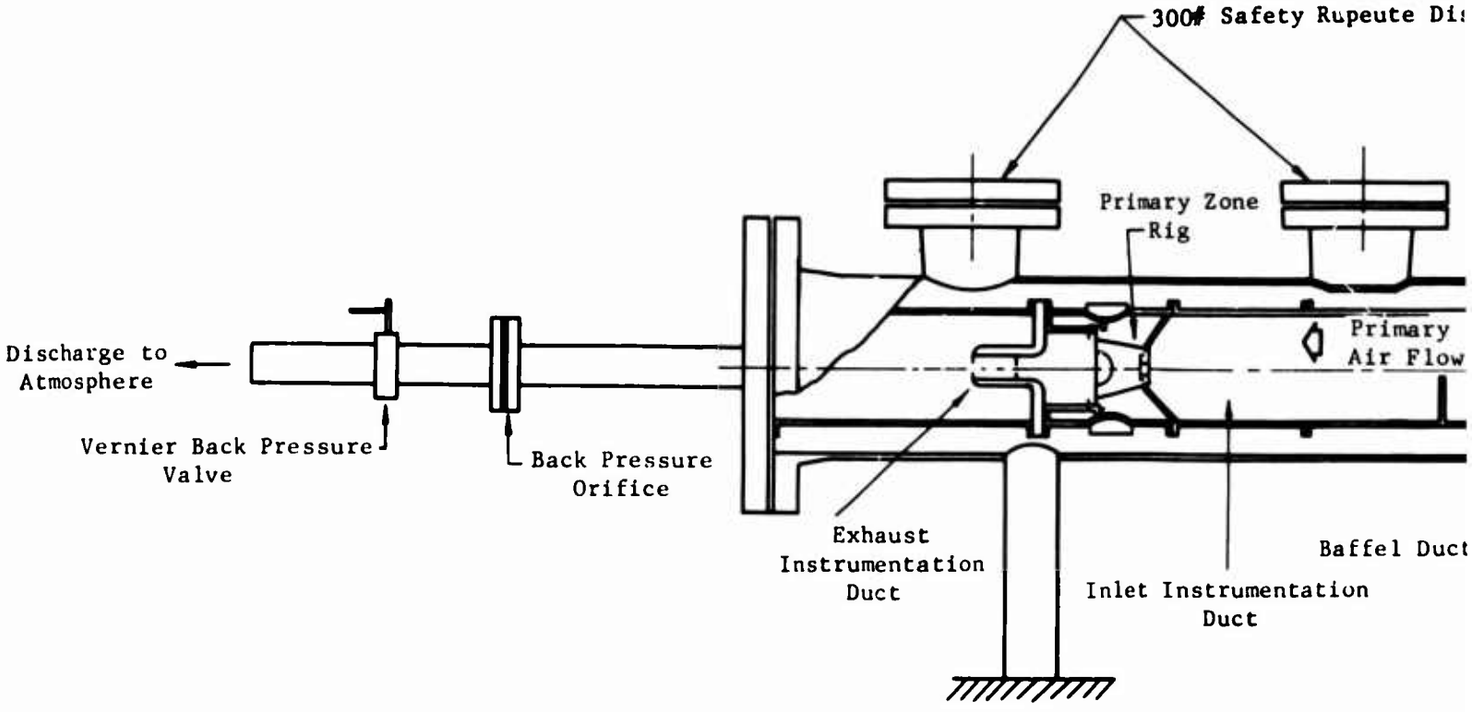

Figure 75. Primary Zone Rig High Pressure Test Stand Installation.

ety Rupeute Discs

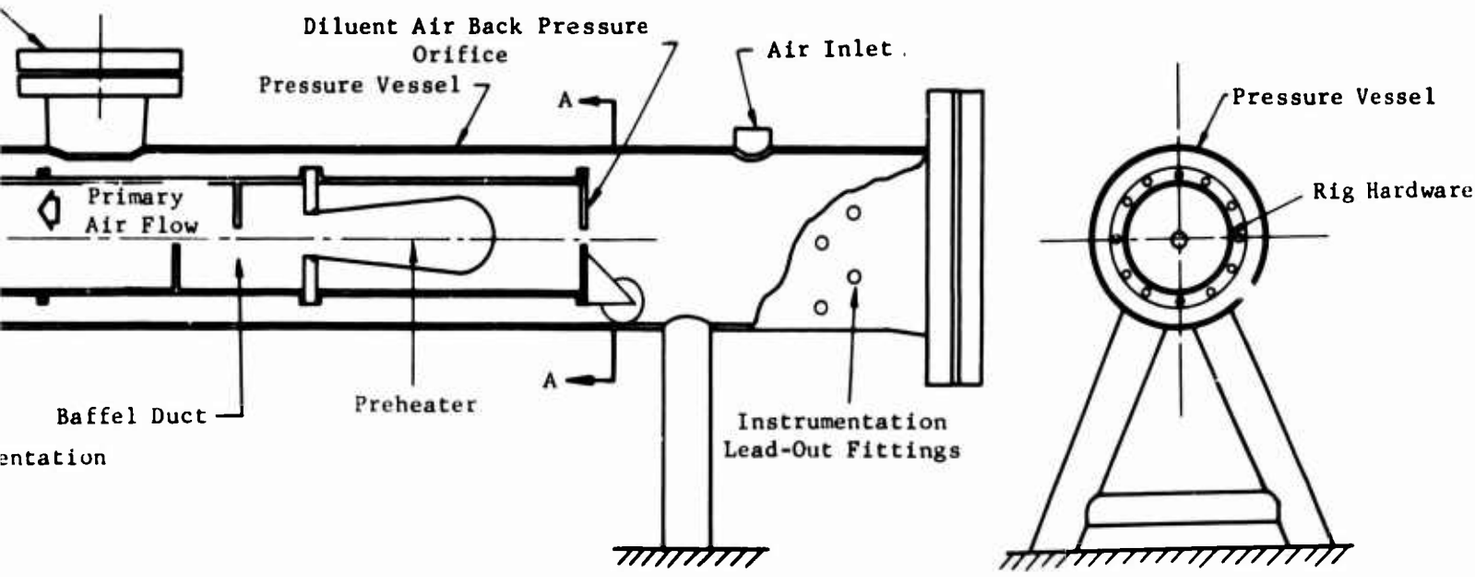

Section A - A

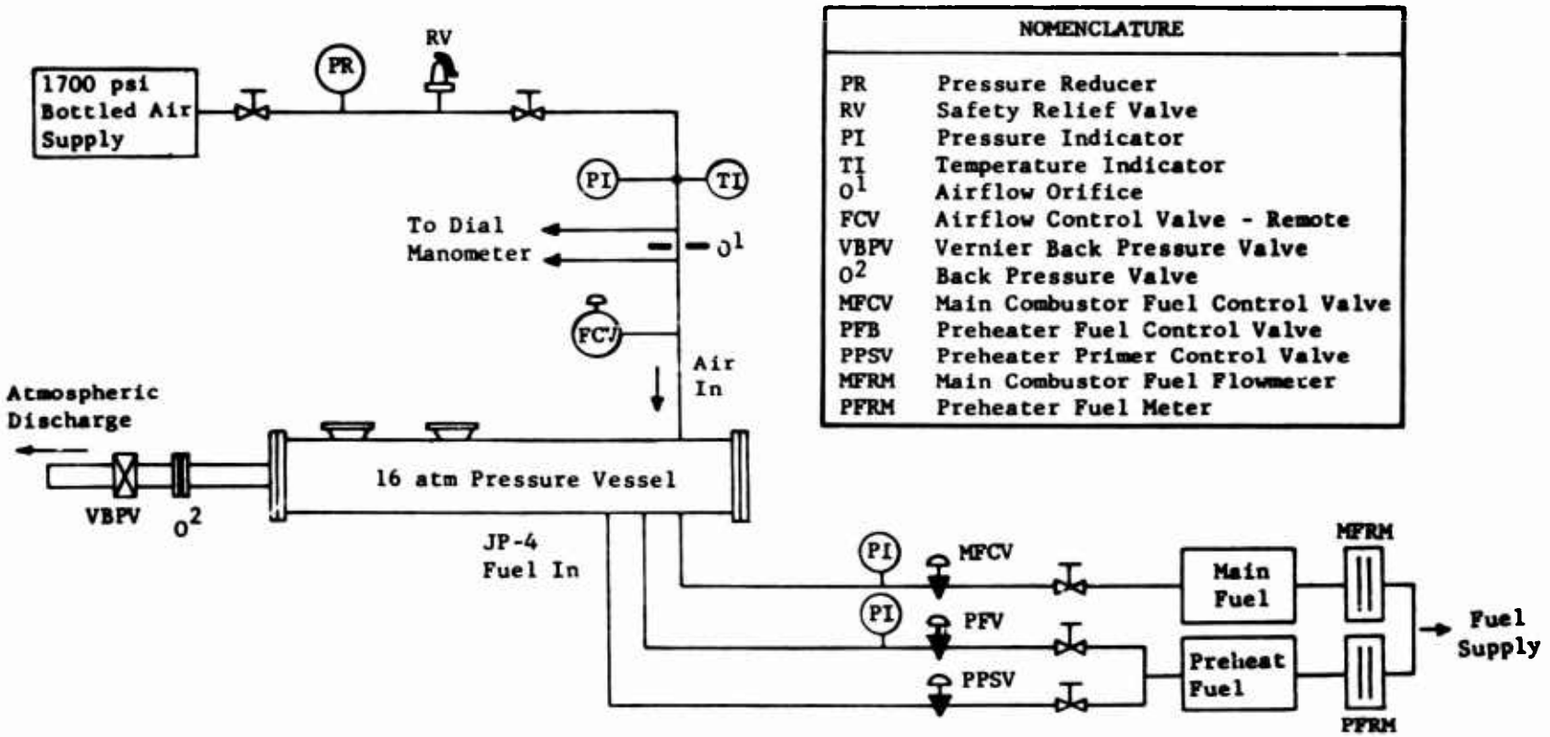

Figure 76. Primary Zone Rig High Pressure Test Facility Fuel and Air Supply Schematic.

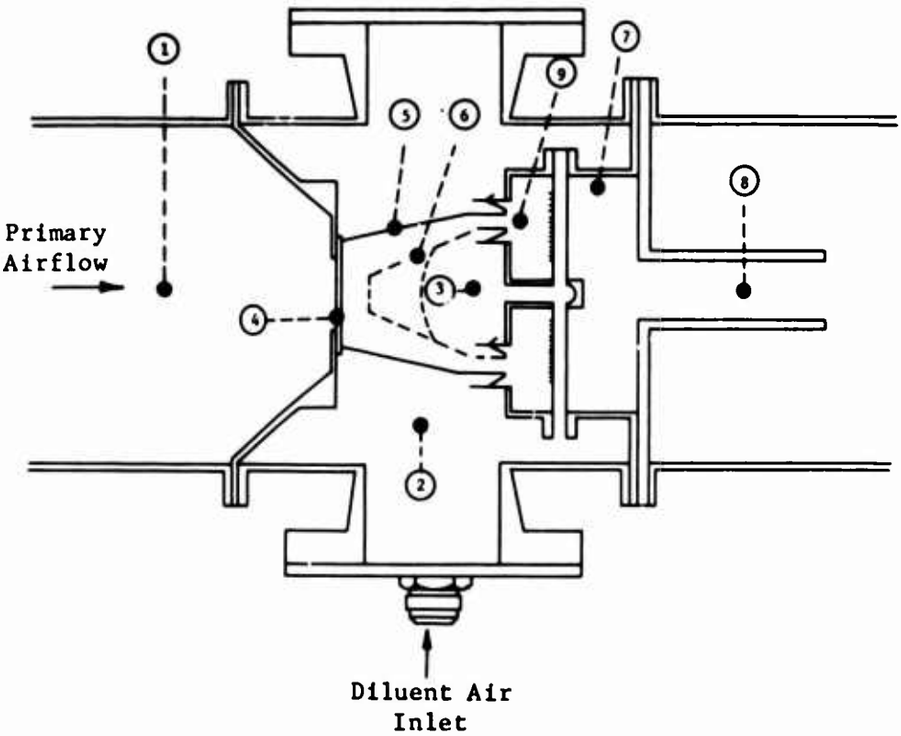

Station Number	Station Description	Type Reading	Number Of Readings
1	Primary Air-Rig Inlet	P_S T_T	2 2
2	Diluent Air-Rig Inlet	P_S T_T	2 2
3	Inner Liner-Inlet	P_S T_T	2 11
4	Headplate - Downstream	P_S	2
5	Outer Liner Metal	T_M	5
6	Inner Liner Metal	T_M	3
7	Exit Plenum	P_S	2
8	Exhaust	T_T	12
9	Primary Exit	T_T	32

Figure 77. Schematic Of Primary Zone Rig Instrumentation.

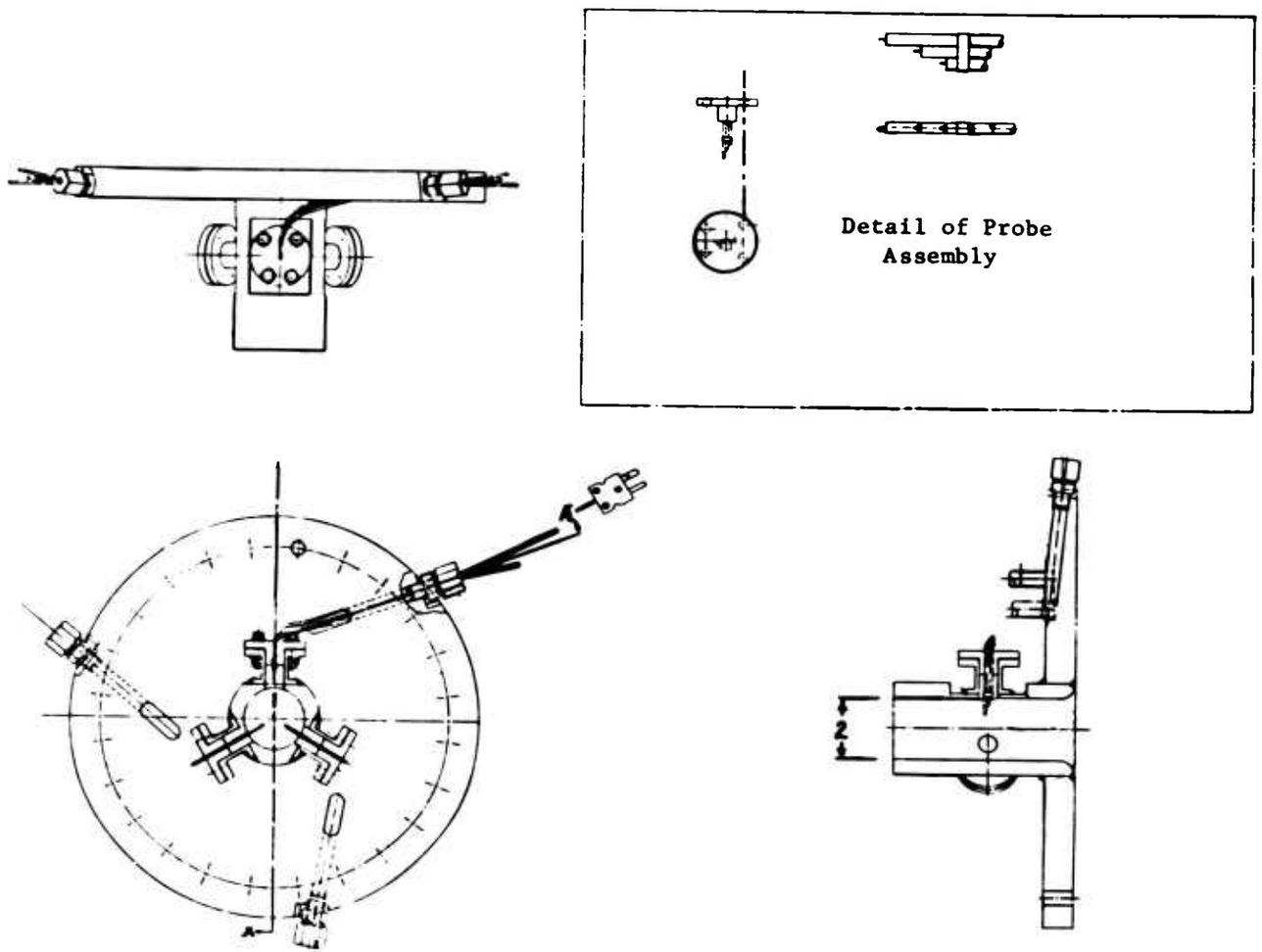

Figure 78. Primary Zone Rig Exhaust Temperature Instrumentation Section.

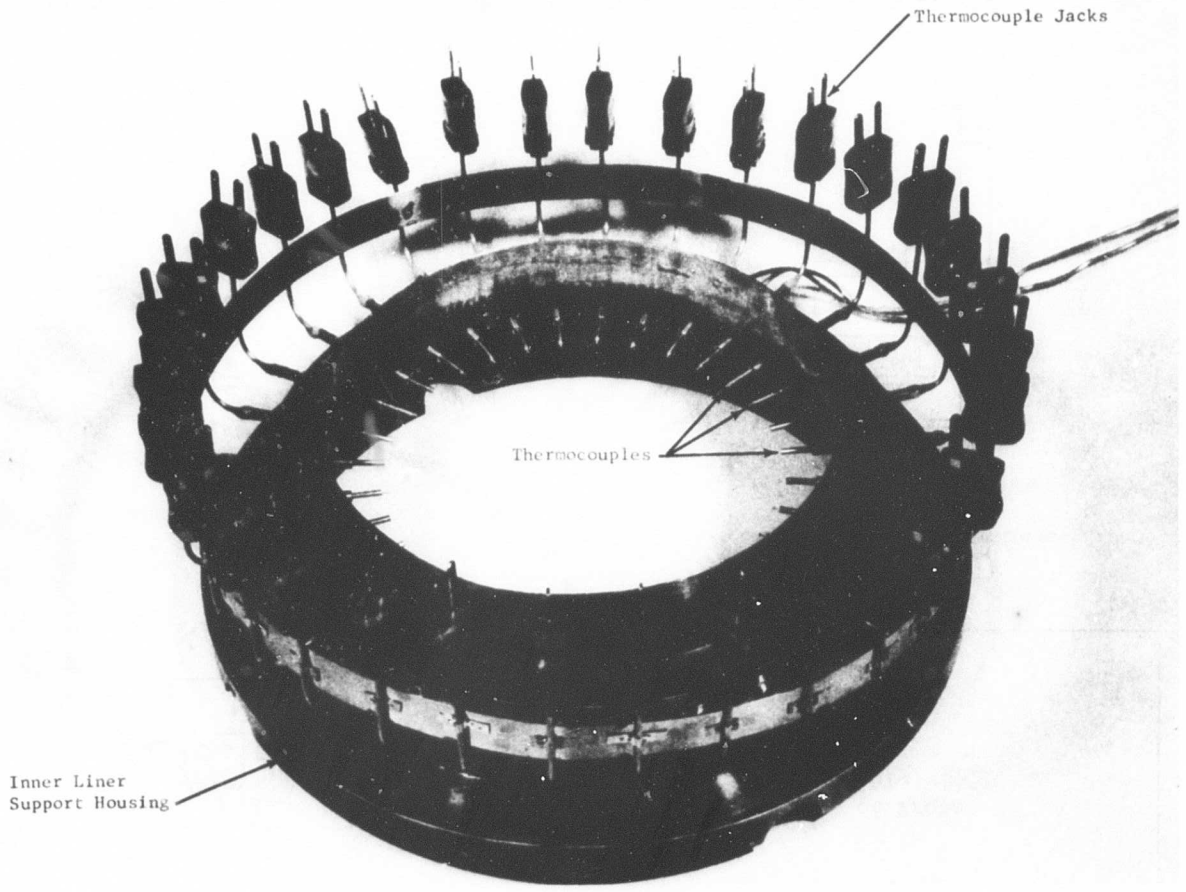

Figure 79. Platinum-Platinum 10% Rhodium Thermocouples Installed in the Inner Liner Support Housing.

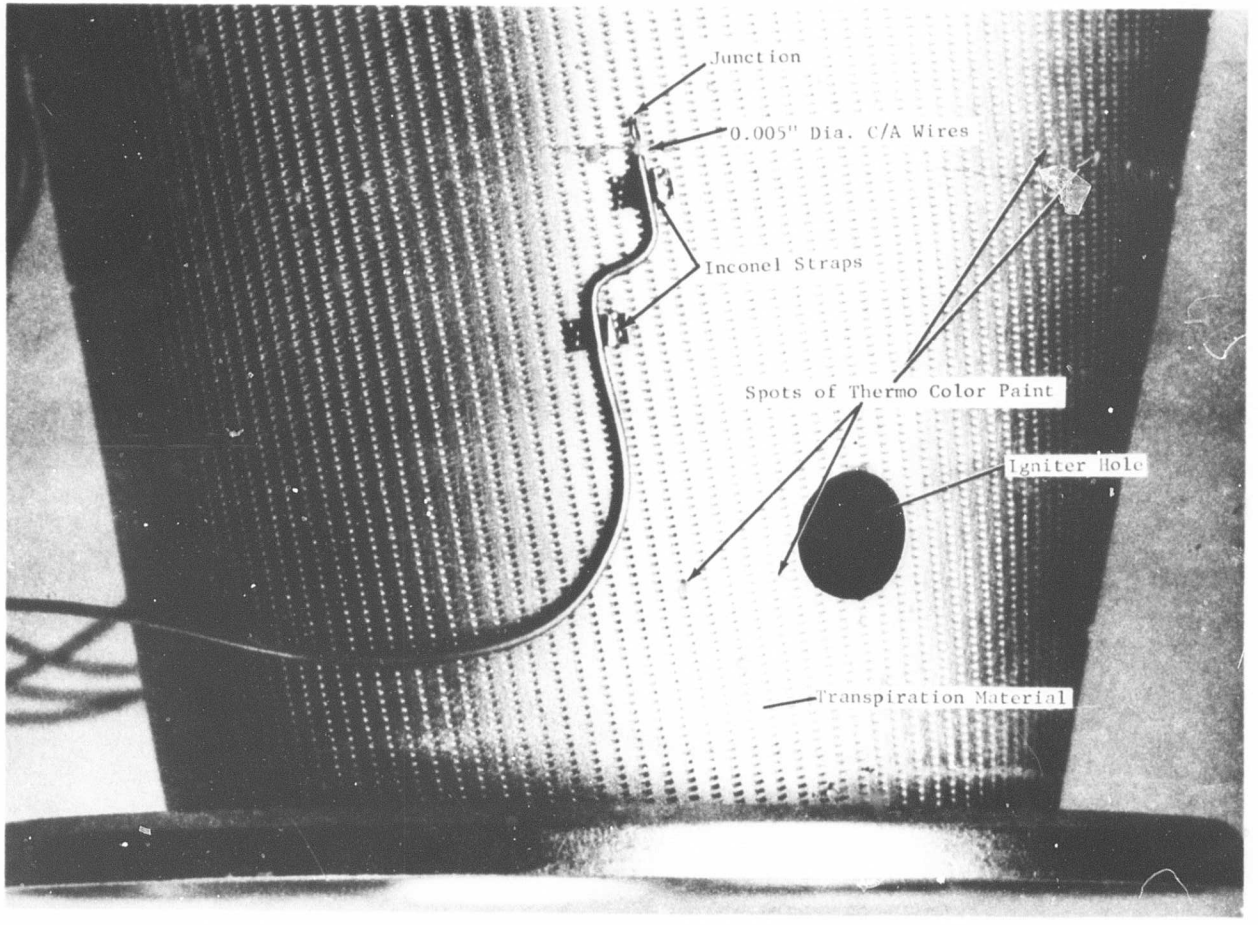

Figure 80. Details of Typical Chromel-Alumel Thermocouple Installation on Transpiration Liner Material.

TABLE XV. PRIMARY ZONE CONFIGURATIONS AND M

Configuration	Build	Time		Fuel Introduction System	Fuel Feed System	
		Test	Burn			
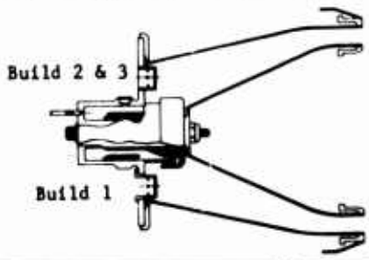 1	1	17:00	6:30	Annular Vaporizer	8-Point Radial-Internal Manifold	
	2	16:40	13:55	Annular Vaporizer	4-Point Axial	J
	3	5:30	4:25	Annular Vaporizer	8-Point Radial-External Manifold And 4-Point Axial	
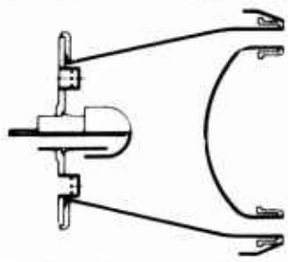 2	1	4:20	3:25	Mushroom Vaporizer	Single Point Axial	
	2	10:35	9:20	Mushroom Vaporizer	Single Point Axial	J
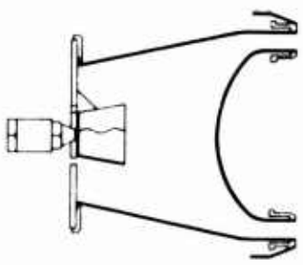 3	1	6:30	3:30	Atomizer-Educer	Simplex Atomizer	
	2	10:50	8:35	Atomizer-Educer	Simplex Atomizer	J
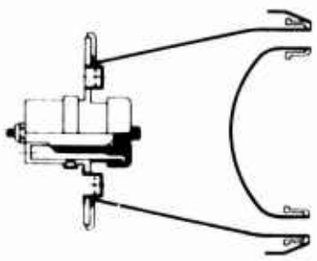 4	1	5:55	4:00	Annular Vaporizer	8-Point Radial-External Manifold	
	2	7:20	3:00	Annular Vaporizer	8-Point Radial-External Manifold	

ZONE CONFIGURATIONS AND MODIFICATIONS TESTED

Fuel Feed System	Fuel	Inner Liner	Diluent Holes in Outer Liner	Inlet Temperature (°F)	General Information
adial-Internal Manifold	JP4	Conical	8	700	Preliminary Tests at Design Inlet Conditions
4-Point Axial	JP4 & JP5	Conical	8	700, 500, 300	Off Design Evaluation - Braze Flow Damaged Inner Liner
adial-External Manifold 4-Point Axial	JP5	Conical	16	700	Circumferential Exit Temperature Distribution Evaluation
gle Point Axial	JP4	Dome	8	700	Preliminary Tests at Design Inlet Conditions
gle Point Axial	JP4 & JP5	Dome	16	700, 500, 300	Off Design and Circumferential Exit Temperature Distribution Evaluation
mplex Atomizer	JP4	Dome	8	700	Preliminary Tests at Design Inlet Conditions
mplex Atomizer	JP4 & JP5	Dome	16	700, 500, 300	Off Design and Circumferential Exit Temperature Distribution Evaluation
adial-External Manifold	JP4	Dome	16	700	Preliminary Evaluation of Configuration Prior to 16 Atm. Test
adial-External Manifold	JP4	Dome	16	700	Configuration Evaluation on High Pressure Facility Including 16 Atmospheres Pressure Test

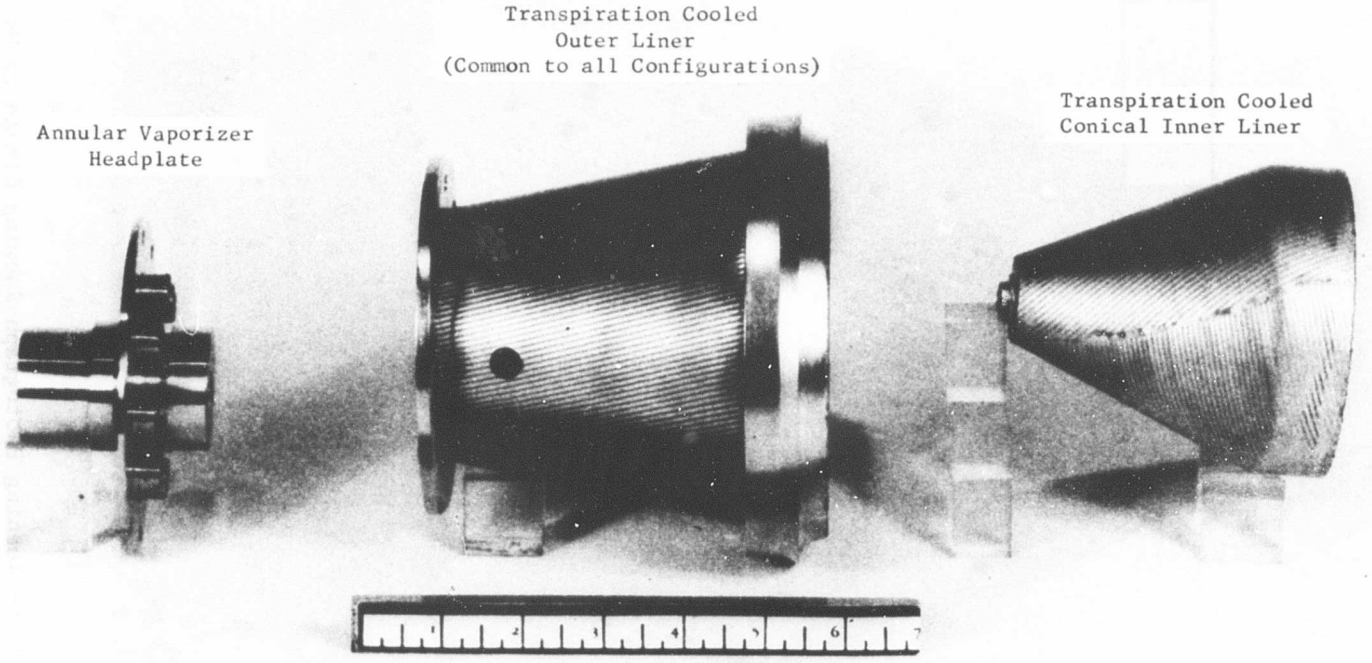

Figure 81. Exploded View of Primary Zone Configuration 1 Hardware (New).

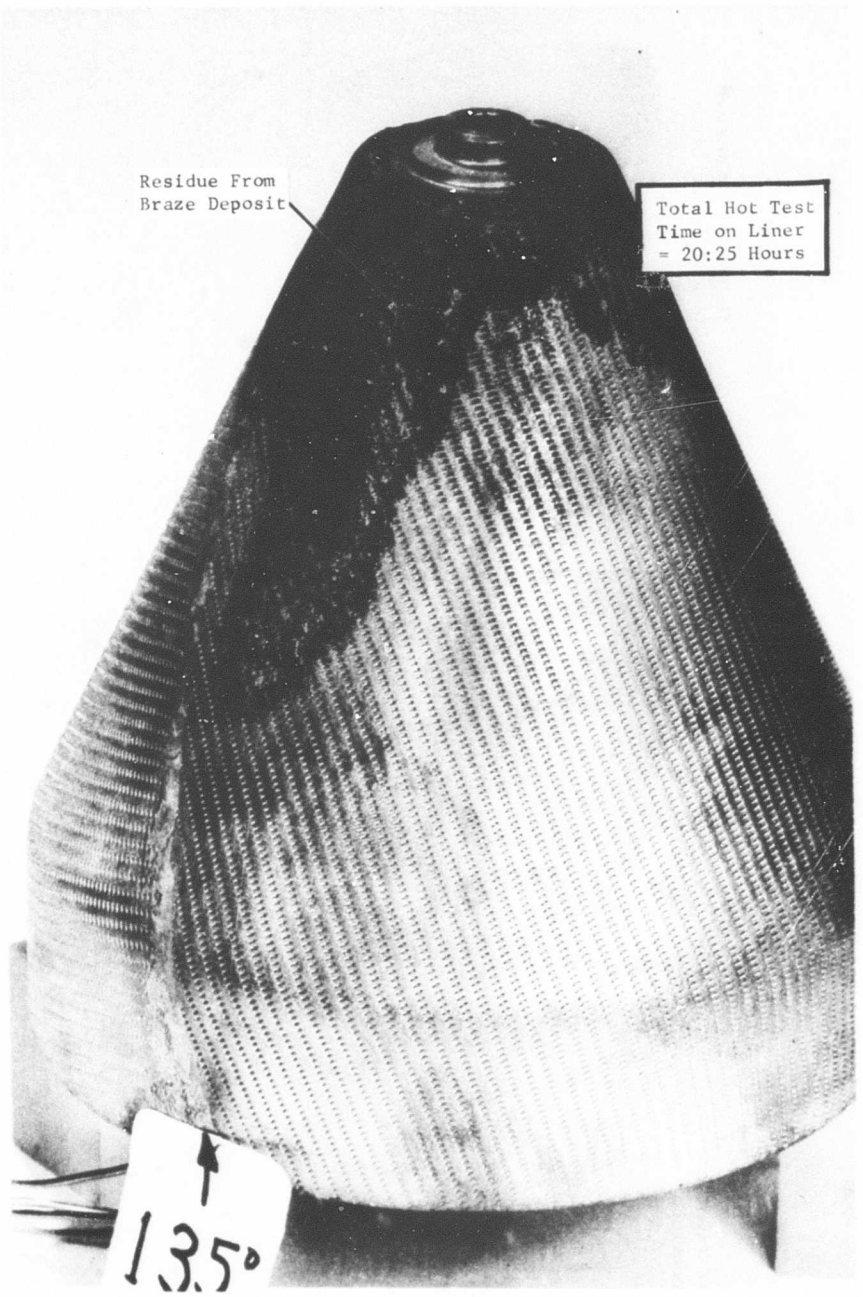

Figure 82 Post-Cleaning Photograph Showing Damage to Hot Side of Transpirationally Cooled, Conical Shaped, Inner Liner Due to Braze Deposit.

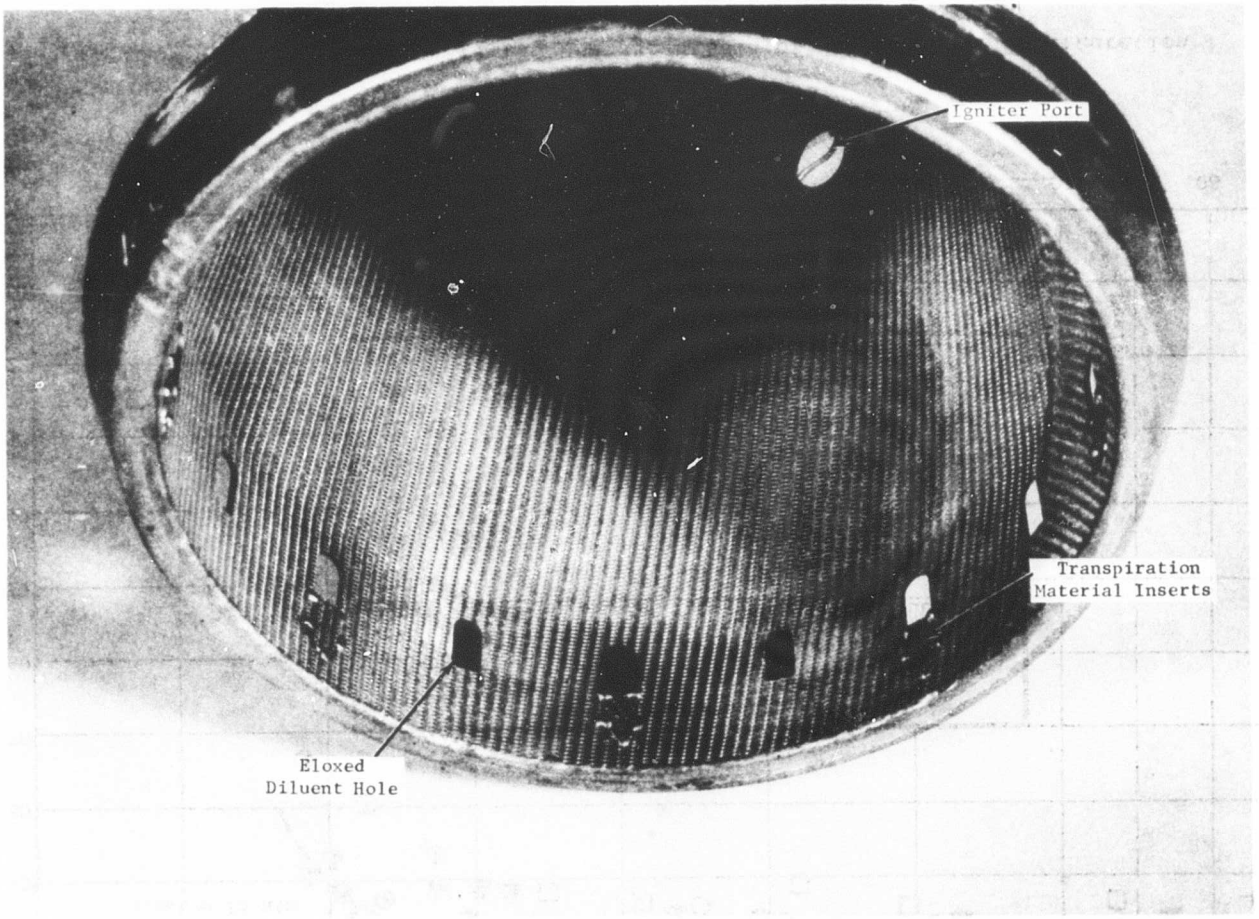

Figure 83. Revised Diluent Slot Geometry On Transpirationally Cooled Outer Liner.

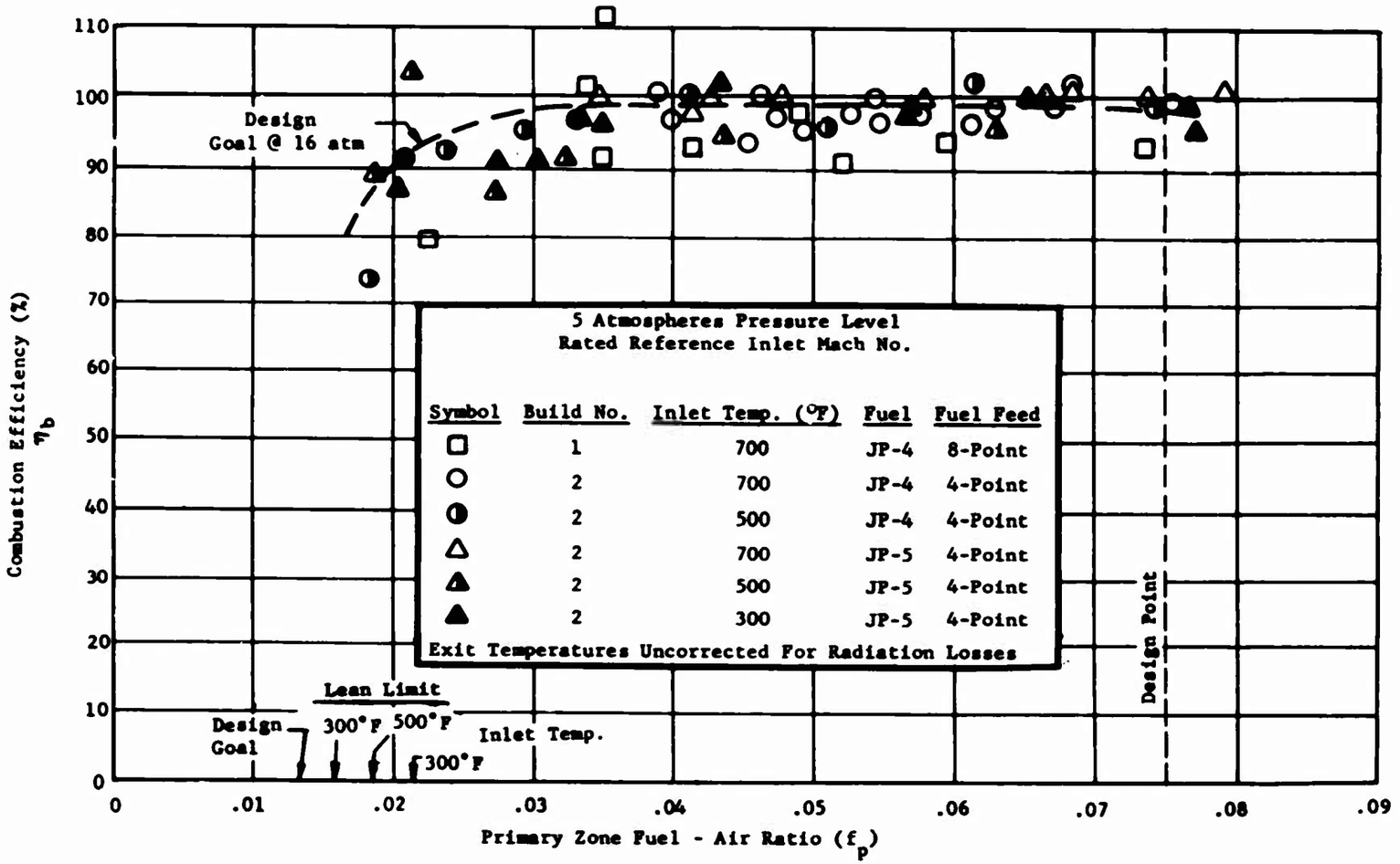

Figure 84. Combustion Efficiency Characteristic of Primary Zone Configuration 1, Builds 1 and 2.

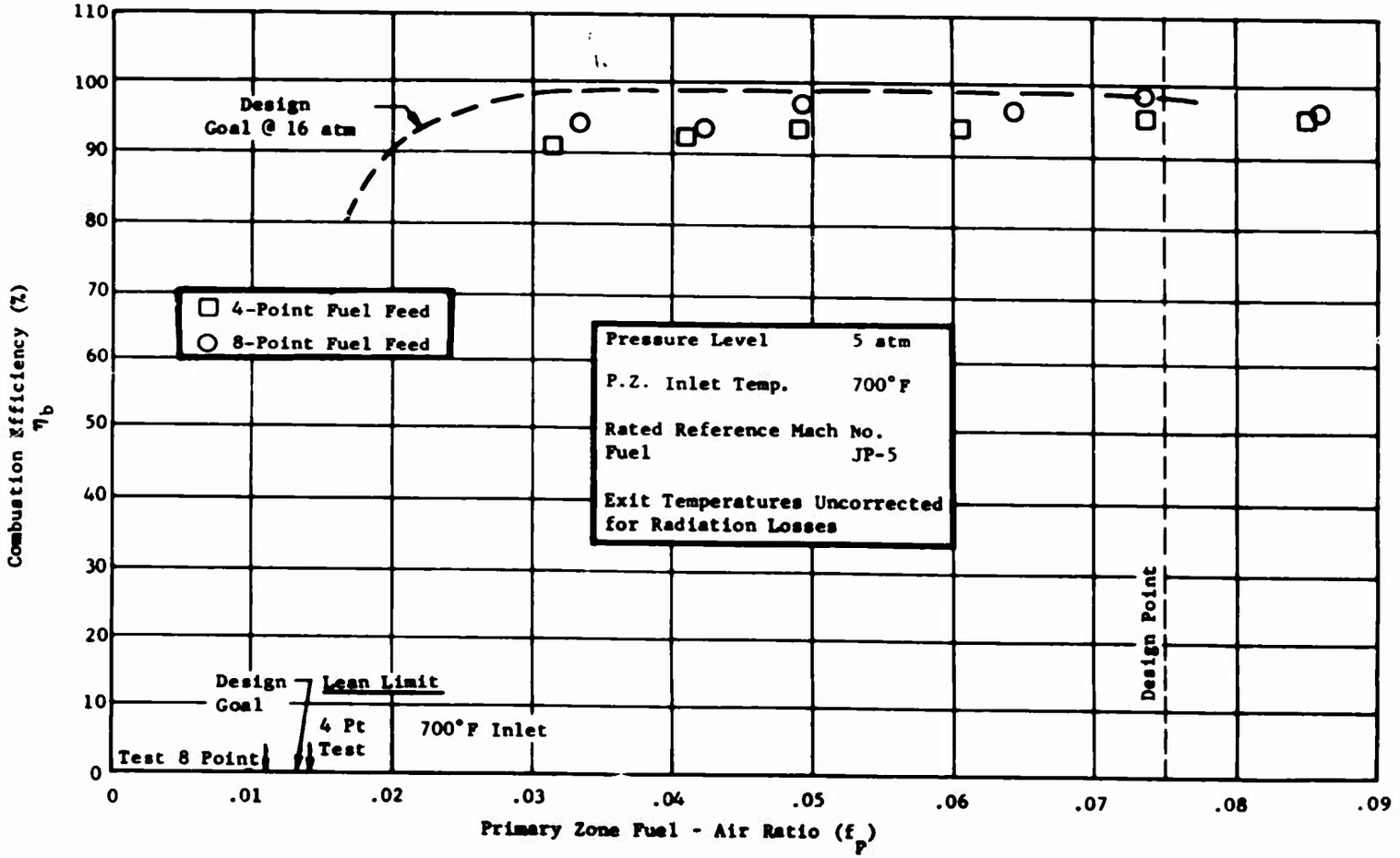

Figure 85. Comparison of Combustion Efficiency Characteristics of Four-Point Axial and Eight-Point Radial Fuel Feed Systems of Primary Zone Configuration 1, Build 3.

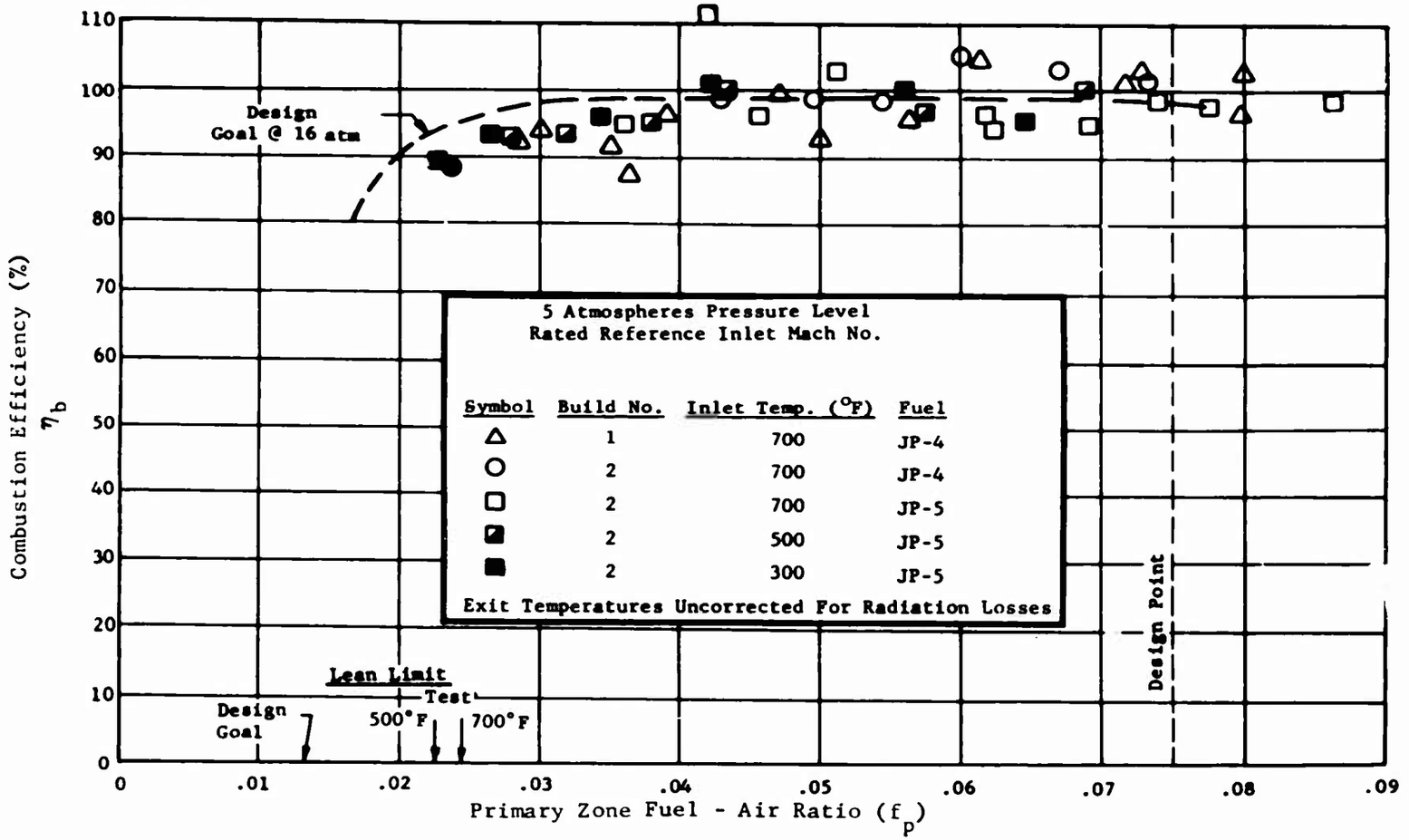

Figure 86. Combustion Efficiency Characteristic of Primary Zone Configuration 2.

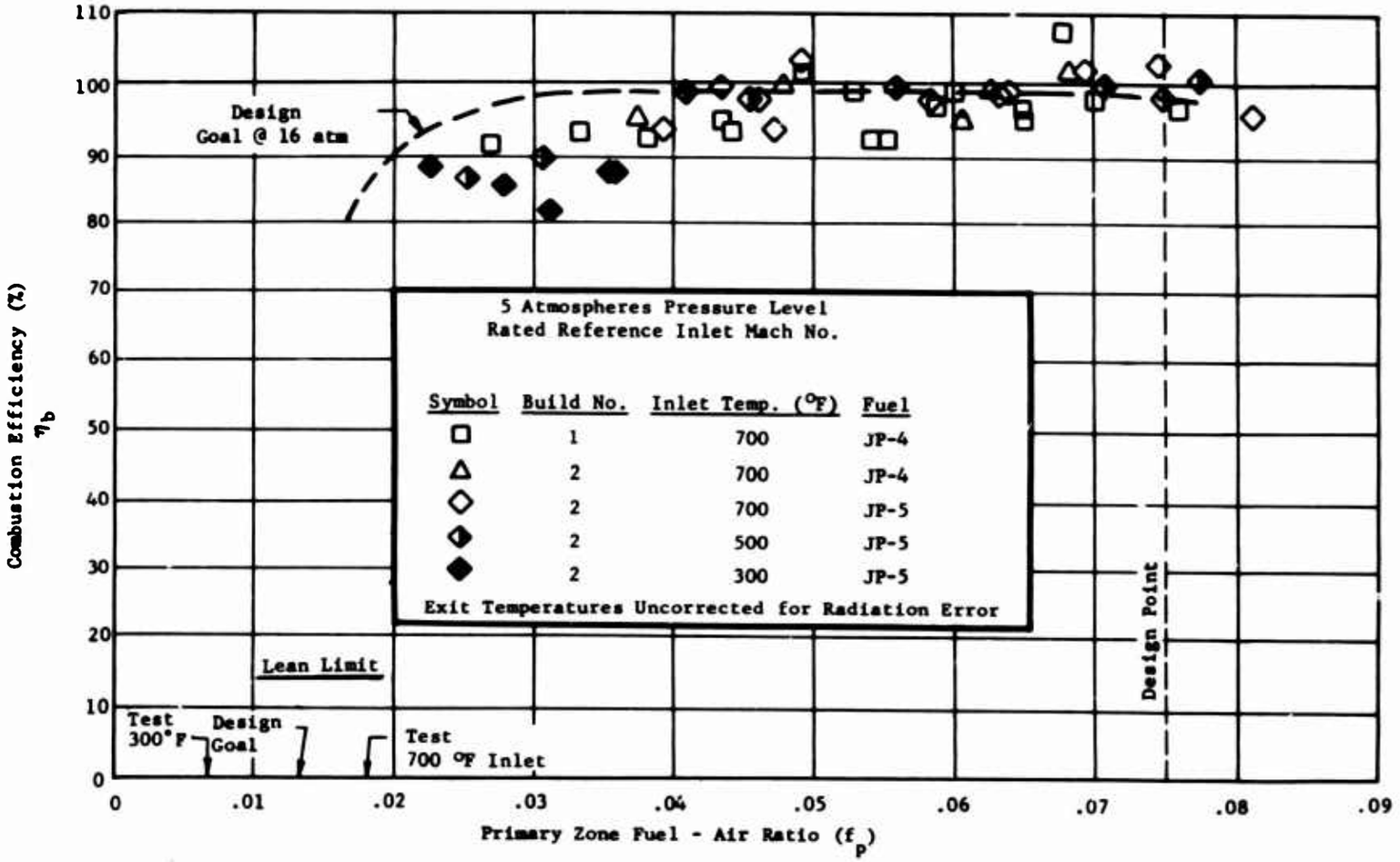

Figure 87. Combustion Efficiency Characteristic of Primary Zone Configuration 3.

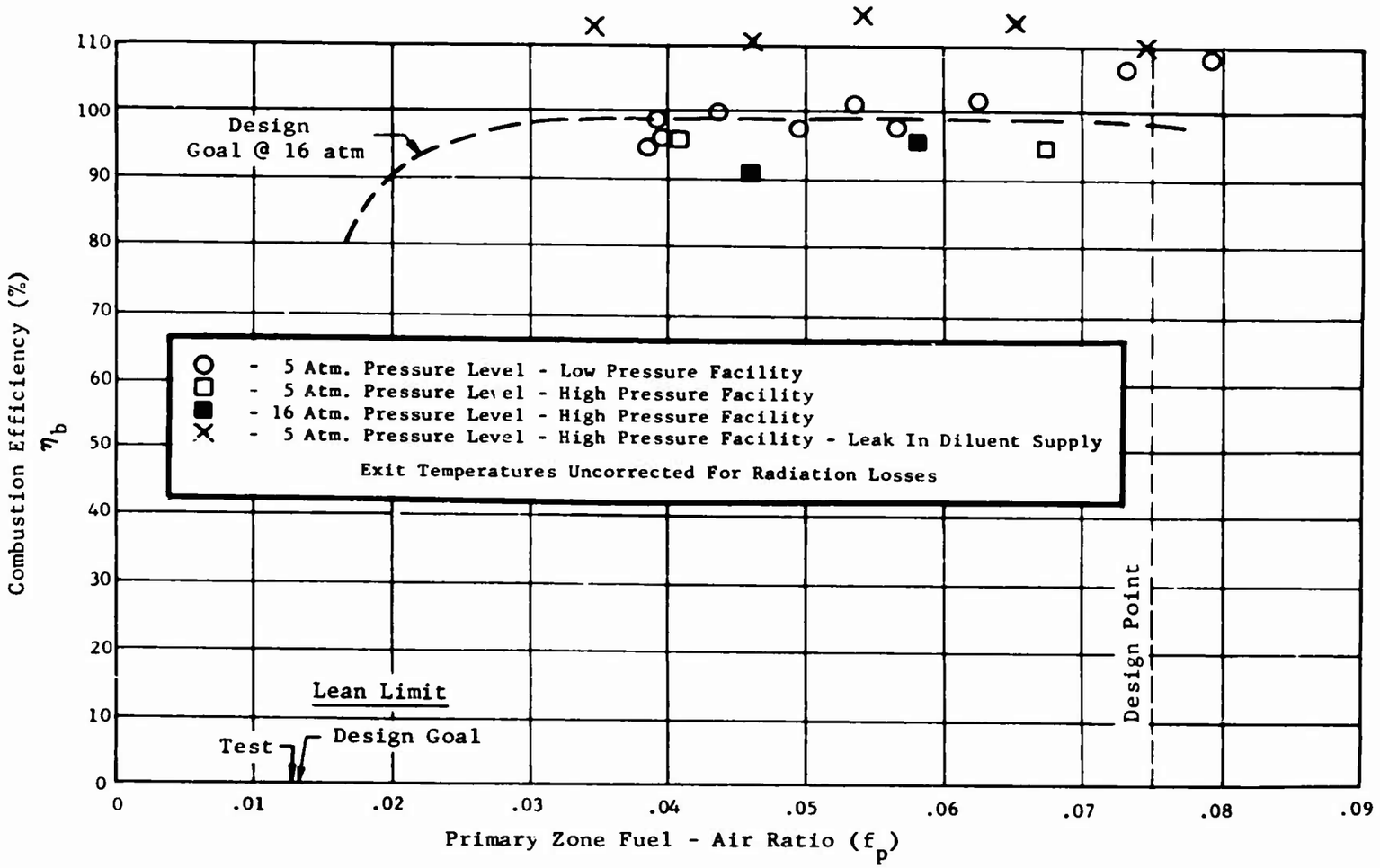

Figure 88. Combustion Efficiency Characteristic of Primary Zone Configuration 4 for Low and High Pressure Facility Tests.

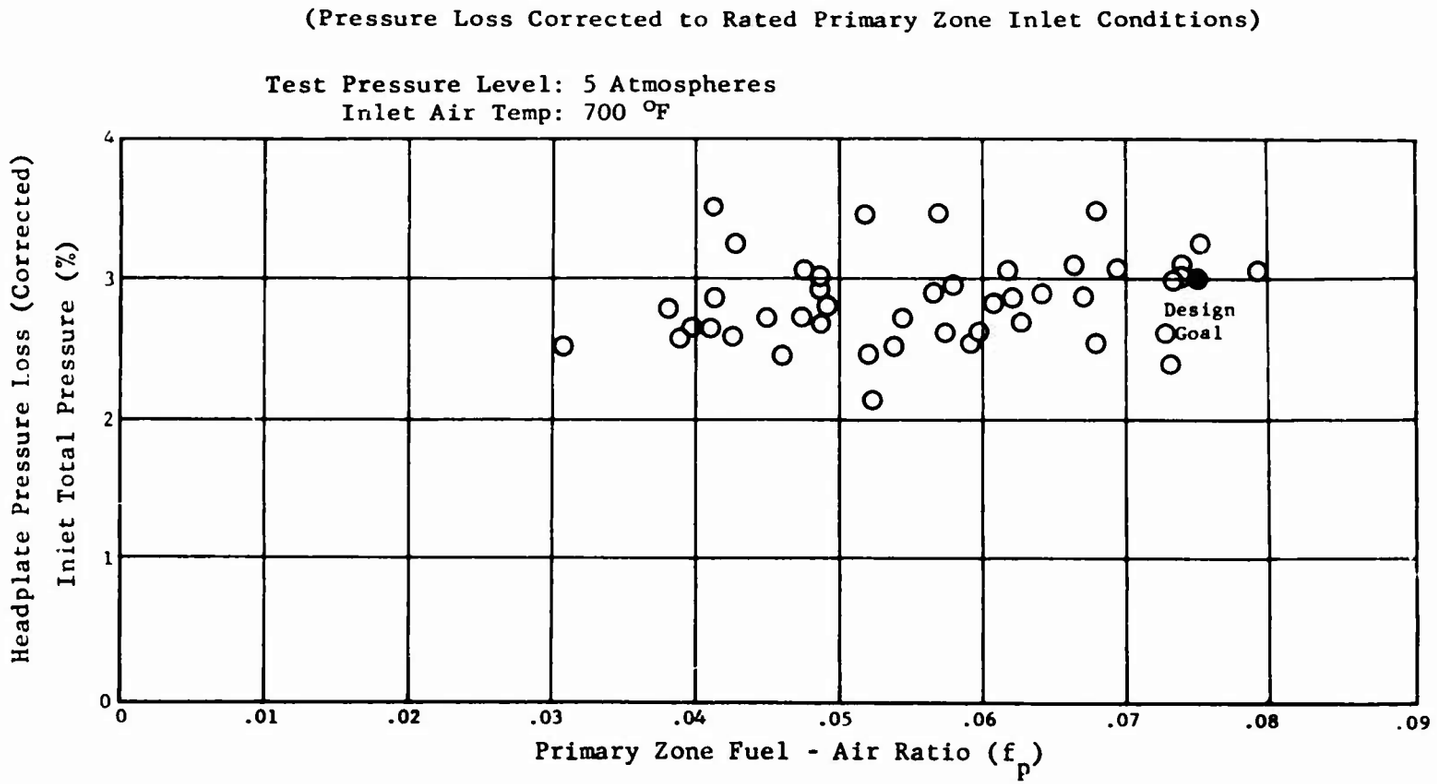

Figure 89. Headplate Pressure Loss Characteristic for Primary Zone Configuration 1.

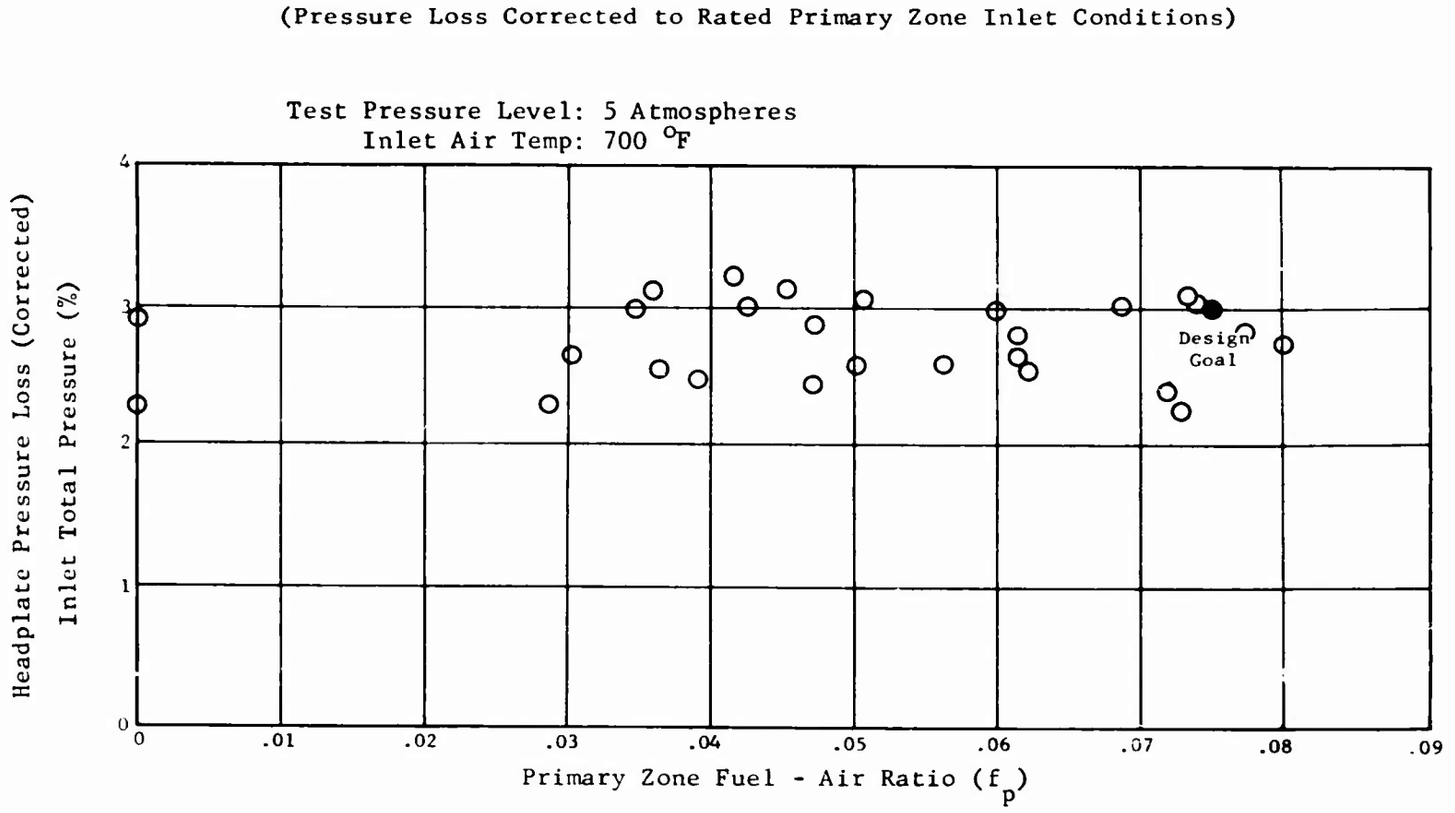

Figure 90. Headplate Pressure Loss Characteristic of Primary Zone Configuration 2.

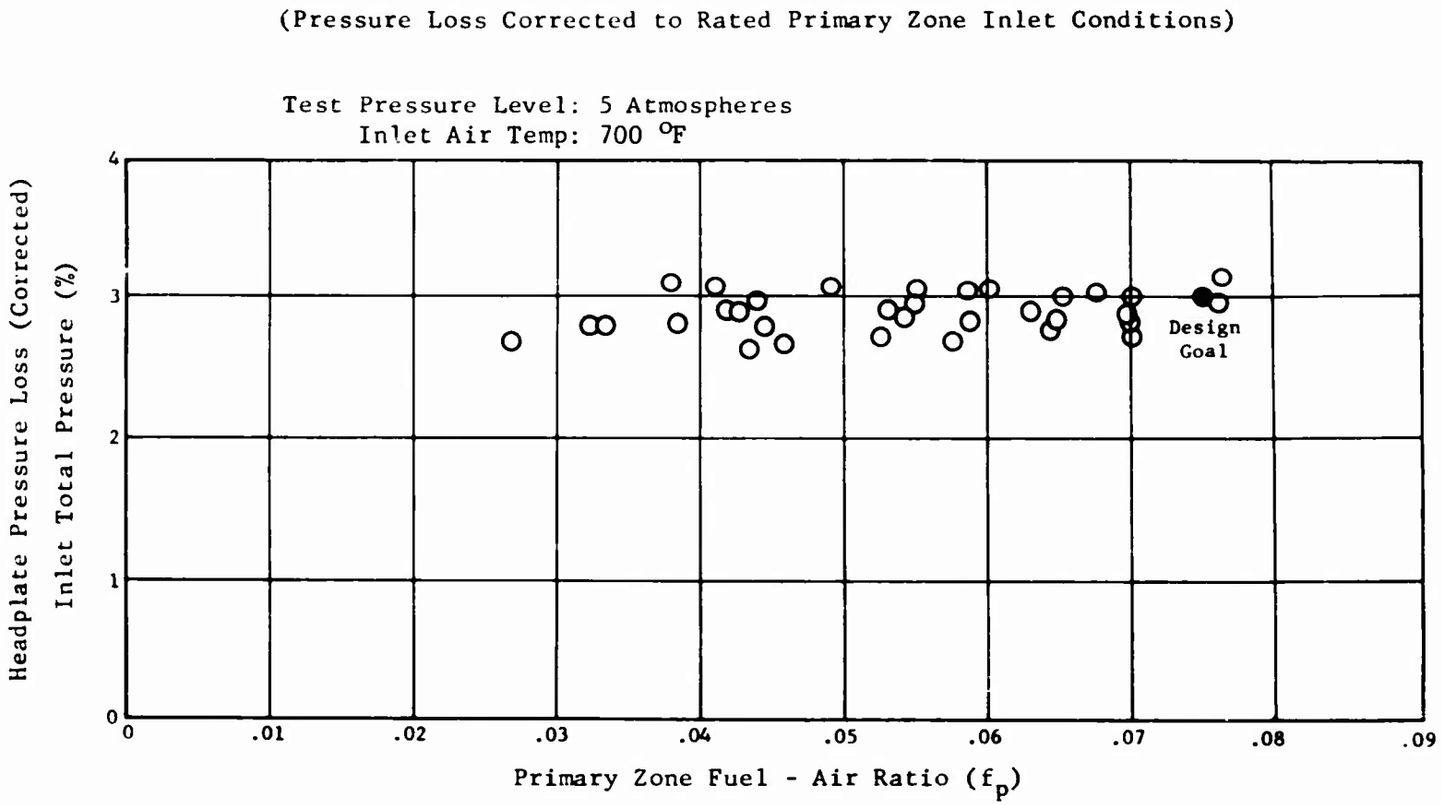

Figure 91. Headplate Pressure Loss Characteristic of Primary Zone Configuration 3.

Inlet Pressure - 5 Atm. Fuel JP-5

Inlet Temperature - 1160°R

Diluent Slot Locations

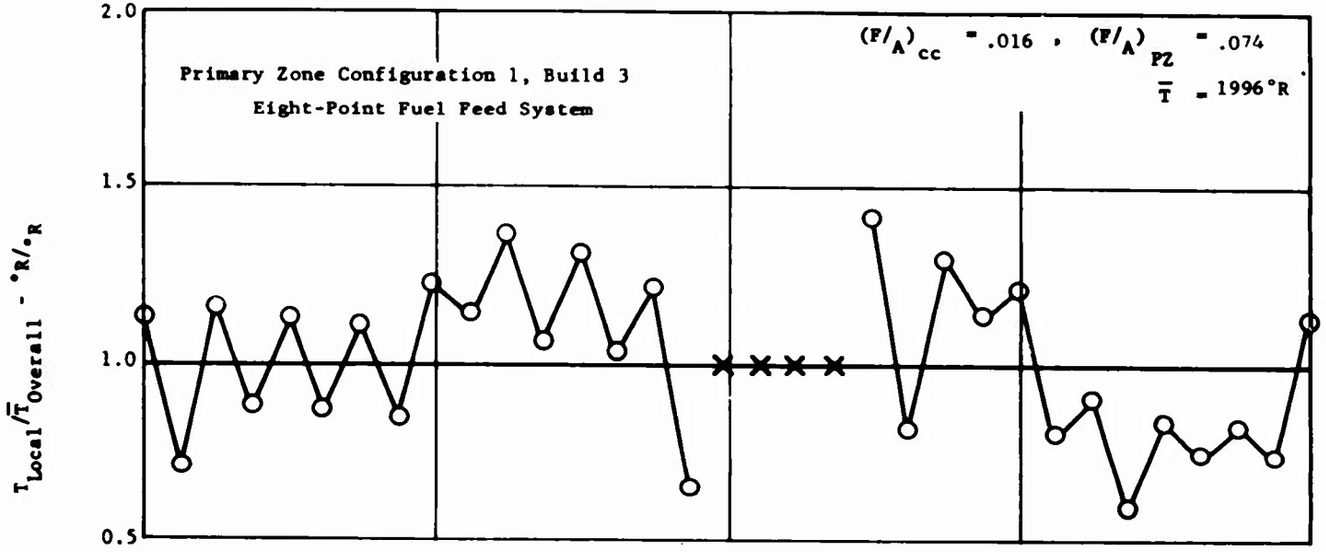

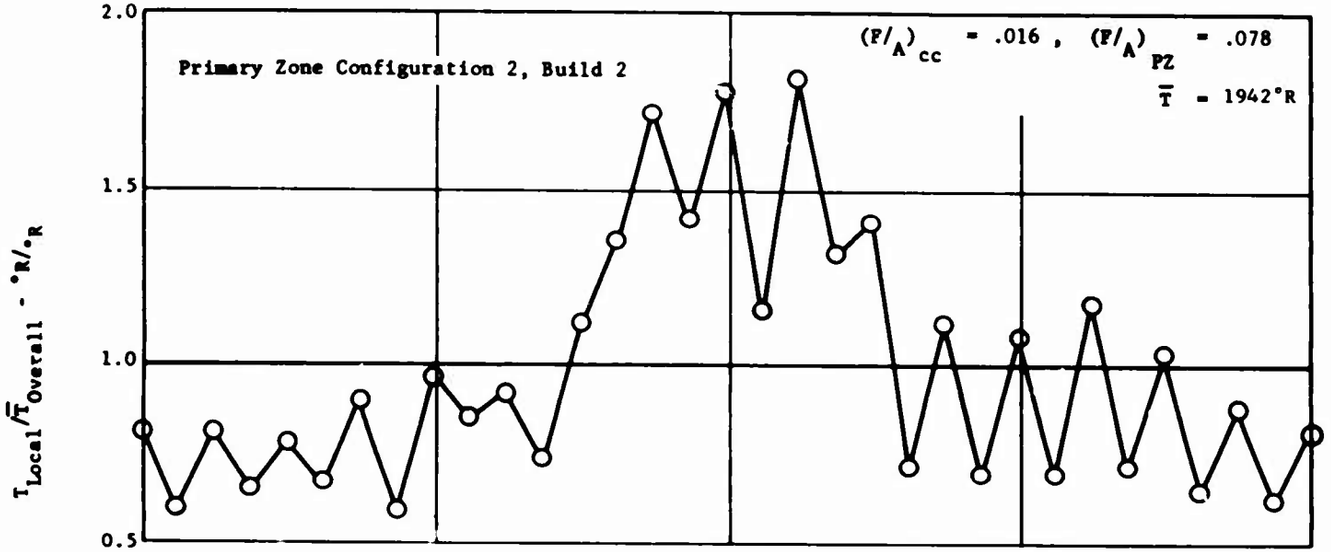

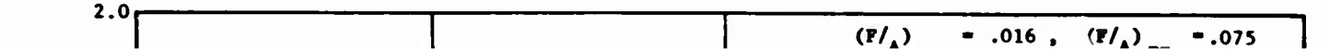

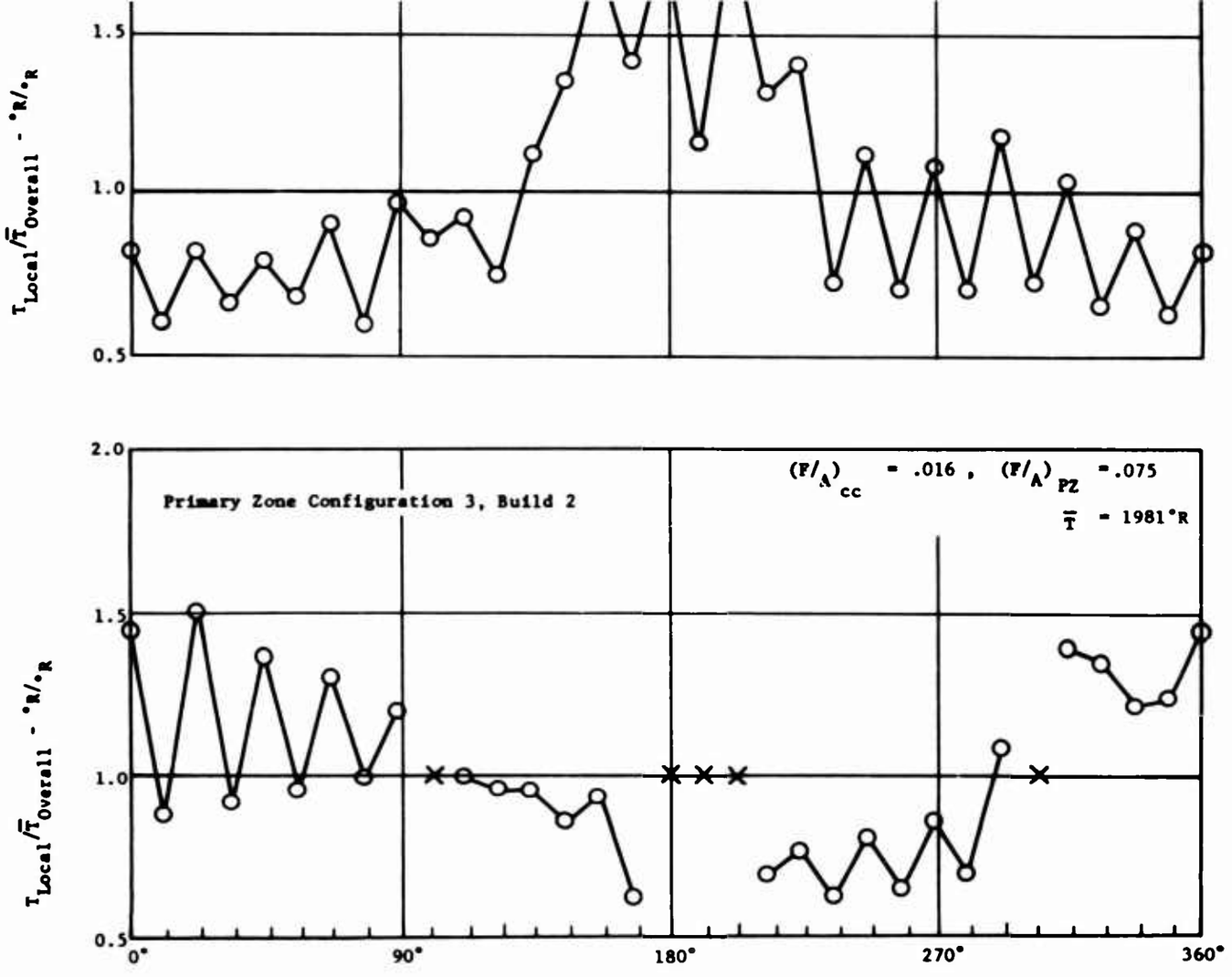

Figure 92. Comparison of Typical Circumferential Exit Temperature Distributions for Primary Zone Configurations 1, 2 and 3.

Inlet Pressure - 5 Atm. Fuel JP-5

Inlet Temperature - 1160°R

Diluent Slot Locations

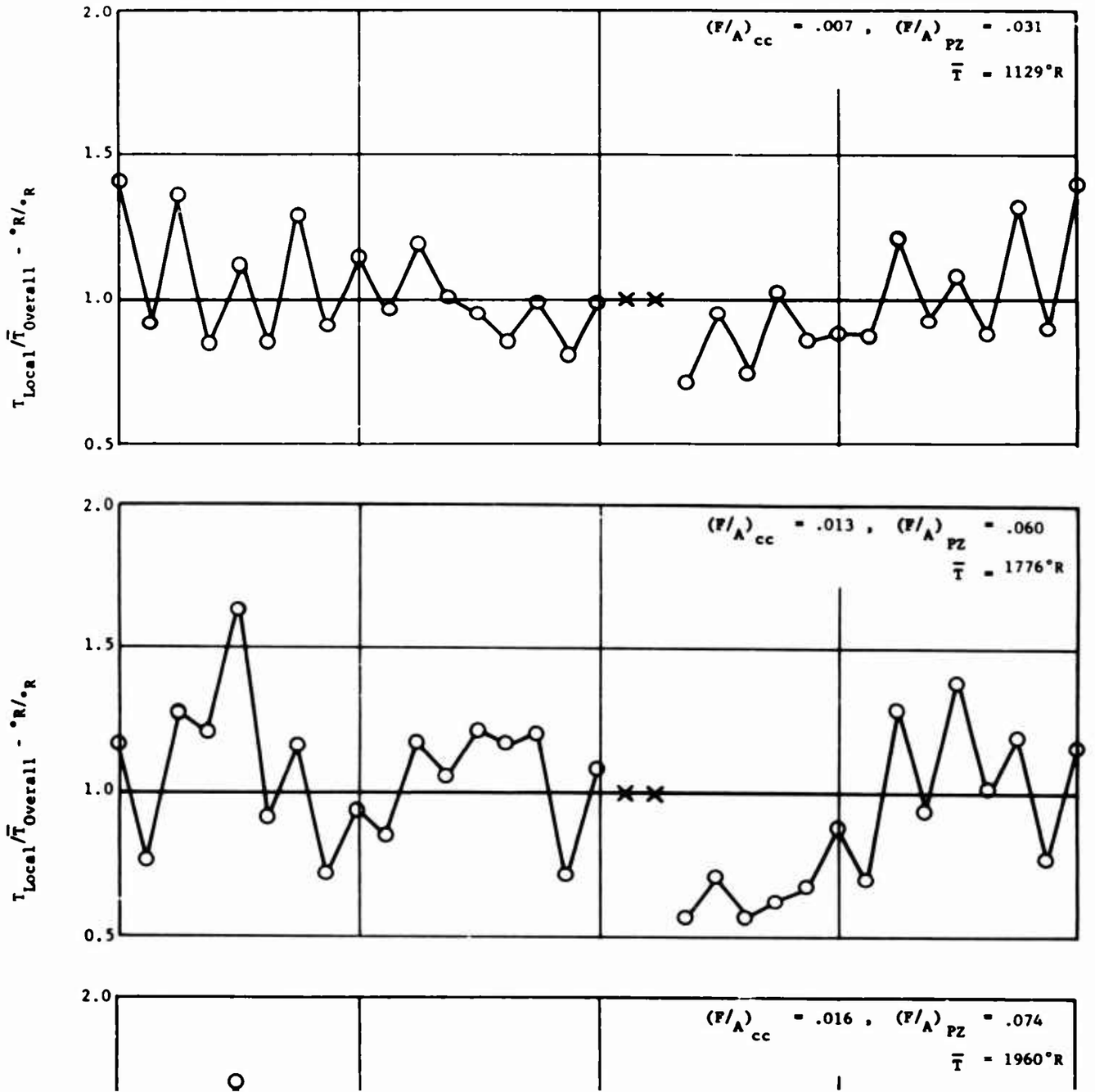

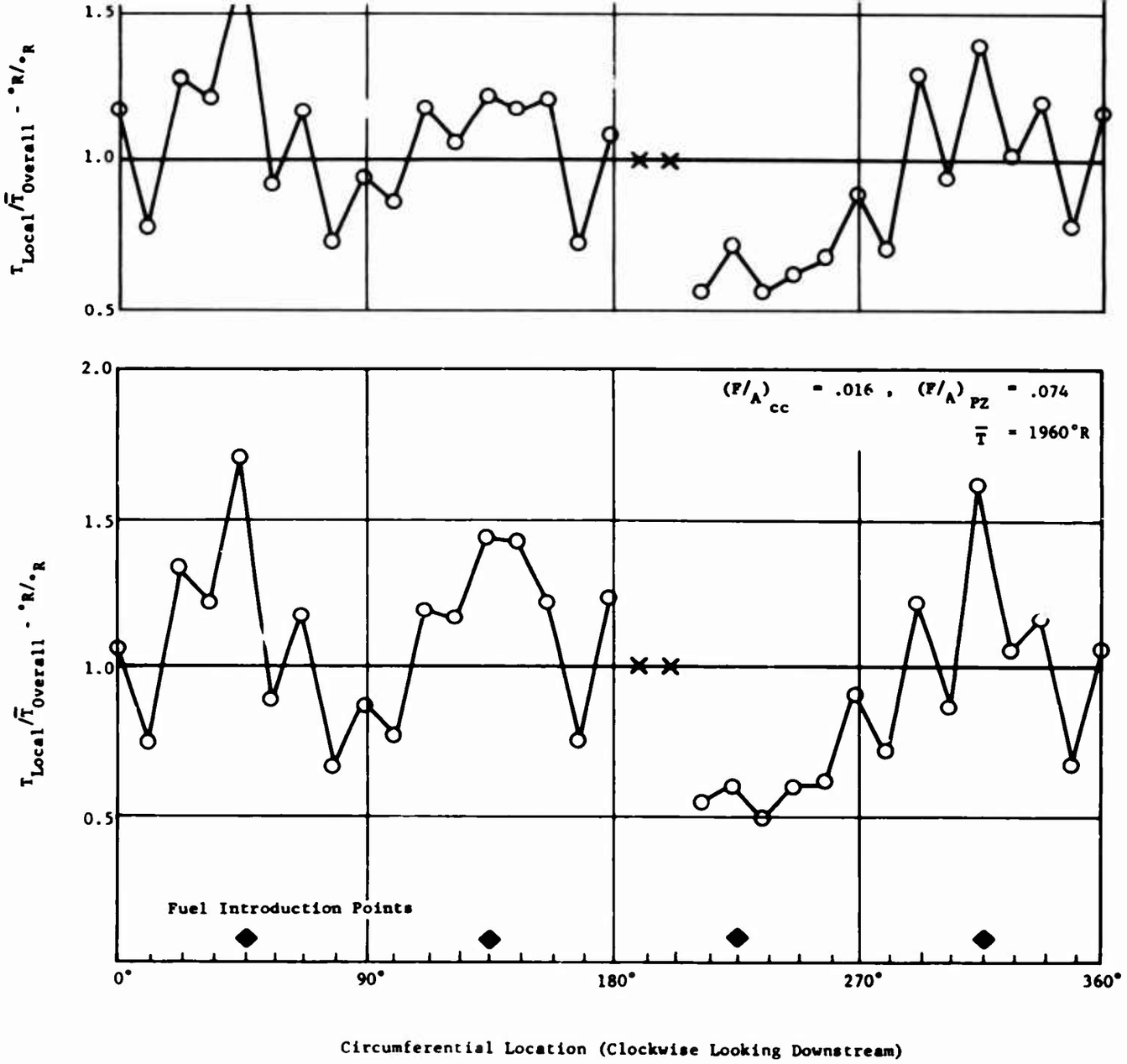

Figure 93. Circumferential Exit Temperature Distributions of Primary Zone Configuration 1, With Four-Point Axial Fuel Feed System for Varying Fuel Flows.

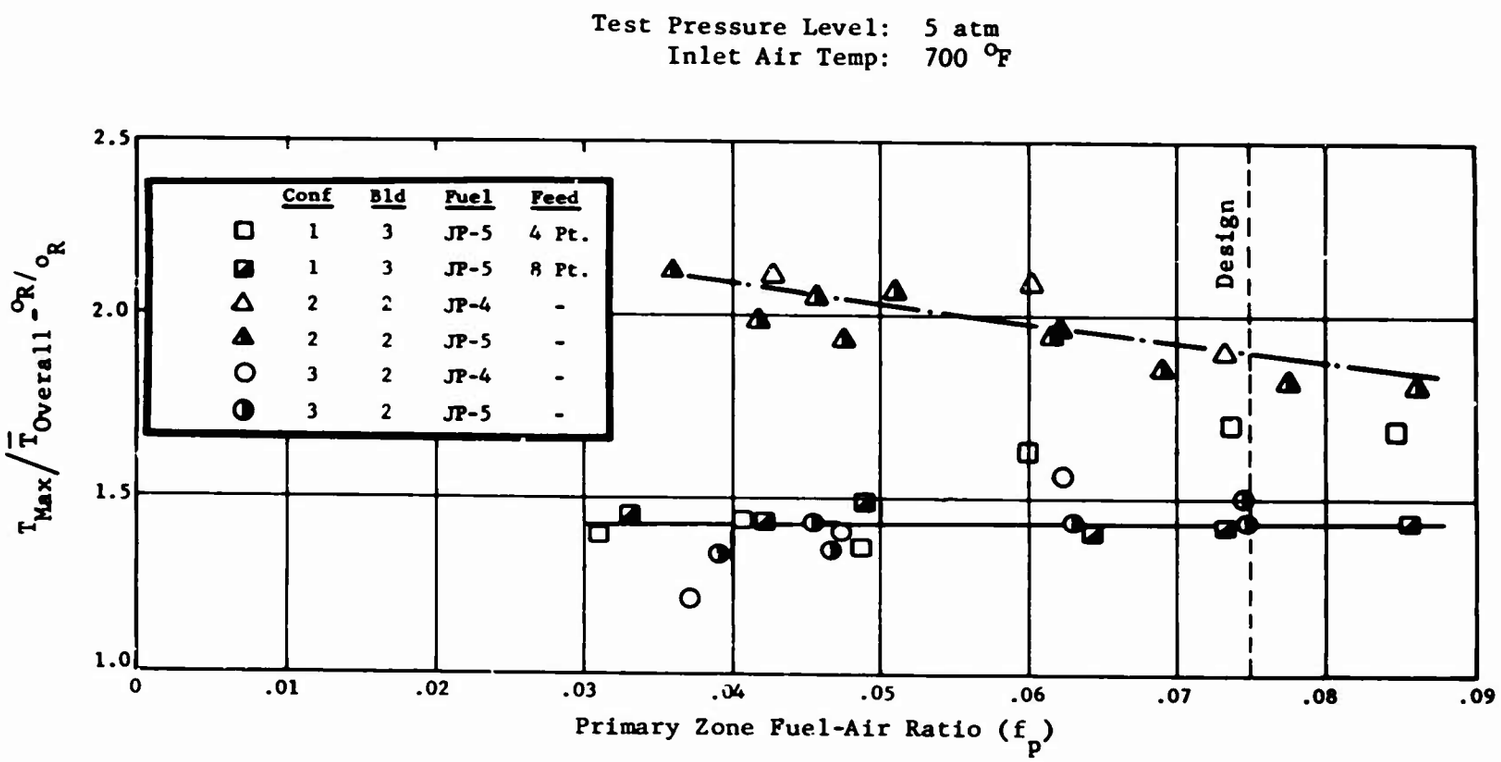

Figure 94. Comparison of Maximum Exit Temperature Characteristics for Primary Zone Configurations 1, 2 and 3.

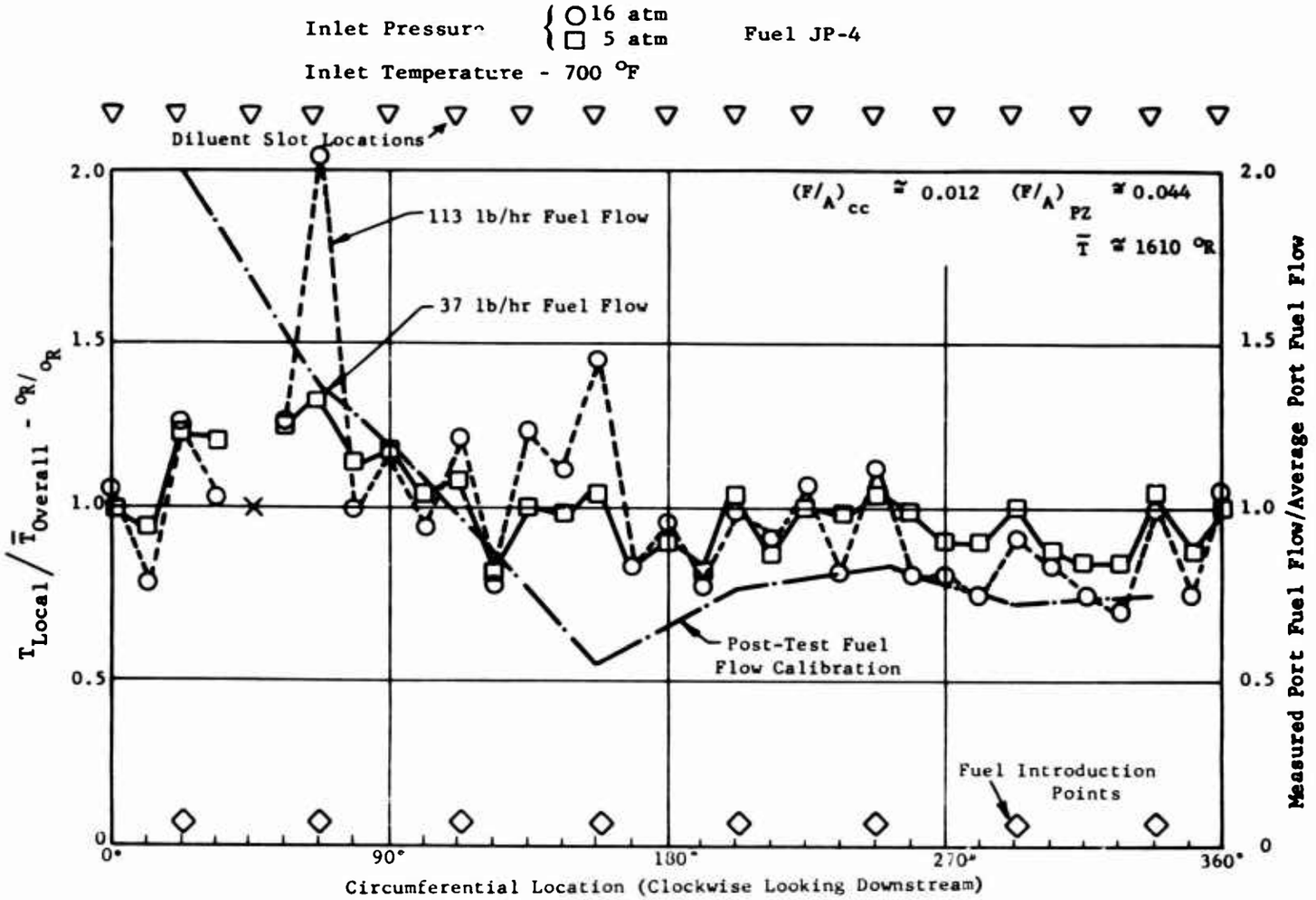

Figure 95. Circumferential Exit Temperature Distribution for Primary Zone Configuration 4 for 5 and 16 Atmospheres Pressure Level Tests (Post-Test Fuel Flow Calibration Superimposed).

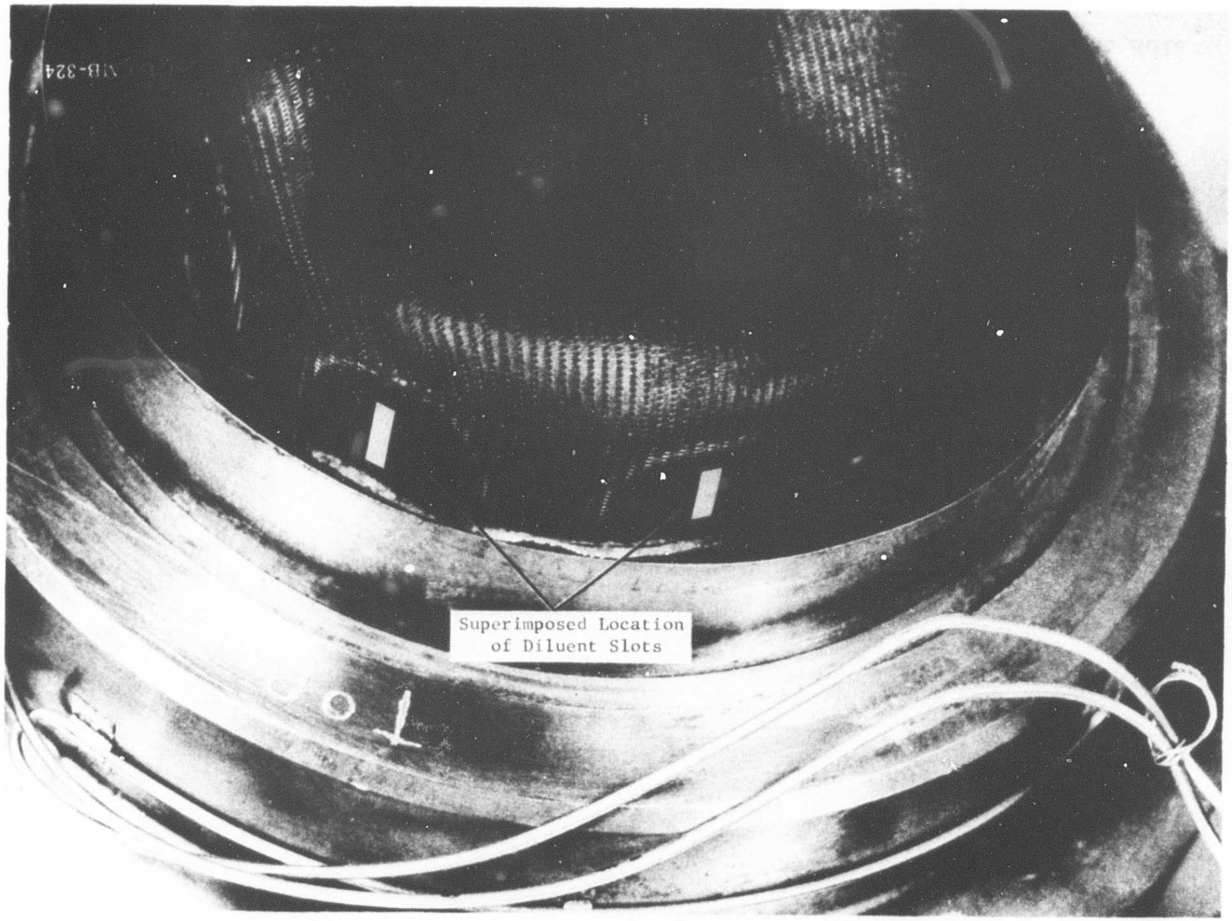

Figure 96. Pattern on Inner Liner After Testing With Original (8) Diluent Hole Configuration in Outer Liner.

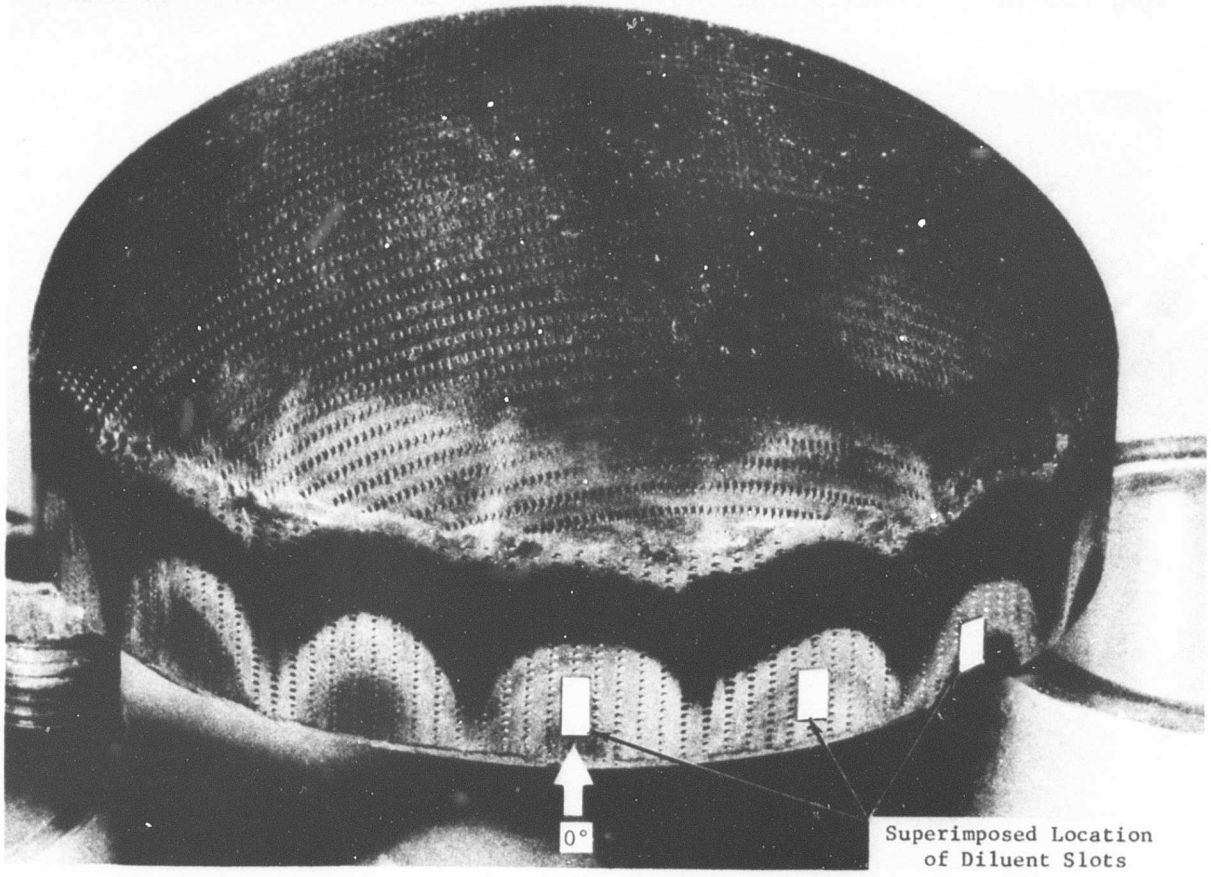

Figure 97. Pattern on Inner Liner After Testing With Revised (16) Diluent Hole Configuration in Outer Liner.

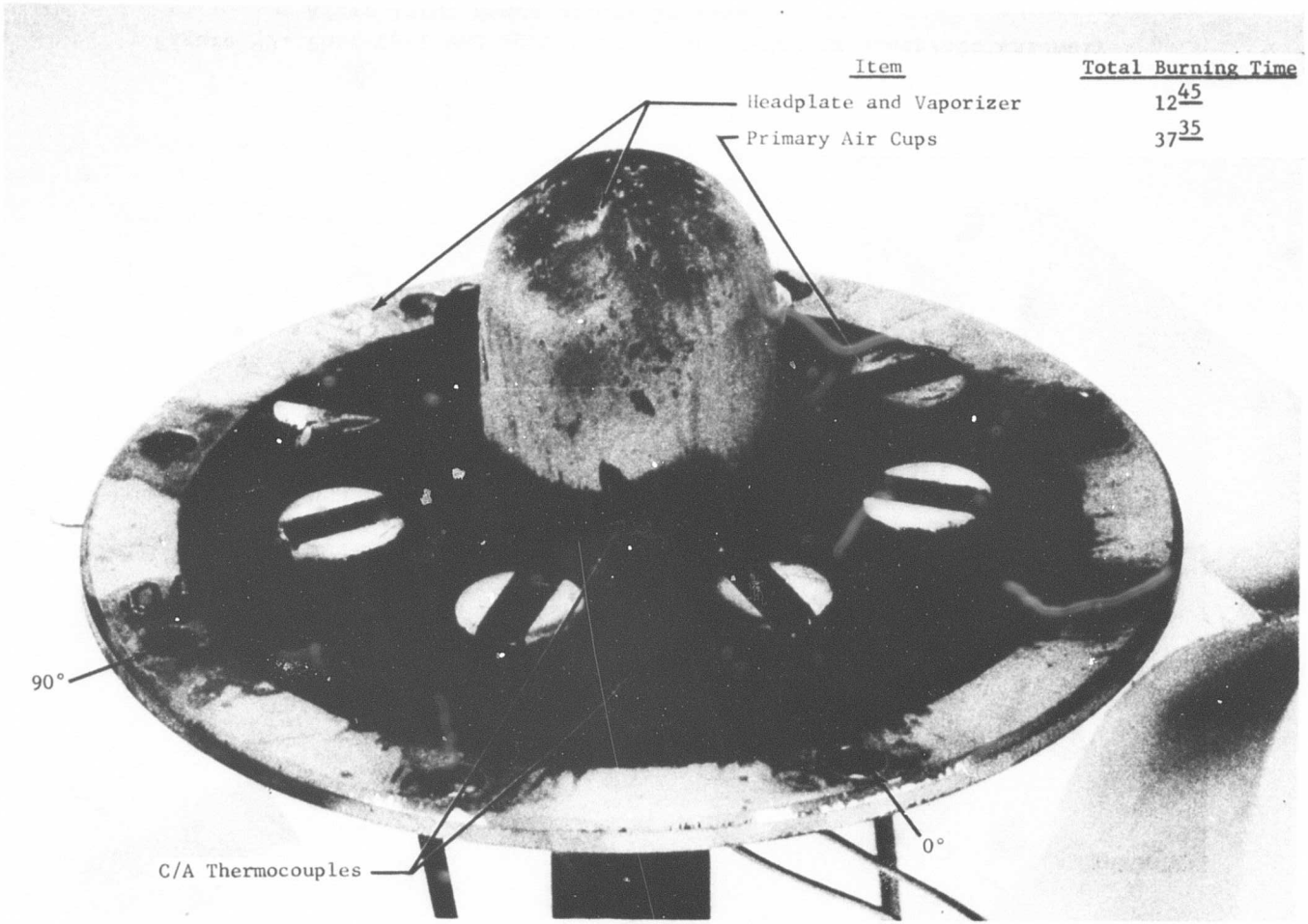

Figure 98. Post-Test Photograph of Mushroom Vaporizer Headplate Assembly After 12:45 Hours of Hot Testing.

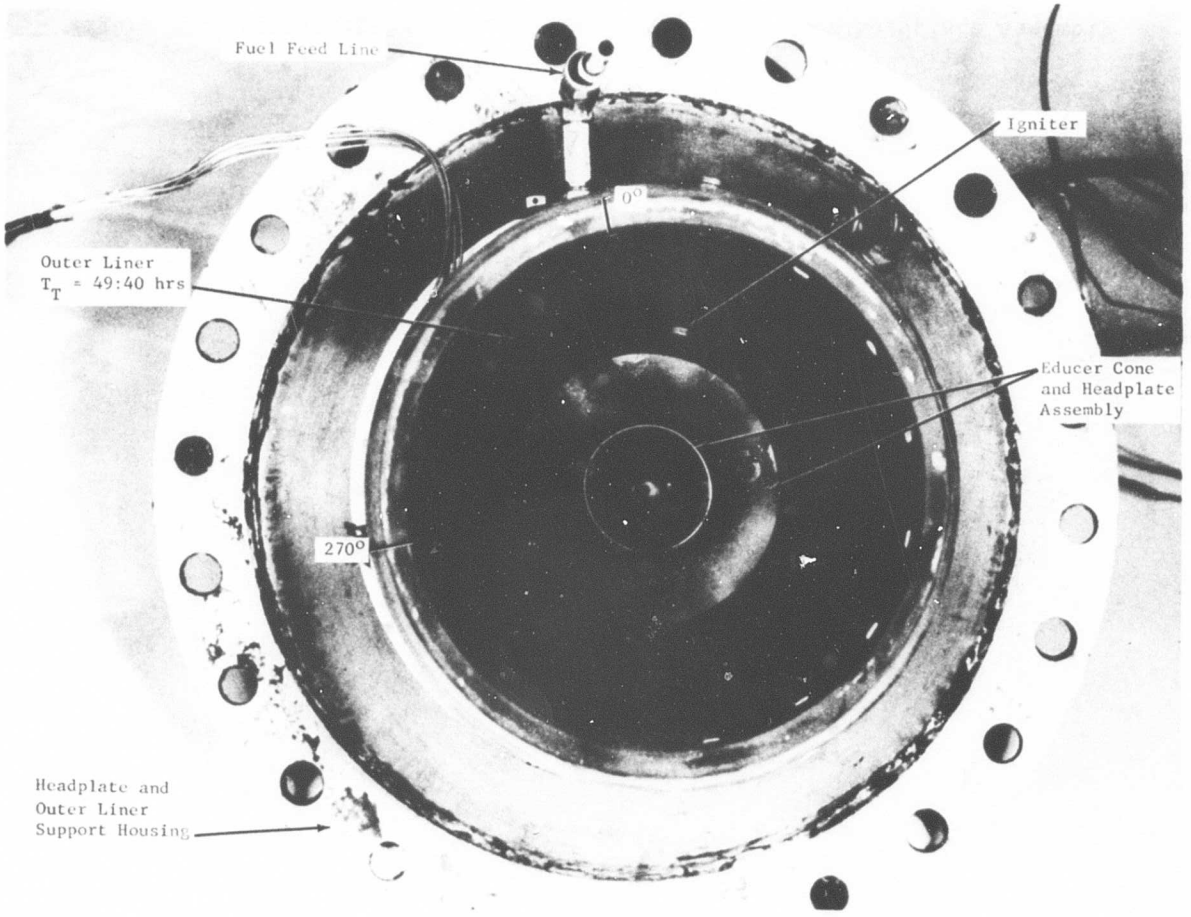

Figure 99. Post-Test Photograph of Atomizer-Educer Headplate Assembly After 12:05 Hours of Hot Testing.

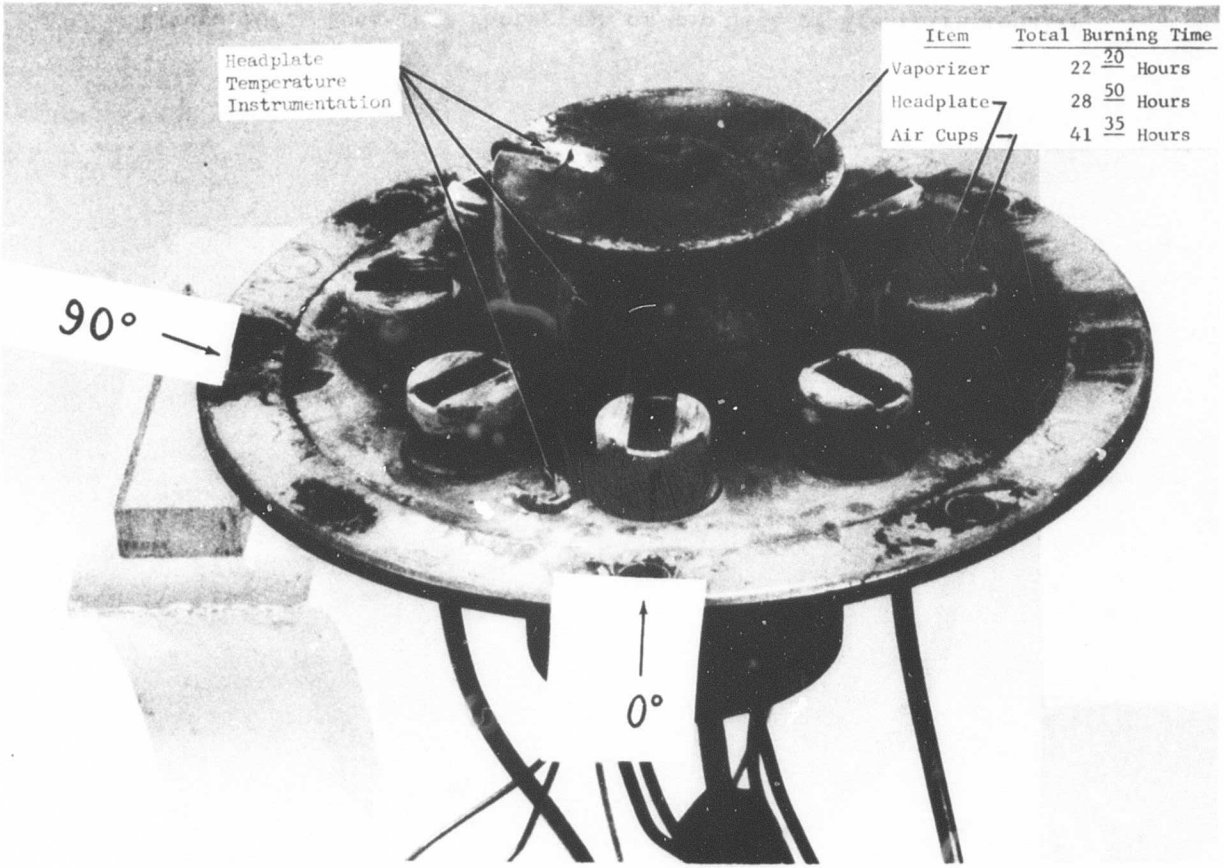

Figure 100. Post-Test Photograph of Annular Vaporizer Headplate Assembly.

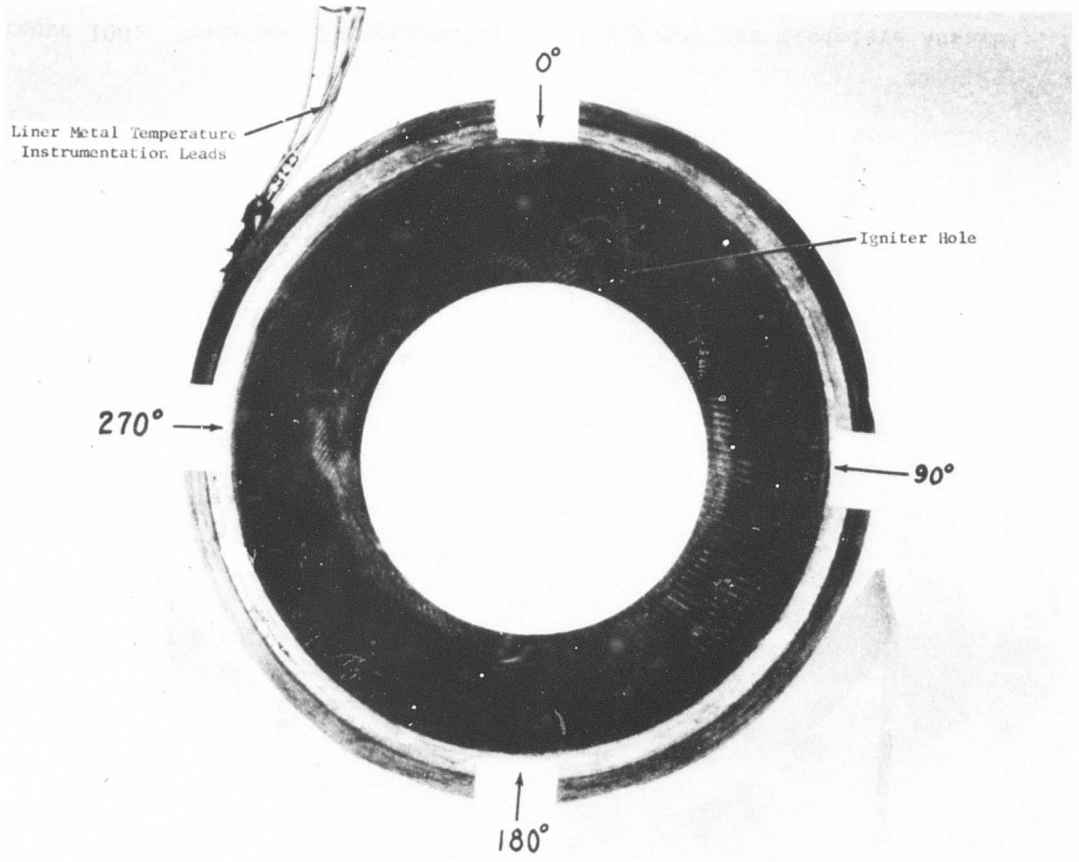

Figure 101. Post-Test Photograph of Hot Side of Transpirationally Cooled Outer Liner After 53:40 Hours of Hot Testing.

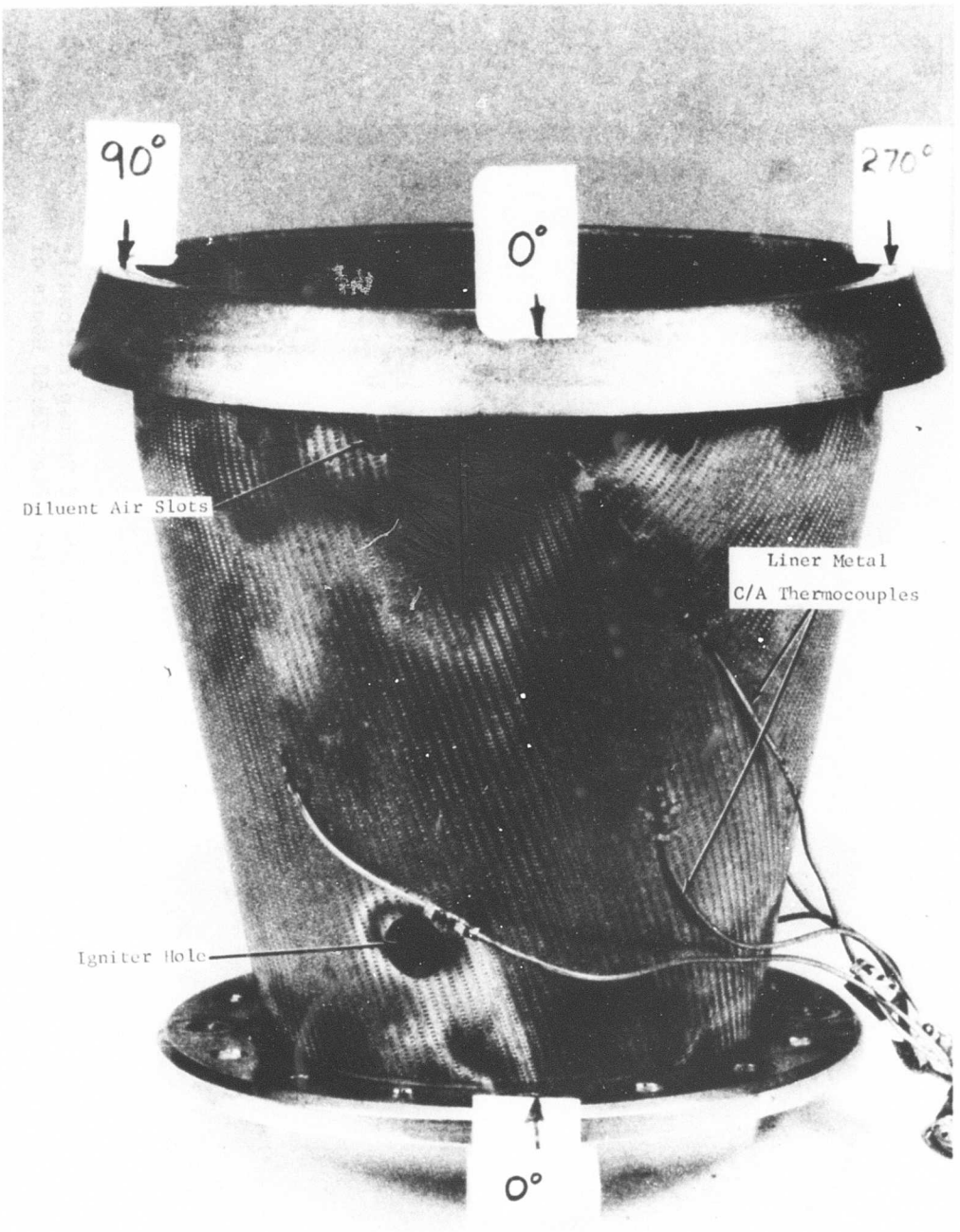

Figure 102. Post-Test Photograph of Cold Side of Transpirationally Cooled Outer Liner After 53:40 Hours of Hot Testing.

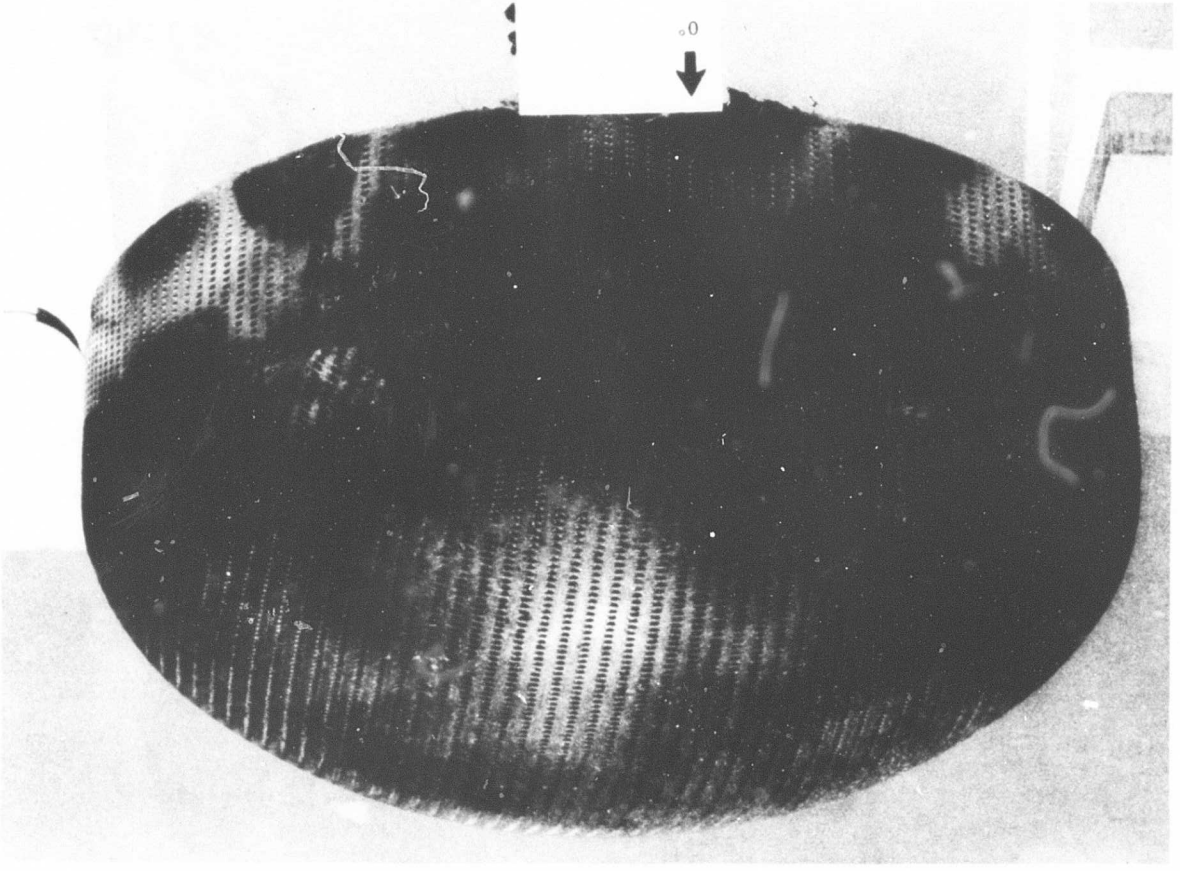

Figure 103. Post-Test Photograph of Hot Side of Transpirationally Cooled, Dome Shaped, Inner Liner After 28:50 Hours of Hot Testing.

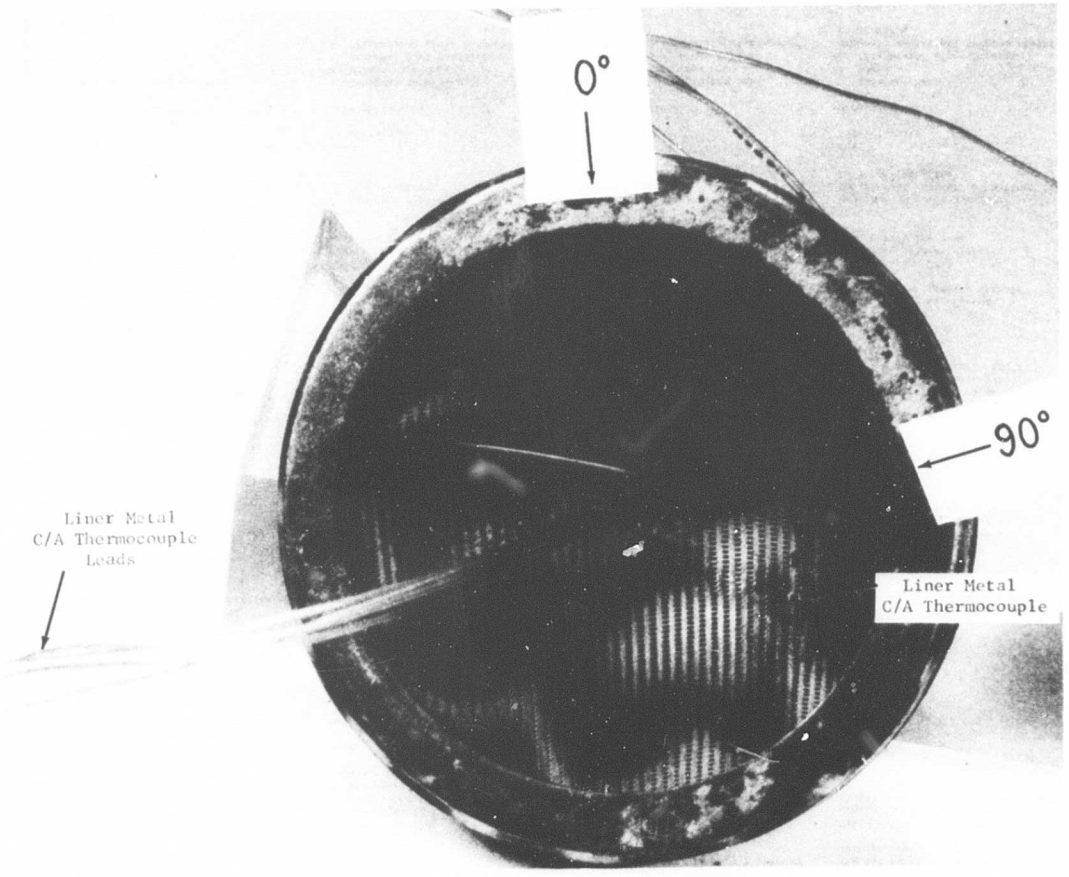

Figure 104. Post-Test Photograph of Cold Side of Transpirationally Cooled, Dome Shaped, Inner Liner After 28:50 Hours of Hot Testing.

TABLE XVI. COMPARISON OF PRIMARY ZONE COMBUSTOR CONFIGURATIONS

		Configuration 1 5 Atm - Low Pressure Facility	Configuration 2 5 Atm - Low Pressure Facility	Configuration 3 5 Atm - Low Pressure Facility
1	Engine Packaging	End-mounted Independent of turbine stator design	End-mounted Complex inner liner and turbine cooling air routing. (Probably through turbine stator blades.)	End-mounted Complex inner liner and turbine cooling air routing. (Probably through turbine stator blades.)
2	Combustion Efficiency and Stability Range	Test Design Point Eff^{7}., η_b > 98% Stable Combustion 8-Point Fuel Feed 0.011 < fp < 0.085 4-Point Fuel Feed 0.016 < fp < 0.085	Test Design Point Eff^{7}., η_b > 98% Stable Combustion 0.022 < fp < 0.085	Test Design Point Eff^{7}., η_b > 98% Stable Combustion 0.007 < fp < 0.08
3	Combustor Exit Temperature Distribution (@ Design Primary Zone Fuel-Air Ratio 700°F Inlet Air Temperature, JP-5 Fuel)	Test 8-Point Fuel Feed $\frac{T_{max.}}{T_{avg.}}$ = 1.416 4-Point Fuel Feed $\frac{T_{max.}}{T_{avg.}}$ = 1.706	Test $\frac{T_{max.}}{T_{avg.}}$ = 1.818	Test $\frac{T_{max.}}{T_{avg.}}$ = 1.499
4	Combustor Pressure Loss	Test $\frac{\Delta P_T}{P_T}$ < 3%	Test $\frac{\Delta P_T}{P_T}$ < 3%	Test $\frac{\Delta P_T}{P_T}$ < 3%
5	Fuel System Complexity and Susceptibility to Contamination	Test External Radial Fuel Feed Manifold with eight 0.020" dia. orifices Upstream Axial Fuel Feed with four 0.030" dia. orifices	Test Axial Fuel Feed Impinging on Mushroom Dome One 0.060" dia. orifice	Test One 24 G.P.H. Simplex Atomizer
6	Liner Surface Area and Cooling Effectiveness	Liner Surface Area Outer 62 in^2 Inner 35 in^2 Test - Metal Temperatures Outer: T_{max} 620 °F, $T_{coolant}$ 86 °F, fp 0.085 Inner: 1270, 87, 0.073 Dome Deposit: 1640, 270, 0.066	Liner Surface Area Outer 62 in^2 Inner 25 in^2 Test - Metal Temperatures Outer: 600, 101, 0.073 Inner: 790, 442, 0.086	Liner Surface Area Outer 62 in^2 Inner 25 in^2 Test - Metal Temperatures Outer: 770, 96, 0.071 Inner: 920, 410, 0.081
7	Durability of Vaporizing Components	Test No visible evidence of deterioration. T_{max} 1775°F @ Design Point 1160°F	Test No visible evidence of deterioration. T_{max} 1780°F @ Design Point - (Lost Thermocouple)	Test No visible evidence of deterioration. T_{max} 1910°F @ Design Point 800°F
8	Carbon, Smoke & Coke Characteristics	Test JP-4 and JP-5 No Coke Negligible Carbon Smoke emission unknown	Test JP-4 and JP-5 No Coke Negligible Carbon Smoke emission unknown	Test JP-4 and JP-5 No Coke Negligible Carbon Smoke emission unknown
9	Multifuel Capability	Test JP-4 and JP-5 Combustion characteristics essentially the same	Test JP-4 and JP-5 Combustion characteristics essentially the same	Test JP-4 and JP-5 Combustion characteristics essentially the same
10	Ease of Ignition	Test No ignition problems (2 Joule igniter)	Test No ignition problems (2 Joule igniter)	Test Required 20 Joule igniter Position of igniter not optimum for this configuration.
11	Response Rate	Test Indeterminate	Test Indeterminate	Test Indeterminate
12	Fabrication Complexity and Comparative Requirements	Straightforward 1 Integral Vaporizer 8 Primary Air Cups 1 External Fuel Manifold 2 "Fishmouth" Liner Supports	Straightforward 1 "Mushroom" Vaporizer Tube 8 Primary Air Cups 1 "Fishmouth" Liner Support Probable additional turbine stator complexity.	Straightforward 1 Atomizer Nozzle 1 Eductor 1 "Fishmouth" Liner Support Probable additional turbine stator complexity.

TABLE XVI - Continued

		Configuration 4, Build 1 5 Atm - Low Pressure Facility	Configuration 4, Build 2 5 Atm - High Pressure Facility	Configuration 4, Build 2 16 Atm - High Pressure Facility
1	Engine Packaging	End-mounted Complex inner liner and turbine cooling air routing. (Probably through turbine stator blades.)	End-mounted Complex inner liner and turbine cooling air routing. (Probably through turbine stator blades.)	End-mounted Complex inner liner and turbine cooling air routing. (Probably through turbine stator blades.)
2	Combustion Efficiency and Stability Range	Test Design Point Eff., $\eta_b > 98\%$ $\eta_b = 98\%$ @ .055 fp Stable Combustion : 8-Point Fuel Feed $0.012 < fp < 0.079$	Test $\eta_b = 95\%$ @ .058 fp Stable Combustion : Similar to Build 1	Test $\eta_b = 94\%$ @ .067 fp Stable Combustion : Similar to Build 1
3	Combustor Exit Temperature Distribution (@ Design Primary Zone Fuel-Air Ratio 700°F Inlet Air Temperature, JP-5 Fuel)	Test 8-Point Fuel Feed $\frac{T_{max.}}{T_{avg.}} = 1.51$	Test 8-Point Fuel Feed $\frac{T_{max.}}{T_{avg.}} = 1.45$	Test 8-Point Fuel Feed $\frac{T_{max.}}{T_{avg.}} = 2.07$
4	Combustor Pressure Loss	Test $\frac{Pt}{Pt} \leq 3\%$	Test $\frac{Pt}{Pt} \leq 3\%$	Test $\frac{Pt}{Pt} \leq 3\%$
5	Fuel System Complexity and Susceptibility to Contamination	Test External Radial Fuel Feed Manifold with eight 0.020" dia. orifices	Test External Radial Fuel Feed Manifold with eight 0.020" dia. orifices	Test External Radial Fuel Feed Manifold with eight 0.020" dia. orifices
6	Liner Surface Area and Cooling Effectiveness	Liner Surface Area Outer 62 in^2 Inner 25 in^2 Test - Metal Temperatures Outer: Tmax 755 °F, Tcoolant 120 °F, fp .044 Inner: Tmax 960 °F, Tcoolant 398 °F, fp .079	Liner Surface Area Outer 62 in^2 Inner 25 in^2 Test - Metal Temperatures Outer: Tmax 935 °F, Tcoolant 100 °F, fp .067 Inner: Tmax 795 °F, Tcoolant 600+ °F, fp .067	Liner Surface Area Outer 62 in^2 Inner 25 in^2 Metal Temperatures - Test Outer: Tmax 550 °F, Tcoolant 79 °F, fp .058 Inner: Tmax 600 °F, Tcoolant 305 °F, fp .058
7	Durability of Vaporizing Components	Test No visible evidence of deterioration. Tmax. 1035°F @ Design Point 1015°F	Test No visible evidence of deterioration. Tmax. 915°F @ Design Point -	Test No visible evidence of deterioration Tmax. 995°F @ Design Point -
8	Carbon, Smoke & Coke Characteristics	Test JP-4 No Coke Negligible Carbon	Test JP-4 No Coke Negligible Carbon and Smoke emission	Test JP-4 No Coke Negligible Carbon and Smoke emission
9	Multifuel Capability	Test JP-4	Test JP-4	Test JP-4
10	Ease of Ignition	Test No ignition problems (low energy igniter)	Test No ignition problems (low energy igniter)	Test No ignition problems (low energy igniter)
11	Response Rate	Test Indeterminate	Test Indeterminate	Test Indeterminate
12	Fabrication Complexity and Comparative Requirements	Straightforward 1 Annular Vaporizer 8 Primary Air Cups 1 External Fuel Manifold 2 "Fishmouth" Liner Supports	Straightforward 1 Annular Vaporizer 8 Primary Air Cups 1 External Fuel Manifold 2 "Fishmouth" Liner Supports	Straightforward 1 Annular Vaporizer 8 Primary Air Cups 1 External Fuel Manifold 2 "Fishmouth" Liner Supports

TABLE XVII. COMBUSTOR DESIGN-POINT OPERATING CONDITIONS AND PERFORMANCE OBJECTIVES

Combustor Inlet	
Airflow Rate, W_e (lb/sec)	2.0
Combustor Bypass Flow Bleed Air, W_{bleed} (lb/sec)	0.57
Combustion Chamber Airflow Rate, W_{cc} (lb/sec)	1.43
Total Pressure (atm)	16.0
Total Temperature (°F)	700
Combustion Chamber Fuel-Air Ratio, f_{cc}	0.04
Fuel Flow Rate (lb/hr)	208
Combustor Exit	
Total Temperature (°F)	3000
Performance Objectives	
Combustion Efficiency (%)	98.5
Combustor Pressure Loss Percent of Inlet Total Pressure (%)	3.0
Exhaust Temperature Variation (°F)	$\pm$200

Note: Primary Zone Fuel-Air Ratio = 0.075

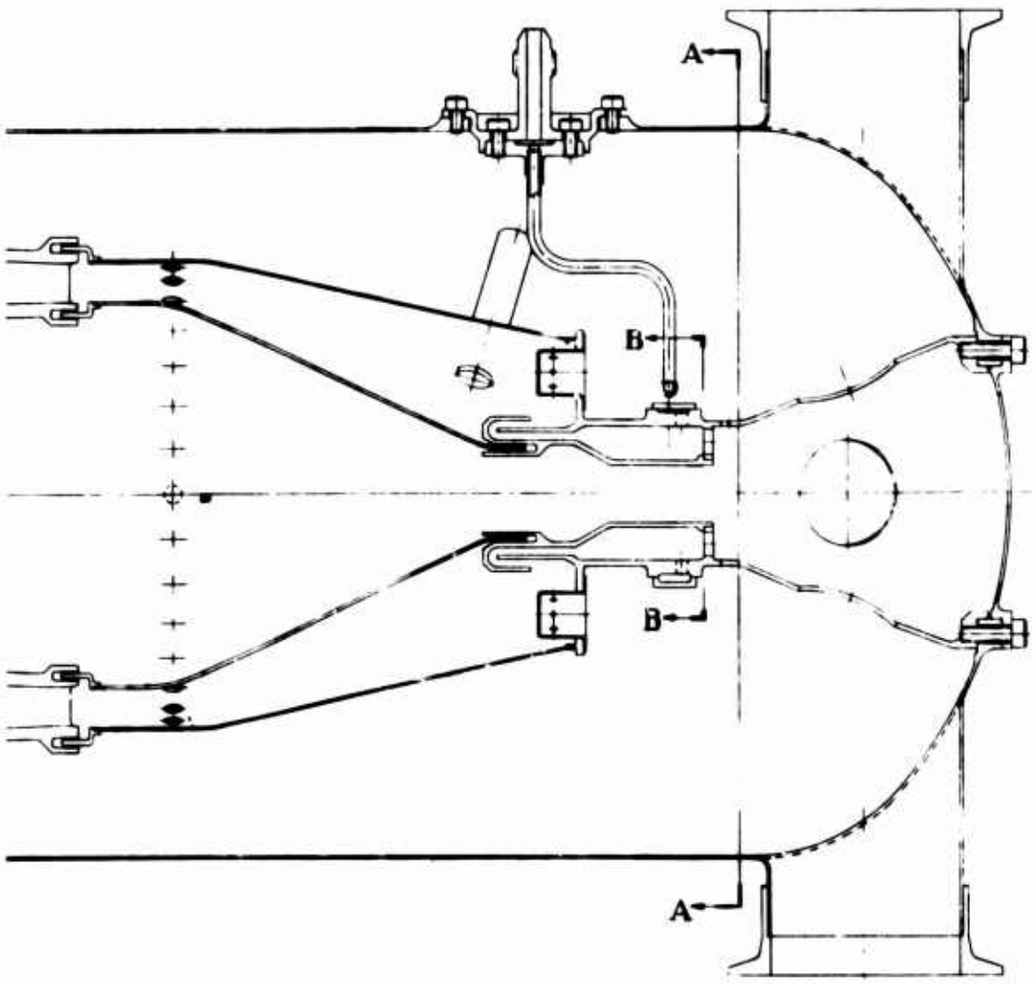

Figure 105. Preliminary Flight Weight End-Mounted Annular Combustor Design Incorporating Eight Point Tangential Fuel Feed System.

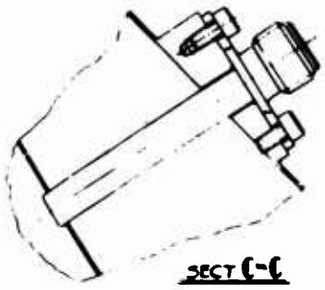

SECT C-C

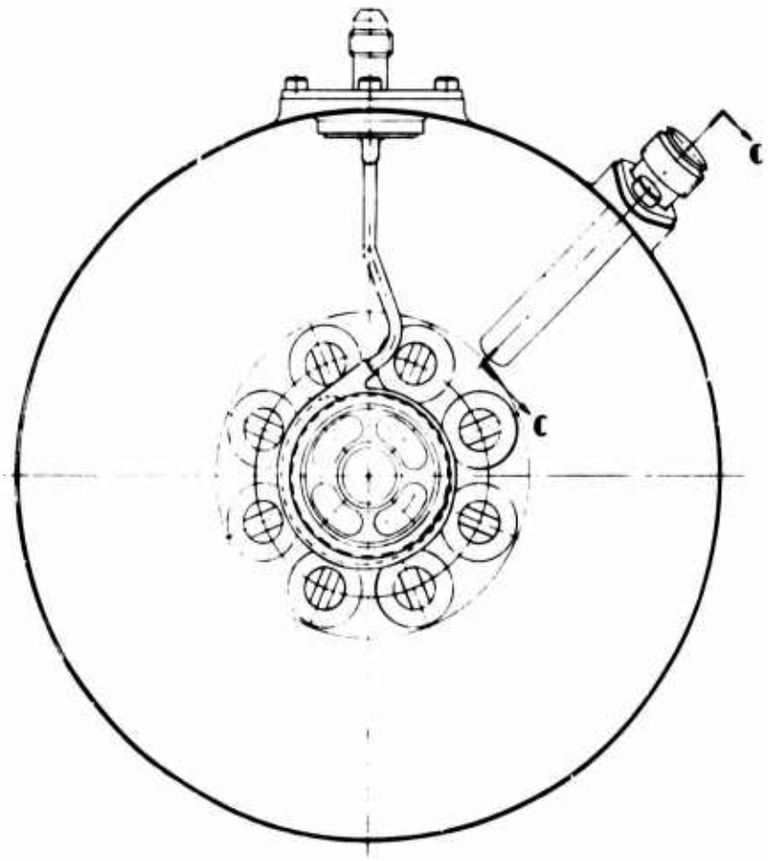

SECT A-A

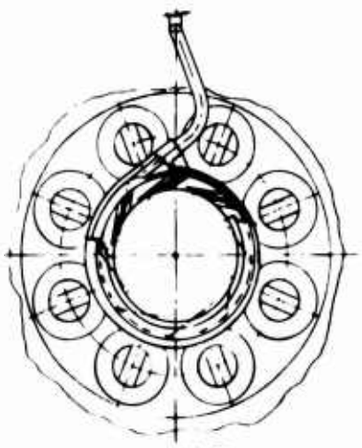

SECT B-B

B

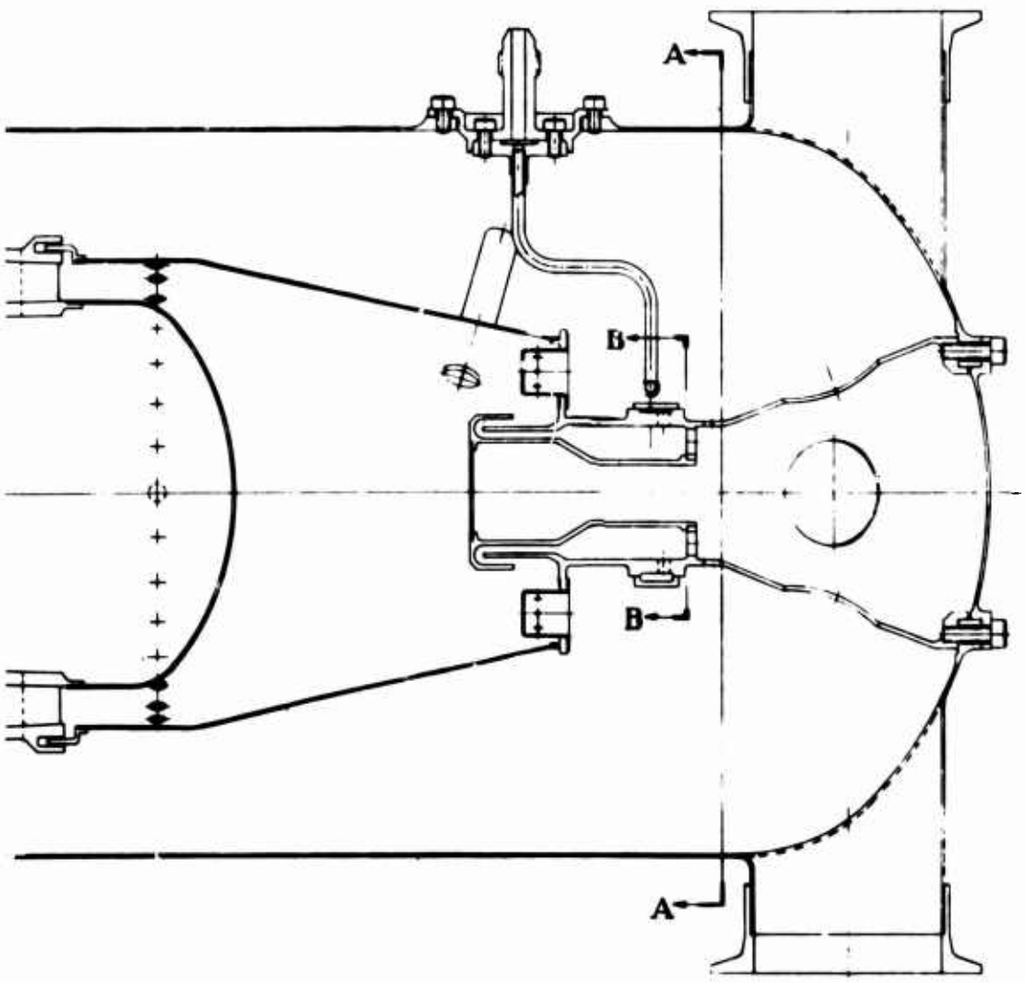

Figure 106. Preliminary Flight Weight End-Mounted Can Combustor Design Incorporating Eight-Point Tangential Fuel Feed System.

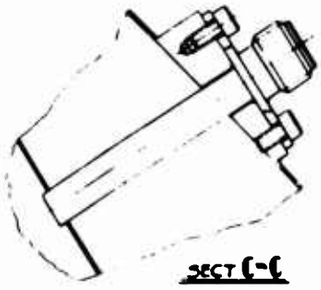

SECT C-C

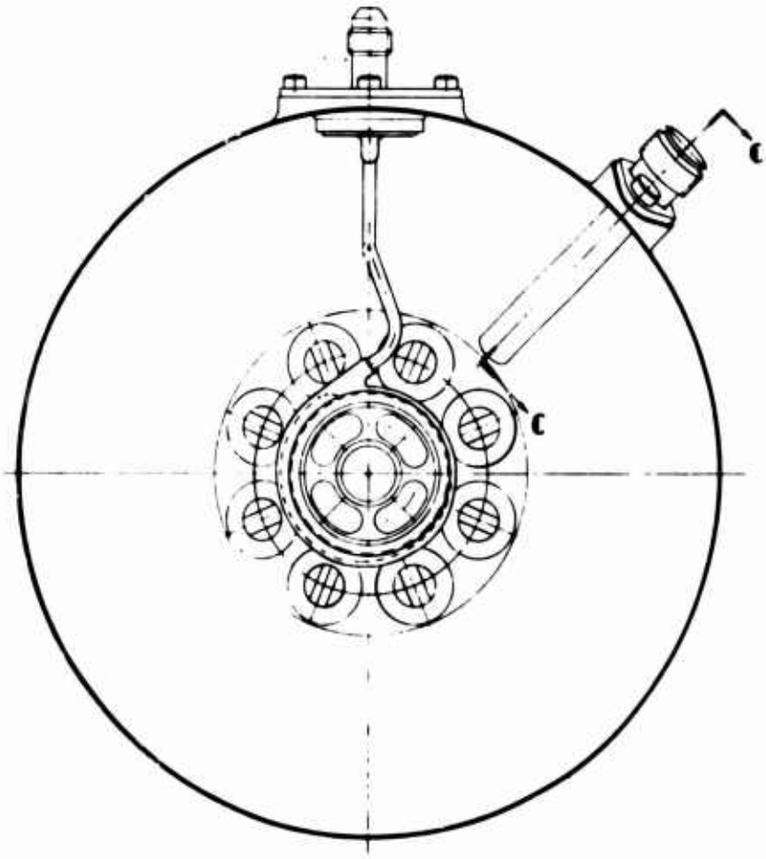

SECT A-A

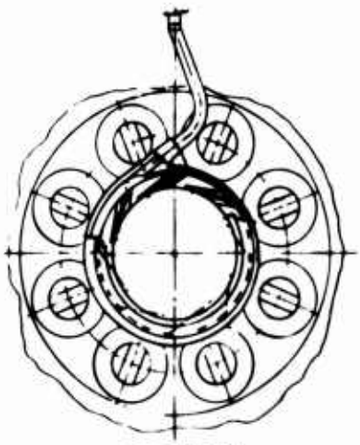

SECT B-B

B

Unclassified
Security Classification

DOCUMENT CONTROL DATA - R & D

(Security classification of title, body of abstract and indexing annotation must be entered when the overall report is classified)

1. ORIGINATING ACTIVITY (Corporate author) Curtiss-Wright Corporation Wood-Ridge, New Jersey	2a. REPORT SECURITY CLASSIFICATION None 2b. GROUP

3. REPORT TITLE

Advanced High Temperature Combustor Research for Small Gas Turbine Engines

4. DESCRIPTIVE NOTES (Type of report and inclusive dates)

Final

5. AUTHOR(S) (First name, middle initial, last name)

Richard H. Andersen

6. REPORT DATE	7a. TOTAL NO. OF PAGES	7b. NO. OF REFS
October 1968	201	

8a. CONTRACT OR GRANT NO.	9a. ORIGINATOR'S REPORT NUMBER(S)
DA 44-177-AMC-375(T) b. PROJECT NO. Task 1G125901A01409 c. d.	USAAVLABS Technical Report 68-63 9b. OTHER REPORT NO(S) (Any other numbers that may be assigned this report) 68-050180.F

10. DISTRIBUTION STATEMENT

This document has been approved for public release and sale; its distribution is unlimited.

11. SUPPLEMENTARY NOTES	12. SPONSORING MILITARY ACTIVITY
	U.S. Army Aviation Materiel Laboratories Fort Eustis, Virginia

13. ABSTRACT

Design studies and an experimental test program have been conducted to provide basic technology and preliminary flight-weight designs for a small (2-5 lb/sec total engine airflow) high temperature rise combustor with a 3000°F exit temperature, as a first step towards demonstration in an advanced engine. Tests were conducted to evaluate the combustor design parameters developed in the initial design study phase of the program pertaining to liner cooling techniques, primary-diluent air mixing, fuel introduction and patternization, and primary zone performance. The preliminary designs optimize the technology developed in this program and comprise both annular and can end-mounted combustor configurations incorporating an annular vaporizer fuel introduction system and transpirationally cooled liners.

DD FORM 1 NOV 68 1473 REPLACES DD FORM 1473, 1 JAN 64, WHICH IS OBSOLETE FOR ARMY USE.

Unclassified
Security Classification

14. KEY WORDS	LINK A		LINK B		LINK C	
	ROLE	WT	ROLE	WT	ROLE	WT
Combustors, Small Combustor Cooling Fuel Injection Design High Temperature Rise						